DESIGN SCOPING STUDY OF THE 12T YIN-YANG MAGNET SYSTEM FOR THE TANDEM MIRROR NEXT STEP (TMNS)

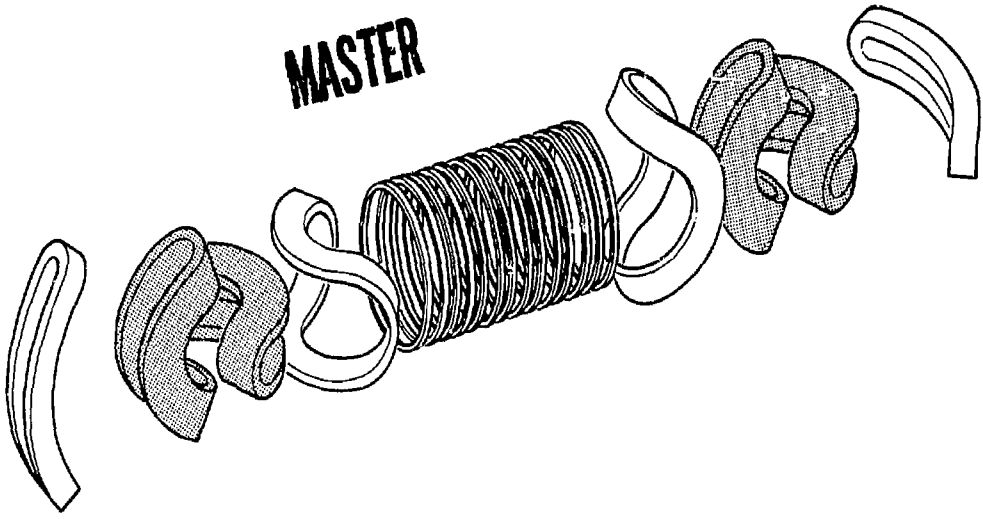

FINAL REPORT

SEPTEMBER 1981

GENERAL DYNAMICS
Convair Division

DESIGN SCOPING STUDY OF THE 12T YIN-YANG MAGNET SYSTEM FOR THE TANDEM MIRROR NEXT STEP (TMNS)

FINAL REPORT

September 1981

PRESENTED TO:
LAWRENCE LIVERMORE NATIONAL LABORATORY
P.O. BOX 808
LIVERMORE, CALIFORNIA 94550

PREPARED BY:
GENERAL DYNAMICS CONVAIR DIVISION
P.O. BOX 80847
SAN DIEGO, CALIFORNIA 92138

FOREWORD

This report documents the conceptual design study performed on the Tandem Mirror Next Step superconducting 12-Tesla Yin-Yang magnet winding. The work was sponsored by the Department of Energy under University of California-Lawrence Livermore National Laboratory Subcontract 2212201. This work was performed during the 7½-month time period beginning 25 February 1981.

ACKNOWLEDGMENTS

The Lawrence Livermore National Laboratory personnel who made significant contributions to this program are:

R.H. Bulmer	Project Advisor
D.N. Cornish	Project Manager
Dr. R.W. Hoard	Project Advisor
Dr. R.M. Scanlan	Project Advisor

General Dynamics Convair Division personnel who made significant technical contributions to this program are:

K. L. Agarwal	Materials & Processes
R. W. Baldi	Chief Engineer
J. L. Christian	Materials & Processes
M. S. Herrington	Cost Estimating
W. L. Johnston	Quality Assurance
P. L. Koppel	Cost Estimating
G. D. Magnuson	Electromagnetic Analysis
R. C. McCool	Structural Analysis
D. D. Stenger	Manufacturing/Producibility
R. A. Sutton	Structural Design
R. E. Tatro	Program Manager
W. D. Taylor	Thermodynamic Analysis

TABLE OF CONTENTS

TABLE OF CONTENTS (Continued)

TABLE OF CONTENTS (Continued)

TABLE OF CONTENTS (Concluded)

LIST OF FIGURES

LIST OF FIGURES (Continued)

LIST OF FIGURES (Continued)

LIST OF FIGURES (Continued)

LIST OF FIGURES (Concluded)

LIST OF TABLES

LIST OF TABLES (Concluded)

SUMMARY

The overall objective of this engineering study was to determine the feasibility of designing a Yin-Yang magnet capable of producing a peak field in the windings of 12T for the Tandem Mirror Next Step (TMNS) program. As part of this technical study, a rough order of magnitude (ROM) cost estimate of the winding for this magnet was undertaken.

The preferred approach to the winding design of the TMNS plug coil utilizes innovative design concepts to meet the structural, electrical and thermodynamic requirements of the magnet system. Structurally, the coil is radially partitioned into four sections, preventing the accumulation of the radial loads and reacting them into the structural case. To safely dissipate the 13.34 GJ of energy stored in each Yin-Yang magnet, the winding has been electrically subdivided into parallel or nested coils, each having its own power supply and protection circuitry. This arrangement effectively divides the total stored energy of the coils into manageable subsystems. The windings are cooled with superfluid helium II, operated at 1.8K and 1.2 atmospheres. The superior cooling capabilities of helium II have enabled the overall winding envelope to be minimized, providing a current density of 2367 A/CM^2, excluding substructure. Design highlights are tabulated below:

- Condutor Pack Cross Section — 3.75 x .70 M (12.3 x 2.8 ft.)
- Spherical Size — 17.4 M (57.0 ft.) Dia.
- Spreading Force — 1.6×10^9 Newtons (350×10^6 lbs)
- Stored Energy — 13.34 GJ per Yin-Yang
- Projected Weight — 4.5×10^6 KG (6670 tons)
- Projected Cost — \$166 M (R.O.M. Estimate) not including contingency or fee)
- Refrigeration Requirements — 4.0 KW (per Yin-Yang)

The conceptual design activities reported herein resulted in a superconducting magnet concept for the Yin-Yang system for the next generation of mirror machines. Detail analysis and evaluation of the TMNS Yin-Yang magnets indicates that they will meet all performance requirements and they can be built with few extensions of today's technology.

1.0 INTRODUCTION

The overall goals of this engineering study were to determine the technical feasibility and to establish the ROM cost estimate of the electrical windings for a 12 Tesla Yin-Yang magnet for the Tandem Mirror Next Step (TMNS) program. This study was based upon the following specific objectives in support of the overall program goals:

- Analyze and design the conductor winding, substructure, and conductor joining process.
- Evaluate techniques to limit the heat load to the superfluid helium II.
- Evaluate the electrical effects of operating parallel windings.
- Prepare a ROM cost estimate for conductor fabrication and winding.

The initial design requirements parameters for the TMNS Yin-Yang magnet system are presented in Table 1-I.

TABLE 1-I

INITIAL DESIGN REQUIREMENT PARAMETERS FOR TMNS

M1, M2		YIN-YANG PAIR
MAJOR RADIUS	:	3.7m
MINOR RADIUS	:	1.5m
SWEEP ANGLE	:	65^{o}
COIL SECTION	:	2.72 x 0.68m
CURRENT DENSITY	:	17.1 - 20.4 MA $\cdot$ M^{-2}
CURRENT/COIL	:	37.7 MA
TOTAL MAGNETIC ENERGY	:	10^{10} j

As part of this study, four different conductor concepts were investigated. Each of these concepts are illustrated in Figure 1-1.

The first conductor studied was the baseline conductor for the High Field Test Facility (HFTF) program shown on the left-hand side of Figure 1-1. This concept was quickly discarded for application in TMNS after detail analysis indicated a prohibitive quench protection problem. Due to the high stored energy in the TMNS magnet, this relatively low current conductor results in a rather challenging design to provide adequate quench

protection. Based on our studies, an excessive number of separate parallel windings (i.e., greater than 20) are required to maintain the conductor quench temperature and voltage within acceptable limits. Therefore, this conductor was discarded from further consideration for TMNS.

The second configuration studied was a scaled-up version of the HFTF conductor as shown in the left center portion of Figure 1-1. This conductor was sized to be as large as possible within the allowable winding strain limitations of the brittle Nb_3Sn superconductor. This larger conductor substantially reduced the number of parallel windings for safe quench/discharge of the magnet. For this concept, a total of 12 parallel windings per coil was estimated.

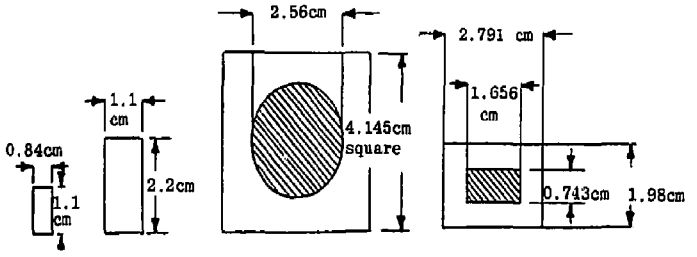

TYPE	MONOLITH	MONOLITH	COPPER STABILIZED CABLE CONDUCTOR	COPPER STABILIZED MONOLITH
CURRENT RATING @ 12T - AMPS	4000	10400	50000	15600
COMMENT	BASELINE HFTF CONDUCTOR	HFTF SCALE-UP	SINGLE CONDUCTOR SERIES WOUND	FIVE NESTED COILS

Figure 1-1. FOUR DIFFERENT CONDUCTORS WERE STUDIED FOR TMNS

Although the use of parallel windings was beginning to show technical feasibility, the mechanical problems with actually fabricating a winding in a parallel fashion appeared to be prohibitive. Therefore, a nested coil approach was adopted. In this approach, the windings are divided into separate series wound "C" shaped coil. They are designed to nest together forming the composite magnet upon assembly.

In conjunction with the study of the scaled-up conductor, substructure detail studies were also conducted. Both electrically insulated 304LN stainless steel and solid G-10CR fiberglass/epoxy substructure materials were studied. These studies showed that the substructure was inefficient. Inclusion of substructure resulted in an unsatisfactory reduction in overall current density to below 1200A/cm^2. Also, the substructure concepts considered did not aid in reacting the axial stresses with the conductor. Consequently, these axial stresses were found to be excessive and this concept was discarded from further consideration for TMNS.

The third configuration studied was an in situ fabricated 50KA copper stabilized cable conductor shown in the right-center portion of Figure 1-1. This conductor had a much larger current rating and cross-section than the other conductors studied. The 50KA operating current required only a single series winding per coil to safely maintain the quench voltage and temperature within acceptable limits. Also, the cross-section was structurally sufficient to react the transverse and radial electromagnetic forces. However, the axial stresses within the conductor were still excessive. Also, the producibility of the conductor was questionable. The two major problems identified were:

- Fabricating a Nb_3Sn cable with good solderability. The addition of barriers encompassing the cable strands to inhibit diffusion bonding of the strands during the reaction process also inhibit subsequent solder bond integrity as well.

- Winding tolerance control. Internal gaps could be difficult to control for an in situ fabricated winding.

Consequently this concept was discarded.

The fourth concept studied is the rectangular copper stabilized monolithic conductor shown in the right-hand portion of Figure 1-1. This conductor design, with five separate nested windings per coil (i.e., 10 separate nested windings per Yin-Yang magnet), provided safe quench performance. A structural case with an integral substructure, as shown in Figure 1-2, was studied in conjunction with this conductor. This arrangement enabled the conductor to adequately react all of the electromagnetic forces with acceptable axial stresses. Consequently, based on these technical advantages, this concept was selected to be the preferred choice for the TMNS Yin-Yang magnet. GDC and LLNL's (Appendix E) detailed analyses of this conductor have shown that all technical requirements have been satisfactorily met, and that the conductor is producible and inspectable within a reasonable extrapolation of today's technology. A summary of the essential design characteristics of the TMNS Yin-Yang magnet with the selected conductor is presented in Table 1-II.

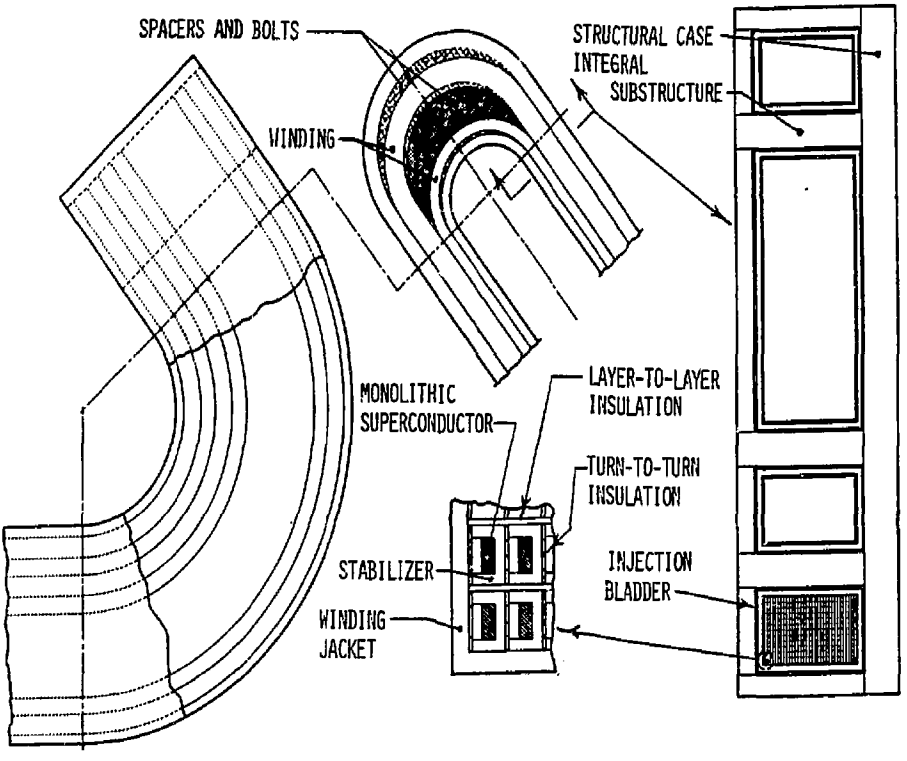

FIGURE 1-2. PREFERRED CONDUCTOR CONCEPT IN CONJUNCTION WITH STRUCTURAL CASE WITH INTEGRAL SUBSTRUCTURE

This report fully documents the work performed to develop the conceptual design of the TMNS Yin-Yang winding. The report is organized in accordance with the evolution phases of the design. Chapter 2 describes the trade studies performed on concepts that were eventually discarded. Chapter 3 describes the detailed efforts performed to verify the suitability of the selected preferred concept. Chapter 4 details the cost estimating task for the preferred concept. This chapter includes groundrules, assumptions, and methodology for establishing cost estimates of the winding. An overall estimate of the Yin-Yang magnet, including a rough estimate of the structural case cost, is also included.

Table 1-II

DESIGN CHARACTERISTICS SUMMARY
FOR TMNS 12T YIN-YANG MAGNET

GENERAL DATA	UNITS	
Magnet Type	-	Yin-Yang Magnet Pair
Number of Units	-	2 (per reactor)
Overall Size	m	17.4m Spherical
Stored Energy	MJ	13340
Ampere Turns	MAT	46,332/Coil
Inductance	H	5.52, 12.1, 13.0 for three nested coils/yin
Charging Time	Min	TBD
Peak Field	Tesla	12
Central Field	Tesla	6
Uniformity Requirements	%	NA
Uniformity Region	M	NA
Discharge Time Constant	Sec	TBD
Operating Temperature	K	1.8
Cooldown Time	Hr	TBD
Helium Volume	L	3000
Conductor Cooling Mode	-	Subcooled HeII
Warmup Time	Hr	TBD

CONDUCTOR DATA			
Grade	-	I	II
Conductor Type	-	Monolithic Stabilizer	Solid in
Operating Current	Amps	15600	15600
S/C Current Density	Amps/cm sq	30934	40847
Pack Current Density	Amps/cm sq	1762	1762
Critical Current	Amps	22286 @ 1.8K/12.0T	22286 @ 1.8K/9.0T
Length	km	61.3	111.0
Superconducting Material	-	Nb_3Sn	NbTi
Cu:Non-Cu Ratio	-	9.98	13.1
Cross-Sectional Area	cm sq	5.39	5.39
Conductor Packing Factor	-	0.818	0.818
He Vol to Cond Vol	-	0.187	0.187
Stabilizer Heat Flux	W/cm sq	0.77	0.76
Stabilizer Material	-	OFHC cu	OFHC cu
RRR Stabilizer	-	75	75
Solder Material	-	63% Sn 37% Pb	63% Sn 37% Pb

Table 1-II (continued)

DESIGN CHARACTERISTICS SUMMARY
FOR TMNS 12T YIN-YANG MAGNET

PROTECTION SYSTEM DATA	UNITS	
Dump Resistor	Ohms	0.0641
Dump Trigger Voltage	Volts	TBD
Term Peak Voltage	Volts	1000
Fast Dump Time Constant	Sec	86.1, 188.8, 202.8 for three nested coils/yin
Stabilizer Peak Temp	K	<200
Peak Dump Pressure	psia	TBD
MATERIALS		
Winding Substructure	-	304LN
Winding Superstructure	-	304LN
Helium Vessel	-	304LN
Tension Bands	-	NA
Winding Pack Insulation	-	G10CR
Cold Mass Supports	-	TBD
Multi-layer Insulation	-	NA
Vacuum Vessel	-	TBD
Magnetic Shield	-	NA
Radiation Shield	-	TBD
Dump Resistor	-	TBD
WEIGHTS		
Total	K lbs	TBD
Cold Mass	K lbs	13,340
Conductor	K lbs	1828
Winding Structure	K lbs	11512
Tension Bands	K lbs	NA
LN_2 Radiation Shield	K lbs	TBD
LHe Radiation Shield	K lbs	TBD
Vacuum Vessel	K lbs	TBD
Magnetic Shield	K lbs	TBD

2.0 ENGINEERING TRADE STUDIES

The trade studies performed during the initial phase of this study are documented in this chapter. The work is organized into seven sections describing the work performed by key discipline. In sequence, design, stress analysis, materials, electromagnetic analysis, thermodynamic analysis, manufacturing, and quality assurance are included.

2.1 CONDUCTOR/SUBSTRUCTURE DESIGN

Much of our study activity encompassed conductor and substructure box arrangements simultaneously, but to simplify the discussion the various elements of the magnets will be presented separately.

2.1.1 Conductor

The first conductor considered was the HFTF monolith with a cross section of 1.1 cm high by 0.54 cm wide. This conductor fits well into the small substructure boxes which we investigated, but was impractical since over 20 parallel windings (and separate power sources) would be required per coil.

The second conductor considered was a scaled up version of the HFTF one; the scaling was limited by the amount of strain that would be experienced by a Nb_3Sn conductor, and resulted in a conductor twice the size of the HFTF conductor. This conductor fit quite well with the substructure box arrangements that were investigated, but it requires twelve parallel power sources per coil to keep the quench temperature and voltages within acceptable limits. Basically this concept was dropped when it was demonstrated that the separated substructure approach is not space efficient and creates problems routing the conductors from box to box.

The third basic concept for a conductor is based on the approach of eliminating the substructure completely and filling the winding envelope with just conductors and insulation. The conductor was originally conceived to be a cable (similar to a wire rope) in a 1/2 hard copper square substrate. Electrically this is an excellent concept in that it requires just one power source per coil. Although, the 1 KV circuit breakers are not off-the-shelf items, they are considered to be feasible. However, problems did arise with this conductor which caused it to be discarded. With a circular superconductor in a substrate, there are some severe problems in verifying the solder bond integrity. In addition, to fabricate the superconductor as a wire rope would require the use of diffusion barriers which would inhibit subsequent solder bonding (the wire rope approach was needed to bend the superconductor without overstraining it). The size of the substrate is such (4.145 cm square) that it would have to be pre-formed in sections and the superconductor bonded in place (this makes the inspection task even more difficult).

For the above reasons the 50,000 ampere cable conductor in a substrate was discarded.

Since a cabled superconductor in a substrate is not currently feasible, we tried a monolith superconductor in a 1/2-hard copper substrate. This resulted in the recommended configuration that is presented in Section 3.

2.1.2 Insulation

In most of our preliminary study work we did not concentrate on the insulation. In general, it was sufficient to postulate insulation of a certain thickness and void percentage. As we closed in on our conductor the specific type of insulation became more important. Snowfence-type insulation was preferred for layer-to-layer use, and the "button-on-a-string" type for turn-to-turn insulation. The button-on-a-string is attractive financially although the adhesives holding the string to it are subject to radiation deterioration. It is felt that this limitation can be overcome by some means of mechanically locking the string to the button (for example, the string could make a full wrap around the button) so that this concept remains the preferred one.

2.1.3 Box Substructures

The first substructure box arrangement considered used the HFTF conductor. Each box had ten conductors in width and five high. The ten conductors were to be connected in parallel. This configuration allowed seven boxes wide and 27 high within the 68 x 272 cm envelope, using 2 mm of insulation thickness, 2.41 cm of substructure between the sides and 3.50 cm of substructure between the tops of the boxes. This arrangement, shown in Figure 2.1-1 was discarded from further study for several reasons.

- The allowable space for substructure between boxes was insufficient to react the magnetic pressure developed in the pack.
- If the substructure were made of a conducting material, then some of its thickness - over 1 cm - would have to allow for ground insulation further weakening the structure for reacting magnetic pressures.
- The problem of routing ten parallel conductors simultaneously through the side plates would further weaken the substructure.
- It was calculated that over 20 groups of nested coils would be required to reduce the quench effects within acceptable levels. This was considered unacceptable.

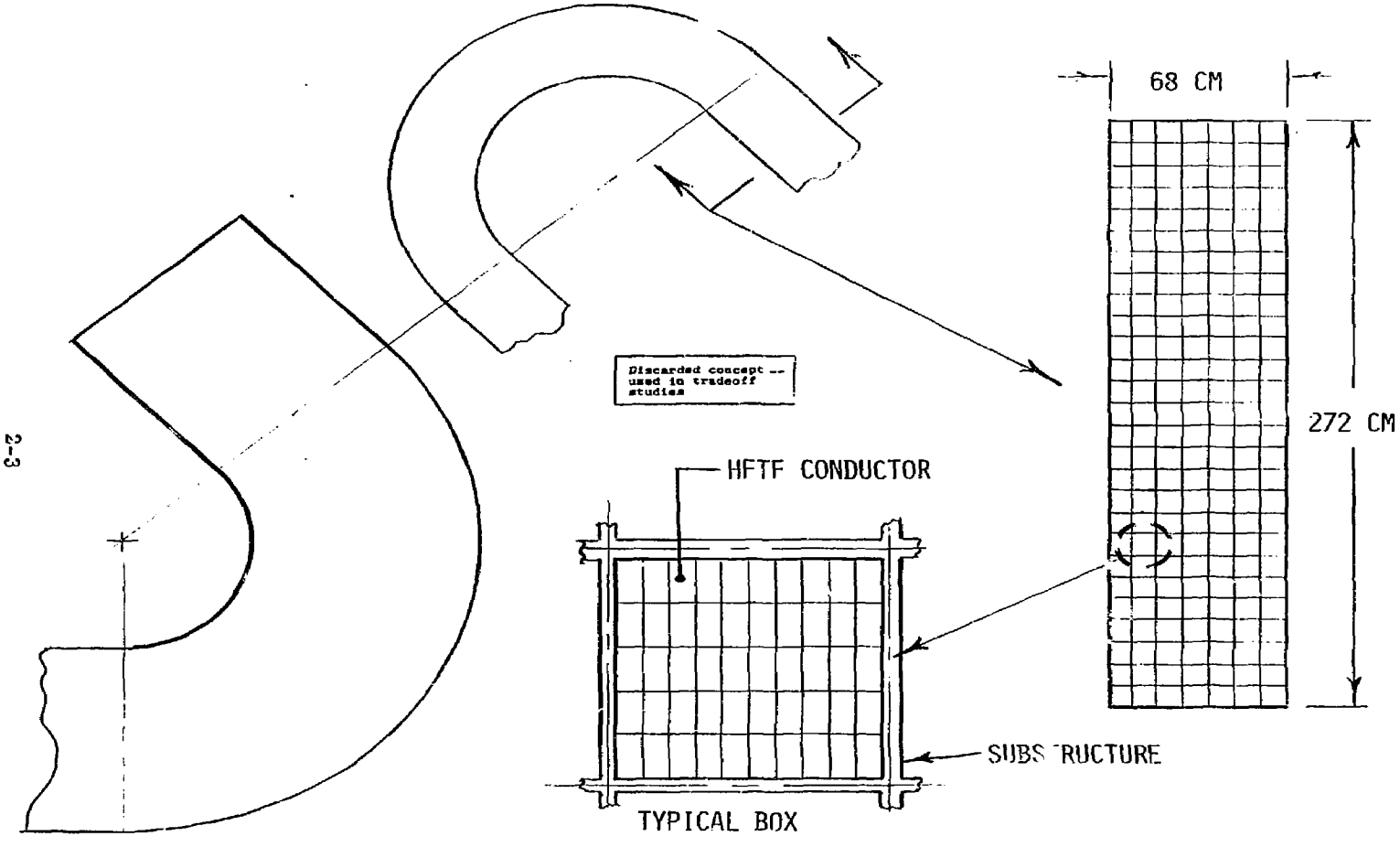

FIGURE 2.1-1 HFTF CONDUCTOR IN 7 x 27 BOX ARRAY

Before considering alternate conductors for the substructure box approach, it was felt that additional understanding of the substructure box concept was needed. Besides being able to react the magnetic pressures the concept must allow for sequential installation of the box sides and tops as the winding progresses. Our initial studies, which utilized 304LN material, focused on the arrangement shown in Figure 2.1-2. This concept was discarded because the tapered ends of the box walls caused distorted box shapes under unequal wall loading.

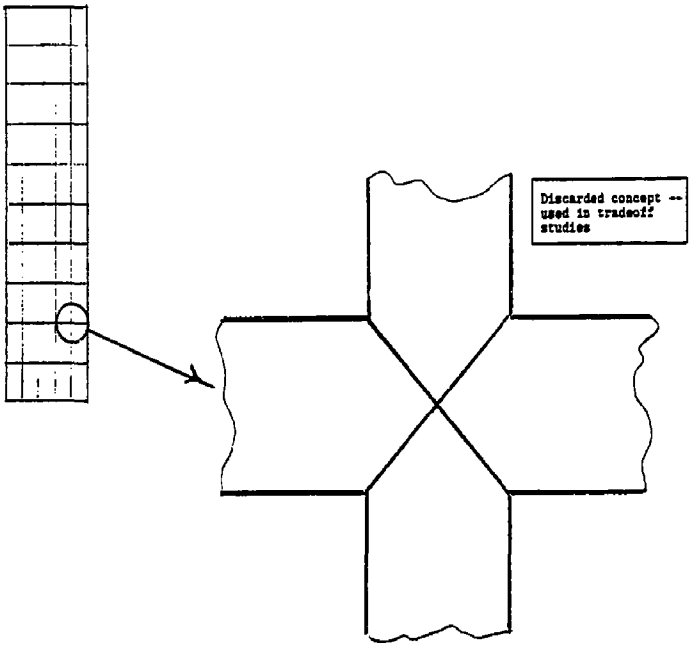

Figure 2.1-2 Symmetrical Box Wall Arrangement

Another concept considered is shown in Figure 2.1-3. This arrangement had the advantage of maintaining alignment under magnetic forces, but resulted in excessive bearing pressures on the vertical sides.

The most suitable box arrangement was the "swastika" concept shown in Figure 2.1-4. This arrangement provided equal bearing areas for all sides, and it can be installed sequentially to accommodate any normal winding arrangement. It should be pointed out that none of these arrangements require the use of welding at the box corners which eliminates a heat problem during assembly.

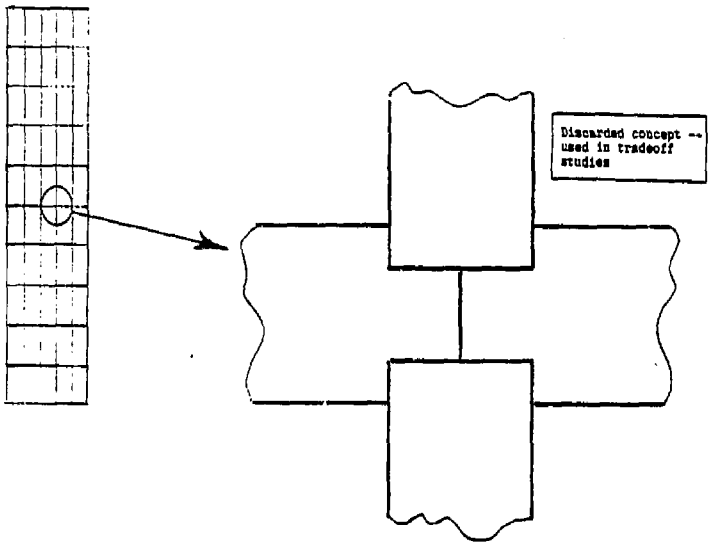

Figure 2.1-3 Unsymmetrical Box Wall Arrangement

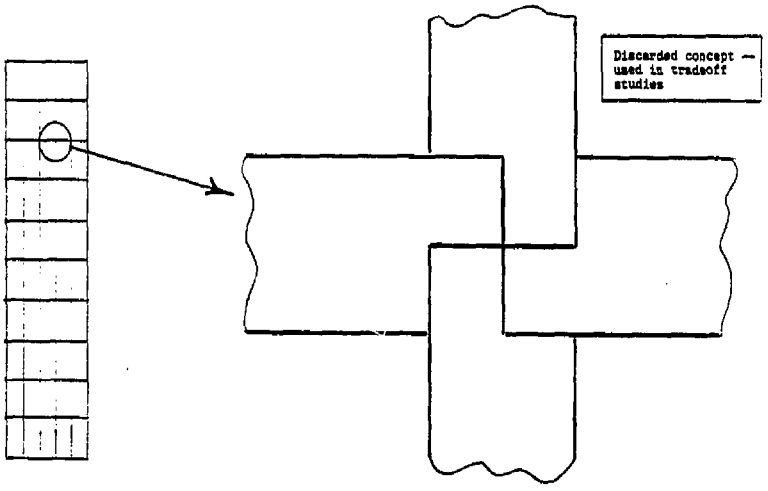

Figure 2.1-4 Swastika Box Wall Arrangement

None of the substructure box concepts considered here used bolts as structural members. It was felt that the use of bolts would:

- o weaken the box sides
- o not be able to react sufficient bending loads
- o not be effective in preventing internal motion
- o interfere with the winding of the conductor

For the above reasons the use of bolted substructure was dropped from further consideration.

2.1.4 Box/Conductor Arrangements

Having selected a candidate box arrangement the next step was to try specific conductors and box size arrangements. The conductor chosen was the scaled-up HFTF conductor which has already been presented. The following goals were established to direct our approach.

- o Only one grade of series wound conductor per box
- o Nested coils are to have equal numbers of boxes (turns) to balance approximately the stored energy
- o Box arrangements must allow for grading
- o Installation of substructure box sides must be compatible with the winding operation
- o The 68 x 272 cm envelope must be maintained.

One of the first arrangements tried using the scaled-up HFTF conductor and the "swastika" box substructure consisted of nine conductors wide by five high for a total of 45 turns. The inside box dimensions for this configuration are 12.72 cm wide x 12.8 cm high. With this configuration, no more than four boxes wide and 16 boxes high can fit into the 68 x 272 cm envelope and still leave room for the substructure. This 64-box arrangement did not allow the use of an equal number of boxes for 12-parallel conductors, but it came reasonably close. Figure 2.1-5 shows the arrangement along with the grading plan which allows 33 of the 64 boxes to use NbTi and 31 boxes to use Nb_3Sn. Any box in a nine Tesla field or less used a NbTi conductor. Nested boxes are shown in heavy outlines in all these arrangements.

This concept was discarded because it provided insufficient ampere-turns and it did not leave sufficient room for the substructure.

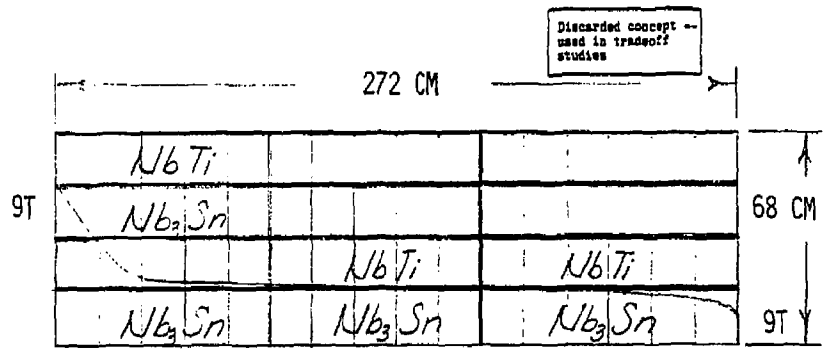

Figure 2.1-5 64-Box, 12 Nested Coil Arrangement

Another box arrangement tried, Figure 2.1-6, consisted of seven conductors wide by seven high to give a box inside dimension of 9.96 cm wide x 17.8 cm high. Since the vertical pressures are greater than the lateral ones, this arrangement tended to equalize the box forces in both the radial and transverse directions. This arrangement resulted in five boxes wide by 13 boxes high. It met the requirement and allowed 50% grading of NbTi. However, this concept was later discarded because of the structural deficiency of the box side plates.

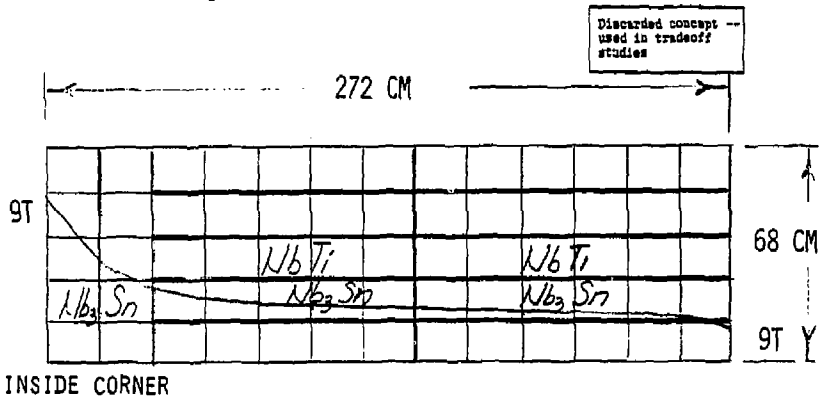

Figure 2.1-6 65-Box, 12 Nested Coil Arrangement

Since it became apparent that the strength of the box substructure was going to limit the box size, a smaller box arrangement was tried. For this concept (Figure 2.1-7) six conductors wide by four high was tried giving inside box dimensions of 8.58 cm wide by 10.3 cm high. Using six boxes wide by 20 high gave a total of 120 boxes. This arrangement met the field requirement and was compatible with using 12 parallel conductors, but it, too, was structurally inadequate when fitted into the given envelope.

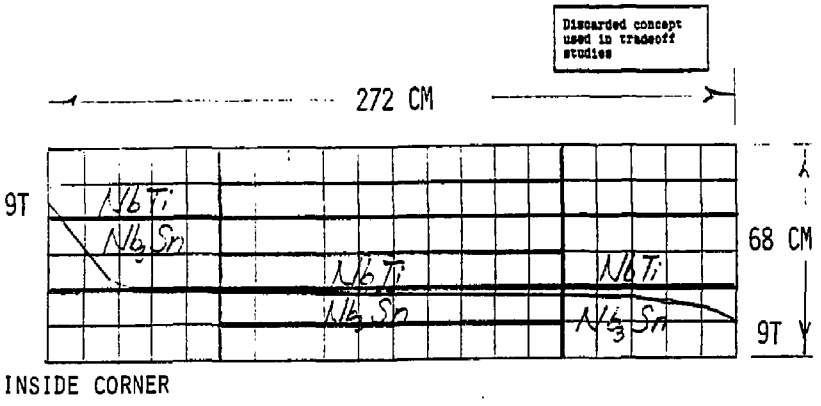

Figure 2.1-7 120-Box, 12 Nested Coil Arrangement

At this point, a check was made of the actual thicknesses of substructure required to withstand the magnetic pressures. Using the smallest box concept (six conductors wide by four high) the thicknesses in Table 2.1-I were calculated for the materials shown:

TABLE 2.1-I. Substructure Material Thickness for 120 Box Arrangement

MATERIAL	SIDE THICKNESS (IN)	TOP THICKNESS (IN)
304L	3.35	2.40
304LN	2.35	1.72
G-10CR	3.72	2.71

Although the metal thicknesses are smaller, they are misleading. Additional ground insulation would be required inside each box thus effectively making the assembly even larger. It was our conclusion that G-10CR was the logical choice for the substructure, but that any of the substructure materials results in overall box area which exceeds the allowable space in the given winding pack envelope. For example, using 304LN plus 1 cm of insulation results in a pack cross-sectional size of 95.7 cm by 321.4 cm which is 66% greater than the required envelope. Our final conclusion was that the use of an independent substructure results in inefficient use of available space, so the separate box substructure concept was completely discarded.

2.1.5 Cask 50 KA Conductor

Since a workable box arrangement was unobtainable, the idea of a scaled-up HFTF conductor was also dropped and alternate approaches were considered. One of these was the conductor proposed for the CASK Commercial Demo Plant (reference 1). This is a 50,000 ampere

conductor which has nine superconducting monoliths (in parallel) set in a copper substrate. Provision is made for regular transposition of the superconductors, as shown in figure 2.1-8. With such a large substrate, normal winding is not considered feasible. The Cask concept of electron-beam welding preformed substrate sections around the magnet and then placing and soldering the superconductors insitu was considered. This concept allowed five conductors across the width and 121 conductors high (alternatively 30 wide by 19 high) but it did not meet the field requirement due to the high aspect ratio of the substrate and the resulting inefficient use of insulation. In addition, the copper substrate was structurally inadequate in this application. The stresses in the reduced area in the region of the transposition groove located underneath the superconductors were excessive.

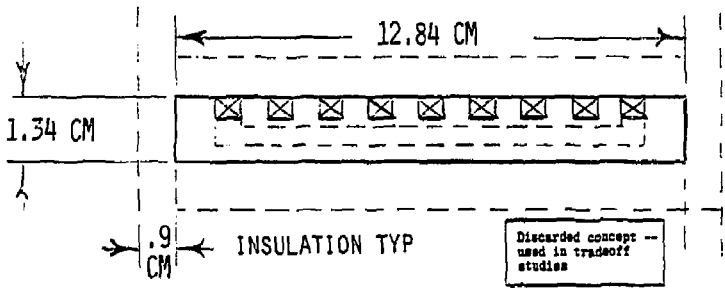

Figure 2.1-8 Cask 50KA Conductor

2.1.6 Cable Conductor In A Copper Substrate

The results of the analysis of the previous conductor hinted that we should seek a more compact substrate. This thought was pursued along with the idea of a circular cable for a superconductor. The cable was envisioned to be similar to a wire rope and thus relatively flexible. The substrate would be pre-formed into half-turns (i.e., in the shape of hair pins) and electron-beam welded to the existing windings; the superconductor would be placed in the groove in the substrate, the copper insert added and both would be soldered to the substrate insitu. This conductor is rated nominally at 50,000 A; it provides 14 turns wide by 56 turns high, it meets field requirements, and it can be graded to use about 36% Nb_3Sn. The basic conductor dimensions are shown in Figure 2.1-9.

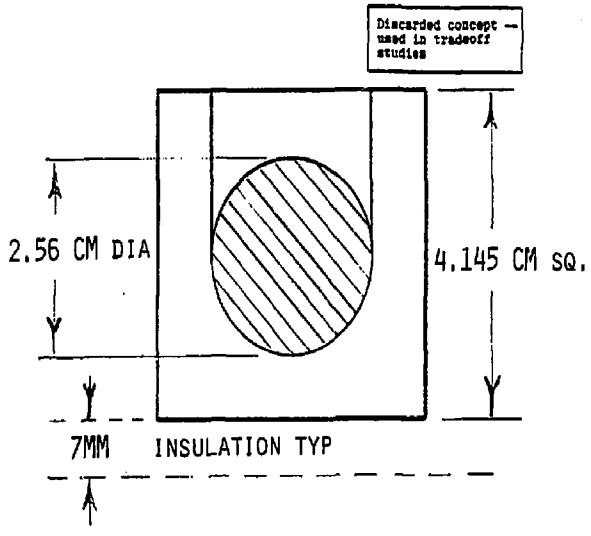

Figure 2.1-9 Cable Conductor In A Copper Substrate

The 1/2-hard copper substrate when filled with the soldered-in-place superconductor and insert can react the magnetic pressure generated in the pack. However, the superconducting cable could not be economically manufactured as a wire rope with separate strands and still have good solderability. An alternative would be to make the superconductor a monolith. Unfortunately, however, a monolith of this diameter (2.56 cm) would receive excessive bending strains (1.1%) during placement into the substrate; therefore, this approach also was discarded.

2.1.7 Conclusions

A review of our trade study activity points out the close interdisciplinary relationships required to reach a workable solution. Each proposed concept must run the gauntlet of the various disciplines, and, as shown here, many proved inadequate. For this study, it can be concluded that the use of a separate box substructure arrangement is inefficient in space utilization. Finally, it was concluded that the use of nested coils is preferable to the use of multiple parallel wound conductors.

2.2 CONDUCTOR/SUBSTRUCTURE STRESS ANALYSIS

2.2.1 Introduction

This section covers the stress analysis that was done to support the Trade-Study portion of the TMNS Design Study. The configurations of TMNS conductor pack examined were: 1) HFTF conductor with substructure, 2) HFTF scale-up conductor with substructure, 3) 50 KA conductor without substructure.

Of particular significance to the analysis of this section was the ground rule pertaining to the assumption of conductor axial strain. Even though a conductor axial strain of 0.1% was assumed, it was found that the configurations studied here did not provide conductor support that would insure that the axial strains remained below 0.1%. For this reason a study was done to evaluate the interaction effects between conductor pack and case and thus guide a selection of a case/substructure configuration which was most favorable from the standpoint of minimizing conductor axial strains. The stress analysis of this "selected configuration" is given in Section 3.2.

2.2.2 Design Criteria and Material Properties

Design Criteria

The following design criteria was established for use during the TMNS Design Study. These criteria are based on those used on other magnet programs such as MFTF-A and MFTF-B together with the strain criteria for the Nb_3Sn superconductor.

- Conductor

  Yield F.S. = 1.50
  4K Material Properties Used
  VonMises Equation Used for Combined Stresses
  Maximum Integrated Strain for Nb_3Sn < 0.4% Prior to Operation
  Ideal Integrated Strain During Operation -0.4% to 0.0%

- Substructure/Case

  Yield F.S. = 1.5
  Ultimate F.S. = 3.0
  Primary Bending Allowable = 1.5 × Tension Allowable
  4K Material Properties Used

Material Properties

The properties for the materials used in the TMNS Design Study are given in Table 2.2-I. The stress-strain curves established for the HFTF superconductor and 1/2 H copper were used for the TMNS analysis. These are shown in Figure 2.2-1.

Table 2.2-I

Materials Properties for TMNS Materials

MATERIAL	MODULUS-MSI		YIELD-KSI		ULTIMATE-KSI		CTE (RT-4K) 10^{-6}/ K
	RT	1.8K	RT	1.8K	RT	1.8K	
COPPER							
1/2 HARD	17.	18.	32.	42.			11.2
304 L CRES	29.	32.	30.	65.	70.	170.	10.6
304 LN CRES	28.	30.	35.	100.	80.	170.	10.6
G-10 CR F/G							
WARP	4.3	5.0			60.	125.	8.1
FILL	3.9	4.8			43.	78.	9.2
NORMAL	2.0	3.2			61.(1)	109.(1)	25.2

HFTF CORE - STRESS STRAIN CURVE GIVEN ON FOLLOWING PAGE

(1) COMPRESSION ALLOWABLE

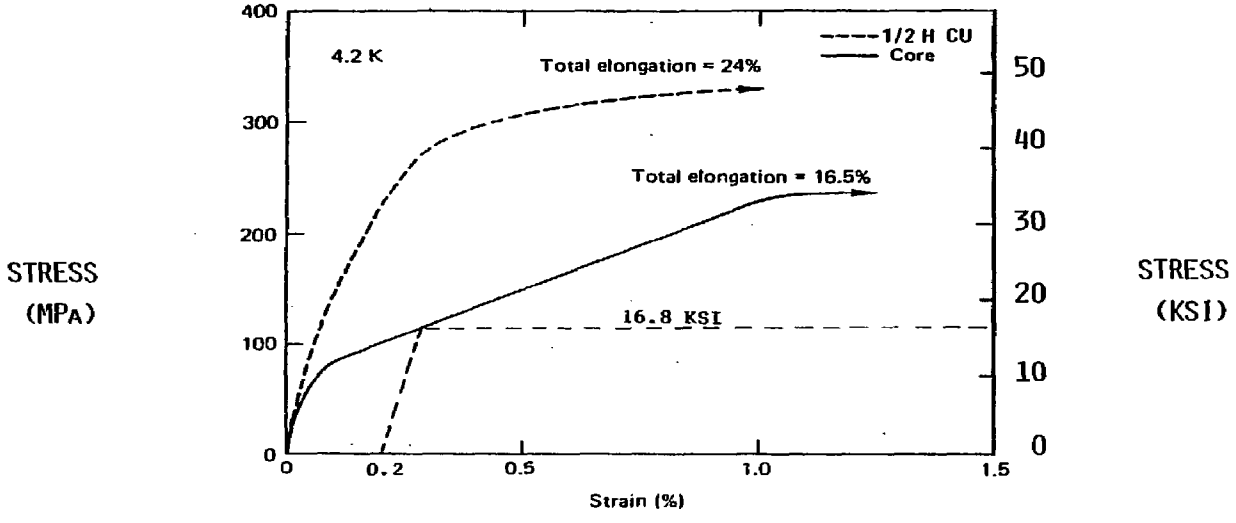

REF. - UCRL - 84040, FIG. 5, LAWRENCE LIVERMORE LABORATORY, 23 MAY 1980.

Figure 2.2-1. HFTF Conductor Properties at 4.2K

2.2.3 Magnetic Loads

The TMNS magnetic fields and conductor pack pressures were calculated by LLNL (Reference 2). The results were given at only the mid-plane of the major axis and the mid-plane of the minor axis. For the purpose of this analysis it was assumed that these fields and pressures remained constant throughout the sweep of the major and the minor axes. Furthermore, it was assumed that the plot of pressures in the long dimension direction of the pack is constant from side to side and is equal to the plot through the maximum pressure. The same was assumed for the pressures in the short dimension direction of the pack. With these assumptions the total pressure configuration can be represented by the curves given in Figures 2.2-2 and 2.2-3.

2.2.4 Analysis Assumptions

The following assumptions were used for the stress analysis during the Trade Study portion of the TMNS Design Study.

1) The axial loads in the case were assumed to be of a magnitude which would cause 0.1% axial strain in the case.

2) The conductor pack pressures can be represented by the maximums given by Figures 2.2-2 and 2.2-3.

3) The material properties at 1.8K were assumed to be the same as those at 4.2K.

2.2.5 HFTF Conductor Configuration With Substructure

The HFTF conductor was the first configuration considered in the TMNS Design Study. This configuration used the HFTF conductor in a substructure arrangement in which the coil pack was divided into seven substructure boxes wide by 27 boxes high with 5 by 10 conductors per box. It follows that the accumulation of pressures on the conductors is obtained by segmenting the coil pressure plots into 27 divisions in the long direction and 7 divisions in the width direction.

The maximum pressure which can build up within one box division occurs at the steepest portion of the coil pressure plot and is shown in Figure 2.2-4. The number of substructure boxes was set so that these pressures could be tolerated with an insulation footprint requirement of no more than 50%.

Only the insulation footprint requirements were calculated for this configuration before it was abandoned because of problems with quench voltages and temperatures.

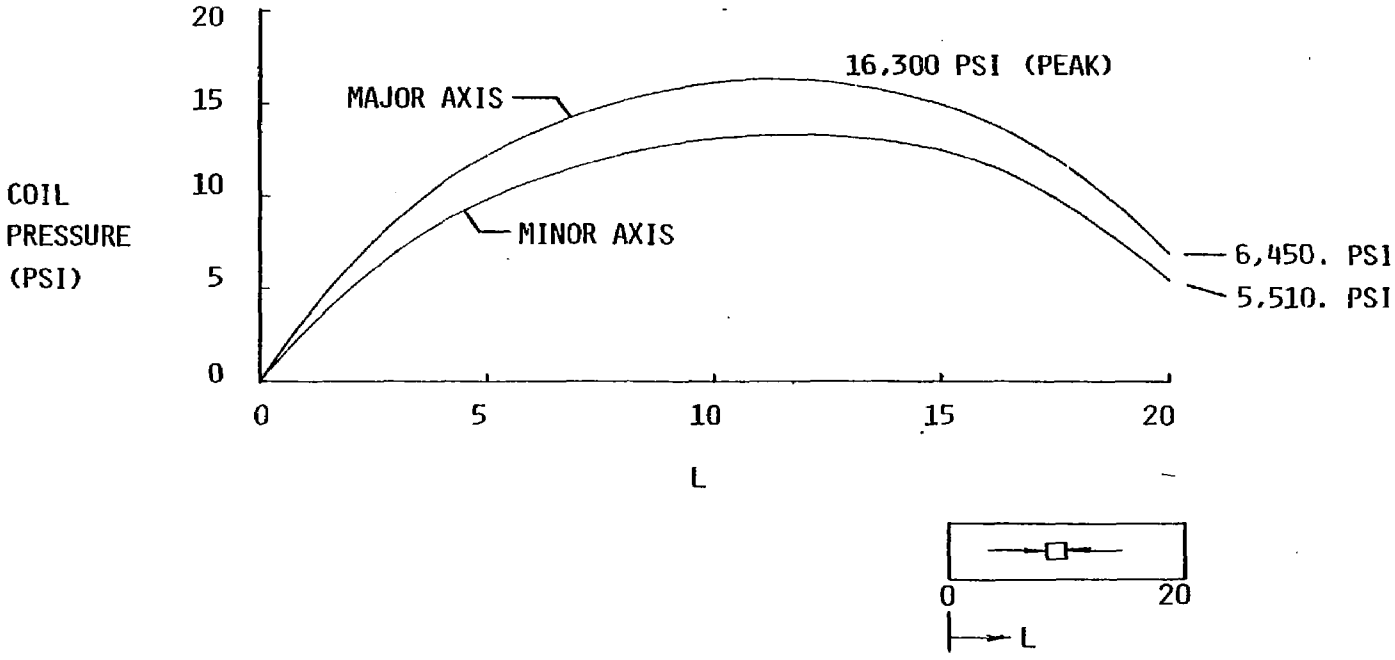

Figure 2.2-2. TMNS Design Study Coil Pack Longitudinal Pressure

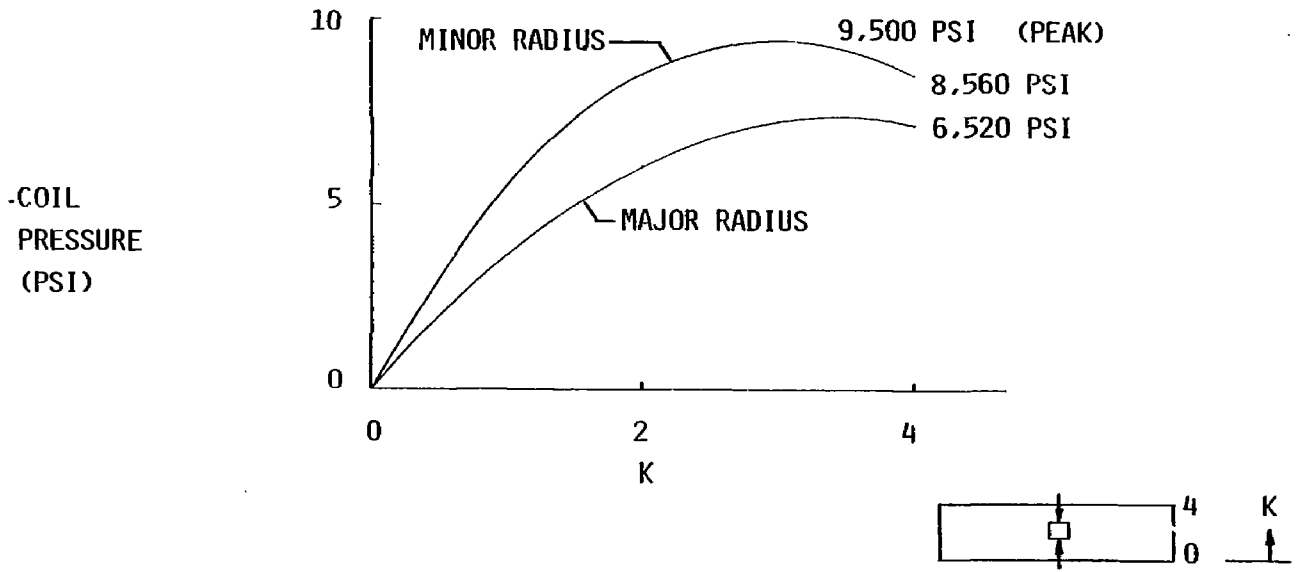

Figure 2.2-3. TMNS Design Study Coil Pack Width Pressure

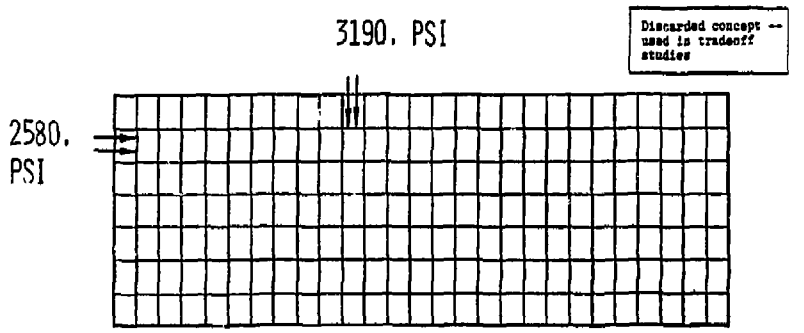

Figure 2.2-4. Substructure Maximum Member Lateral Pressure for the HFTF Conductor Configuration

Insulation Footprint Requirements

$$A\% = \frac{\text{Box Width (Height)}}{\text{No. Conductors} \times \text{Conductor Width (Height)}}$$

$$X \frac{\text{Box Press.}}{F_{allow}\ \text{(Conductor or Insul.)}} X\ 100$$

The results of these calculations for this configuration and for the HFTF Scale-up configuration given in Section 2.2.6 are shown in Table 2-2-II.

2.2.6 HFTF Scale-up Conductor Configuration With Substructure

The HFTF Scale-up conductor with substructure was the second configuration considered in the TMNS Design Study. This configuration used the HFTF type conductor with the conductor set as large as possible within the limits of the maximum allowable peak winding strains.

Maximum Allowable Winding Strain

$$\epsilon \leq \frac{1}{2}\ (0.8\%) = 0.4\%$$

$$\epsilon = \frac{1/2\ \text{(Conductor Width or Height)}}{\text{Winding Radius}}$$

Table 2.2-II. Conductor and Insulation Footprint Requirements for the HFTF and HFTF Scale-up Conductor Configurations

	HFTF (7 X 27 BOXES)		HFTF SCALE-UP (6 X 20 BOXES)	
	WIDTH	HEIGHT	WIDTH	HEIGHT
BOX DIMENSIONS	3.824 IN	3.966 IN	4.461 IN	5.354 IN
CONDUCTORS IN BOX	10	5	6	4
CONDUCTOR DIMENSIONS	0.213 IN	0.433 IN	0.416 IN	0.866 IN
PRESS. ON BOX	2580. PSI	3190. PSI	3480. PSI	4000. PSI
PRESS. ON CONDUCTOR	4632. PSI	5844. PSI	6220. PSI	6182. PSI
FOOTPRINT REQUIREMENT				
CONDUCTOR	41.3%	52.1%	55.5%	55.1%
INSULATION	17.0%	21.5%	22.8%	22.7%

The HFTF Scale-up size conductor exhibited winding strains which were slightly higher than the 0.4% but was selected on the basis that it was a convenient two times HFTF size.

This configuration used a substructure arrangement in which the coil pack was divided into six boxes wide by 20 boxes high with 4 by 6 conductors per box. The accumulation of pressures on the conductors is obtained by segmenting the coil pressure plots into 20 divisions in the long direction and 6 divisions in the width direction. The maximum pressure which can build up within one box division is shown in Figure 2.2-4.

Insulation Footprint Requirement

The calculation of insulation footprint requirement was given in Section 2.2.5 and the results are given in Table 2.2-II.

Substructure Thickness Requirement

The pressures given in Figure 2.2-5 are the pressures which cause the substructure member bending. Note that it was assumed that the 4,000 psi has no variation along the length and that the 3480 psi has no variation across the width.

The loads which cause compression in the substructure members are taken directly from the coil pressure plots. These are a maximum of 16,300 psi for the longitudinal members and 9,500 psi for the lateral members.

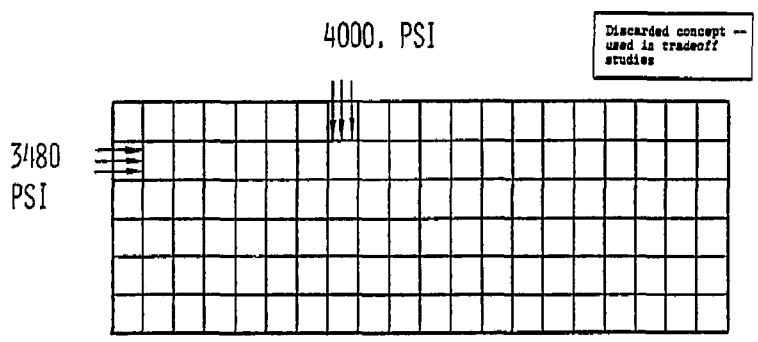

Figure 2.2-5. Substructure Maximum Member Lateral Pressure for the HFTF Scale-up Conductor Configuration

The maximum loads on the substructure members are summarized as follows:

Member	Max. Compression	Max. Moment
Lateral	50,866 lb	6,718 in-lb
Longitudinal	72,725 lb	11,660 in-lb

These loads were calculated from the following with an assumed 2 inch member thickness.

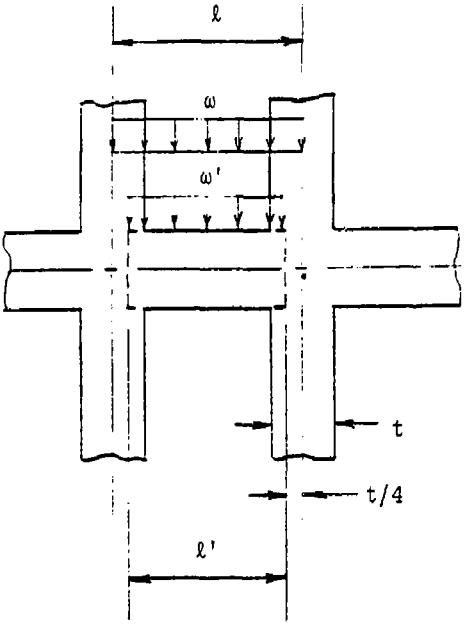

ℓ = Substructure Box Pitch

ω = Press. for Each Box

t = Substructure Thickness

ℓ' = Effective Beam Length

ω' = Effective Beam Pressure

ℓ' = ℓ - (t/2)

ω' = ω (ℓ/ℓ')

t = 2. in. First Try Thickness

Maximum Comp. = p_{coil} (ℓ) Maximum Moment = $\frac{\omega' \ell^2}{8}$

Member	ℓ	ω	t	ℓ	ω'	p_{coil}
Lateral	4.462"	3480 psi	2"	3.462"	4485 psi	9,500 psi
Longitudinal	5.355"	4000 psi	2"	4.355"	4918 psi	16,300 psi

The substructure members were sized for 304L Cres, G10-CR Fiberglass, and 304 LN Cres. The following equation was used to determine the maximum allowable combined compression and bending stresses.

$$\frac{f_c}{F_c} + \frac{f_b}{F_b} \leq 1.0$$

where:

f_c = calculated compressive stress

F_c = allowable compressive stress ($F_c = F_t$ assumed)

f_b = calculated bending stress

F_b = allowable bending stress ($F_b = 1.5\ F_t$)

304L Substructure

For 304L at 4K

$F_{ty} = 65$ ksi

$F_c = 43.3$ ksi

$F_b = 65$

Lateral Members

$$\frac{50,866}{t\ (43,300)} + \frac{6,719\ (6)}{t^2\ (65,000)} = 1$$

$t = 1.56$ in. $\Rightarrow 2.40$ in. for 35% ventilation

Longitudinal Members

$$\frac{72,725}{t\ (43,300)} + \frac{11,660\ (6)}{t^2\ (65,000)} = 1$$

$t = 2.18$ in. $\Rightarrow$ 3.35 in. for 35% ventilation

G-10CR Substructure

For G-10CR at 4K

$F_{tu} = 125$ ksi

$F_c = 41.7$ ksi

$F_b = 41.7$ ksi ($F_b \neq 1.5\ F_t$ for G-10CR)

Lateral Members

$$41.7 \text{ ksi} = \frac{50,866}{t} + \frac{6719}{t^2} \cdot 6$$

$t = 1.76$ in. $\Rightarrow$ 2.71 in. for 35% ventilation

Longitudinal Members

$$41.7 \text{ ksi} = \frac{72,725}{t} + \frac{11,660}{t^2} \cdot 6$$

$t = 2.42$ in. $\Rightarrow$ 3.72 in. for 35% ventilation

304LN Substructure

For 304LN at 4K

$$F_{ty} = 100 \text{ ksi}$$

$$F_c = 66.7 \text{ ksi}$$

$$F_b = 100 \text{ ksi}$$

Lateral Members

$$\frac{50,866}{t\ (66,700)} + \frac{6719\ (6)}{t^2\ (100,000)} = 1$$

$t = 1.12 \Rightarrow 1.72$ for 35% ventilation

Longitudinal Members

$$\frac{72,725}{t\ (66,700)} + \frac{11,660\ (6)}{t^2\ (100,000)} = 1$$

$t = 1.53 \Rightarrow 2.35$ for 35% ventilation

The plots in Figure 2.2-6 were constructed in an effort to evaluate the substructure thickness requirements as compared to the thickness requirement at the maximum compression plus maximum moment location. The thickness required for each load component alone (i.e., compression or bending) was normalized to the thickness required where the load component is maximum. These ratios were plotted as a function of the location across the coil cross-section (K and L as defined by Figure 2.2-2 and 2.2-3).

If these curves can be visualized as a topographical map then the following is noted.

1) The longitudinal members will have the minimum thickness requirements in the corners near K = 4, L = 0 and K = 4, L = 20.

2) The lateral members will have the minimum thickness requirements near K = 0, L = 11.

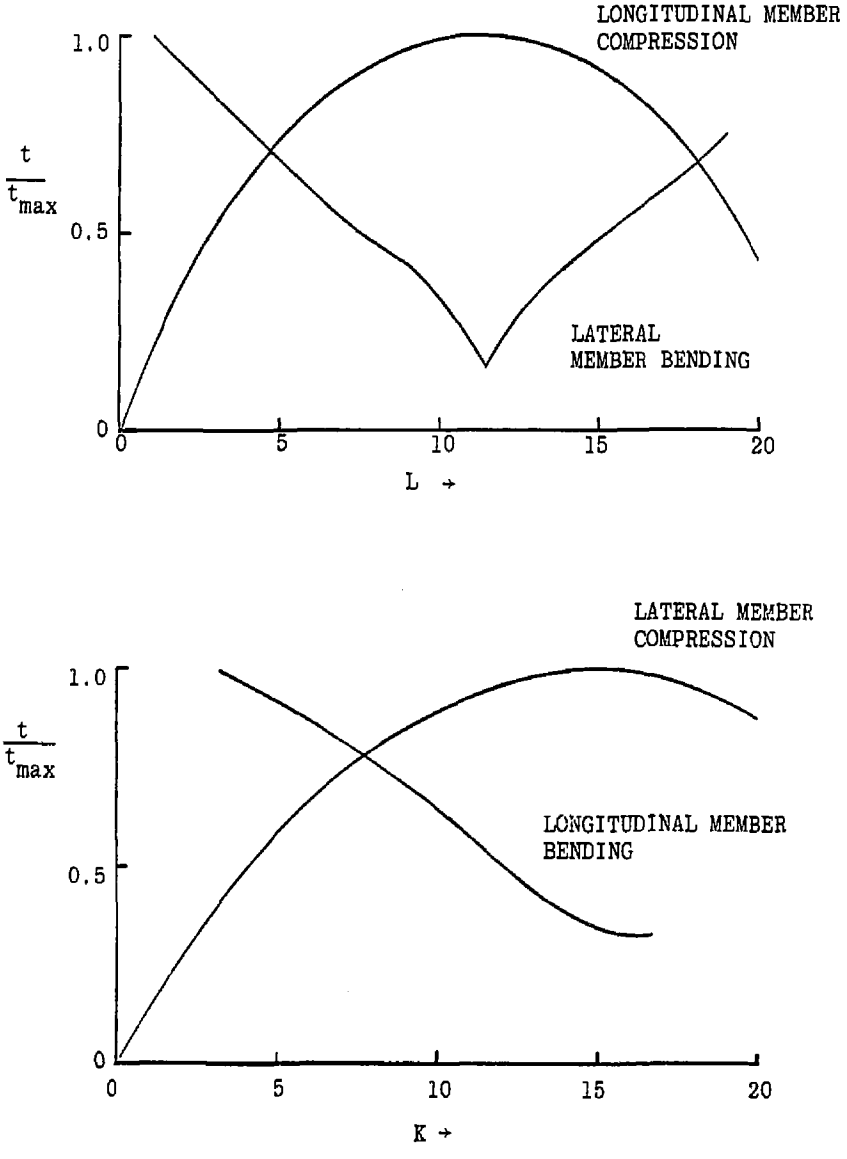

Figure 2.2-6. Substructure Bending and Compression Requirement for HFTF Scale-up Conductor Configuration

It is seen from this that substructure grading would be asymmetrical. It is also noted that any thinning of the substructure below the initially assumed 2.0 inch thickness would increase the effective beam length and thus the thickness of the perpendicular members.

2.2.7 50 KA Conductor Configuration - No Substructure

This was the third configuration considered in the TMNS Design Study. The objective of this design was to 1) make the conductor as large as practical and 2) eliminate the substructure. Objective number 1 was accomplished by the use of a cabled superconductor which is installed in-situ thereby eliminating the winding strains and thus removing the size constraint. Objective number 2 was accomplished by the use of a 1/2 H copper stabilizer which would have adequate strength to carry the full conductor pack crushing pressures.

The selected configuration for the 50 KA conductor together with the G10-CR insulation and the compressive loads are shown in Figure 2.2-7.

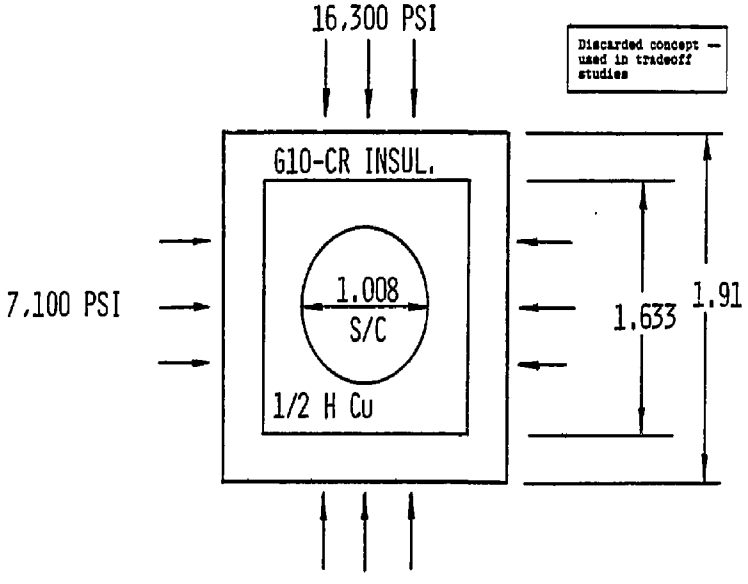

Figure 2.2-7. 50 KA Conductor and Insulation Cross-Section With Maximum Compressive Loads

Conductor Stresses

The composite modulus of elasticity for the conductor in the width direction was calculated with the superconductor assumed to be 65% copper and 35% solder. By the law of mixtures:

$$E\ (S/C) = \frac{65\%\ (E\ Cu) + 35\%\ (E\ Solder)}{100\%}$$

$$= \frac{0.65\ (17 \times 10^6\ psi) + 0.35\ (4 \times 10^6\ psi)}{1.00}$$

$$= 12.45 \times 10^6\ psi$$

The equivalent modulus for the total conductor cross-section is

$$E_{TOT} = \frac{(12.45 \times 10^6)\ (1.008) + (17 \times 10^6)\ (0.625)}{1.633}$$

$$= 14.19 \times 10^6\ psi$$

The strain and then the stresses in the height direction are calculated by

$$\varepsilon(height) = \frac{16{,}300\ (1.91/1.633)}{14.19 \times 10^6}\ in/in$$

$$= 0.00134\ in/in$$

$$f(cu) = 22.81\ ksi \qquad f\ (s/c) = 16.71\ ksi$$

Likewise for the width direction

$$\varepsilon(width) = 0.000586\ in/in$$

$$f(cu) = 9.94\ ksi \qquad f\ (s/c) = 7.28\ ksi$$

At point A where f (cu) = 22.81 ksi (height)

$$f(cu) = 7100\ (1.912/1.633)$$

$$= 8{,}325\ psi\ (width)$$

The stress and strain in the axial direction is 0.1% and 17,000 psi by assumption.

The VonMises stress in the copper is then

$$f_{V.M.} = \frac{1}{\sqrt{2}} \left[(17.0 + 22.81)^2 + (22.81 - 8.33)^2 + (8.33 + 17.0)^2 \right]^{1/2}$$

$$= 34.9 \text{ ksi} \leftarrow \text{too high}$$

If the axial stress in the conductor was limited to 10 ksi, then

$$f_{V.M.} = 28.5 \text{ ksi}$$

The superconductor strain would be

$$\langle \varepsilon \rangle = \frac{1}{\sqrt{2}\ (1+\nu)} \left[(0.059 + 0.134)^2 + (0.134 - 0.059)^2 + (0.059 + 0.059)^2 \right]^{1/2}$$

$$= 0.127\%$$

This configuration was abandoned when it was learned that it would be difficult to produce a Nb_3Sn cable with good solderability. A monolith was considered but produced prohibitively high strains during winding for this large of a conductor.

Insulation Footprint Requirement

The footprint requirements for the conductor and insulation are found by the equation of Section 2.2.5. These are:

Conductor	58%
Insulation	55%

Free-Standing Conductor Hoop Loads

Figure 2.2-8 shows the plot for the By vector component of the magnetic field in the minor radius area of the magnet. This is the component of the field which creates the radial load (P_r) and thereby the hoop load in the conductor pack. The calculations determined the average tensile stress in the conductor pack due to this magnetic field if no radial support is provided by the magnet case (free standing conductor pack). These stresses are excessive for a 1/2 H copper conductor.

2.2.8 Conclusions

The conductor pack arrangements with internal segmented substructure or no substructure do not provide adequate conductor axial strain control.

The internal segmented substructure has inefficient use of structural materials.

2.3 MATERIALS

The effects of He II environment on the properties of materials were evaluated and materials were selected to support the conceptual design of the TMNS magnet.

2.3.1 Effect of Helium II Environment on Materials

On the basis of a literature search and telephone conversations with the technical people engaged in He II research, no detrimental effects on the mechanical properties of materials like 304LN CRES stainless steel, OFHC copper, aluminum, G-10CR, etc., are anticipated in the He II environment as compared to normal liquid helium environment. Additionally, there are no surprises in the thermophysical properties of materials.

2.3.2 Criteria for Material Selection

Many criteria must be considered when selecting a material for use at cryogenic temperatures. A number of these are listed in Table 2.3-I. Of uppermost importance in this application and the ones that were the limiting factors were cost, cryogenic strength and toughness, availability, and fabricability.

Following the precedents set by previous magnet programs, the guidelines listed below were established for material selection.

- Excellent mechanical and physical properties at room and cryogenic temperatures.
- High degree of fabricability and producibility.
- Large data base and ASME specification coverage.
- Reliability established by service history.
- Proven fabrication methods and processes.
- Availability in required sizes and shapes.
- Previous design and fabrication experience.

The following materials were selected for the TMNS magnet.

Superconductor — Nb_3Sn and NbTi

Stabilizer — CDA10100 copper — 1/2 hard

Solder — PbSn eutectic and indium

Electrical Insulation — G-10CR fiberglass/epoxy

Structure — 304LN CRES stainless steel

Table 2.3-I. Criteria Considered During Material Selection Process.

Mechanical	Physical	Chemical	Metallurgical	Fabrication	Misc.
Tensile	Thermal Conductivity	Composition	Microstructure	Machining & Grinding	Cost
Compressive	Thermal Diffusion	Compatibility	Response to Thermal/ Mechanical Treatments	Forming	Availability
Shear & Torsion	Thermal Expansion	Corrosion Resistance		Welding Bonding	Tolerances Toxicity
Bearing	Specific Heat	Oxidation Resistance	Phase Diagrams	Brazing	Specifications
Fatigue	Emissivity	Stability		Surface Treatment	Design Allowables
Creep	Density				
Ductility	Coefficient of Friction				Service Data
Toughness	Electric, Magnetic, & Nuclear Properties				
Stress-Strain Cruve					
Hardness					

Superconductor — Nb_3Sn and NbTi

Based on reliability, proven fabrication methods and processes, availability in required sizes and shapes and cost, Nb_3Sn is the choice superconductor for higher magnetic field (9-12T) applications and NbTi for magnetic field applications below 9T.

Electrical Insulation — G-10CR Fiberglass/Epoxy Laminate

Selection of G-10CR fiberglass/epoxy is based on materials porosity to helium, tolerance to the operating voltages, and ability to transmit the compressive conductor loads. Table 2.3-II shows some mechanical properties of G-10CR laminate.

Table 2.3-II. Mechanical Properties of G-10CR Laminate

Properties	No. of Laminate	R.T.	20°K
Tensile			
Ultimate strength, ksi	12	47.3	95.1
Initial modulus, 10^6psi	12	3.38	4.0
Secondary modulus, 10^6psi	12	2.60	2.34
Edgewise compression			
Ultimate strength, ksi	6	56.8	115.9
Elastic modulus, 10^6psi	6	3.87	4.53
Flexural			
Ultimate strength, ksi	5	83.5	155.3
Elastic modulus, 10^6psi	5	3.89	4.82

Structure — Type 304LN CRES Stainless Steel

Type 304LN stainless steel is a low carbon, high nitrogen/ chromium-nickel corrosion resistant steel which in the annealed condition, possesses an austenitic face-centered cubic structure having low magnetic permeability and freedom from grain boundary carbide precipitation during welding. Of the available 300 series corrosion resistant steels, type 304LN possesses the best combination of mechanical and physical properties, fabricability, and availability in various forms and sizes and has a large data base and service reliability in cryogenic applications. Figure 2.3-1 shows the variation of low temperature yield strength of 304L stainless steel with N2 content and Figure 2.3-2 shows the strength and fracture toughness of 304LN stainless steel.

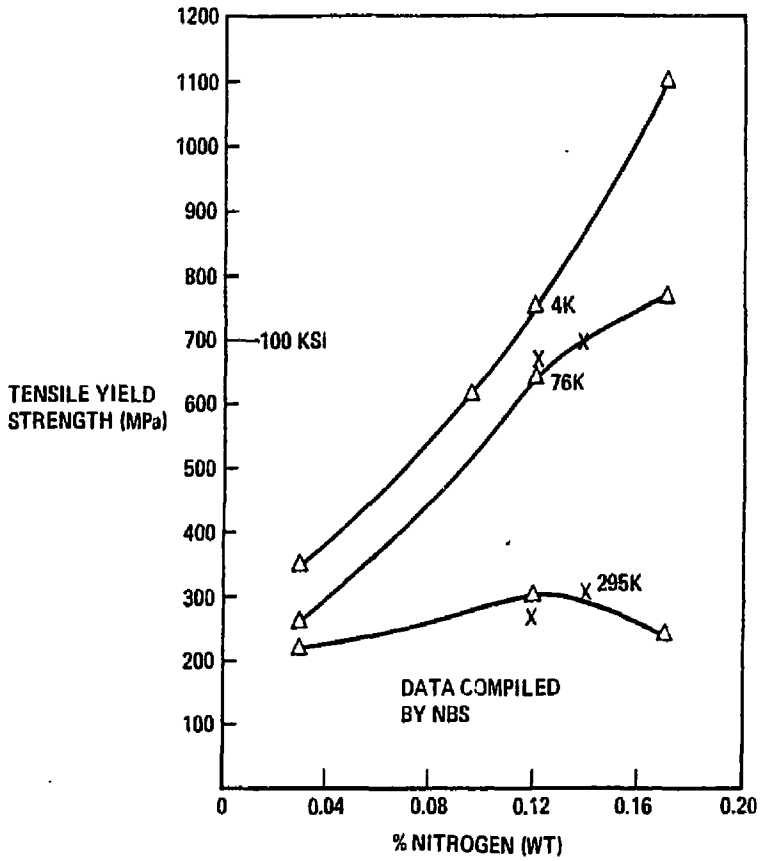

07078474J5320

Figure 2.3-1. Low Temperature Yield Strength of Type 304L Stainless Steel is Dependent on N_2 Content.

2.4 ELECTROMAGNETIC ANALYSIS

In this section, the results of our calculations on the adiabatic temperature rise of the conductor during an emergency dump are presented. These calculations were performed using GDC's computer program SUPERQ. A brief description of SUPERQ is given in Appendix D.

2.4.1 Introduction

One of the most important parameters that must be considered in the event of an emergency discharge of a superconducting magnet is the temperature rise of the conductor. If the temperature excursion is too large, it may result in a high stress level in the conductor and causing the superconductor to be strained above its elastic limit, and thus degrading the current-carrying capabilities of the conductor. To keep the conductor temperature low during a dump, one would like to reduce the current and, hence, the stored energy in the magnet as quickly as possible. However, there is a limit to how fast one can reduce the current, since larger inductive potentials are generated the more quickly the current is reduced. Hence, the time constant of an emergency dump is always a compromise determined by the conflicting requirements of dump voltage and conductor temperature rise.

For the calculations reported herein, we found that in most cases it was necessary to consider the magnet as consisting of several nested magnets, each operating with its own power supply. This reduces the conductor temperature, for a given dump voltage, since we assume the total stored energy of the magnet is shared equally by all the nested magnets. The restrictions we worked within were to limit the dump voltage to a maximum of 1000 V and the conductor temperature to a value not greater than 250K.

2.4.2 HFTF Conductor

Table 2.4-I gives some of the pertinent parameters of those conductors, the temperatures of which have been calculated. The initial concept considered was the HFTF conductor. The cases tried, listed in Table 2.4-I, show that even when using 20 or more coils in parallel, the conductor temperature was still too high, i.e., greater than 500K.

2.4.3 HFTF Scale-up

The next attempt scaled up the HFTF core, roughly doubling the linear dimensions. As can be seen from Table 2.4-I, that case where the current was 10,000 A and there were 10 nested coils, the temperature rose to 294K. Using 11 parallel coils dropped the conductor temperature to 244K, within the self-imposed limit of 250K. When a current of 12,866 A was used, the decay time

Table 2.4-I. Summary of Pertinent Parameters for Various Coil and Conductor Configurations Calculated by SUPERQ

E (MJ)	No. of Parallel Coils	I_o (A)	V_d (V)	J_o (A/cm^2)	Cu/Sc Ratio	τ (Sec)	T_{max} (K)
			HFTF Coil				
500	10	4,000	1,000	4,050	5.0	250	503
454.5	11	4,000	1,000	4,050	5.0	227	503
416.7	12	4,000	1,000	4,050	5.0	208	503
384.6	13	4,000	1,000	4,050	5.0	192	503
333.3	15	4,000	1,000	4,050	5.0	167	503
250	20	4,000	1,000	4,050	5.0	125	503
200	25	4,000	1,000	4,050	5.0	100	503
500	10	4,000	1,000	3,015	6.0	250	503
			Scale-Up HFTF Coil				
500	10	10,000	1,000	3,198	4.8	100	294
454.5	11	10,000	1,000	3,198	4.8	91	244
500	10	12,866	1,000	3,397	3.5	78	503
500	10	12,866	1,000	3,016	3.5	78	503
500	10	12,866	1,000	3,858	3.5	78	503
500	10	12,866	1,000	3,528	3.5	78	503
			50,000 A Conductor				
5000	-	50,000	1,000	2,411	8.1	200	173
			Alternate Conductor				
5000	-	13,000	1,000	2,039	9.0	769	503
2500	2	13,000	1,000	2,039	9.0	385	495
1666.7	3	13,000	1,000	2,039	10.0	256	220
1250	4	13,000	1,000	2,041	10,0	192	153
1000	5	13,000	1,000	2,039	9.0	154	122
416.7	12	13,000	1,000	2,039	9.0	64	68
			Miscellaneous				
5000	-	5,000	1,000	2,000	20.0	2000	500
5000	-	5,000	5,000	2,000	20.0	400	500
5000	-	5,000	6,000	2,000	20.0	333	500
5000	-	5,000	6,500	2,000	20.0	308	456
5000	-	5,000	7,000	2,000	20.0	286	382
5000	-	5,000	10,000	2,000	20.0	200	197
5000	-	35,000	1,000	2,034	7.3	286	503
5000	-	35,000	2,000	2,034	7.3	143	180

constant decreased and the temperature rose above 500K, assuming 10 nested coils.

2.4.4 Cask CDP

Also considered was a CASK CDP type conductor carrying nominally 50,000 A. In this case, the conductor temperature rise is moderate, reaching a maximum of 173K. This conductor contains more copper than the previous conductors and, hence, eliminates the need to use nested coils.

2.4.5 50KA and Alternative Conductor Approaches

Also listed in Table 2.4-I are several miscellaneous conductors that were evaluated. For the 5000-A conductor, an iteration procedure was undertaken to determine what dump voltage would be required to keep the conductor temperature below our maximum of 250K. As can be seen in Table 2.4-I, the dump voltage had to be increased to about 10KV to get the temperature below 200K. Also, for the 35KA conductor, the dump voltage had to be doubled to 2KV to obtain temperatures below 200K.

2.4.6 Conclusion

The alternate conductors listed in Table 2.4-I represent a viable candidate for the next design iteration. This conductor employs about 13 KA and has a temperature rise of 220K if three nested coils are used to limit the stored energy discharged through the coil.

2.5 THERMODYNAMIC ANALYSIS

2.5.1 Introduction

The basic thermodynamic criteria for any conductor concept considered during the course of this study was that it should be unconditionally stable during steady-state operation in helium II at 1.2 atmospheres and 1.8K. Using a method outlined by Hoard (Reference 3), the amount of insulation required to just meet the unconditional stability requirements could be determined for given operating and design parameters. By manipulation of Hoard's equations, this is expressed mathematically by the following two equations:

$$\frac{I_o^2 \rho / A_{cu}}{n_h\left[1 + \left(\frac{af_v}{bf_h}\right)\left(\frac{L_H}{L_v}\right)^{1/3}\right]} \leq \frac{7.4}{L_H^{1/3}} bf_h \qquad \text{for horizontal channels} \qquad (1)$$

$$\frac{I_o^2 \rho / A_{cu}}{n_v\left[1 + \left(\frac{bf_h}{af_v}\right)\left(\frac{L_v}{L_H}\right)^{1/3}\right]} \leq \frac{7.4}{L_v^{1/3}} af_v \qquad \text{for vertical channels} \qquad (2)$$

Where

I_o = operating current - amps

ρ = effective copper resistivity - Ω-cm

A_{cu} = effective area of copper stabilizer cm^2

n_h = number of horizontal cooling channels — generally a total of four for rectangular conductors

n_v = number of vertical cooling channels — generally a total of four for rectangular conductors

a = side insulation thickness — cm (see Figure 2.5-1)

b = top, bottom insulation thickness — cm (see Figure 2.5-1)

x = conductor height — cm (see Figure 2.5-1)

y = conductor width — cm (see Figure 2.5-1)

L_H = horizontal cooling channel length — cm = (y + a/2)

L_v = vertical channel length — cm = (x + b/2)

f_v = helium void fraction in the side insulation

f_h = helium void fraction in the top, bottom insulation

Equations 1 and 2 determine the insulation needed for unconditional stability requirements for a given conductor. The conductor itself is sized from the following equation:

$$\dot{q} = \frac{I_o^2 \rho}{(A_{cond} - A_{sc})P_w} \qquad (3)$$

Where

$\dot{q}$ = generated joule heat flux — w/cm^2

A_{cond} = cross-sectional area of the conductor — cm^2

A_{sc} = cross-sectional area of the superconductor — cm^2

$A_{sc} = I_o/J_c$ where J_c is the critical current density on the superconductor in A/cm^2

P_w = the wetted perimeter of the conductor — cm^2/cm

Since A_{cond} and P_w are functions of the conductor's dimensions, choosing two of the parameters (i.e., $\dot{q}$, I_o, conductor dimensions) allows the third to be determined and hence the insulation thickness. This then determines the minimum conductor unit cell (excluding any required substructures) area for the given conditions. From this, the substructure can be added, if that approach is being considered, and the number of amp-turns that that conductor concept can supply calculated for the given pack envelope. To meet field requirements, $37.7 * 10^6$ amp-turns are required in the given envelope as described in Table 1-I.

2.5.2 HFTF Conductor

The first conductors considered for TMNS were versions of the HFTF monolithic core being developed by LLNL. As applied to TMNS, this conductor was assumed to be rectangular in shape and to be made up of annealed copper, Nb_3Sn, bronze, and tantalum. Only the annealed copper was assumed to carry any current once the Nb_3Sn was normalized. The superconducting portion of the conductor was sized using HFTF core data, considering the superconductor to be everything but the annealed copper. Using an operating-to-critical current density ratio (over the superconductor) of 0.7, led to an operating current density of 24255 A/cm^2 (Note: This was later revised to 26460 A/cm^2 based on a 20% improvement due to a decrease in operating temperature between 4.2K test data and 1.8K operating temperature, rather than 10% previously assumed). With the chosen operating current, the non-copper portion of the conductor could be sized. Equations 1 through 3 could then be applied to determine the remaining conductor parameters. The HFTF analysis presented in Reference 3 was used as a check against the above procedure. Using a

current of 4000A and a conductor cross section of 1.1cm X 0.54cm, a heat flux of 1.62 w/cm^2 was calculated, and this required 0.67mm of insulation to be unconditionally stable. These numbers vary slightly from those in Reference 3, mainly because of different copper resistivity data used, but not enough to invalidate the procedure.

2.5.3 Parametric Studies

At this point, a variety of parametric studies were performed to determine the effects of heat flux, conductor unit cell current density, and insulation void fraction on conductor design in superfluid helium. The results are presented in Figures 2.5-2 through 2.5-4.

Figure 2.5-2 is a plot of the unit cell area (considering only the conductor and insulation) versus the conductor's normalized heat flux as a function of operating current and conductor aspect ratio λ. As can be seen, the unit cell area begins to minimize at a heat flux between 1.0 to 1.5 w/cm^2. Above these values, the stabilizing copper begins to trade off one-for-one with the insulation. Thermodynamically, this reduction in copper area is of little consequence. However, from an electrical quench standpoint and from a structural footprint standpoint, this reduction is disastrous. Thus, the optimum heat flux for a conductor in this magnet application appears to be between 1.0 and 1.5 w/cm^2, especially for higher operating currents.

Unit cell current density is plotted against operating current in Figure 2.5-3. This graph indicates that like conductors cooled by helium I, those cooled in helium II approach a minimum unit cell current density beyond a certain operating current. However, in helium II, the maximum unit cell current density is much higher and appears at a lower current than in helium I. Also, to construct this curve, the design heat flux for helium II is 1.0 w/cm^2 instead of 0.25 w/cm^2 for helium I, which helps to increase unit cell current density by reducing the required stabilizer area. Insulation thickness required for unconditional stability on the other hand, typically varies almost linearly with operating current as shown in Figure 2.5-4. Also, required insulation thickness varies inversely to the insulation void fraction.

2.5.4 HFTF Scale-up Conductor

The next conductor considered after the HFTF core was a scale-up of that conductor. Its cross section was set at 2.2cm X 1.08cm with a joule heat flux of 1.0 w/cm^2. These parameters dictated a maximum operating current of 10,400 amps and a minimum insulation thickness requirement of 2.1mm. With a nominal substructure assumed, this conductor could achieve the required number of amp-turns in the given envelope only if the current were graded throughout the conductor pack. Current

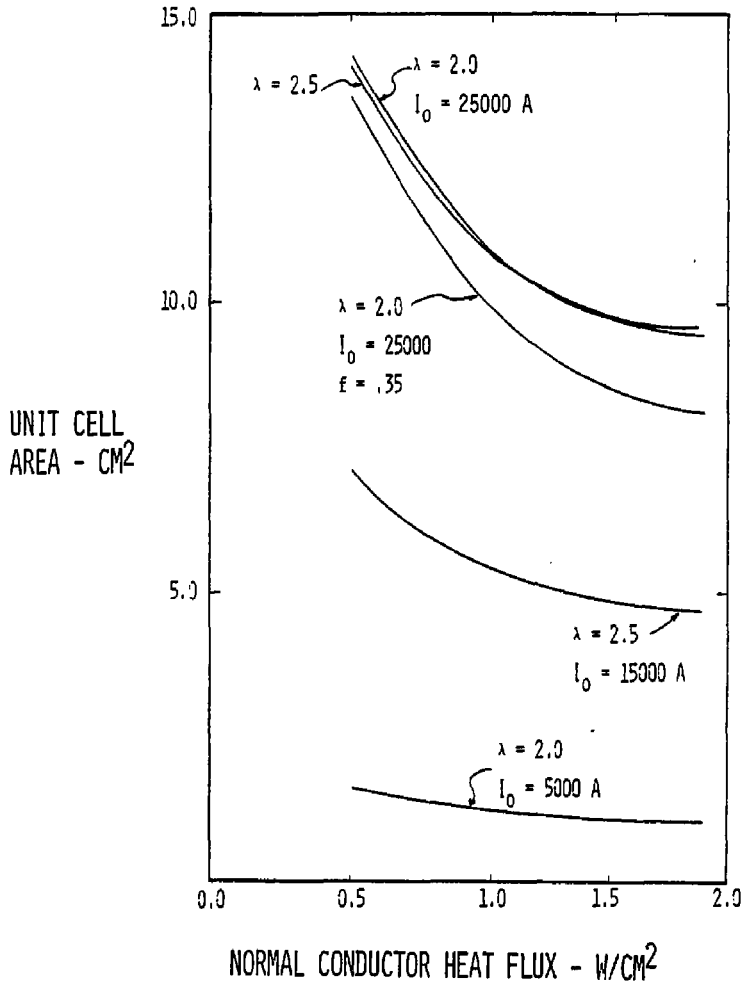

Figure 2.5-2. Copper/Insulation Ratio is Optimized for a Heat Flux $\dot{q}$ = 1.0 ~1.5 W/CM^2.

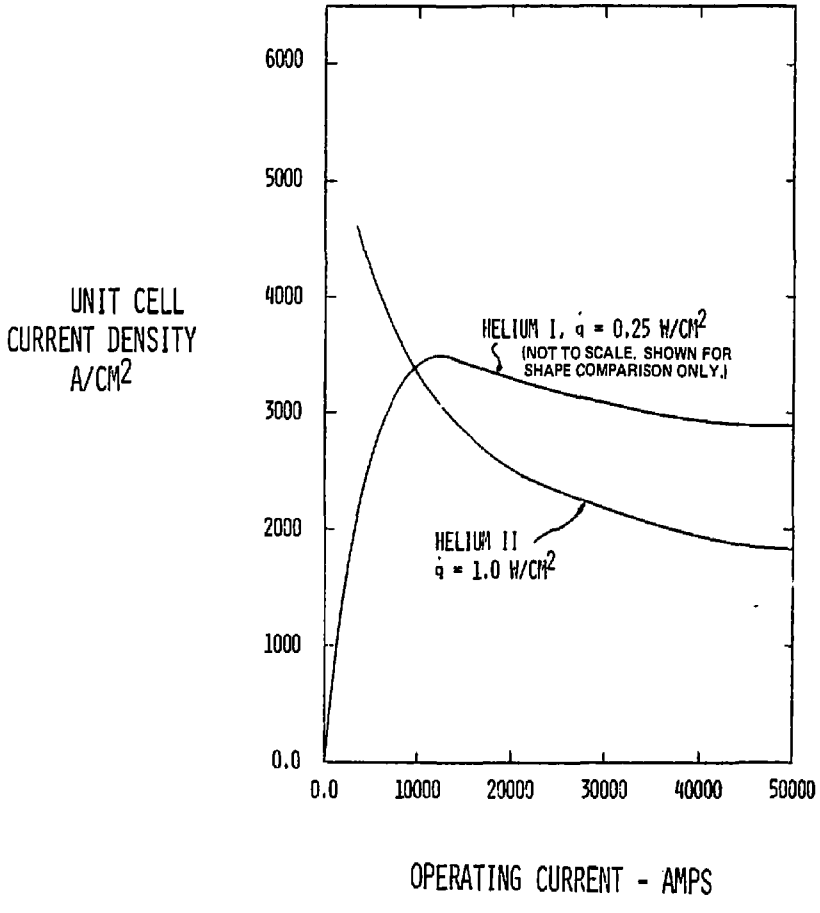

Figure 2.5-3. Required Unit Cell Quantities of Insulation and Copper Increase More Quickly than Current Resulting in Decreasing Current Densities with Increasing Current.

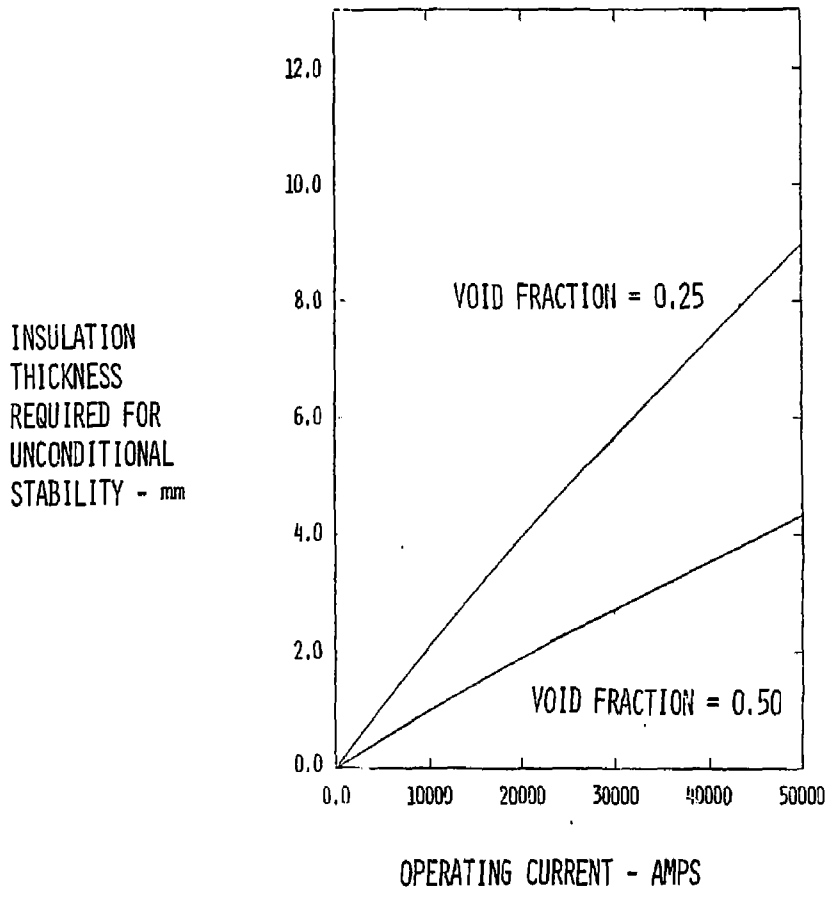

Figure 2.5-4. Required Insulation Thickness Increases Almost Linearly with Operating Current.

grading was accomplished by subdividing the pack into separate coils, each with its own power supply, operating so as to produce the same joule heat flux throughout the pack (copper resistivity varies with field; lower field implies lower resistivity which implies higher current to maintain a constant joule heat flux). This concept was later rejected when the assumed substructure dimensions were found to be far too small to handle the expected loads.

2.5.5 Cask CDP Conductor

Conductors capable of reacting the magnet loads without additional substructure were considered next. Initial consideration was given to a Cask CDP (Reference 1) type conductor. From a thermodynamic standpoint, this conductor is acceptable with a heat flux of 0.75 w/cm^2, an insulation thickness of 6.75cm and a cross section of 12.84cm X 1.34cm. However, structural and manufacturing problems led to the rejection of this concept.

2.5.6 50KA Conductor

While attempting to make the nine individual monolithic conductors in the Cask CDP approach transpose without overstraining the Nb_3Sn superconductor, it was proposed that the superconductor be a loosely woven cable soldered into a copper substrate instead of the nine monoliths. This concept of using a cabled conductor proved feasible with a heat flux of 1.47 w/cm^2, slightly over 7.0mm of insulation and an operating current of 48087 amps. However, manufacture of a loosely woven solderable cable proved to be impractical. Thus, a cylindrical rod of the same cross section was proposed instead. This was rejected due to the strain limitations on the superconductor being exceeded in parts of the winding.

2.5.7 Conclusions

Thermodynamically, all the conductors considered in this study were analyzed with equations 1 through 3. Each rejected conductor concept was rejected because of consideration other than thermodynamic indicating that in a magnet the size of TMNS, utilizing the excellent heat transfer properties of helium II, thermodynamic requirements are not the major design driver for the conductor.

2.6 PRODUCIBILITY STUDY OF FABRICATING IN SITU 50 KA CONDUCTOR

2.6.1 Introduction

After engineering had made several design trade studies, manufacturing was asked to design a fabrication method for the 50KA conductor shown in Figure 1-1. The following is an outline of that manufacturing process.

2.6.2 Stabilizer

Due to the pack size and the potential for gap problems associated with the large conductor cross-section, a machined stabilizer would be required. Rolling, extrusion or draw methods were considered but it was felt that they would result in tolerances that would be prohibitive in maintaining the proper overall envelope. The proposed stabilizer presented in Figure 2.6-1 would be machined from square shaped OFHC copper bars and subsequently electron beam welded into the required lengths. The groove would be cut using a specially built cutter. Check gages would be employed throughout this process to minimize size variations

Once machined, a series of stabilizers would be formed into the shape of bent hair pins as shown in Figure 2.6-2. These hair pins would then be formed and rolled to build-up one pancake tier. To minimize winding build up tolerance, check templates shown in Figure 2.6-3 would be used to accept each stabilizer at each forming operation. After this final rolling and forming, the stabilizer sections are stored until they are needed in the assembly sequence.

This manufacturing plan was developed around the idea that the coil would be built from the outside to the inside and in an inverted form, which is the reverse of the "MFTF-A" manufacturing technique. This method was selected because it was assumed that the 50 KA conductor would be too large to wind conventionally. Additionally, even if this large of a conductor could be wound, the Nb_3Sn superconductor would be overstrained in the process. The fixture shown in Figure 2.6-4 would hold a coil form with the inside up and rotate it back and forth to keep the working area at the lowest possible point.

2.6.3 Splices

The coil will be progressively spliced together as indicated in Figure 2.6-5. Each "bent hair pin" would be layed up in a position above and away from its final location. While in this preliminary location, an Electron Beam weld head would be brought into place and the stabilizer pieces welded together. The coil would take shape, then, in a spring like configuration.

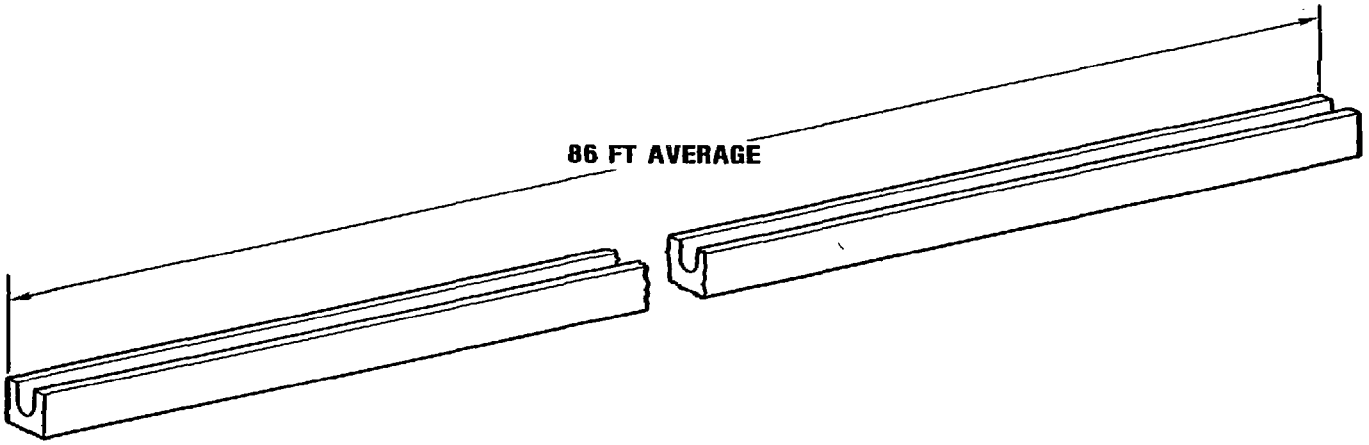

- SIZED (SPLICED)
- SHAPED
- GRADED

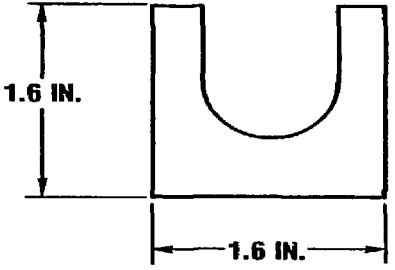

Figure 2.6-1. Stabilizer is Machined for the 50 KA Conductor.

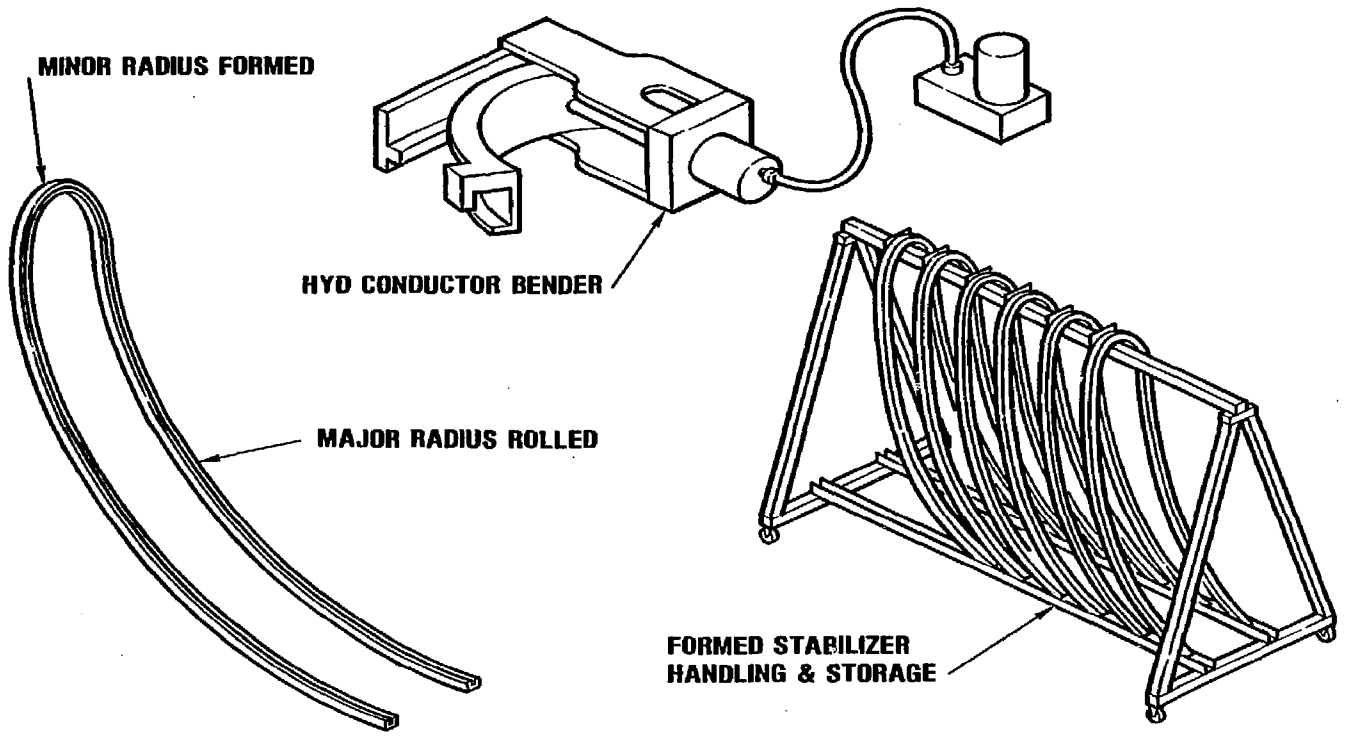

Figure 2.6-2. Stabilizer is Pre-formed to Match Winding Configuration.

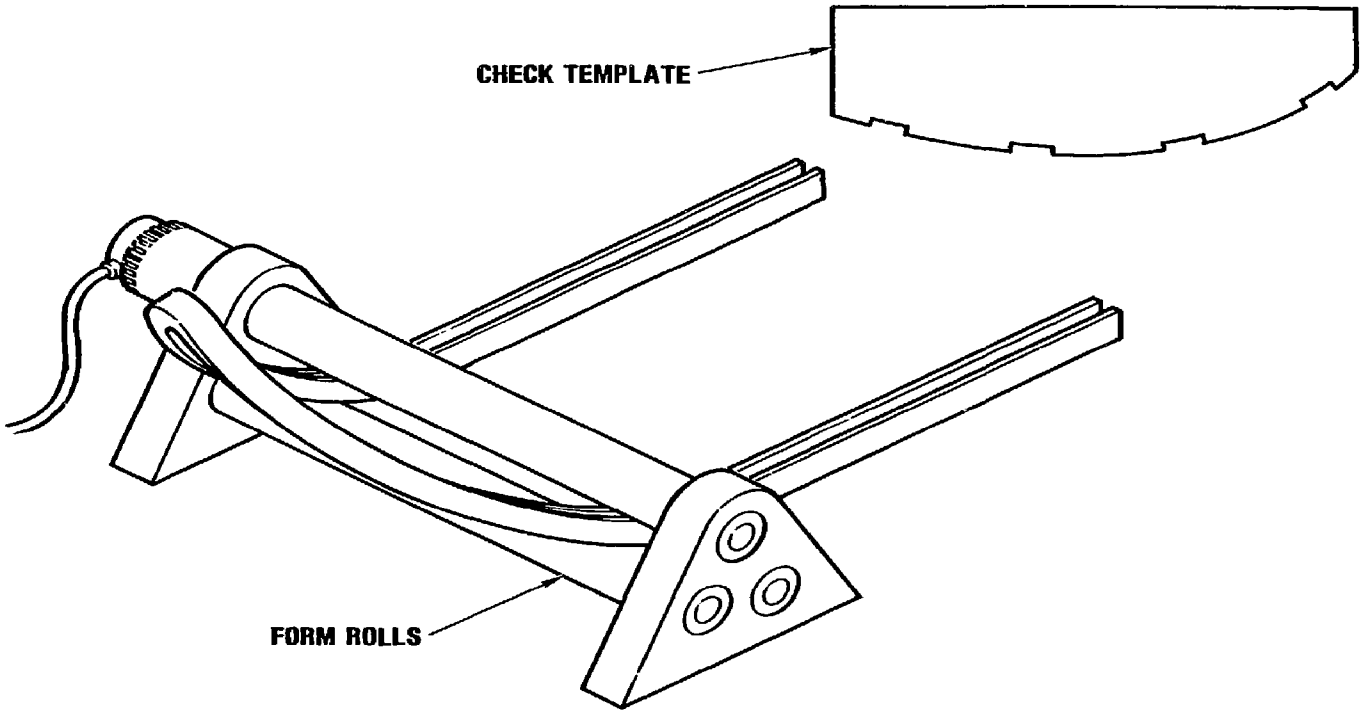

Figure 2.6-3. Winding Build Tolerance is Minimized with Check Templates.

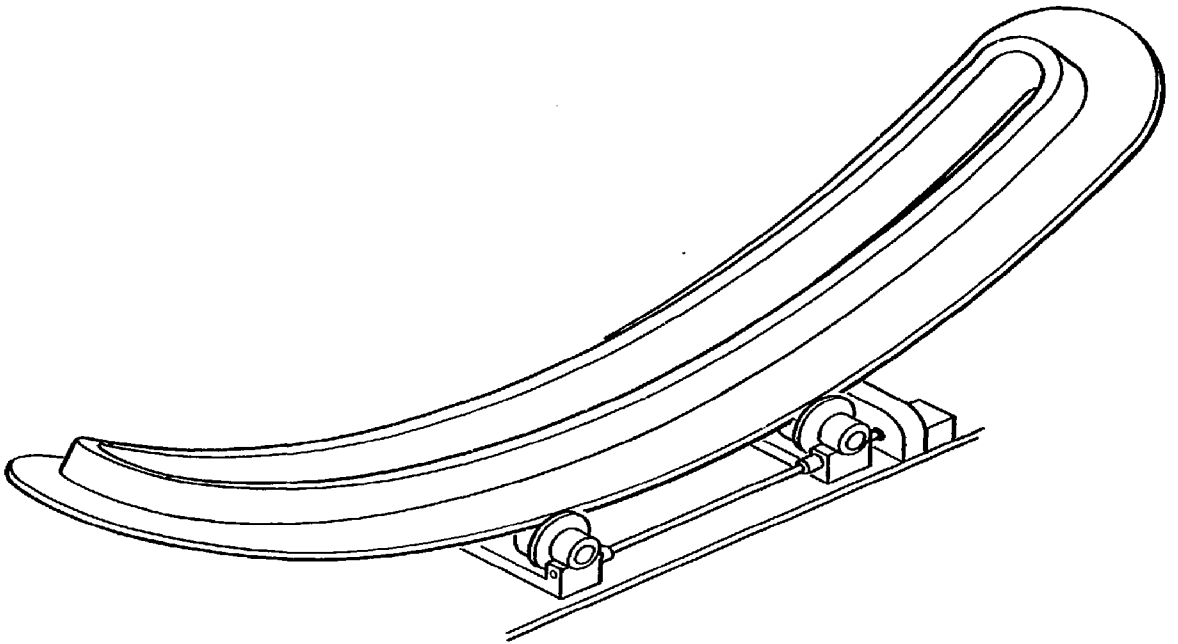

264.766-7

Figure 2.6-4. Coil Handling Fixture Aids Fabrication.

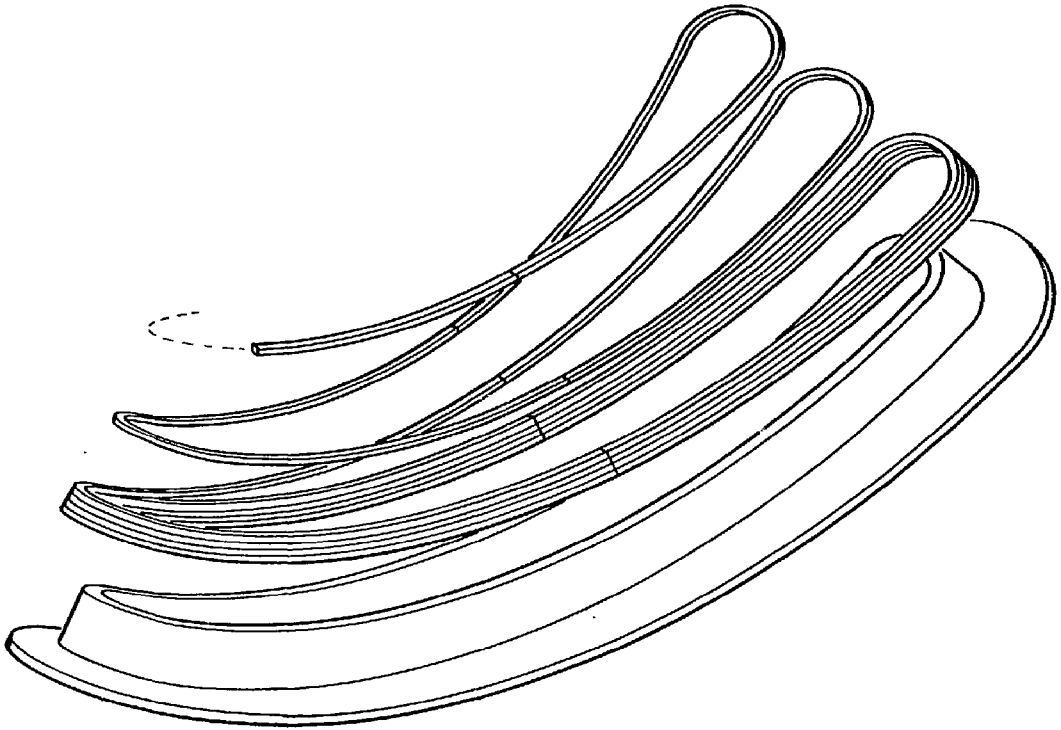

264.766-16

Figure 2.6-5. Pancake In Situ Winding is Built Up by Progressive Splicing.

Although no portable Electron Beam welding equipment exists, it is feasible that the existing welders illustrated in Figure 2.6-6 could be reconfigured for movable applications. Figure 2.6-7 illustrates one possible configuration for a portable Electron Beam welder. A special box would be built that encloses the stabilizer and provides the necessary vacuum for the welding process. Vacuum would be provided by a skid mounted system as shown in Figure 2.6-8 that will be brought to the coil on a track system. Once the weld has been completed, the joint will be stretched, hardened and tested using a proof loading technique developed for the General Dynamics Large Coil program as illustrated in Figure 2.6-9.

2.6.4 Final Conductor Assembly

Final build up of the conductor shown in Figure 2.6-10 would take place on the coil. The plan is to lay the superconducting cable in the stabilizer channel groove while the stabilizer is held up and away from the final location. Solder in a strip form would then be fed in on top of the superconductor. Placement of the insert would be the final assembly task. The soldering heat would be provided by induction coils of the type shown in Figure 2.6-11. This type of heating is very reliable and provides clean solder joints. Manufacturing aids would be used to support and clamp the conductor assembly during this fabrication.

The projected size of the TMNS plug coil system dictates some very specialized handling equipment of the type shown in Figure 2.6-12. Even though this equipment is unique, it does not appear to be beyond the current state-of-the-art.

2.6.5 Fabrication Site Floor Plan

In terms of working area, for support equipment, working from both sides of the coil forms would be the most efficient. The proposed working area layout is shown in Figure 2.6-13. The approach indicated would require two Electron Beam weld heads. However, both heads plus the Electron Beam welder for the stabilizer line could be controlled from a central control unit.

2.6.6 Conclusions

Size alone makes this 50KA conductor coil manufacture difficult. The conductor could not be manipulated or formed with hand tools, necessitating the need for machines and equipment throughout the coil fabrication to ensure a tight coil pack. Even with these difficulties, the fabrication of this coil, as it is designed, is feasible.

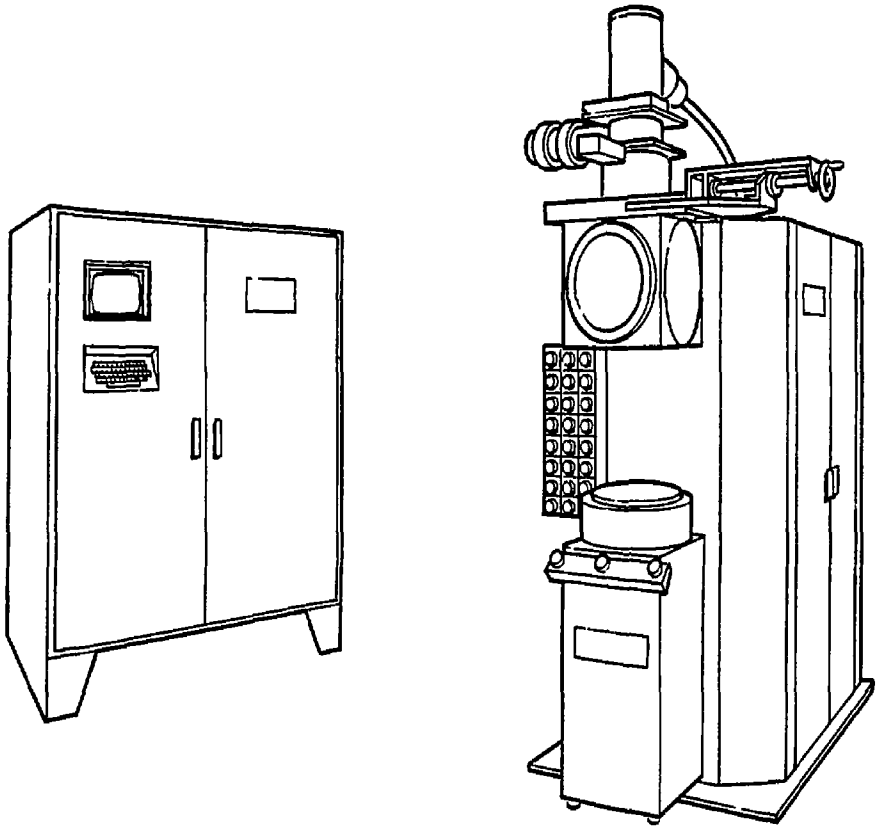

264.766-10

Figure 2.6-6. Current Stationary Electron Beam Welding Equipment can be Modified for Mobility.

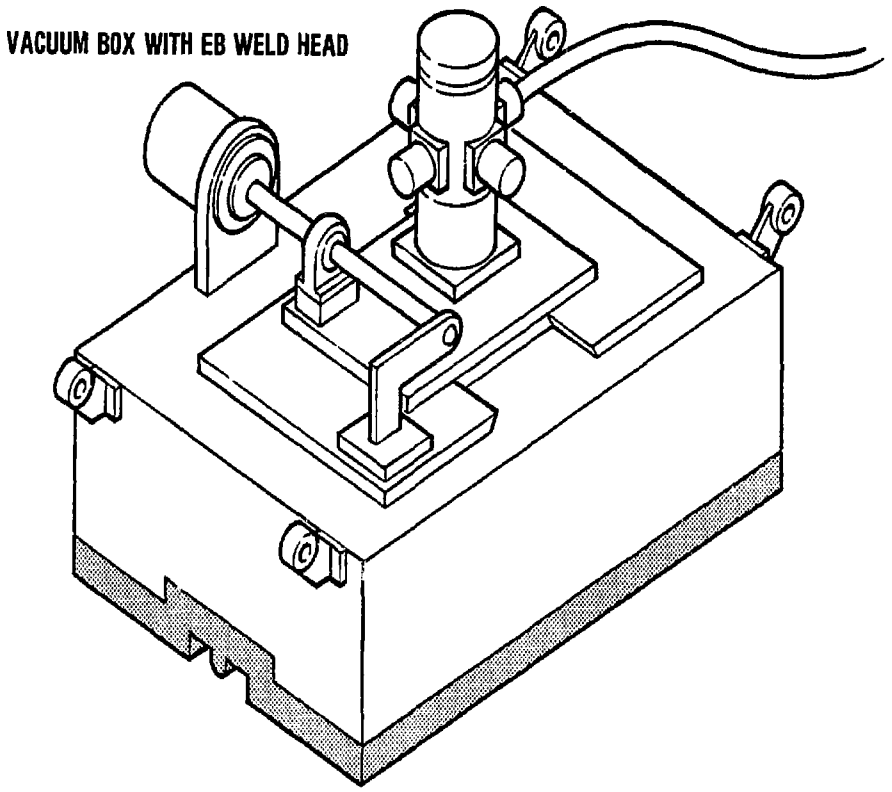

Figure 2.6-7. Proposed Portable Electron Beam Welder Design is Based On Current Technology.

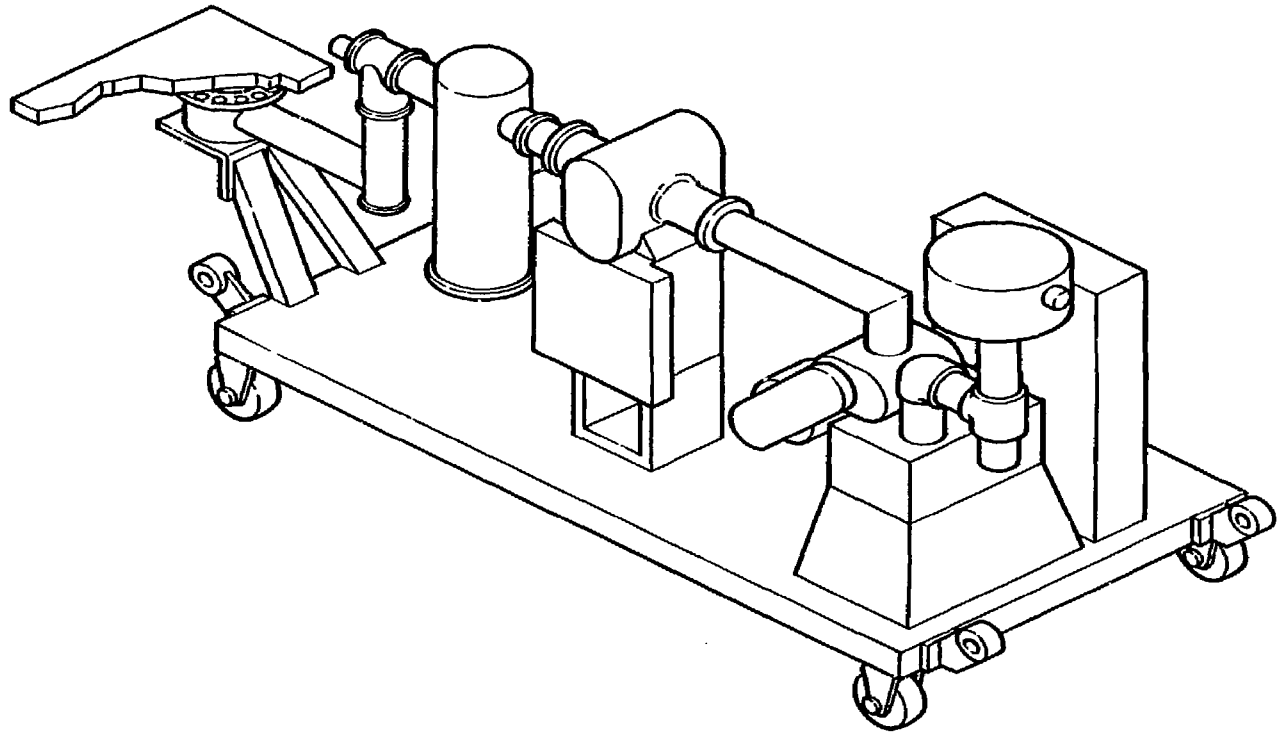

264.766-9

Figure 2.6-8. Vacuum for the Electron Beam Welder Provided by Skid Mounted Vacuum System.

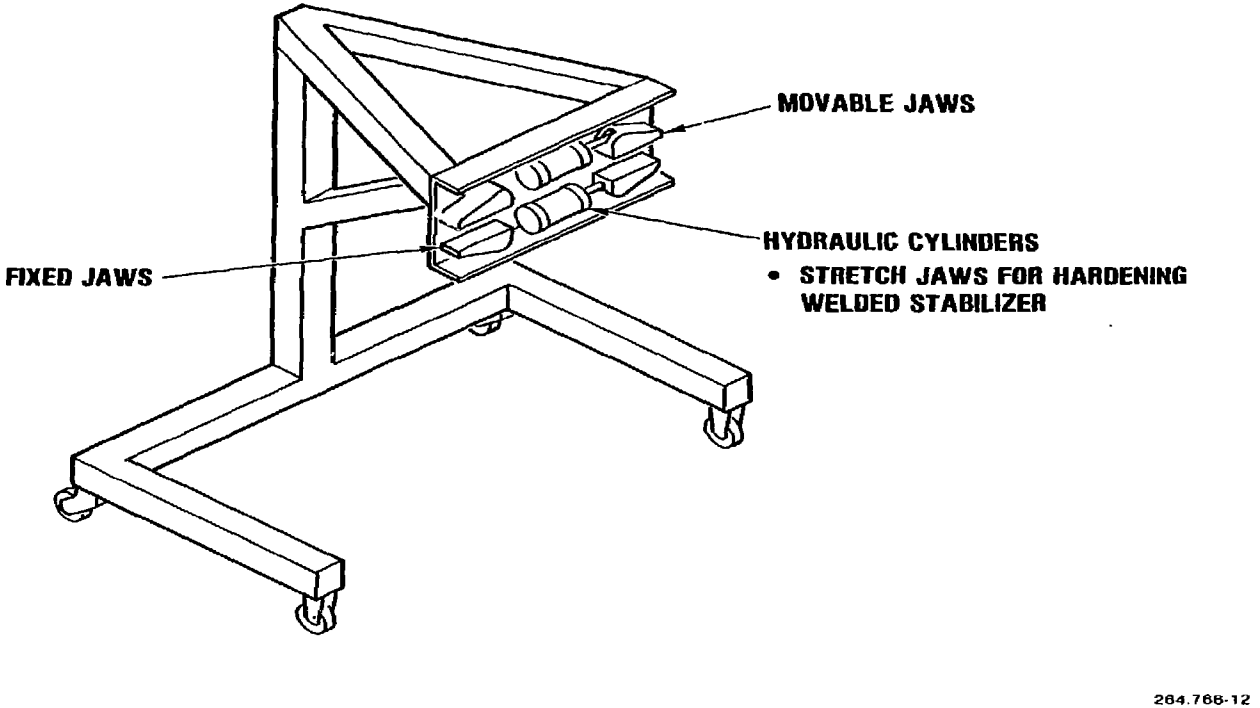

Figure 2.6-9. EB Welded Joint can be Proof Loaded by Proven Methods.

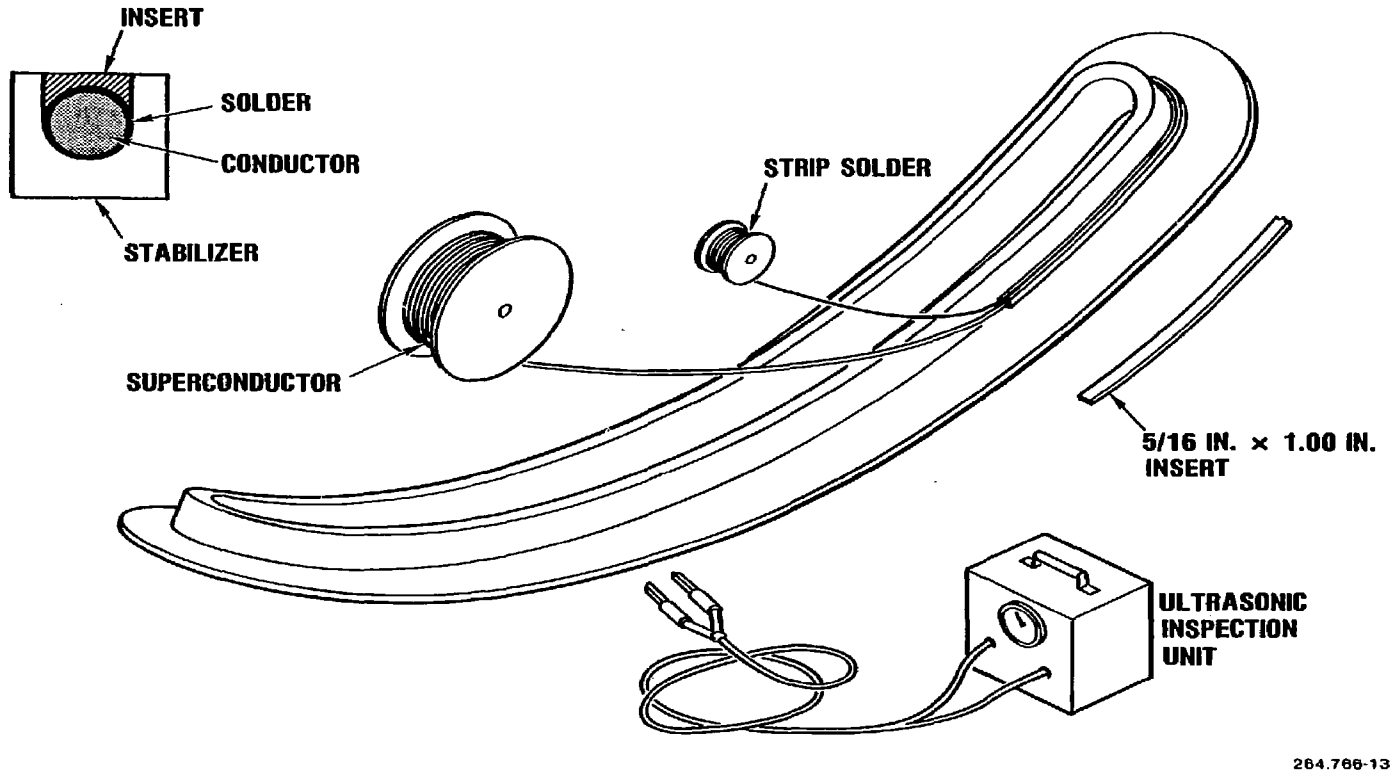

Figure 2.6-10. Conductor Assembly is Accomplished on the Winding Form.

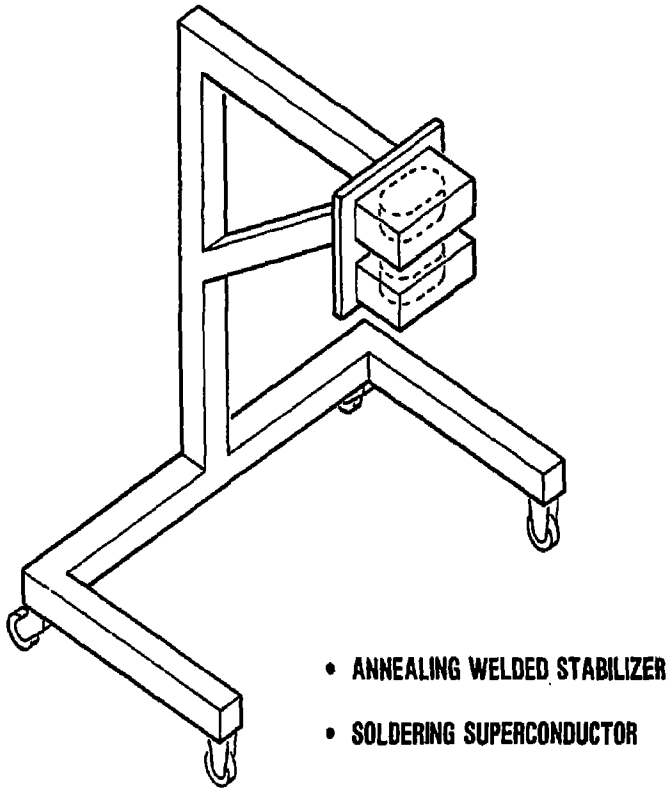

Figure 2.6-11. Induction Coils are used to Solder the Superconductor into the Stabilizer.

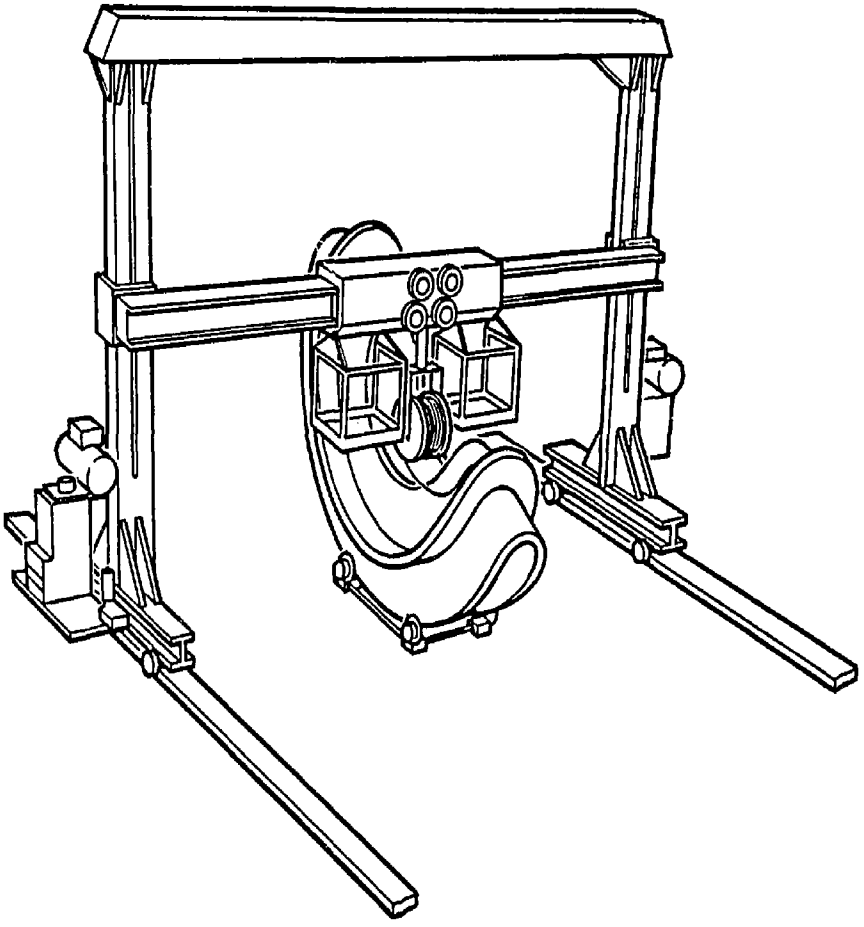

264.766-15

Figure 2.6-12. Gantry Cranes will Handle Production Material.

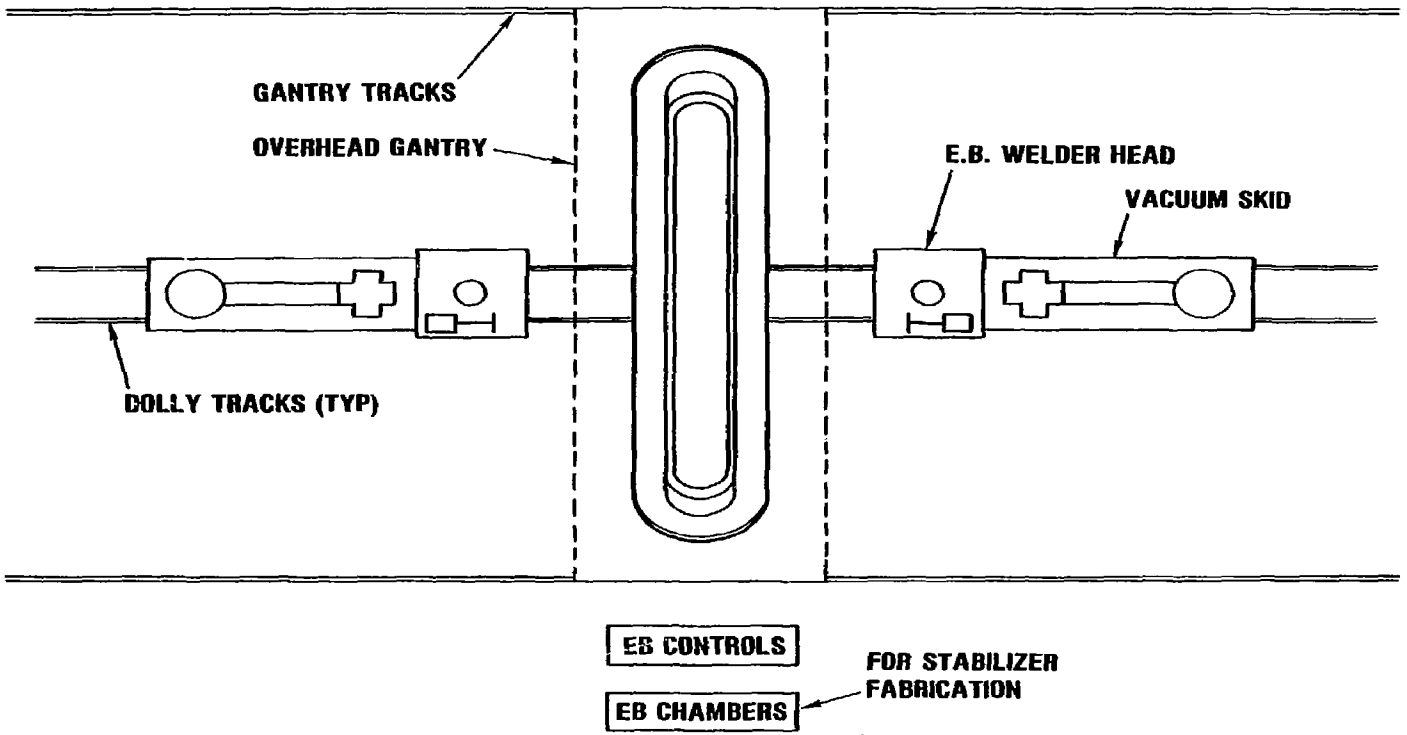

Figure 2.6-13. Working Area is Readily Accessible

2.7 QUALITY ASSURANCE

2.7.1 Proposed Inspection Method

Based on the use of 50KA conductor shown in Figure 1-1 with circular cross-section superconductor and a shaped copper plug for close-out, an ultrasonic inspection method was selected. The specific arrangement is shown in Figure 2.7-1. It is estimated that ultrasonics will provide low cost positive assurance that the solder bond between the stabilizer and the superconductor and at the plug interface meets specifications. It is anticipated that the use of multi-element transducer arrays would simplify the system design and reduce the number of moving parts to a minimum. The plug interface will be inspected first to determine if it will interfere with inspecting the conductor interface. Calculations have been made which show that plug interface solder will not appreciably disrupt signals which must cross it if they are properly phased. Any spurious signal produced by this interface will be delayed in time or scattered so it will not interfere with the information desired.

2.7.2 Alternate Inspection Method

Several other techniques were considered; however, they are not expected to be as effective as the ultrasonic system proposed. These included ultrasonic wave form analysis, process control, microwave techniques, heat transfer, and x-ray tomagraphy.

3.0 PREFERRED DESIGN APPROACH

The preferred design concept for the TMNS Yin-Yang magnet pair is presented in this chapter. Key analyses and extensions of the trade studies in Chapter 2 are discussed. The work is organized into seven sections describing the work performed by key disciplines. These sections discuss the essential features of design, stress analysis, materials, electromagnetic analysis, thermodynamic analysis, manufacturing and quality assurance, respectively.

3.1 CONDUCTOR/SUBSTRUCTURE DESIGN

3.1.1 Conductor

At the time of the Preliminary Design Review, the conductor proposed for TMNS consisted of a loose cable held in a copper stabilizer (the loose cable was needed to minimize bending strains). This conductor was rated at 50,000 amperes and it completely filled the 68 X 272 centimeter winding envelope. When it was recognized that a loose cable with good solderability would be difficult to fabricate in Nb_3Sn, alternate approaches were investigated.

Since the Nb_3Sn superconductor would have to be considered a monolith, the size of it was strain-limited, and this criteria was used to develop the preferred conductor and stabilizer which is shown in Figure 3.1-1.

Initially, it was hoped that this conductor could be wound within the original envelope of 68 cm X 272 cm. To do this would require a pack cross-section of 32 conductors wide by 91 conductors high, operating with a current of approximately 13,000 amperes. Unfortunately, the Stansol analysis (Section 3.2) showed that the conductor axial strains were too great and this approach was dropped. This was the last attempt to remain within the original envelope. Breaking up the coil pack into six sections and adding integral substructure was tried next, but this, too, caused excessive strains. One feature of this approach was that it started opening up space in the minor radius region which was beneficial for getting leads out. This winding arrangement is shown as Figure 3.1-2.

The final approach to this problem was to break up the envelope into four sections, each sized such that the magnetic pressure would give approximately equal loading within each of the sections. With the introduction of substructure, the original envelope was exceeded by quite a large margin, 120 cm X 412 cm, instead of 68 X 272.

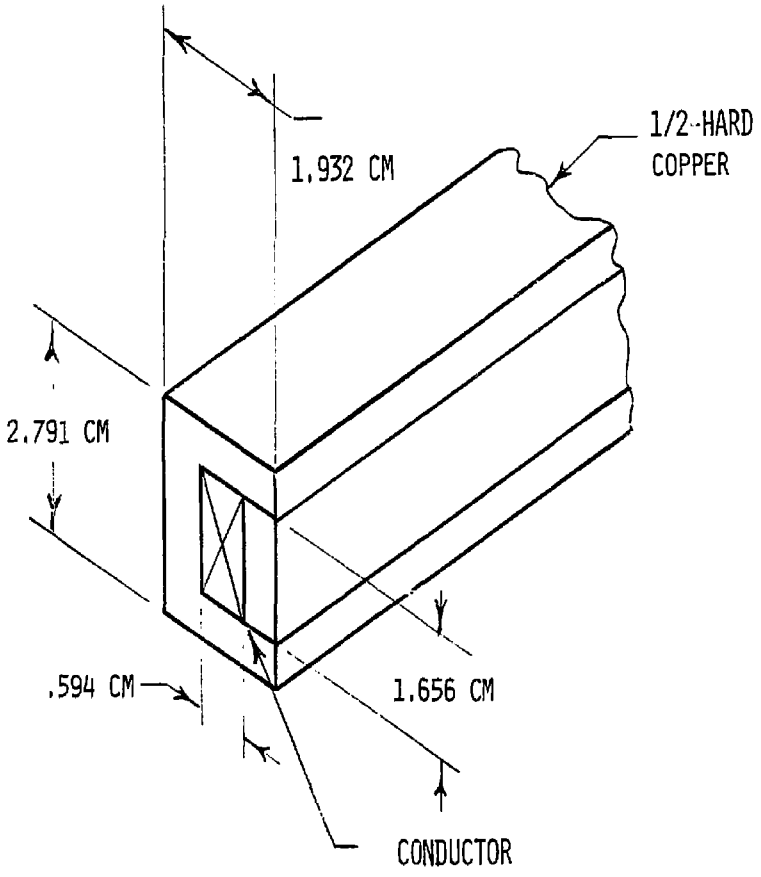

Figure 3.1-1. A Copper Stabilized Monolithic Superconductor is Preferred.

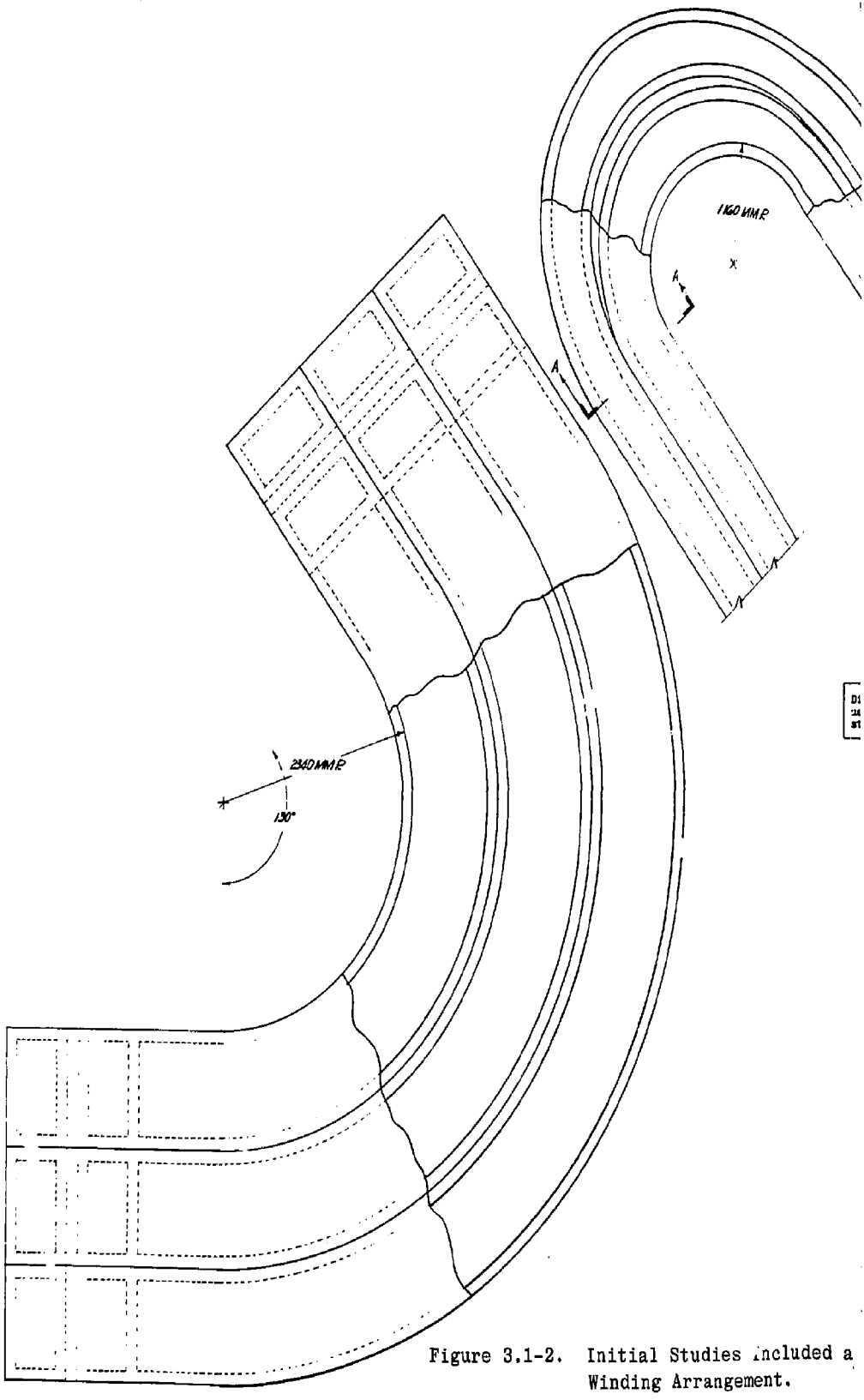

Figure 3.1-2. Initial Studies Included a Winding Arrangement.

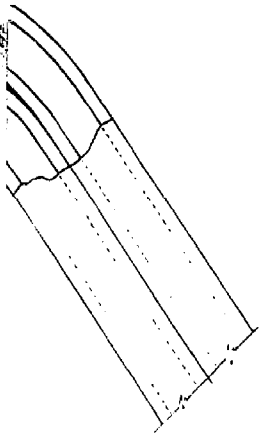

Discarded concept -- used in tradeoff studies

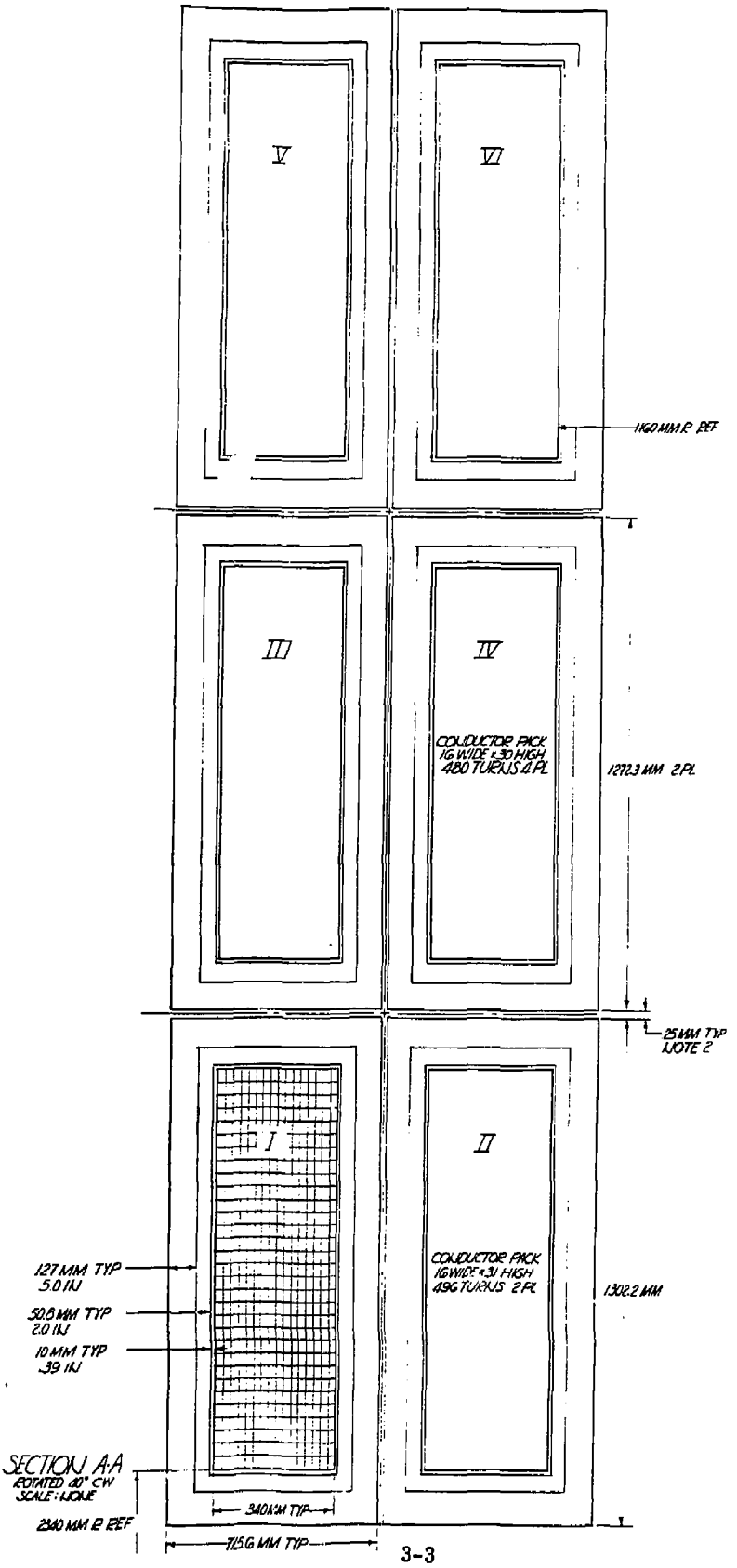

ıded a Six-Section

With this new arrangement, LLNL found that the peak field intensity approached 14 Tesla in the minor radius region. To alleviate this, space was added between the Nb_3Sn and the NbTi conductors. LLNL found that approximately 36 inches of space between these conductors would bring the field intensity to acceptable levels. This winding arrangement is shown in Figure 3.1-3. This space is used to advantage by locating the Nb_3Sn to NbTi splices in this area. Incidentally, additional crescent-shaped spaces are required at the ends of the four sections for the turn-to-turn splices in the minor radius region. The operating current for this winding is 15,600 amperes, the pack width is 33 conductors, and the total height is 90 conductors. This gives 2970 turns and at 15,600 amps, yields 46,332,000 ampere-turns.

3.1.2 Insulation

The basic insulation concept utilizes "button-on-a-string" insulation for the turn-to-turn insulation and "snow-fence" type for layer-to-layer insulation, as shown in Figure 3.1-4. Turn-to-ground insulation is about 1 cm thick. G-10 CR is the preferred insulation.

Initially, it was calculated that three nested windings would be needed, and the insulation thickness requirements were established on this basis. The refined quench analysis presented in Section 3.4 indicates that the number of nested windings should be increased to five. Structurally, the effect of this change is relatively minor, probably only necessitating thicker layer-to-layer insulation which could increase the total pack height about 18 centimeters.

3.1.3 Conductor Grading

The original field plots of the minor and major radius regions were combined to make a composite of the maximum field strengths. Based on this original composite and the goal to keep the NbTi conductors in fields below 9 Tesla, it was determined that all the turns in Section No. 1 (Figure 3.1-5) should be of Nb_3Sn while only the first inside 10 (of 33) pancake layers should be Nb_3Sn in the remaining three sections. There was no time to create a new composite to determine if the 10 layers was still adequate, if there are five nested coils instead of three. A change in this value would make no structural change, but it could cause revisions to the cost estimate.

3.1.4 Splices

There are basically three types of splices: (1) Nb_3Sn to Nb_3Sn, (2) Nb_3Sn to NbTi, and (3) NbTi to NbTi; types (1) plus (2) outnumber type (3). Regarding splice design, the primary concern after low resistance and high strength was protection of the Nb_3Sn superconductor since it is so susceptible

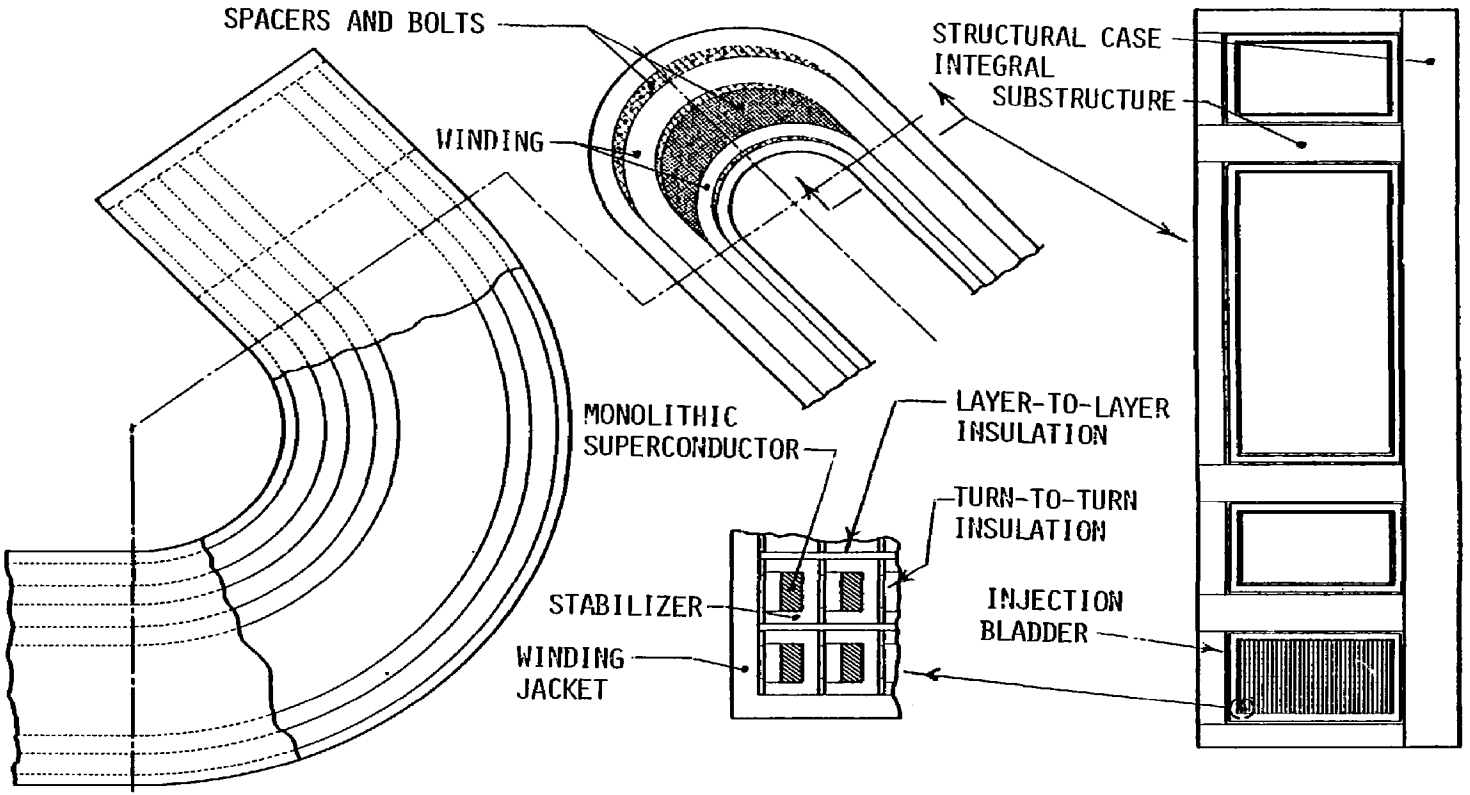

Figure 3.1-3. Preferred Winding Arrangement

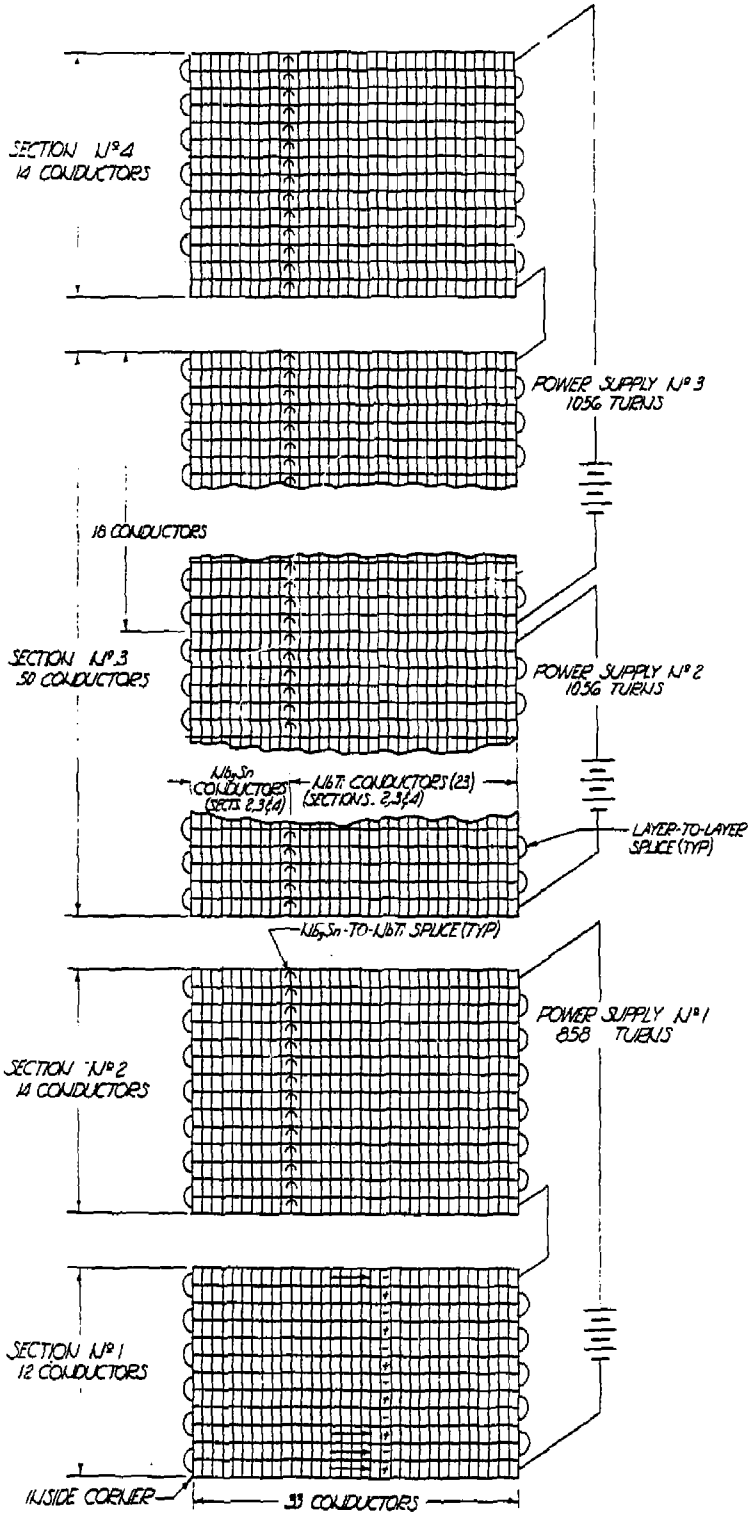

Figure 3.1-5. Grading and Splice Locations.

to brittle cracking. With this in mind, the approach taken was to retain as much of the copper stabilizer as possible and just expose the superconductor for lap splicing. The current design uses indium foil at the lap interface to reduce the electrical resistance. Details of the splice are given in Figure 3.1-6.

The total number of splices for a Yin or a Yang is 163, based on 2600-foot conductor lengths. Of the 163 splices per coil, 35 are NbTi to NbTi, thus the majority of splices have at least one Nb_3Sn conductor involved.

All splices will be made in the minor radius region and G-10 CR crescent-shaped pieces have been planned to accommodate them.

3.1.5 Winding

The winding of the Yin and Yang will be performed by sections. Whether it is better to wind all the sections separately and then assemble into the case or wind them directly into the case should be determined by a tradeoff study, and in either event, the first section will be composed of all Nb_3Sn conductors and the other three sections will contain mixtures of Nb_3Sn and NbTi.

It is planned that all windings will be layer-wound in the major radius regions (which makes it a pancake winding in the minor radius regions) and that all layers start from the inside edge of the substructure/case. This means that alternate layers must be wound in the opposite direction to the previous layer, and that splices will be required at the layer terminations and in between where there is a change from Nb_3Sn to NbTi (an additional splice could be required if the conductor lengths furnished are less than 2600 feet). See Figure 3.1-5 for splice locations.

All the splices will be accomplished in the minor radius region where space has been provided to accommodate them, Figure 3.1-7.

3.1.6 Substructure

The substructure chosen was derived from an analysis of the internal magnetic pressures furnished by LLNL. The substructure arrangement, which was shown on Figure 3.1-3, was chosen in an attempt to equalize the magnetic loads. It should be pointed out that the new winding geometry creates a new force field so that an iterative approach is indicated here. There is also a hazy distinction between where substructure ends and case structure (which is not part of this study) starts.

The design uses 304 LN for the substructure and for part of the filler pieces in the minor radius regions. Note that each of the four coil sections is contained in a 1 1/2-inch thick case;

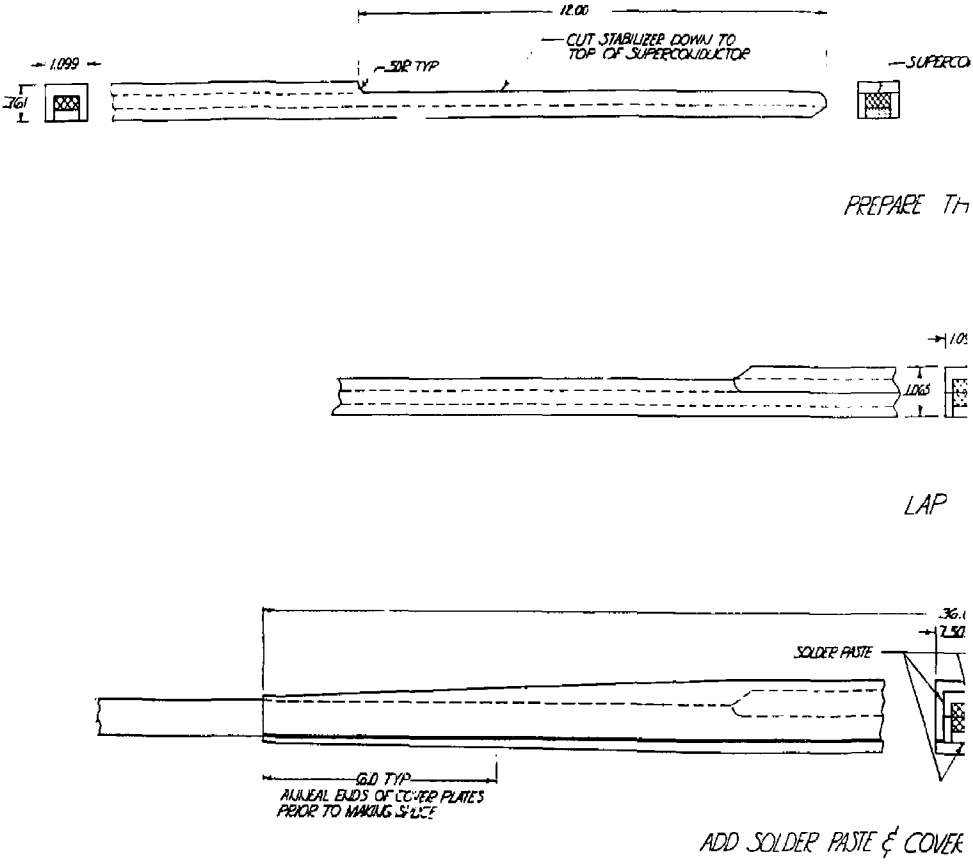

Figure 3.1-6. Conduct

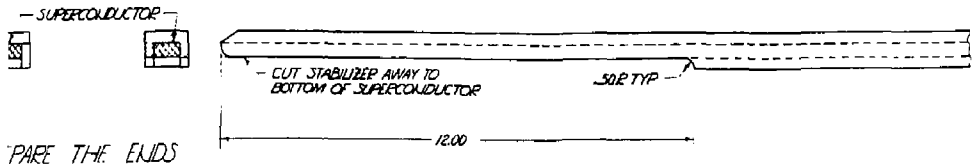

'PARE THE ENDS

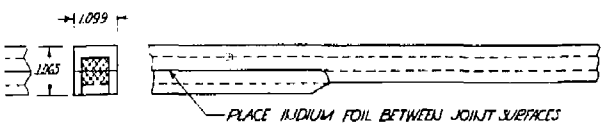

LAP THE ENDS

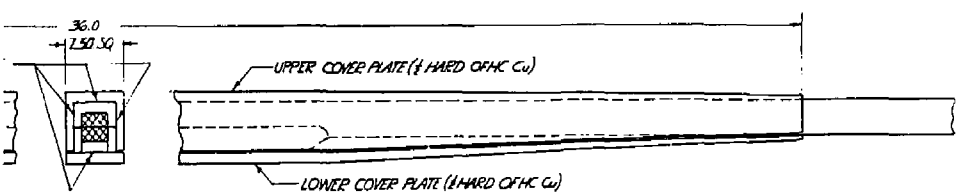

F & COVER PLATES, CLAMP & HEAT

Conductor Splices Details.

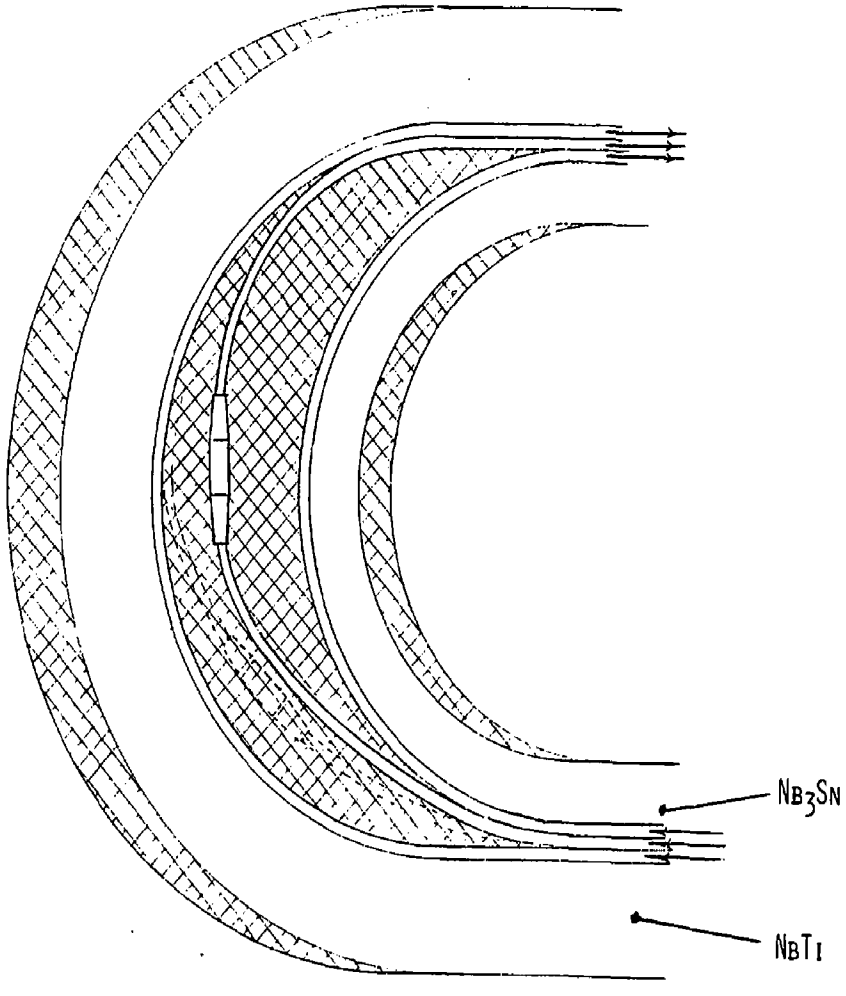

Figure 3.1-7. Typical Splice in Minor Radius Region.

this will provide the flexibility to either wind the section separately and install later or wind directly onto the case. In either event, there will be some large and extensive welds involved in closing out the sections.

3.1.7 Winding Operation

This operation was examined to verify that the proposed winding method is feasible. It is envisioned that the coil sections will be wound separately in cases and that these will be assembled sequentially, see Figure 3.1-8. The largest coil section (No. 3) has 50 layers and is 33 conductors wide. The weight of this coil and its 1 1/2-inch thick case is approximately 571,000 pounds, which far exceeds the approximately 172,000 pound capacity of the winding machine used for MFTF-A. As far as size goes, the winding machine horizontal pivot axis should be around 20% greater than the current machine.

It is obvious that the current machine cannot handle even the small winding sections as each of their weights greatly exceeds its capacity.

It would be possible to break coil section 3 into two parts, thus reducing the maximum weight to around 300,000 pounds, but in any event, we are faced with a winding machine of slightly larger geometric capacity and 75 percent increase in maximum weight capacity. The subject of conductor tension during winding has not been addressed, as it is felt some testing would be required to define this value.

3.1.8 Assembly Sequence and Closeout Welds

While the individual coil sections could be wound into the Yin or Yang sequentially, the weight to be supported by the winding machine would be prohibitive. It was felt the individual coil sections should be wound into a coil case and then assembled sequentially into a structural case. Welding would also have to be performed sequentially. The assembly sequence and closeout welds are shown in Figure 3.1-8.

3.1.9 Weight of Yin-Yang

The estimated total weight of a Yin-Yang is 6670 tons. This estimate was computed as described in Section 4.3 based on a total stored energy of 13.34 GJ. In order to help confirm the accuracy of the estimated weight, the following check was made using the weight of MFTF-A. The total weight of the MFTF-A magnet is 343 tons, and the weight of the structural case which surrounds the windings (excluding conductors, external stiffeners, etc.) is 88 tons which gives a ratio of case to total

1. WELD BOTTOM PLATE TO OUTER CASE
2. PLACE COIL SECTION 1
3. PLACE DIVIDER PLATE 1 AND WELD TO OUTER CASE
4. PLACE CLOSURE PLATE FOR COIL SECTION 1 AND WELD
5. PLACE COIL SECTION 2
6. PLACE DIVIDER PLATE 2 AND WELD TO OUTER CASE
7. PLACE CLOSURE PLATE FOR COIL SECTION 2 AND WELD
8. CONTINUE WITH THIS SEQUENCE TO THE TOP

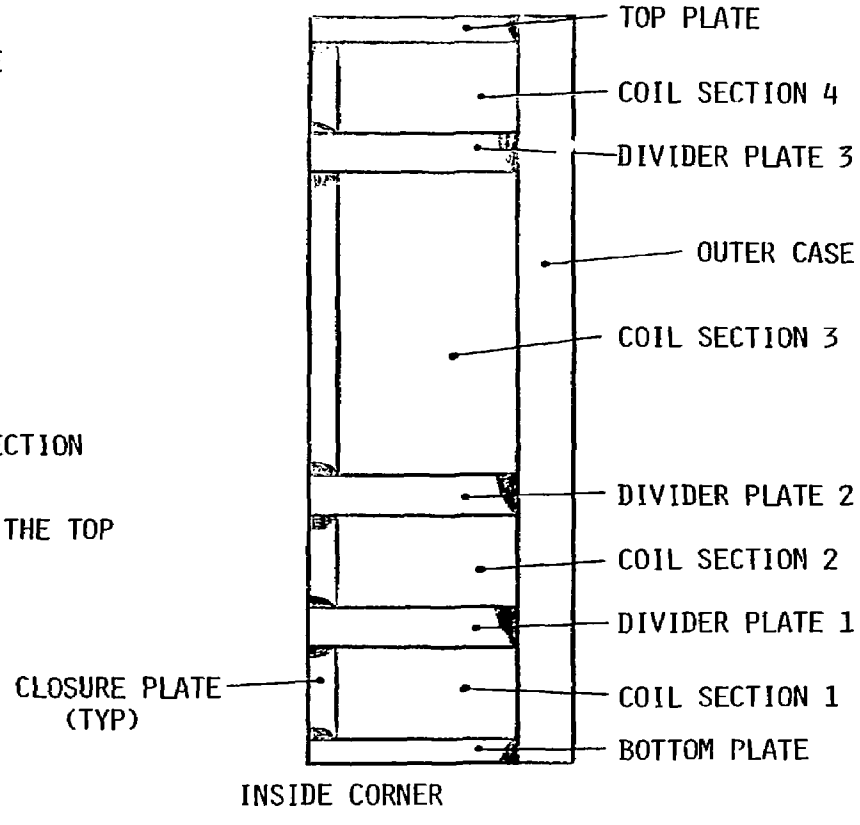

Figure 3.1-8. Structural Case Assembly Sequence and Close-Out Weld Locations.

weight of 25.7%. For TMNS, the weight of the bare case is 1486 tons, and ratioing this with the total estimated weight gives a value of 22.3%. Comparing the two percentages verifies that the stored energy method appears to give valid estimates of magnet weights.

A word of caution should be interjected here. The volume of structure required to react the extremely large magnetic forces is going to be large, and it should be pointed out that regarding clearances for the plasma, due allowances should be made for the necessarily large structure required to contain the magnet forces.

3.1.10 Conclusion

This study has provided a conceptual design of a conductor that is compatible with the various disciplinary requirements. It is a readily producible conductor that can be wound and spliced. We have found that a regionalized winding pack can isolate the magnetic forces so that they can be reacted without overstraining the conductor, and we have found that nested coils give a more practical configuration than do parallel wound conductors. The proposed winding scheme takes full advantage of grading, as well as practical conductor lengths. Finally the problem of accommodating splices has been met by utilizing the crescent-shaped pieces in the minor radius region.

3.2 CONDUCTOR/CASE STRESS ANALYSIS

3.2.1 Introduction

This section covers the stress analysis of the "selected configuration" of the TMNS Design Study.

The selected configuration uses a divided case as shown in drawing TMNS-017, Appendix C. This configuration was determined to be the best arrangement for dividing the case from the standpoint of minimizing the conductor axial strains. The basis for this arrangement was that of dividing the case so that the accumulation of conductor pack pressures in each section was approximately equal as shown in Figure 3.2-1.

One of the major tasks of the analysis in this section was that of evaluating the magnitude of case support by determining the relationship between conductor axial loads, conductor pack pressures, and case loads and deflections. Most of this work was done with the aid of the STANSOL computer code, Reference 4.

3.2.2 Analysis Assumptions

The following assumptions were used during the stress analysis of the TMNS selected design concept:

- The overall magnetic loads are the same with either the undivided or the divided case configurations.
- One third of the lobe spreading force is carried through the minor radius.
- The case is supported to ground at the point where the major axis sweep angle equals 65°. This isolates the case tension loads in the minor and major axis areas.
- All motion between mating surfaces is considered frictionless.
- The material properties at 1.8K were assumed to be the same as those at 4.2K.

3.2.3 Case Overall Magnetic Loads

The case overall magnetic loads were calculated using the conductor pack pressure plots of Reference 5. These pressures were calculated as if the conductors were completely flexible and the case were completely rigid. This means that the total loads calculated

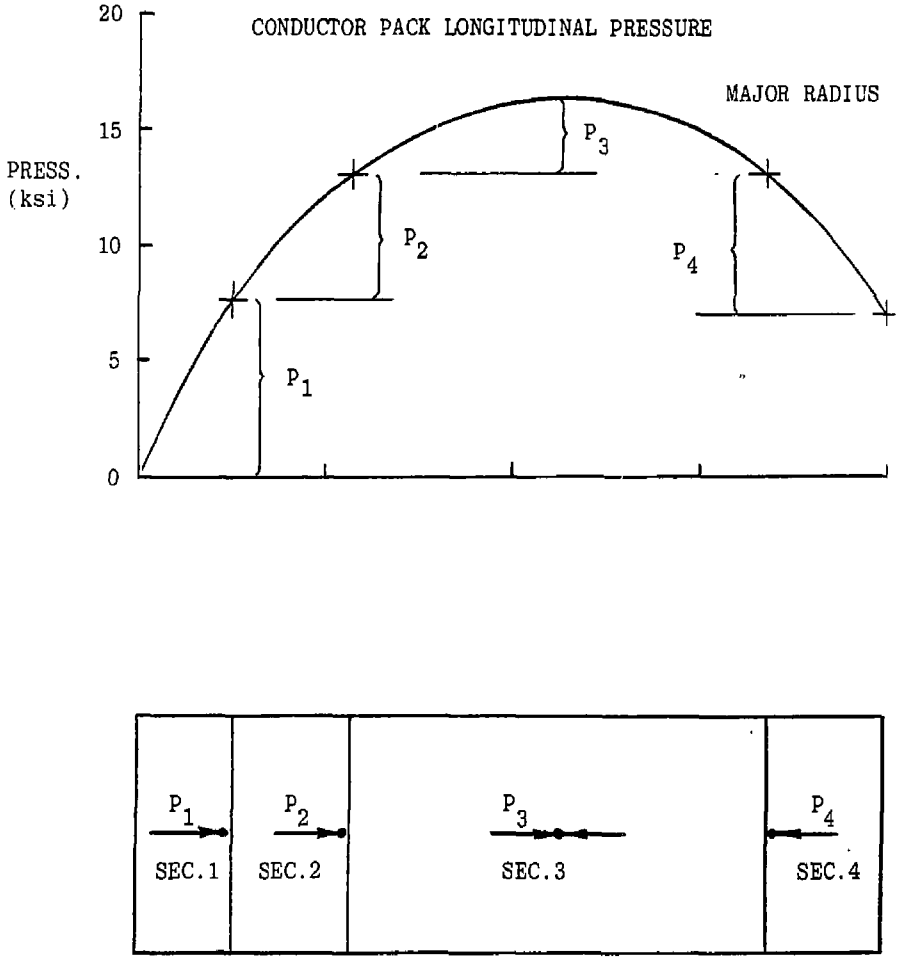

Figure 3.2-1. Case Divisions of Conductor Pack Longitudinal Pressure.

here for the case would be the total load for the case and the conductors regardless of how the loads are shared between the case and conductors.

Figure 3.2-2 shows the equivalent line loads acting on the case surfaces. These line loads are derived from the average pressure acting on each surface times the width of the surface (Table 3.2-I).

Table 3.2-I. Case Overall Magnetic Loads

Load	Radius (in)	Peak Pressure (psi)	Average Pressure (psi)	Line Load (lb/in)
W_1	199.20	7030.	6724.	180.0×10^3
W_2	145.67	7180.	5665.	606.7×10^3
ω_1	72.45	8484.	7687.	823.2×10^3
ω_2	59.06	8963.	4170.	111.6×10^3

Lobe Spreading Force

$$\text{Lobe Spreading Force} = W_2 \pi R \frac{65}{180} + \omega_1 (r)$$

$$= 1.6 \times 10^8 \text{ lb} \quad \text{One Half}$$

$$= 3.2 \times 10^8 \text{ lb} \quad \text{Both Halves}$$

Yin-Yang Closing Force

$$\text{Closing Force} = -\int_0^{65} W_1 R_1 \cos\theta \, d\theta$$

$$-\omega_2 (\pi/2)(r_2)(\cos 65°)$$

$$+\int_0^{\pi/2} \omega_1 (r_1) \sin 65° \cos\phi \, d\phi$$

$$= -180.00 (199.2)(\sin 65°)$$

$$-111.63 (92.77)(\cos 65°)$$

$$+823.20 (72.45)(\sin 65°)$$

$$= 17.18 \times 10^6 \text{ lb} \quad \text{One Quadrant}$$

$$= 68.72 \times 10^6 \text{ lb} \quad \text{Four Quadrants}$$

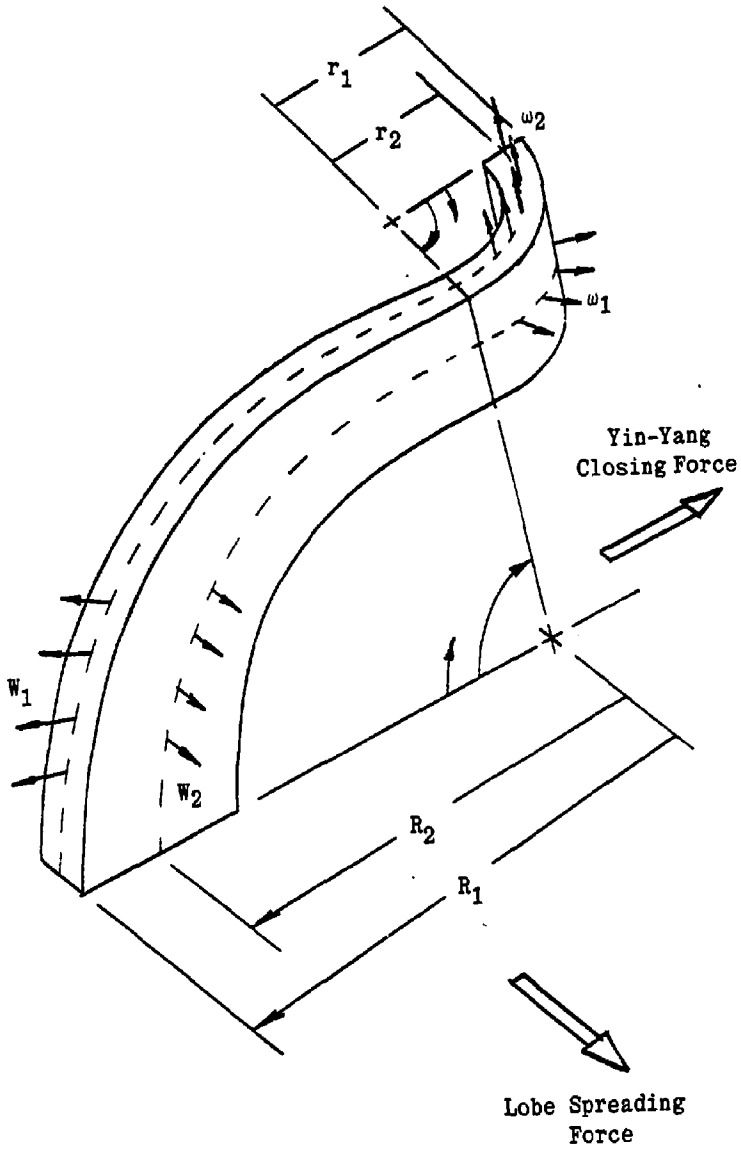

Figure 3.2-2. Magnetic Loads on Magnet Case with Totally Flexible Conductors.

This is felt to be in good agreement with the 76.5 X 10^6 lb calculated by LLNL since the force calculated here was derived from the forces at only the midplane of the major and minor axes.

Conductor Tensile Loads Analysis Model

The conductor tensile loads analysis was done using a conductor quarter-turn model as shown in Figure 3.2-3. From this representation of the conductor, it can be seen that the tensile stress can be found if the changes in the major and minor radii are found. The relationship between the tensile stress and the radii changes is expressed by:

$$\Delta L = 2\pi \Delta R \frac{65}{360}$$

$$\Delta l = 2\pi \Delta r \frac{90}{360}$$

$$\varepsilon_t = \frac{\Delta L + \Delta \ell}{L + l}$$

$$\sigma_t = \varepsilon_t E$$

An examination of the magnetic loads and of the coil/case structure revealed that there were four radial deflection contributions which contributed to the conductor axial strain. These contributions to the radial deflections are shown in Figure 3.2-4.

Figure 3.2-5 shows the locations where conductor axial strains/stresses were calculated and Table 3.2-II tabulates radial deflections due to each contribution and the resulting conductor axial strain. Figure 3.2-6 shows the corresponding conductor axial stress due to each contribution.

Figure 3.2-7 shows the combined conductor tensile loads due to all four effects together with the radial pressures obtained from the STANSOL analyses and the lateral pressures obtained from the pressure curves of Reference 5.

Conductor Tensile Loads Due to Layer-Layer Gapping

Gapping between conductor layers occurs due to manufacturing inaccuracies such as conductor waviness and surface irregularities. The total effect of this is taken to be a gap of 0.002 inch per layer.

THE TENSILE STRESSES CAN BE CALCULATED IF THE R'S ARE KNOWN

$$\Delta l = 2\pi \Delta R \frac{65}{360}$$

$$\delta l = 2\pi \delta r \frac{90}{360}$$

$$\epsilon_t = \frac{\Delta l + \delta l}{L + l}$$

$$\sigma_t = \epsilon_t E$$

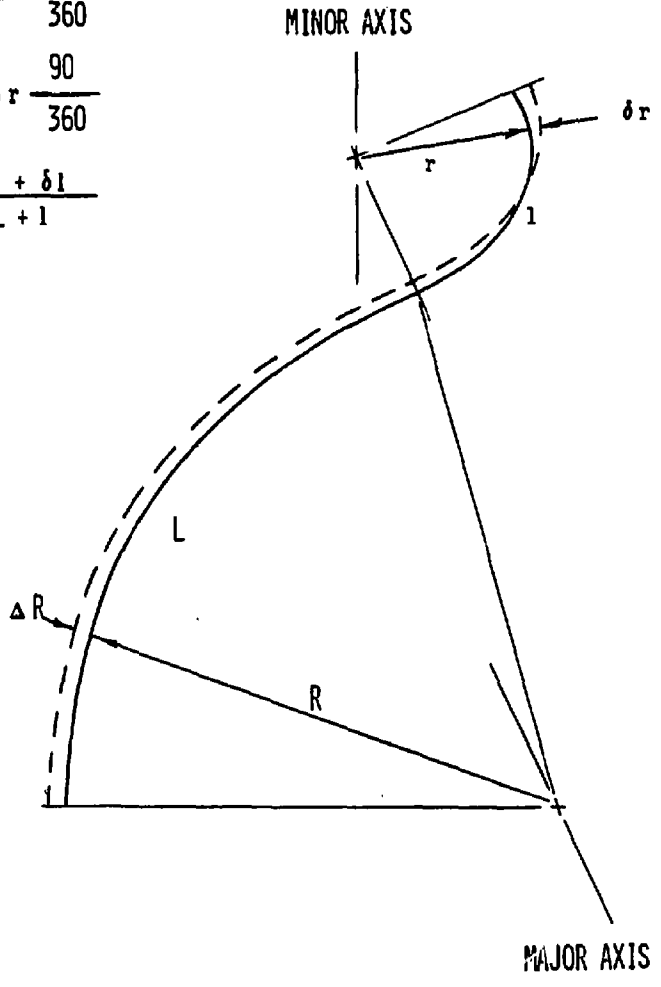

Figure 3.2-3. Conductor Quarter Turn Tensile Loads Analysis Model.

- OVERALL CASE HOOP TENSION

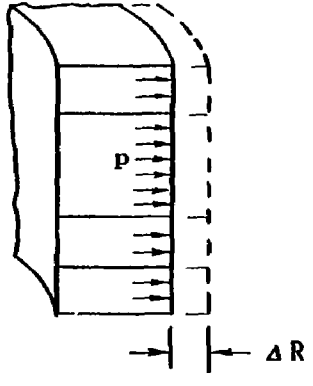

p FROM STANSOL

- LOCAL CASE DEFLECTIONS

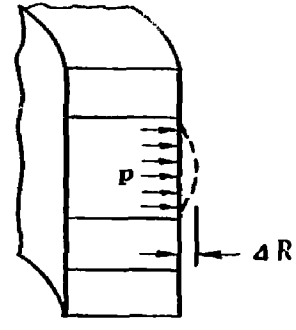

- CONDUCTOR PACK DEFLECTION

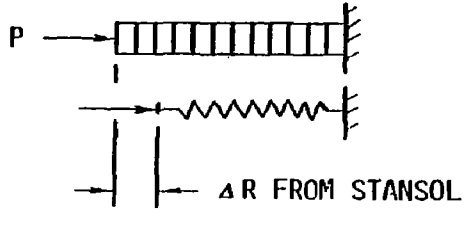

- CONDUCTOR LAYER-LAYER GAPS

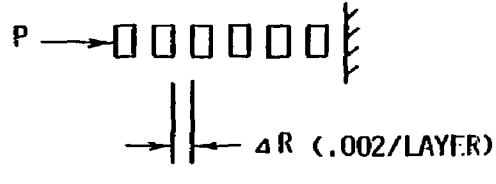

Figure 3.2-4. Effects which Contribute to Conductor Axial Strain.

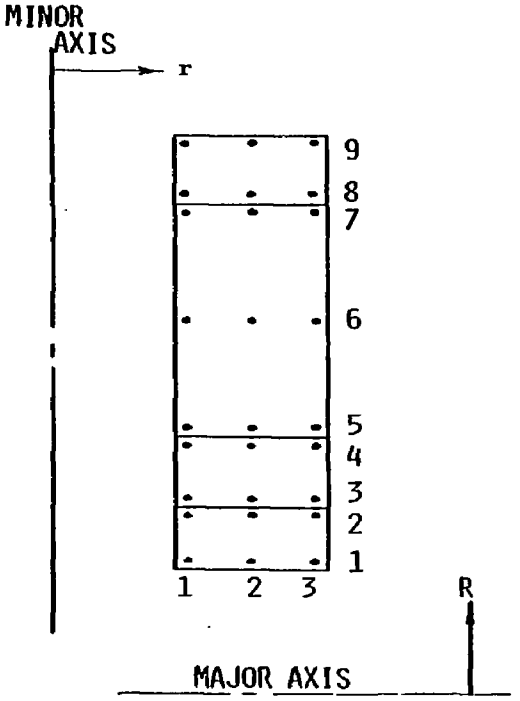

RADIUS TO CONDUCTOR ℄		CONDUCTOR QUARTER LENGTH	
r_1 =	46.05	ℓ_1 =	72.34
r_2 =	59.88	ℓ_2 =	94.06
r_3 =	73.32	ℓ_3 =	115.17
R_1 =	92.68	L_1 =	105.14
R_2 =	106.07	L_2 =	120.33
R_3 =	119.96	L_3 =	136.09
R_4 =	135.78	L_4 =	154.04
R_5 =	149.69	L_5 =	169.82
R_6 =	179.51	L_6 =	203.65
R_7 =	209.32	L_7 =	237.47
R_8 =	223.22	L_8 =	253.24
R_9 =	239.04	L_9 =	271.13

Figure 3.2-5. Geometry for Locations where Conductor Tensile Loads were Calculated.

Table 3.2-II. Conductor Tensile Strains Due to Gaps

r	R	ℓ+L	Δr	$\Delta\ell$	ΔR	ΔL	$\varepsilon = \frac{\Delta\ell+\Delta L}{\Delta r+\Delta R} \times 10^{-3}$
r_1	R_1	177.48	.066	.1037	.024	.027	.7377
	R_2	192.67			0	0	.5843
	R_3	208.43			.028	.032	.6501
	R_4	226.38			0	0	.4975
	R_5	242.16			.100	.113	.8948
	R_6	275.99			.050	.0565	.6615
	R_7	309.81			0	0	.4282
	R_8	325.58			0	0	.3033
	R_9	343.52	.066	.1037	-.028	-.032	.2103
r_2	R_1	199.20	.033	.0519	.024	.027	.4442
	R_2	214.39			0	0	.2921
	R_3	230.15			.028	.032	.4013
	R_4	248.10			0	0	.2488
	R_5	263.88			.100	.113	.6808
	R_6	297.71			.050	.0565	.4474
	R_7	331.53			0	0	.2141
	R_8	347.30			0	0	.1514
	R_9	365.24	.033	.0519	-.028	-.032	.0586
r_3	R_1	220.31	0	0	.024	.027	.1521
	R_2	235.50			0	0	0.
	R_3	251.26			.028	.032	.1526
	R_4	269.21			0	0	0.
	R_5	284.99			.100	.113	.4666
	R_6	318.82			.050	.0565	.2333
	R_7	352.64			0	0	0.
	R_8	368.41			0	0	0.
	R_9	386.35	0	0	-.028	-.032	-.0930

Table 3.2-II. Conductor Tensile Strains Due to Case Axial Loads

r	R	ℓ+L	Δr	Δℓ	ΔR	ΔL	$\varepsilon = \frac{\Delta\ell+\Delta L}{\Delta r+\Delta R} \times 10^{-3}$
r_1	R_1	177.48	.0355	.0558	.0137	.0155	.4019
	R_2	192.67					.3701
	R_3	208.43					.3421
	R_4	226.38					.3149
	R_5	242.16					.2944
	R_6	275.99					.2583
	R_7	309.81					.2301
	R_8	325.58					.2190
	R_9	343.52					.2076
r_2	R_1	199.20					.3579
	R_2	214.39					.3326
	R_3	230.15					.3097
	R_4	248.10					.2874
	R_5	263.88					.2702
	R_6	297.71					.2395
	R_7	331.53					.2151
	R_8	347.30					.2053
	R_9	365.24					.1952
r_3	R_1	220.31					.3236
	R_2	235.50					.3028
	R_3	251.26					.2838
	R_4	269.21					.2648
	R_5	284.99					.2502
	R_6	318.82					.2236
	R_7	352.64					.2021
	R_8	368.41					.1935
	R_9	386.35	.0355	.0558	.0137	.0155	.1845

Table 3.2-II. Conductor Tensile Strains Due to Local Case Defl.

r	R	ℓ+L	Δr	Δℓ	ΔR	ΔL	$\varepsilon = \frac{\Delta\ell+\Delta L}{\Delta r+\Delta R}$ $\times 10^{-3}$
r_1	R_1	177.48					
	R_2	192.67					
	R_3	208.43					
	R_4	226.38					
	R_5	242.16					
	R_6	275.99	.0570	.0895	0	0	.3243
	R_7	309.81					
	R_8	325.58					
	R_9	343.52					
r_2	R_1	199.20	0	0	.0587	.0666	.3343
	R_2	214.39	0	0	.0587	.0666	.3106
	R_3	230.15					
	R_4	248.10					
	R_5	263.88	0	0	.0258	.0293	.1110
	R_6	297.71	.0570	.0895	.0258	.0293	.3990
	R_7	331.53	0	0	.0258	.0293	.0884
	R_8	347.30					
	R_9	365.24					
r_3	R_1	220.31					
	R_2	235.50					
	R_3	251.26					
	R_4	269.21					
	R_5	284.99					
	R_6	318.82	.0570	.0895	0	0	.2807
	R_7	352.64					
	R_8	368.41					
	R_9	386.35					

Table 3.2-II. Conductor Tensile Strains Due to Pack Compression

r	R	ℓ+L	Δr	Δℓ	ΔR	ΔL	$\varepsilon = \frac{\Delta\ell+\Delta L}{\Delta r+\Delta R}$ ×10⁻³
r_1	R_1	177.48	.0347	.0545	.0083	.0094	.3600
	R_2	192.67			.0013	.0015	.2906
	R_3	208.43					
	R_4	226.38					
	R_5	242.16			.0579	.0657	.4964
	R_6	275.99			.0337	.0382	.3359
	R_7	309.81			.0017	.0019	.1820
	R_8	325.58					
	R_9	343.52	.0347	.0545			
r_2	R_1	199.20	.0168	.0264	.0083	.0094	.1797
	R_2	214.39			.0013	.0015	.1301
	R_3	230.15					
	R_4	248.10					
	R_5	263.88			.0579	.0657	.3490
	R_6	297.71			.0337	.0382	.2170
	R_7	331.53			.0017	.0019	.0854
	R_8	347.30					
	R_9	365.24	.0168	.0264			
r_3	R_1	220.31	0	0	.0083	.0094	.0427
	R_2	235.50			.0013	.0015	.0064
	R_3	251.26					
	R_4	269.21					
	R_5	284.99			.0579	.0657	.2305
	R_6	318.82			.0337	.0382	.1198
	R_7	352.64			.0017	.0019	.0054
	R_8	368.41					
	R_9	386.35	0	0			

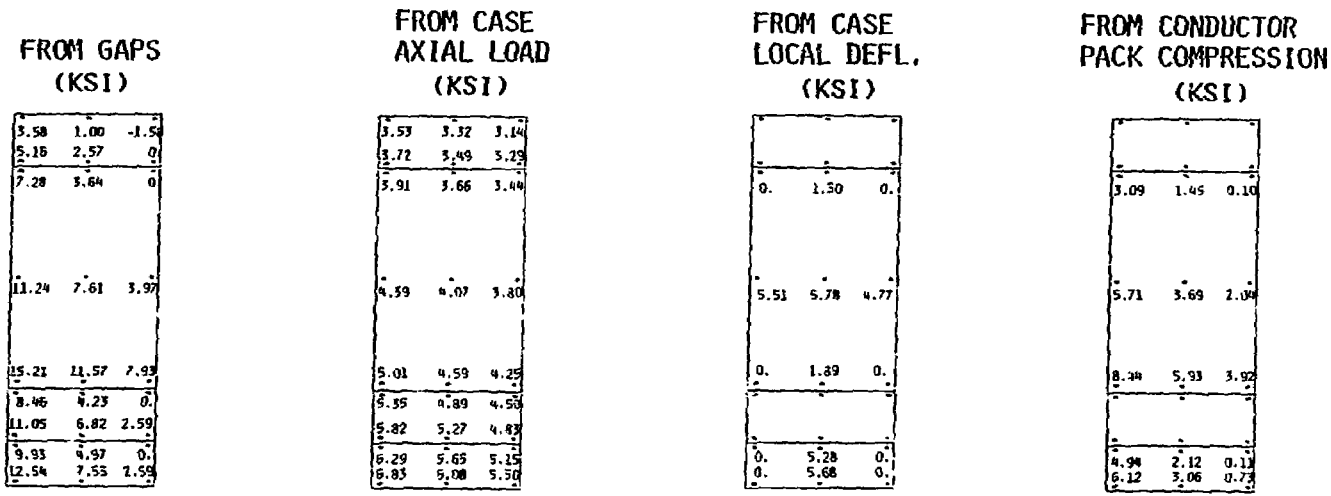

Figure 3.2-6. The Conductor Axial Stress is shown for each Contribution.

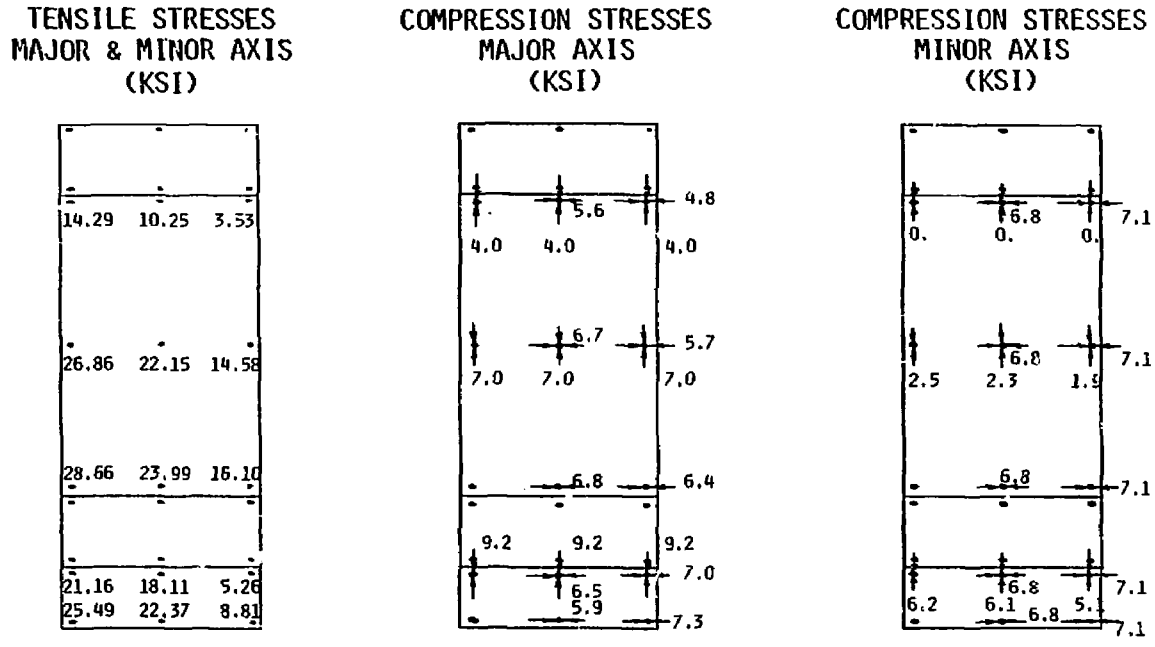

Figure 3.2-7. Conductor Total Stresses at the Major and Minor Radii.

The effect of the gaps is that the conductor can move radially through these gaps before contacting and thus transferring radial load to the case. The radial motion for the inner turn will be 0.002 inch times the number of layers and the radial motion for the outer turn will be zero. The radial motion of the remaining turns will be a linear distribution between the inner and outer turns.

For the purpose of this analysis, it was assumed that all gaps close simultaneously, i.e., no radial pressures occur in the pack until the gaps close.

3.2.4 Conductor Tensile Loads Due to Pack Compaction (STANSOL Analysis)

The STANSOL-II computer code (Reference 4) developed by Mechanics Research Inc. calculates internal loads and deflections in solenoid magnets. The STANSOL code was used here to evaluate the interacting effects of the radial pressures and hoop loads due to radial magnetic loads in the major and minor radius areas of TMNS.

The analytical models used to represent the conductor pack and case in the major and minor radius areas are shown in Figures 3.2-8 and 3.2-9. Figures 3.2-10 through 3.2-12 show the location of the line through the iso-field plots that was used to generate the field plot for each STANSOL analysis. Two items of special note to the STANSOL analyses are:

1) The outer case in each model was rigid in order to maximize the coil pressure on the case and to maximize the amount of conductor pack compression.

2) The hoop modulus of the conductors was modified to represent the flexibility of a complete conductor one turn length rather than a $2\pi R$ length as calculated by STANSOL.

A summary of the STANSOL analyses performed is given below.

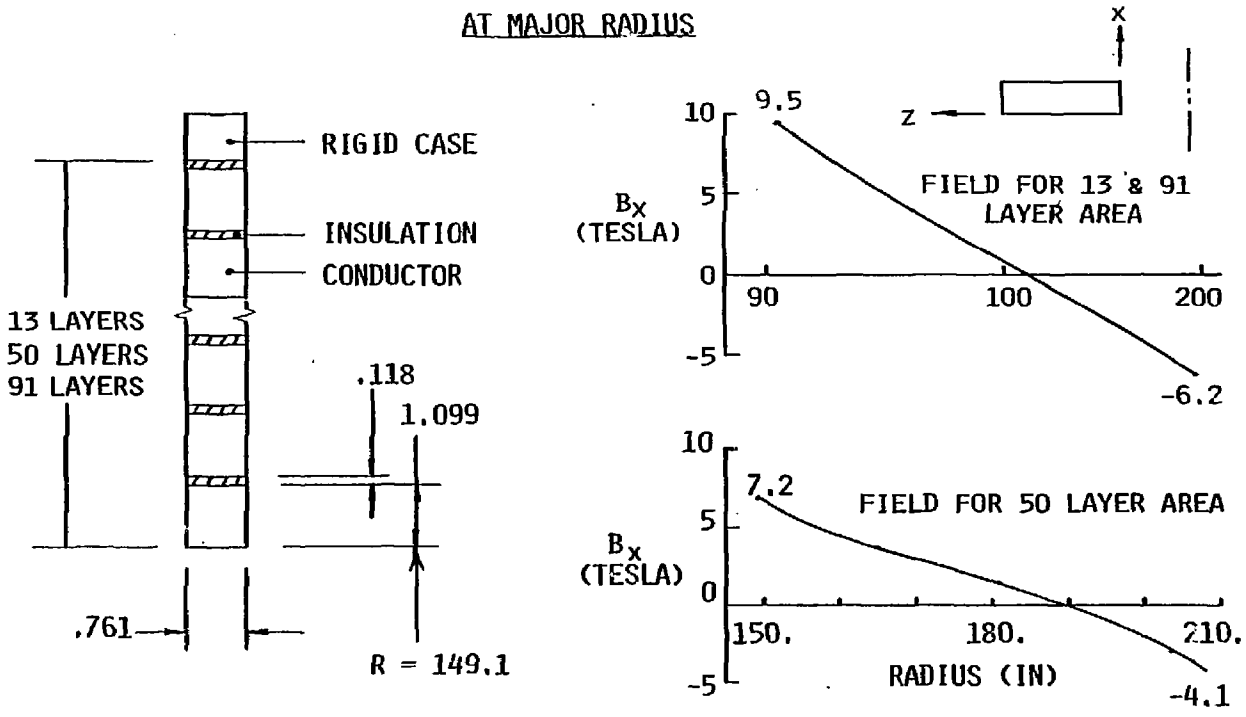

Figure 3.2-8. Conductor Pack STANSOL Model for Major Radius Area.

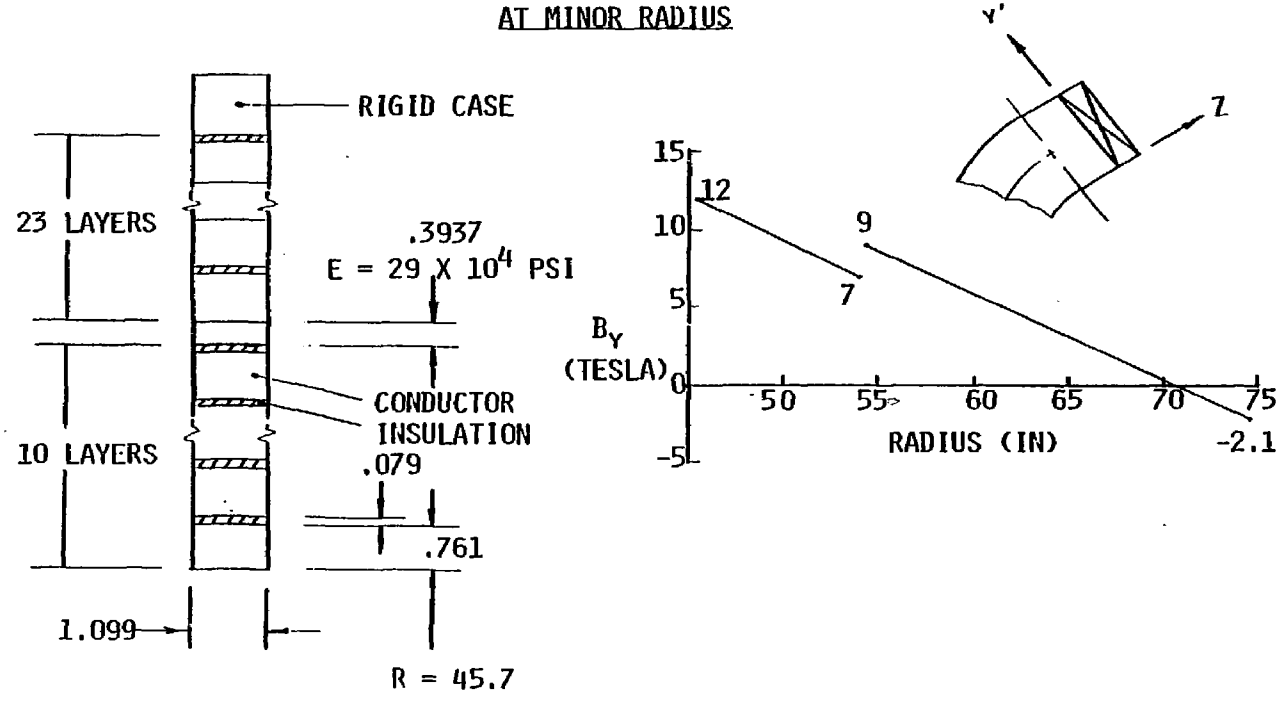

Figure 3.2-9. Conductor Pack STANSOL Model for Minor Radius Area.

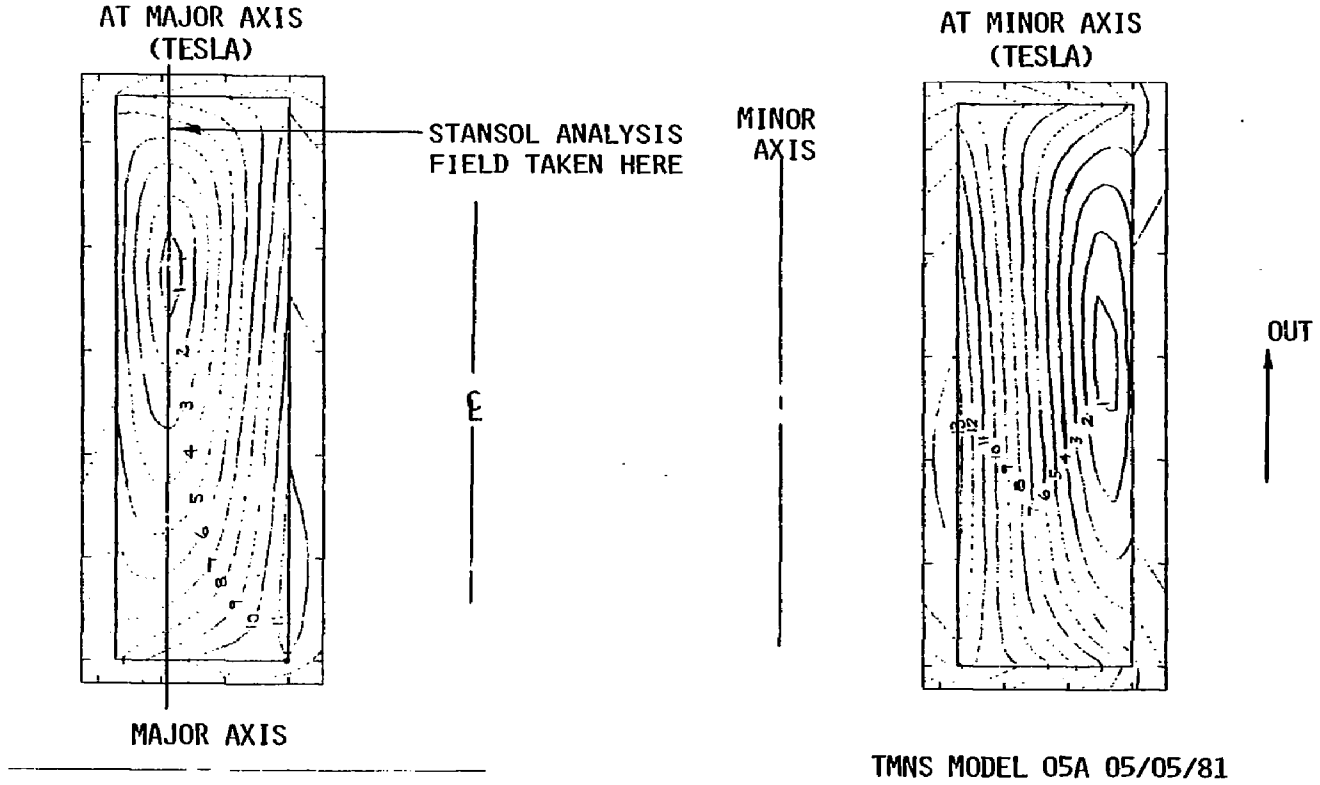

Figure 3.2-10. The Iso-Field Plots from TMNS Model 05A shows where the STANSOL 13 Layer and 91 Layer Model Magnetic Loads were Taken.

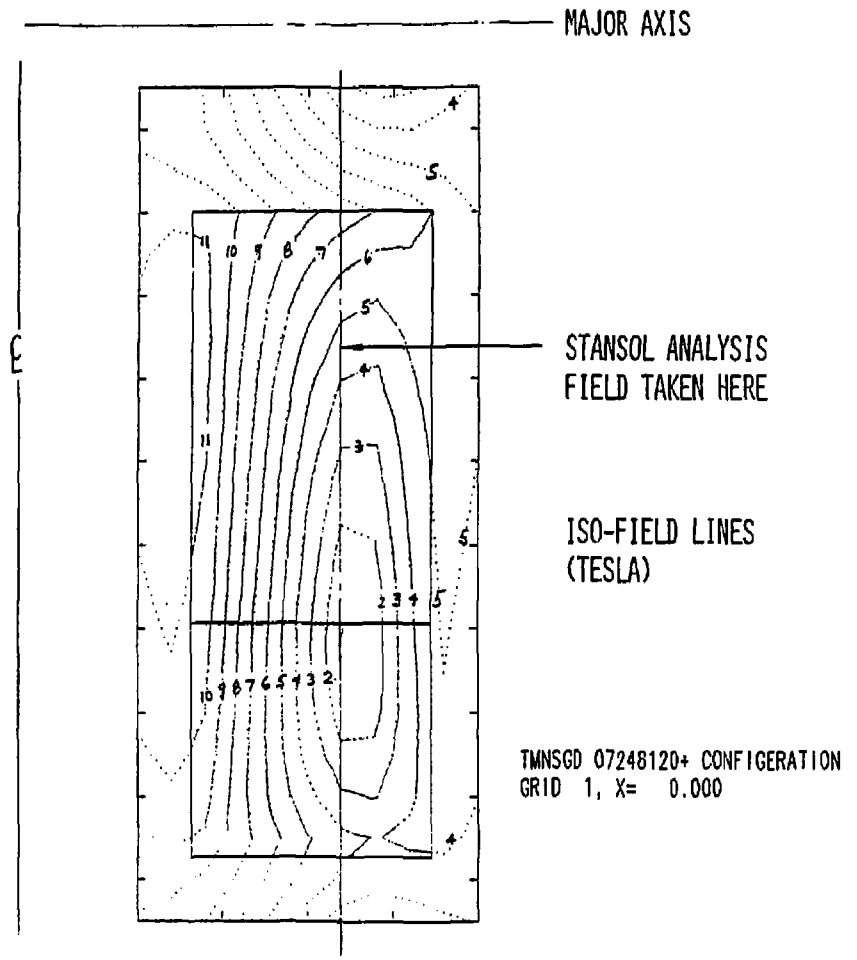

Figure 3.2-11. The Iso-Field Plots from TMNS Configuration 3 shows where the STANSOL 50 Layer Model Magnetic Loads were Taken.

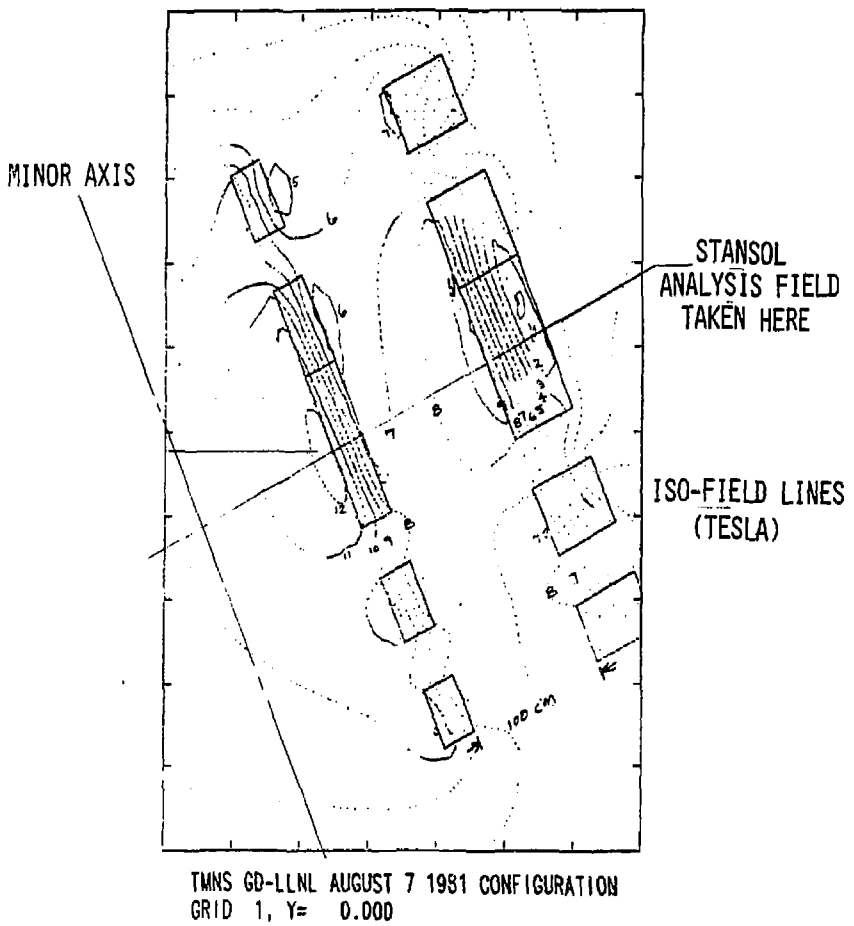

Figure 3.2-12. The Iso-Field Plots from TMNS Configuration 3 were used to Generate the STANSOL Minor Radius Model Magnetic Loads.

Area	Layers	Field	Output
Major Radius	91	Figure 3.2-10	Case pressure to generate case axial loads in major radius.
Major Radius	13	Figure 3.2-10	Case local pressure in Section 1. Conductor pack radial pressures. Conductor pack radial deflections.
Major Radius	50	Figure 3.2-11	Case local pressure in Section 3. Conductor pack radial pressures. Conductor pack radial deflections.
Minor Radius	33	Figure 3.2-12	Case pressure to generate case axial loads in minor radius. Case local pressure for all sections. Conductor pack radial pressures. Conductor pack radial deflections.

Conductor Tensile Loads Due to Case Axial Loads

The case overall axial load in the major radius area due to the magnetic pressure was calculated by STANSOL. It was assumed that this maximum pressure acts across the full width of the case.

$$P(\text{STANSOL}) = 8.27 \times 10^6 \text{ lb}$$

$$\sigma_{case} = \frac{P}{A} = \frac{8.27 \times 10^6}{3536.} \text{ psi}$$

$$= 2{,}339. \text{ psi}$$

$$\Delta R = \varepsilon R = \frac{2339.}{29. \times 10^6} (169.8)$$

$$= 0.0137 \text{ inch}$$

The case overall axial load in the minor radius area was calculated from the magnetic pressures generated by STANSOL together with one-third (estimated) of the lobe spreading force acting on the major radius areas. The portion of the lobe spreading force acting on the minor radius area is included in P(STANSOL).

$P(STANSOL) = 35.56 \times 10^6$ lb

$P(Lobe\ Spreading) = (1.253 \times 10^8/3)$ lb

$$\sigma_{case} = \frac{P}{A} = \frac{(35.56 + 41.77)}{4874.} \times 10^6 \text{ psi}$$

$$= 15{,}866. \text{ psi}$$

$$\Delta R = \varepsilon R = \frac{15{,}866.}{29. \times 10^6} (64.91) \text{ inch}$$

$$= 0.0355 \text{ inch}$$

Conductor Tensile Loads Due to Case Local Deflections

The case local deflections were calculated from a simple beam/ring model that considers the beam stiffness to be acting in parallel with the ring hoop stiffness. The pressures acting on this model were conservatively taken as being undiminished from the pressures used to calculate the case overall axial loads.

Bending Stiffness -

Assume ends are mid-way between fixed and pinned

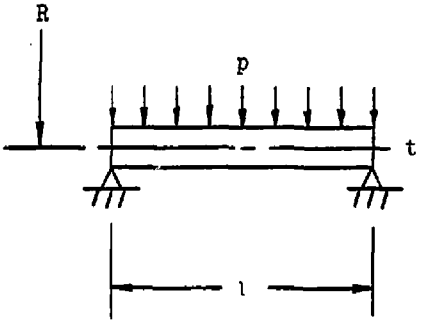

$$Y_b = \frac{3pl^4}{384\ EI}$$

Hoop Stiffness -

$$Y_h = \frac{pR^2}{Et}$$

Combined Stiffness -

$$Y_{TOT} = \frac{1}{\frac{1}{Yb} + \frac{1}{Yh}} = \Delta R$$

Area	t (in)	l (in)	p (psi)	Y_b (in)	Y_h (in)	ΔR (in)
Major Radius Section 1	8	32.4	9498.	.0661	.528	.0587
Major Radius Section 3	8	32.4	3843.	.0267	.775	.0258
Minor Radius Section 1	10	19.3	7007.	.0031	.157	.0031
Minor Radius Section 3	10	65.5	7007.	.418	.157	.114*

*This deflection was taken to be .057 inch for the remainder of the analysis under the assumption that the case could have local beef-up to reduce this deflection by one half.

3.2.5 Conductor Stress/Strain Analysis

A cross-section of TMNS conductor is shown in Figure 3.2-13 together with the lateral compressive load. The location of the conductors with critical loading was found by inspection of Figure 3.2-7 to be at (r_1,R_2), (r_1,R_5), and (r_1,R_6).

Since the stress-strain curves for the superconductor and the stabilizer are not equal, a trial and error solution was needed to determine the superconductor and stabilizer stresses. In each case, a set of stresses was found that would balance the external load and at the same time would have equal strains in the superconductor and stabilizer. It is realized that this solution would not yield a totally compatible load-deflection relationship but is a substitute for a very extensive non-linear analysis.

Table 3.2-III lists the stresses and strains for the stabilizer and conductor in each direction at each critical location.

Table 3.2-IV lists the Von Mises stresses and the integrated strain at each of the critical locations calculated from the following equations:

$$\sigma_{(\text{VON MISES})} = \frac{1}{\sqrt{2}}\left[\sigma_A^2 + \sigma_L^2 + (\sigma_A - \sigma_L)^2\right]^{\frac{1}{2}}$$

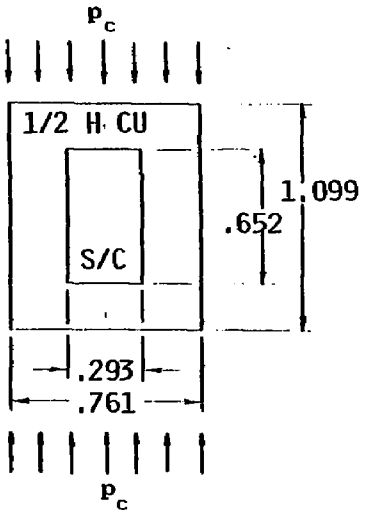

DIMENSIONS IN INCHES

CRITICAL LOCATION	σ (V.M.) COPPER (KSI)	σ (V.M.) S/C (KSI)	$\langle\epsilon\rangle$ (%)
r_1, R_2	29.9	17.4	.184
r_1, R_5	32.6	14.7	.200
r_1, R_6	34.9	18.0	.214

$$\langle\epsilon\rangle = \frac{\sqrt{2}}{2(1+\nu)}\left[(\epsilon_1-\epsilon_2)^2+(\epsilon_2-\epsilon_3)^2+(\epsilon_3-\epsilon_1)^2\right]^{1/2}$$

(1) THE STRESSES ON THE COPPER AND THE SUPERCONDUCTOR ARE DETERMINED FROM THE MATERIAL STRESS-STRAIN CURVES AT EQUAL STRAINS AND P/A REQUIRED FOR LOAD BALANCE.

(2) THE S/C STRAINS ARE CONTROLLED BY AND EQUAL TO THE COPPER STRAINS.

Figure 3.2-13. The Conductor Stresses and Strains were Calculated at the Three Critical Areas.

Table 3.2-III. Stresses and Strains in the Copper Stabilizer and Superconductor for each Load Direction.

Loc.	Dir.	P	σ_{cu}	$\sigma_{s/c}$	ε
R_2, r_1	Axial	17,697.	23.5	12.2	.120
	Long	- 7,010.	-10.2	- 7.8	-.060
R_5, r_1	Axial	23,970.	32.6	14.7	.200
	Long	0.	0.	0.	0.
R_6, r_1	Axial	22,464.	30.55	14.21	.186
	Long	- 5,304.	- 7.55	- 6.04	-.044

Table 3.2-IV. Von Mises Stresses and Integrated Strain in the Copper Stabilizer and Superconductor.

Loc.	$\sigma_{V.M.cu}$	$\sigma_{V.M.s/c}$	ε_A	ε_L	(ε)
R_2, r_1	29.94	17.41	.120	-.060	.184
R_5, r_1	32.60	14.70	.200	0.	.200
R_6, r_1	34.95	18.01	.186	-.044	.214

The ½-hard copper in the stabilizer remains essentially linear while the superconductor insert due to its annealed copper matrix is non-linear. Therefore, the strains are calculated from:

$$(\varepsilon) = \frac{\sigma_{cu}\ (\text{Von Mises})}{E_{cu}}$$

3.2.6 Superconductor Strains

The total integrated strains in the superconductor accumulated for all processes up to the time of operation are given in Table 3.2-V. The strain calculated for "straightening" is based on a reaction spool diameter of approximately 13 feet. The winding strains are calculated as follows:

$$(\varepsilon) = \frac{h}{4R} \qquad \begin{array}{l} h = \text{superconductor height} \\ R = \text{winding radius} \end{array}$$

$$= \frac{.652}{4(92.68)}$$

$$= 0.00175 \text{ in/in Major Radius}$$

$$(\varepsilon) = \frac{.293}{4(46.05)}$$

$$= 0.0016 \text{ in/in Minor Radius}$$

The range of total integrated strain for the TMNS (-.451% to +.079% including thermal strains) is compared to the HFTF conductor critical current versus strain curve, Figure 3.2-14. This would indicate that the strain range for TMNS would be acceptable since the I_c/I_{co} for this range is largely greater than 1.0. This strain range would also compare favorably with the strain/critical current curves of Reference 6. It should be noted that the accumulated strain prior to operation exceeds the 0.4% criteria if the absolute value of strain is compared. However, the relationship of current degradation to negative strains (including thermal strains) should be verified by test.

3.2.7 Case Stress Analysis

The case stresses at the critical location on the major and minor radii are shown in Figure 3.2-15. These stresses were calculated from the case radial deflections as follows:

$$\sigma_{HOOP} = \frac{\Delta R}{R} \cdot E + \sigma_{HOOP}\ (\text{Overall})$$

$$\sigma_{BEND} = \frac{\Delta R}{36} \frac{384EI}{l^2} \frac{6}{t^2}$$

(See Section 3.2.4.)

Area	ΔR (in)	σ_{HOOP} (ksi)	σ_{BEND} (ksi)	$\sigma_{V.M.}$ (ksi)
Major Radius Section 1	.0587	17.33	69.18	79.29
Minor Radius Section 3	.0570	36.36	29.03	56.76

Table 3.2-V. Superconductor Strains were Calculated for Four Quadrants of the Cross-Section for All Process Steps.

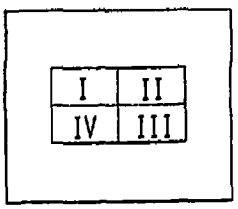

	I	II	III	IV
COOLDOWN FROM REACTION	-.3%	-.3%	-.3%	-.3%
STRAIGHTENING	-.09	-.09	+.09	+.09
WINDING	-.175	+.175	+.175	-.175
MAGNET COOLDOWN	-.1	-.1	-.1	-.1
MAGNETIC FORCES	+.214	+.214	+.214	+.214
Σ	-.451	-.101	+.079	-.271

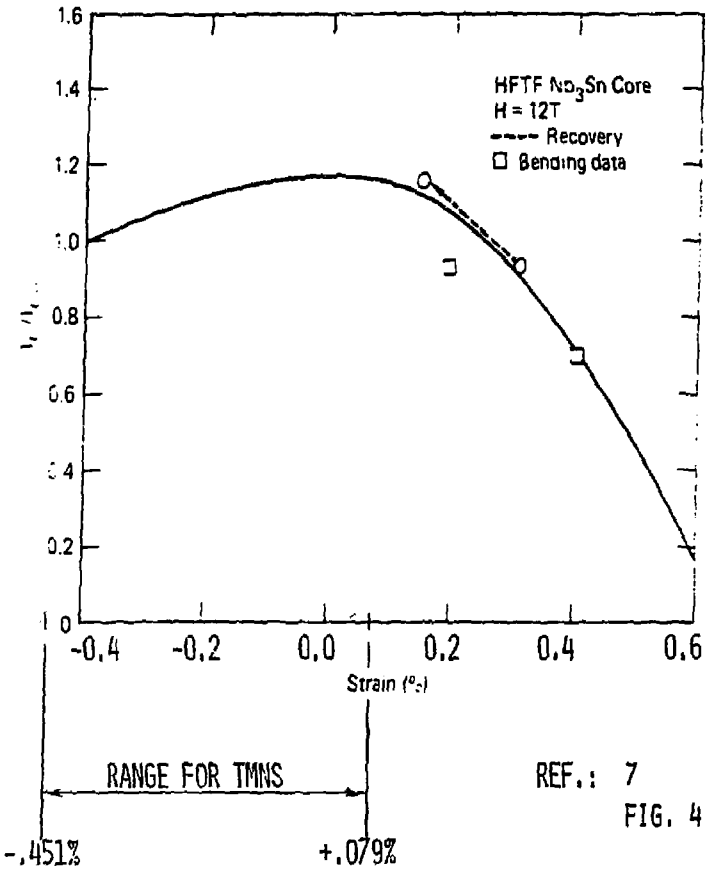

Figure 3.2-14. The TMNS Superconductor Strains were Compared to the HFTF Conductor Critical Current vs. Strain Curve.

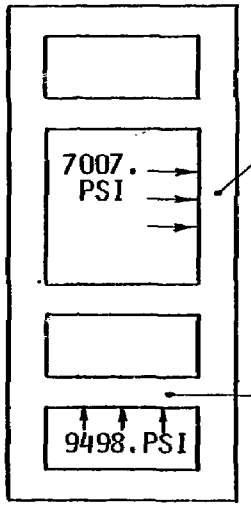

MINOR RADIUS
RADIAL LOAD
CARRIED BY
HOOP TENSION
+ PLATE BENDING

MAJOR RADIUS
RADIAL LOAD
CARRIED BY
PLATE BENDING
+ HOOP TENSION

	MAJOR RADIUS	MINOR RADIUS
% LOAD CARRIED IN HOOP	11%	73%
% LOAD CARRIED IN PLATE BEND	89%	27%
HOOP TENSION σ	17.3KSI	36.4KSI
PLATE BEND σ	69.2KSI	29.0KSI
VON MISES σ	79.3KSI	56.8KSI

MAX. HOOP LOAD IN RIGID CASE: NO WINDING GAPS

MINOR RADIUS	50.59×10^6 LB	
MAJOR RADIUS	17.25×10^6	(NO DIVISIONS)

Figure 3.2-15. The Case/Substructure Maximum Stresses we e Calculated.

3.2.8 Reconciliation of Case Loads

The following is a check to determine if overall loads on the case and conductors will check with those calculated in Section 3.2.3.

If the summation of forces is taken at a plane through the case where the major and minor axes meet, then:

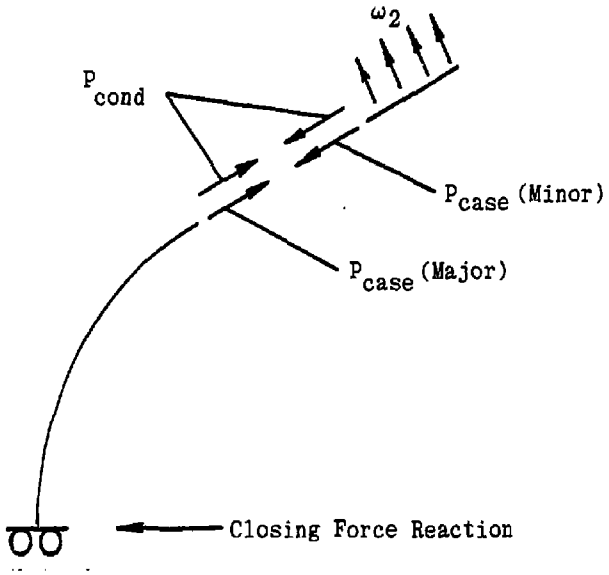

$$\text{Closing Force} = -P_{case}\,(\text{Major})\cos 25°$$

$$-\omega_2\,(\pi/2)(r_2)\cos 25°$$

$$+P_{case}\,(\text{Minor})\cos 25°$$

$$= -(8.27 \times 10^6\ \text{lb})\cos 25°$$

$$-(111.63 \times 10^3\ \text{lb/in})(59.06\ \text{in})\frac{\pi}{2}\cos 65°$$

$$+(35.56 \times 10^6\ \text{lb})\cos 25°$$

$$= 20.36 \times 10^6\ \text{lb}$$

This, however, is based on the peak loads calculated by STANSOL. If it is assumed that the ratio of the peak load to the average load here is the same as that given in Section 3.2.3, then:

$$\text{Closing Force} = -(8.27 \times 10^6 \text{ lb})\left(\frac{6724}{7030}\right) \cos 25°$$

$$-4.377 \times 10^6 \text{ lb}$$

$$+(35.56 \times 10^6 \text{ lb})\left(\frac{7687.}{8484.}\right) \cos 25°$$

$$= 17.66 \times 10^6 \text{ lb}$$

versus 17.18×10^6 lb from Section 3.2.3.

3.2.9 Conclusions

The "selected configuration" with integral case substructuring provides adequate axial strain control for the conductors. The conductor stresses and Nb_3Sn strain are within acceptable limits. The case stresses are acceptable by a preliminary analysis.

Further refinements of the case division could reduce the conductor stresses and strains. A suggested next iteration would be a combination of 12, 14, 36, and 28 layer divisions.

A loads and stress analysis which would account for friction loads between mating surfaces should be performed.

3.3 MATERIALS

The following items were considered to determine which material and/or process would be the best choice for the TMNS configuration:

- Nb_3Sn processing: Wah-Chang's "Jelly-Roll" process versus present methods.
- Solder process to prevent annealing of half-hard Cu: Indium versus Pb-SN eutectic solder.
- Selection of fiberglass/epoxy laminate for electrical insulation - G-10 versus G-10CR.

3.3.1 Nb_3Sn Processing

Wah-Chang's "Jelly-Roll" process for fabricating Nb_3Sn superconductor was evaluated. Based on the information provided by Wah-Chang, the "Jelly-Roll" process appears to be being successfully developed. The Nb_3Sn superconductor processed by "Jelly-Roll" process potentially will perform as well as the ones produced by present methods and it is expected to cost less. Half-hard CDA 10100 OFHC copper is the best combination of mechanical and thermo physical properties and solderability without softening, and is the material selected for the stabilizer.

3.3.2 Solder Process to Prevent Annealing of Half-Hard Copper: Indium Versus Pb-Sn Eutectic

Exposure of the cold-worked copper to temperatures encountered in soldering processes can anneal or soften the copper. The degree of softening depends on the temperature and the time of exposure. Also, the greater the cold reduction, the lower the softening temperature for a given time of exposure. Use of Indium (melting point 313°F) and/or Pb-Sn eutectic (melting point 361°F) was considered for soldering the superconductor to the copper stabilizer. A literature search was conducted to obtain softening data on cold worked copper. The softening data on cold-worked OFHC copper are given in Figure 3.3-1, and pertinent properties of eutectic and indium solders in Table 3.3-I. According to these data, half-hard OFHC copper anneals or softens at 625°F and loses one half of its cold-worked strength in 30 minutes. Thus use of Pb-Sn eutectic solder (melting point 361°F) to solder superconductor to stabilizer appears safe, and has been selected and is preferred to the more expensive Indium. Indium was used in superconductor to superconductor joints. In view of low mechanical strength of Indium joints, Pb-Sn eutectic soldered stabilizer to stabilizer joints were included to provide additional strength to the superconductor to superconductor joint.

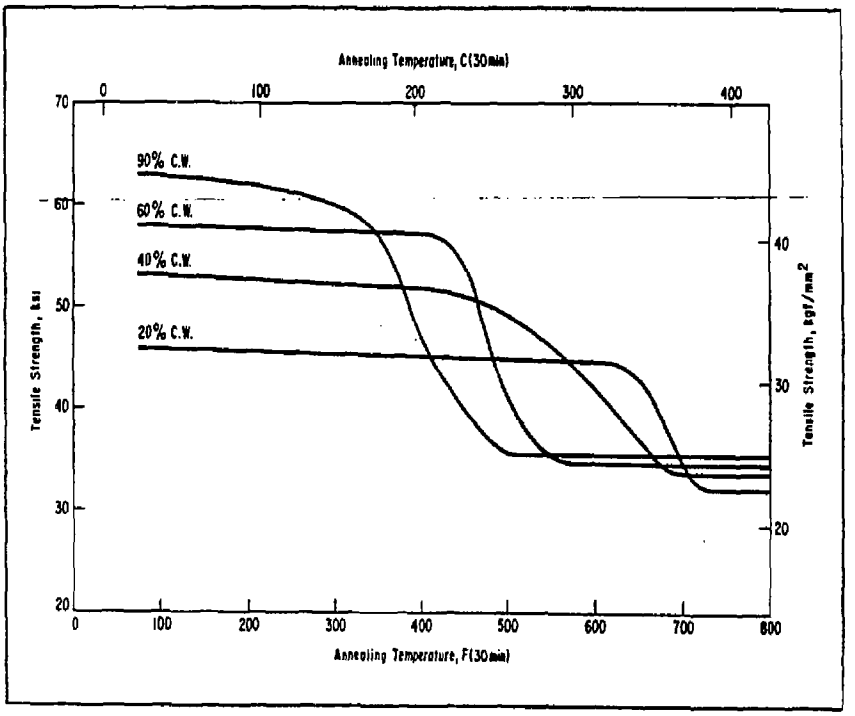

Figure 3.3-1. Softening Curves for Cold Worked OFHC Copper (AMAX Data).

3.3.3 Selection of Fiberglass/Epoxy Laminate for Electrical Insulation

The selection of G-10CR over G-10 fiberglass epoxy laminate for electrical insulation in superconducting magnets has always been challenged because of electrical, physical, and mechanical properties of G-10CR and G-10 laminates are seemingly comparable at room temperature yet G-10CR is higher in cost than G-10.

Table 3.3-I. Mechanical Solders & Physical Properties of Pb-Sn Eutectic and Indium.

	Pb-Sn Eutectic	Indium
Melting Point	361°F	313°F
Tensile Strength (Room Temp)	6,000 PSI	550 PSI
(4.2°K)	15,000	1,250 PSI (estimated)
Bond Holding Strength (Cu-Cu) (Room Temp)	23,000 PSI	890 PSI
(4.2°K)	58,000 PSI (estimated	2,000 PSI (estimated)
Thermal neutron cross-section	Pb 170 mb Sn 600 600 mb	190 barn

In the service environment of the TMNS magnet, such cost reduction attainable by using G-10 rather than G-10CR becomes impractical. Since G-10 laminate varies in formulation and processing, the mechanical properties of the laminate at cryogenic temperatures also vary. G-10CR is fabricated based on a non-proprietary resin formulation and process. Variation in G-10CR laminate properties is minimized. G-10CR laminates fabricated by different manufacturers have shown uniformly good mechanical properties and radiation resistance at cryogenic temperatures. We feel that such reliability is hardly worth sacrificing when the cost difference between G-10CR and G-10 laminate is only 4% to 10%. Therefore, we selected G-10CR for the TMNS cost estimate.

3.4 ELECTROMAGNETIC ANALYSIS

3.4.1 Conductor Quench Protection

The conductor adiabatic temperature rise in the event of an emergency dump has been calculated. This calculation was performed using GDC's computer program SUPERQ. A brief description of SUPERQ is given in Appendix D.

One parameter that SUPERQ requires as input is the total stored energy of the magnet. For this calculation, the self and mutual inductances of the nested coils are needed. LLNL provided these values calculated by their computer program EFFI. The inductance matrix and a brief description of the calculation is given in Appendix E. A tabulation of these inductances, in Henries, is given in Table 3.4-I. With these inductance values, the stored energies in the coils were calculated as listed in Table 3.4-II.

The stored energies given in Table 3.4-II are larger than the stored energies originally contemplated when the present 3 nested coil configuration illustrated in Figure 3.4-1 was selected. At that time, a 13,000 A conductor and a total stored energy in one half of the coil of 5000 MJ were envisioned. Since the inductances were not known, the stored energy was simply distributed equally among the three coils, 1667 MJ, and this value was used for the calculation of the temperature rise. The temperature was calculated to be an acceptable value of 220 K and so the decision was made to consider the magnet as comprised of three nested coils. However, since that time, the conductor parameters have changed slightly and the current has increased to 15,600 A. This necessitated a re-calculation of the conductor adiabatic temperature rise.

A calculation of the temperature rise in coil E2 using these new conductor parameters showed that with its large stored energy (2900 MJ), the temperature rise was excessive, about 500 K. A calculation of the temperature of the conductor in coil E1, with only 1520 MJ of stored energy, results in a maximum temperature of 266 K. However, even this rise is too high since the strains introduced are beyond the elastic limit of the conductor. Stress analysis shows that the temperature increase must be kept below 200 K. Therefore, it was concluded that the present configuration of three nested coils was not acceptable. Without further detailed analysis, precisely how many coils are required is not known. However, it seems certain that 5, or at most 6, nested coils would keep the conductor temperature below a safe value of 200 K.

The input data for SUPERQ in this calculation for coil 1 is presented in Figure 3.4-2. Figure 3.4-3 gives the numerical results of the calculation and Figures 3.4-4 to 3.4-9 present the time and temperature dependence of the various parameters calculated by SUPERQ.

Table 3.4-I. Self and Mutual Inductances of the 3 Nested Coils in Henries.

	COIL NO.	E1	E2	E3	YANG COMPOSITE
YIN	E1	5.52			
	E2	3.33	12.1		
	E3	1.66	6.53	13.0	
	YANG COMPOSITE	1.99	1.86	1.46	49.5

THE YANG COMPOSITE COIL IS THE OTHER HALF OF THE YIN-YANG PAIR, AND IS MODELED AS ONE COIL.

Table 3.4-II. Stored Energy of the 3 Nested Coils, in M.J.

	COIL NO.	YIN E1	YIN E2	YIN E3	YANG COMPOSITE
YIN	E1	671	405	202	242
	E2	405	1470	794	226
	E3	202	794	1590	178
	YANG COMPOSITE	242	226	178	6020
	TOTAL ENERGY ASSOCIATED WITH EACH MAGNET	1520	2900	2760	6670

THE YANG COMPOSITE COIL IS THE OTHER HALF OF THE YIN-YANG PAIR AND IS MODELED AS ONE COIL.

SEE DWG. TMNS-017 FOR COIL CONFIGURATION

COIL	NO. OF TURNS
E1	858
E2	1056
E3	1056
YANG COMPOSITE	2970

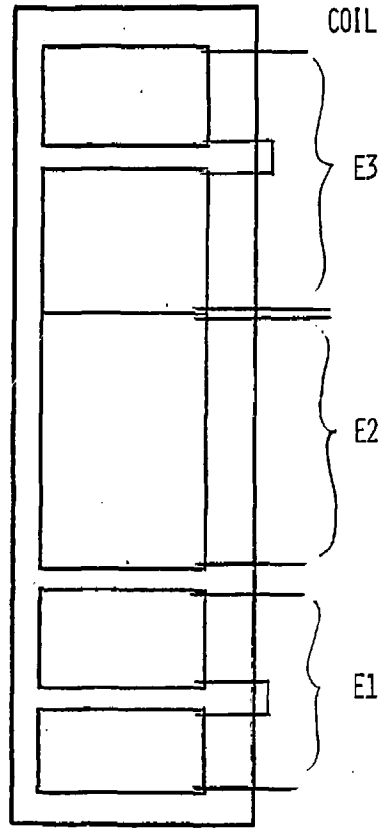

Figure 3.4-1. Quench Analysis was Based on Three Electrical Subdivisions per Coil.

OPERATING CURRENT =	15600.	(AMPS)
MAXIMUM DISCHARGE VOLTAGE =	1000.	(VOLTS)
OVERALL CURRENT DENSITY =	2337.	(AMPS/SQ. CM)
MAGNETIC ENERGY =	1520.00000	(MEGAJOULES)
CRITICAL TEMPERATURE =	5.0	(DEG K)
NORMAL ZONE LENGTH =	300.	(CM)
NORMAL ZONE TRIGGER VOLTAGE =	.00100	(VOLTS)
DELAY =	10.00000	(SEC)
SELF FIELD =	12.00000	(TESLA)
BACKGROUND FIELD =	0.00000	(TESLA)
FIELD ANGLE =	0.00000	(DEGREES)
CU/SC RATIO =	9.7	
PACKING FRACTION =	.80770	
RRR =	97.	

AREA OF UNIT CELL =	6.67522	(SQ. CM)
AREA OF CONDUCTOR =	5.39158	(SQ. CM)
AREA OF COPPER =	4.88769	(SQ. CM)
DUMP RESISTANCE =	.00410	(OHMS)
INDUCTANCE =	12.49178	(HENRIES)

SEE DWG. TMMS-017 FOR COIL CONFIGURATION

Figure 3.4-2. Input Data for TMNS SUPERQ Computer Run.

CURO =	15600.	RRR =	97.	TIMEM =	7.64E+02
VMAX =	1000.	RHOF =	1.55E-08	TC =	5.0
HEN =	12.49	RHOZ =	1.59E-08	DT =	1.00
A =	4.8877	XLN =	300.00	DELAY =	1.00E+01
XJ =	2337.	REX =	.8641	TD =	44.0
SWTDLY =	10.000	VDUMP =	1.000E-03	TMAX =	266.0
BMAG1 =	12.00	BMAG2 =	0.00	THE12 =	0.00

TEMP	TIME	CURRENT	VLTGN	VLTGD	POWER	ENERGY	TAU	RESISTIVITY
5.00	0.	1.000	6.94E-02	0.	1.08E+03	1.000	2.81E+06	7.25E-08
15.00	1.786E-01	1.000	7.02E-02	0.	1.10E+03	1.000	2.77E+06	7.34E-08
25.00	1.374E+00	1.000	7.38E-02	0.	1.15E+03	1.000	2.64E+06	7.71E-08
35.00	4.833E+00	1.000	8.48E-02	0.	1.32E+03	1.000	2.30E+06	8.85E-08
45.00	1.078E+01	.997	1.08E-01	9.97E+02	1.65E+07	.993	1.96E+02	1.13E-07
55.00	1.847E+01	.958	1.37E-01	9.58E+02	1.43E+07	.918	1.95E+02	1.50E-07
65.00	2.715E+01	.916	1.73E-01	9.16E+02	1.31E+07	.839	1.95E+02	1.98E-07
75.00	3.622E+01	.875	2.17E-01	8.75E+02	1.19E+07	.765	1.95E+02	2.59E-07
85.00	4.534E+01	.835	2.59E-01	8.35E+02	1.09E+07	.696	1.95E+02	3.24E-07
95.00	5.457E+01	.796	2.96E-01	7.96E+02	9.89E+06	.633	1.95E+02	3.89E-07
105.00	6.397E+01	.758	3.30E-01	7.58E+02	8.98E+06	.575	1.95E+02	4.54E-07
115.00	7.363E+01	.722	3.59E-01	7.22E+02	8.13E+06	.521	1.95E+02	5.20E-07
125.00	8.346E+01	.686	3.85E-01	6.86E+02	7.35E+06	.471	1.95E+02	5.86E-07
135.00	9.351E+01	.652	4.07E-01	6.52E+02	6.63E+06	.425	1.95E+02	6.51E-07
145.00	1.041E+02	.617	4.24E-01	6.17E+02	5.95E+06	.381	1.95E+02	7.18E-07
155.00	1.153E+02	.583	4.37E-01	5.83E+02	5.30E+06	.340	1.95E+02	7.84E-07
165.00	1.271E+02	.548	4.46E-01	5.48E+02	4.70E+06	.301	1.95E+02	8.50E-07
175.00	1.398E+02	.514	4.51E-01	5.14E+02	4.12E+06	.264	1.95E+02	9.17E-07
185.00	1.535E+02	.479	4.51E-01	4.79E+02	3.58E+06	.229	1.95E+02	9.83E-07
195.00	1.687E+02	.443	4.45E-01	4.43E+02	3.06E+06	.196	1.95E+02	1.05E-06
205.00	1.857E+02	.406	4.34E-01	4.06E+02	2.57E+06	.165	1.95E+02	1.12E-06
215.00	2.052E+02	.367	4.16E-01	3.67E+02	2.11E+06	.135	1.95E+02	1.18E-06
225.00	2.284E+02	.326	3.90E-01	3.26E+02	1.66E+06	.106	1.96E+02	1.25E-06
235.00	2.574E+02	.281	3.54E-01	2.81E+02	1.23E+06	.079	1.95E+02	1.32E-06
245.00	2.968E+02	.229	3.03E-01	2.29E+02	8.21E+05	.053	1.95E+02	1.39E-06
255.00	3.684E+02	.165	2.29E-01	1.65E+02	4.28E+05	.027	1.95E+02	1.45E-06
265.00	5.767E+02	.056	8.11E-02	5.60E+01	4.90E+04	.003	1.95E+02	1.51E-06
266.00	7.642E+02	.028	4.01E-02	2.76E+01	1.19E+04	.001	1.95E+02	1.52E-06

SEE DWG. TMNS-017 FOR COIL CONFIGURATION

Figure 3.4-3. SUPERQ Output for Selected TMNS Configuration.

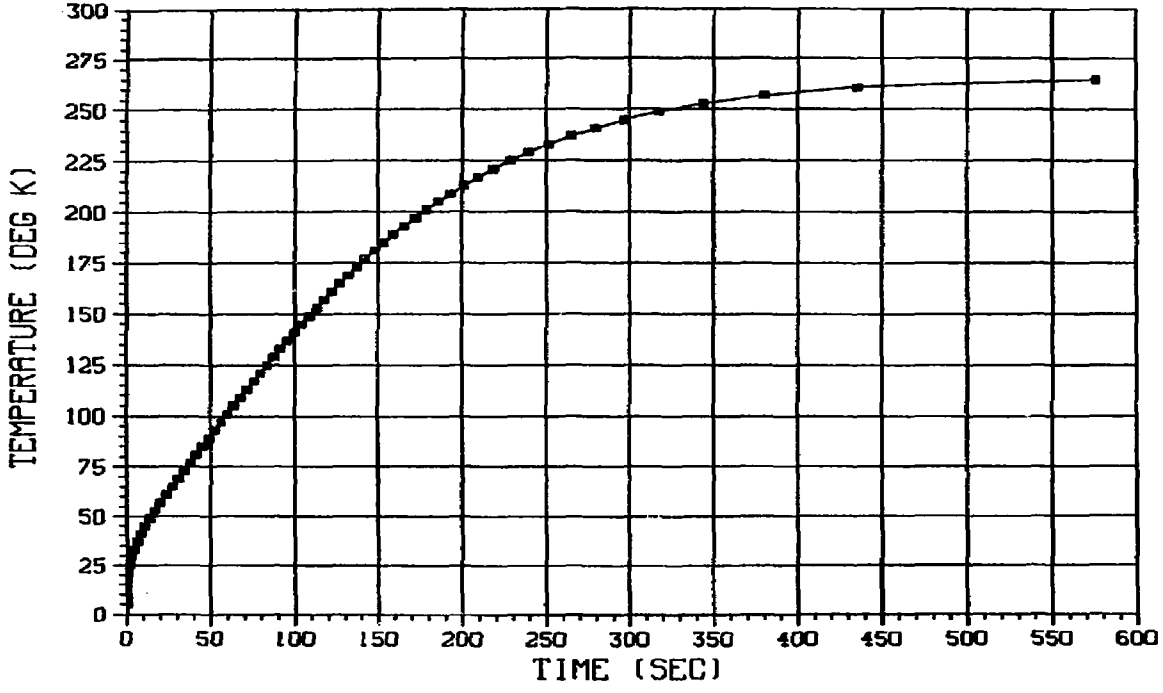

SEE DWG. TMNS-017 FOR COIL CONFIGURATION

Figure 3.4-4. Temperature vs. Time for TMNS Selected Configuration.

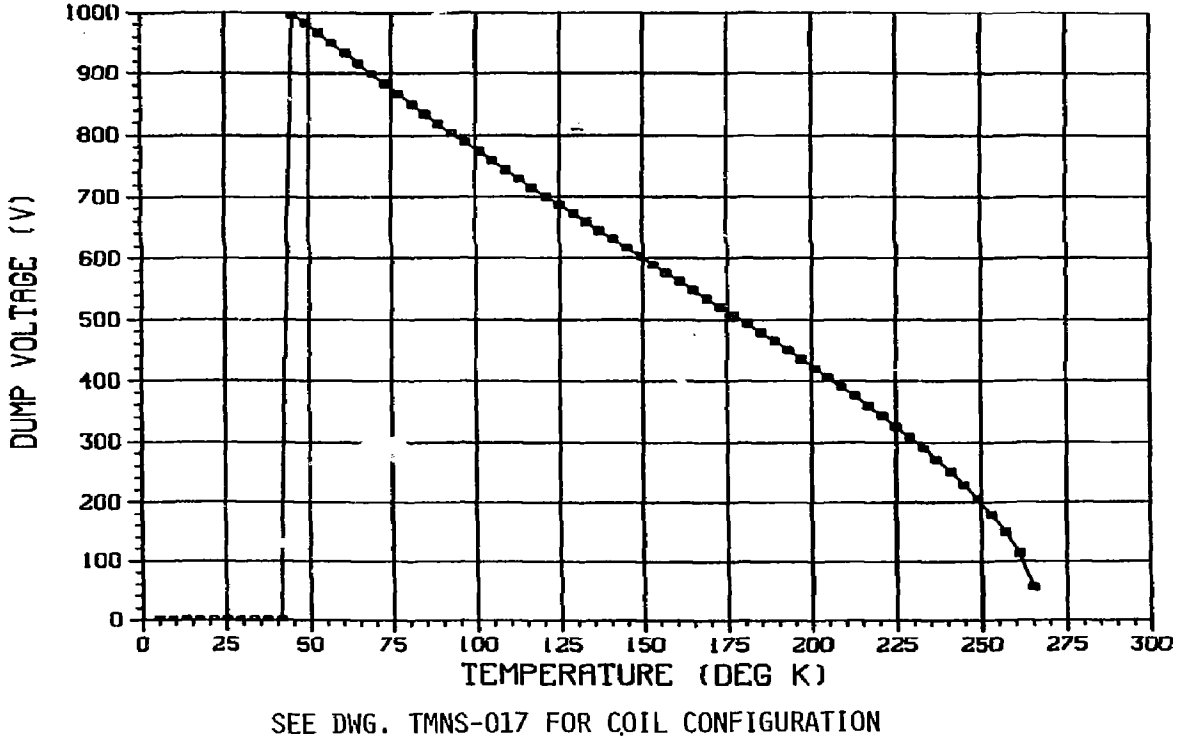

Figure 3.4-5. Voltage vs. Temperature for TMNS Selected Configuration.

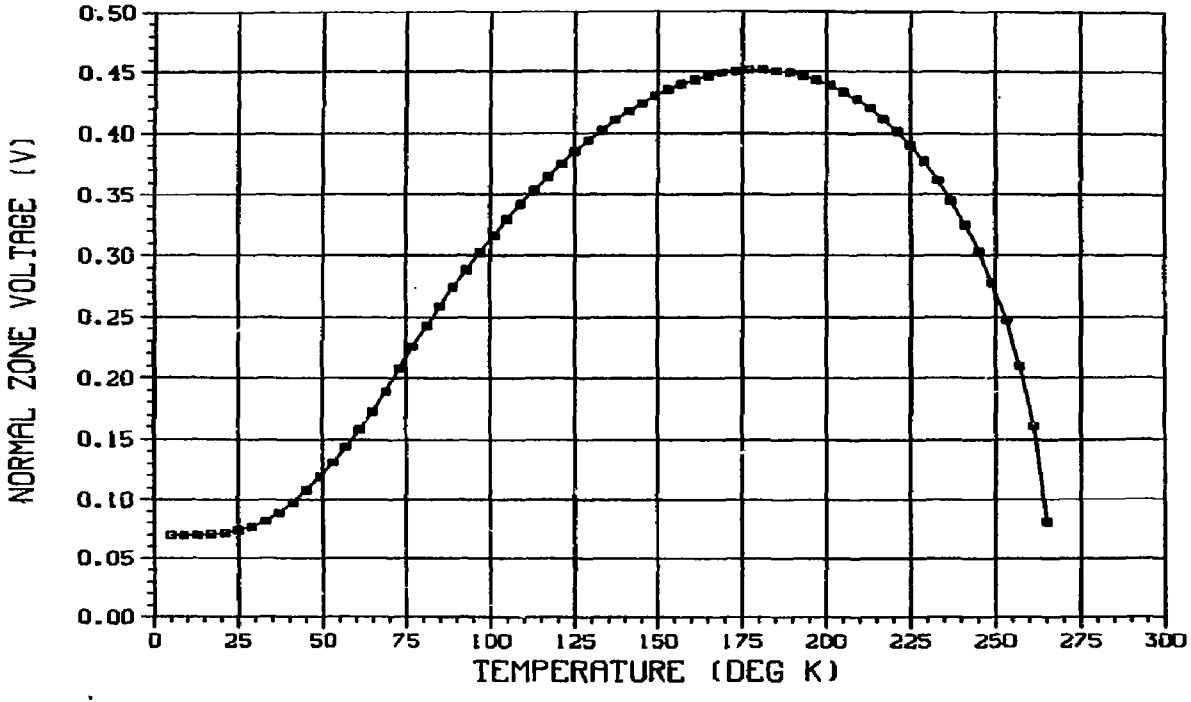

SEE DWG. TMNS-017 FOR COIL CONFIGURATION

Figure 3.4-6. Voltage vs. Temperature for TMNS Selected Configuration.

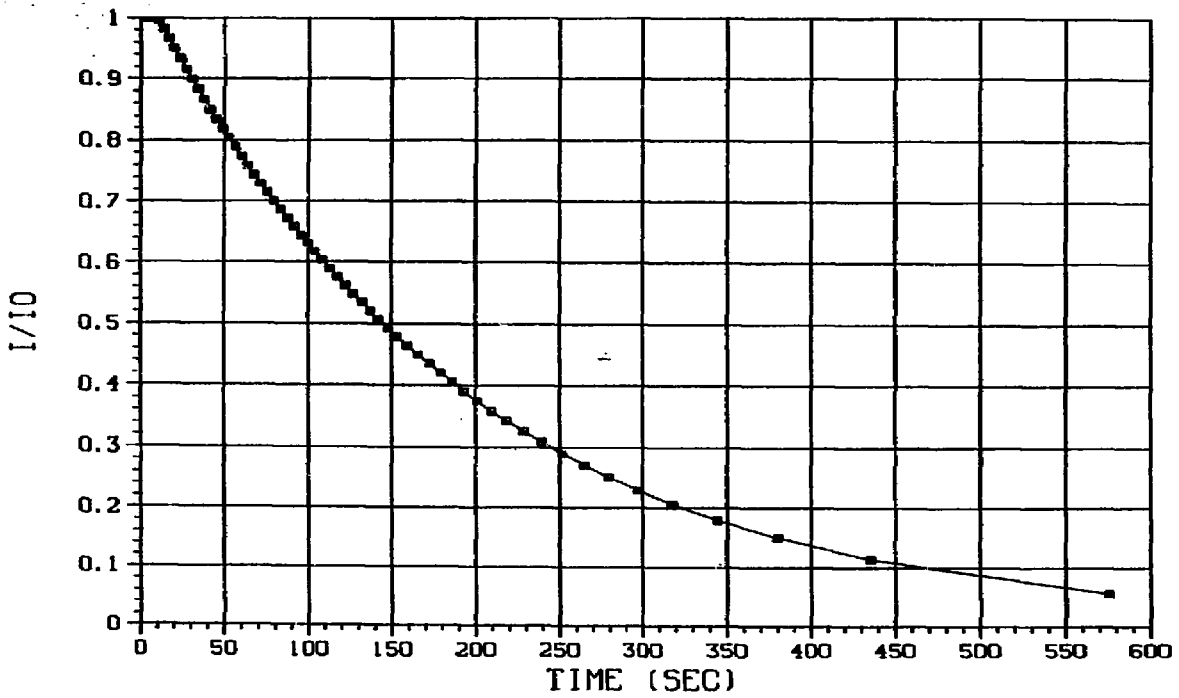

SEE DWG. TMNS-017 FOR COIL CONFIGURATION

Figure 3.4-7. Current vs. Time for TMNS Selected Configuration.

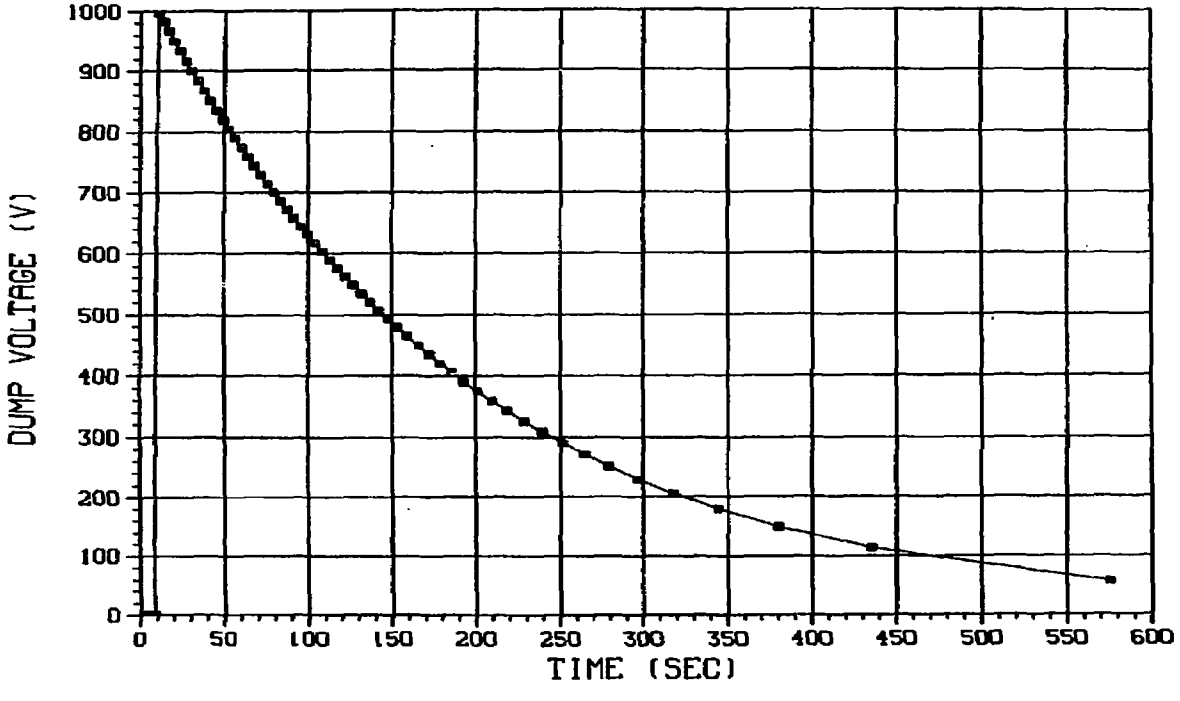

SEE DWG. TMNS-017 FOR COIL CONFIGURATION

Figure 3.4-8. Voltage vs. Time for TMNS Selected Configuration.

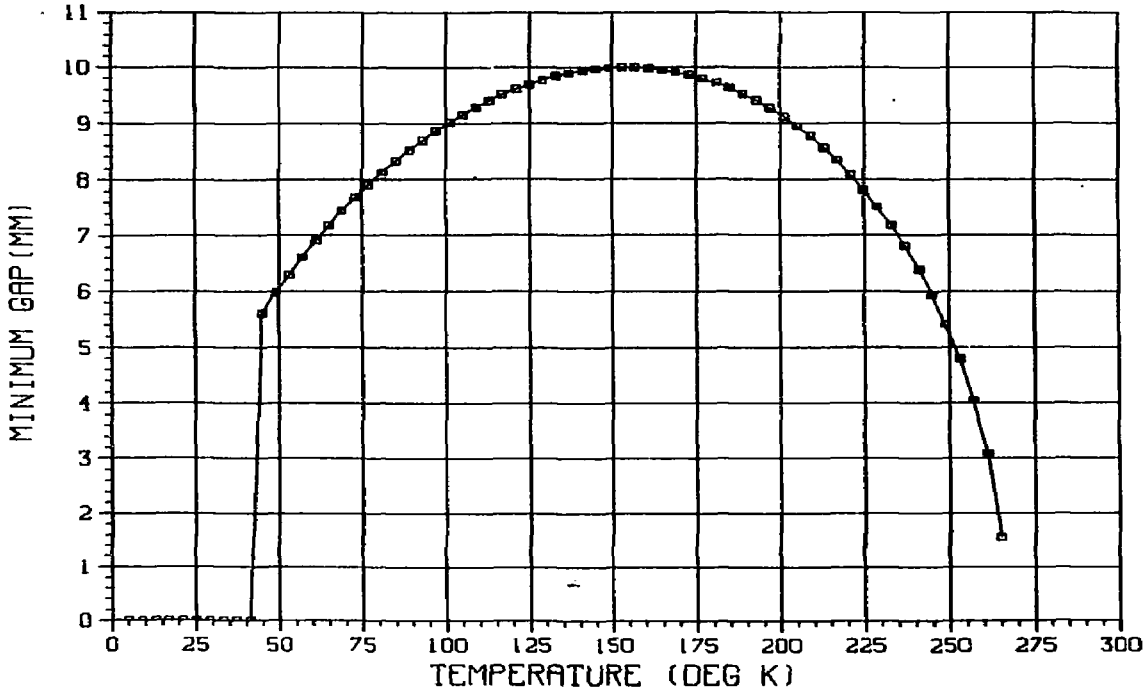

SEE DWG. TMNS-017 FOR COIL CONFIGURATION

Figure 3.4-9. Min. Gap vs. Temperature for TMNS Selected Configuration.

The objective of the quench temperature calculations reported in this section was to determine what quench voltage would be required for each of the nested coils comprising the magnet, in the event of an emergency dump, which would result in a temperature rise less than 200 K, for the conductor in any one of the coils. A further restriction is that the dump voltage, for all the coils, be no larger than 1000 V.

The results of the calculations presented here show that three nested coils are not sufficient to satisfy these requirements. To determine exactly how many nested coils must be used one would proceed in the following fashion. From the number of turns and the geometrical configuration of the chosen nested coils, one must first calculate the self and mutual inductances of the coils. From these inductances the total stored energy associated with each of the coils can be calculated. Since it would be advantageous to make the stored energy in each coil as nearly equal as possible one should choose the number of turns in each coil so as to make the self inductances as nearly equal as possible.

Knowing the stored energy one can then calculate the conductor adiabatic temperature rise using SUPERQ, assuming a given dump voltage. This procedure can be iterated until the temperature rise is less than 200 K for all coils and the dump voltage is 1000 V or less for each coil.

One other consideration should be mentioned. In conjunction with these calculations it is necessary that the current behavior as a function of time, for each of the coils, be also investigated. The presence of the closely coupled coils results in an increase of the time constant for a dumped coil. This increase in effective time constant results in an increase in the conductor temperature. This effect, though relatively small, should be taken into account in this iterative calculation.

3.4.2 Parallel Winding Analysis

As mentioned in Section 3.4.1, each half of the Yin-Yang coil must be separated electrically into 5, or at most 6, nested coils in order to keep the conductor adiabatic temperature rise below 200K, when using a dump voltage of 1000V. However, the analysis presented here was done for the baseline configuration of 3 nested coils.

Figure 3.4-10 represents a cross-section of the conductor pack and schematically shows the winding geometry of the three coils. The number of turns in each coil is also given. The Yang composite is the other half of the Yin-Yang pair and is modeled as one coil.

Each of the three coils will have its own power supply and dump resistor. Using the self and mutual inductances given in Table 3.4-I, the temporal behavior of the currents during an emergency dump were calculated using the computer program SPICE. A brief description of SPICE is given in Appendix D.

The dump analysis was carried out in the following fashion. At initiation of the dump, all the magnet power supplies are turned off. The current of that magnet that is being dumped is allowed to circulate through an appropriately sized dump resistor. For these nested coils, the same value of dump resistor was used for each coil, 0.0641 ohms, which sets a maximum dump voltage of 1000 V. The current in those coils that are not dumped is allowed to "free wheel" through a diode with a voltage drop of about 1 volt, and therefore, will start to decay with a very long time constant. SPICE calculates and plots the current in each coil as a function of time after initiation of the dump.

The case where only coil E1 was dumped was investigated first. The currents in the four coils are plotted in Figures 3.4-11 - 3.4-14 for the first 500 seconds after initiation of the dump. From Figure 3.4-12, it can be seen that the current in coil E2 reaches a peak value of 19,500 A in about 240 sec., or a current increase of about 3900 A. The current in coil E3 shows no increase in current whatever, and the current in coil E4 shows an increase in current of only about 390 A. The induced currents in coils E3 and E4 are small enough that they lead neither to a quench condition of the conductors nor do they pose a threat to the structural integrity of the coils.

The 25% increase in current in coil E2 has greater, possibly more serious consequences. First, this large an increase in current could possibly drive the conductor above its critical current limit. Second, this enhancement of the current could lead to a large increase in the electromagnetic loads acting on coil E2.

COIL	NO. OF TURNS
E1	858
E2	1056
E3	1056
* YANG COMPOSITE	2970

* THE YANG COMPOSITE IS MODELED AS ONE COIL

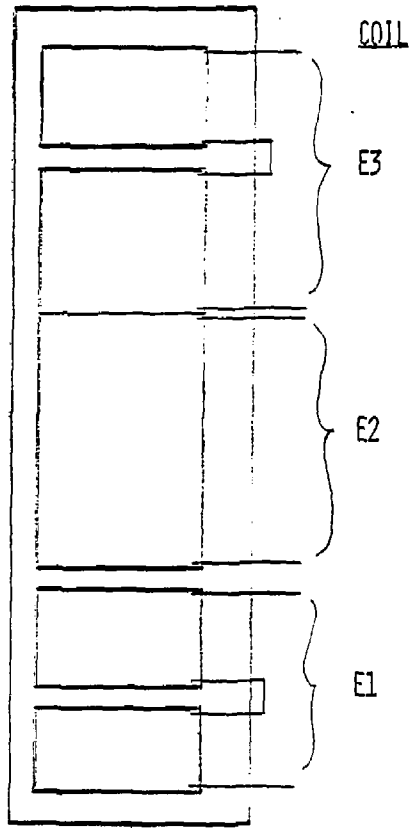

Figure 3.4-10.. Electrical Schematic of Coil Cross-Section used in Electrical Analysis.

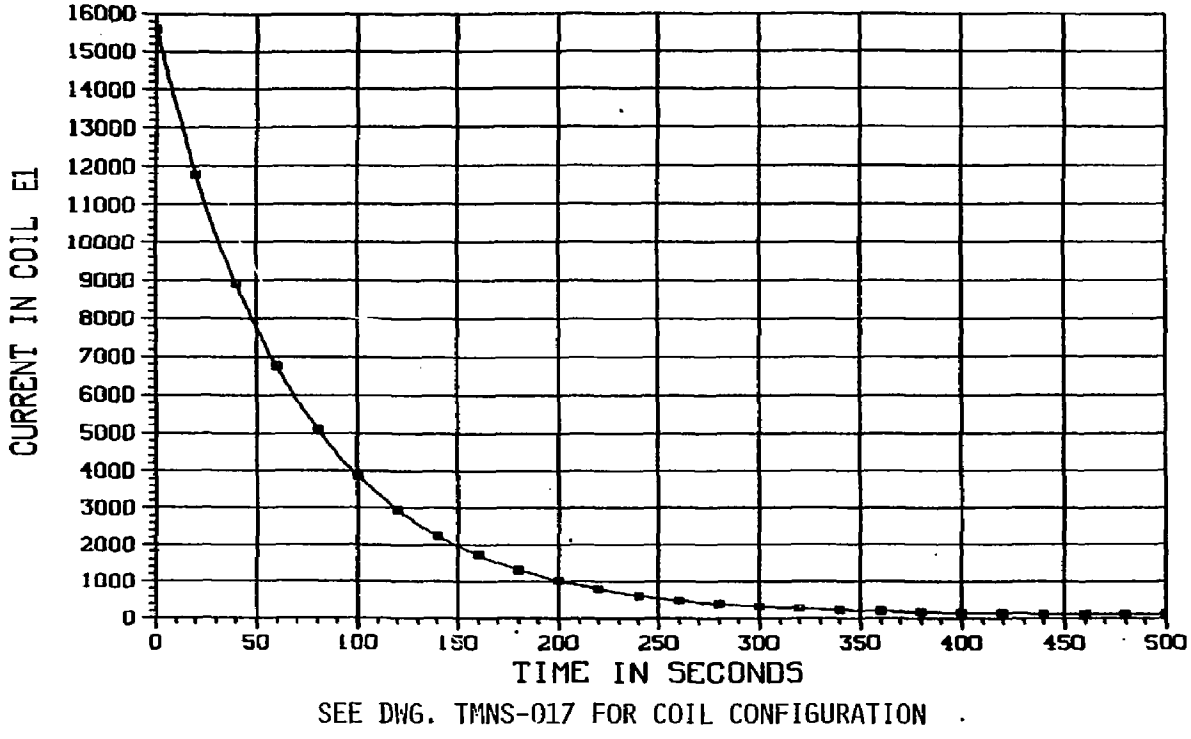

Figure 3.4-11. TMNS Induced Currents for Selected Configuration and Dump of Coil E1.

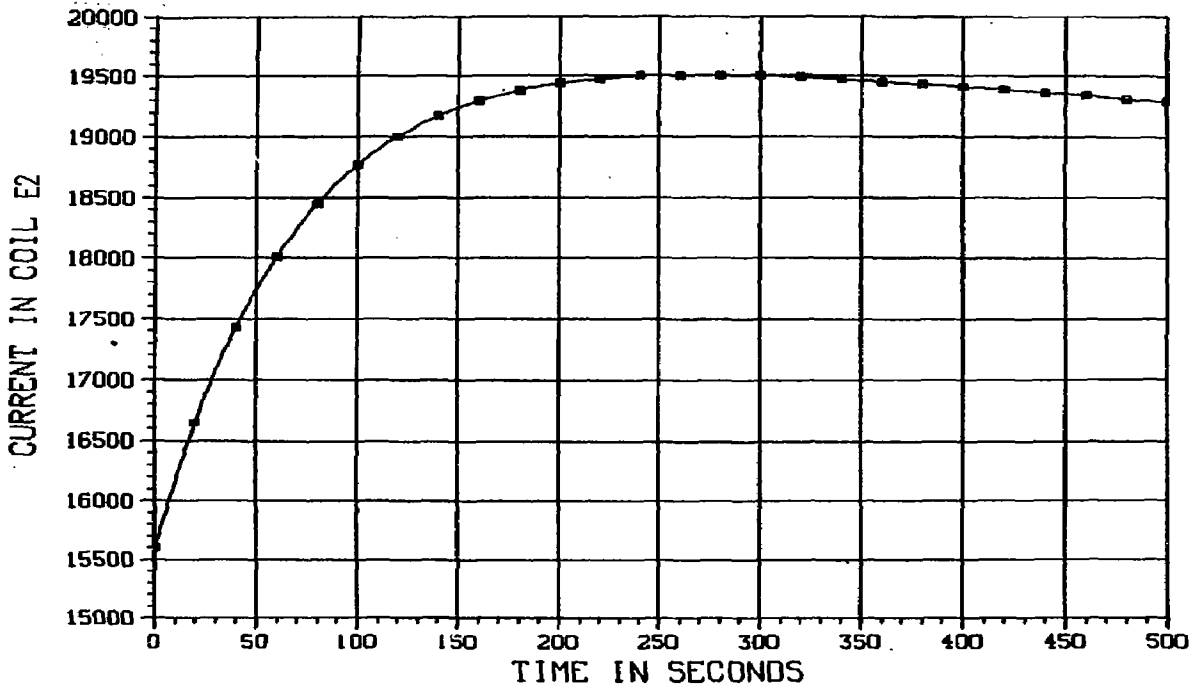

Figure 3.4-12. TMNS Induced Currents for Selected Configuration and Dump of Coil E1.

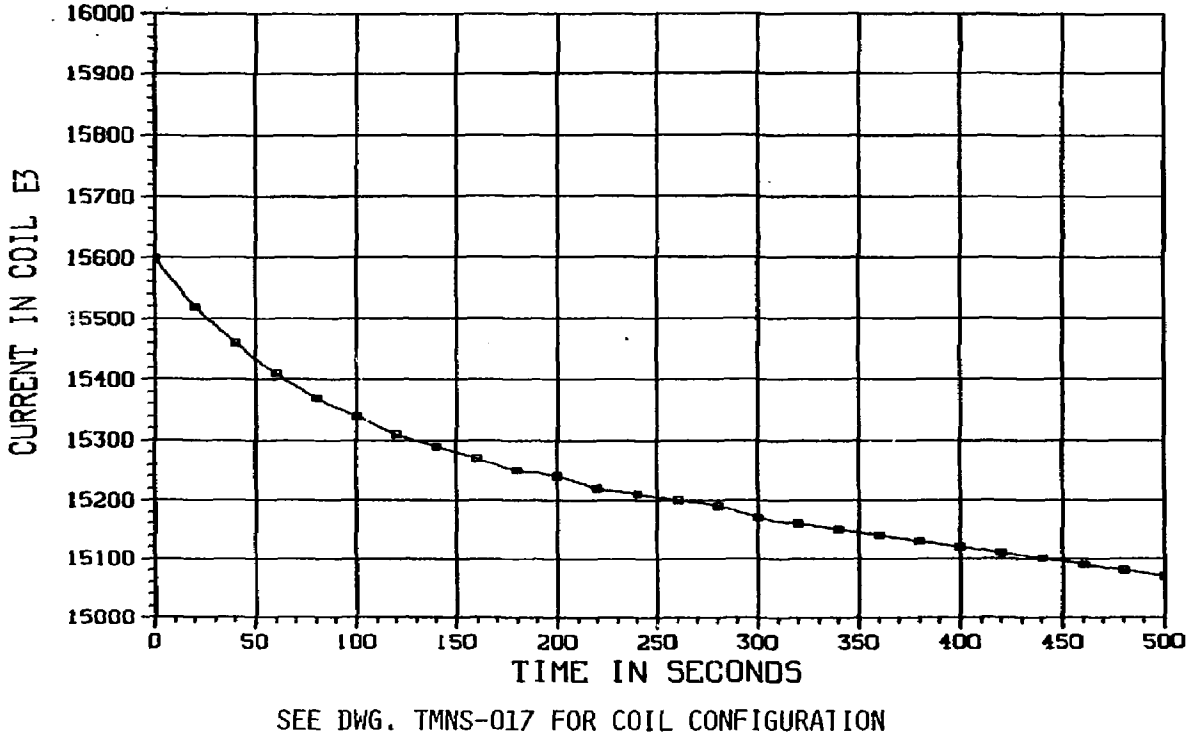

Figure 3.4-13. TMNS Induced Currents for Selected Configuration and Dump of Coil E1.

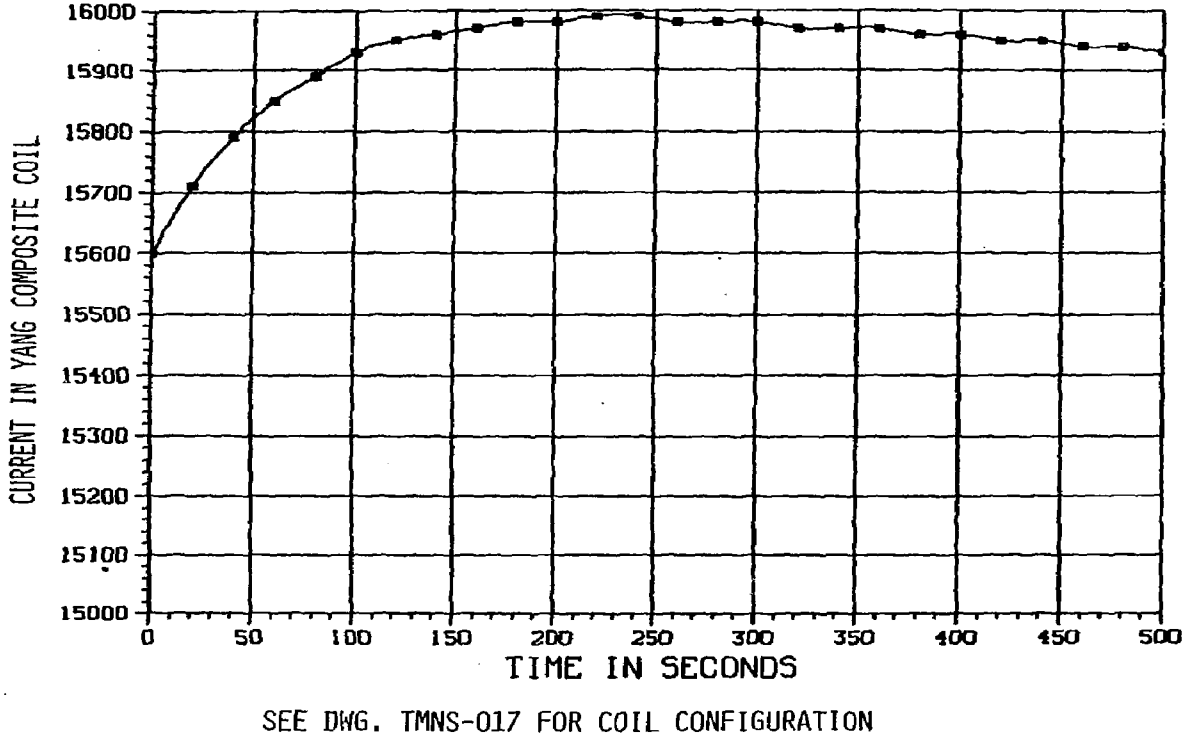

Figure 3.4-14. TMNS Induced Currents for Selected Configuration and Dump of Coil E1.

The simultaneous dump of all the coils was considered next. The results are given in Figures 3.4-15 - 3.4-18. As can be seen from these curves, there is no increase in current in any of the coils. The only effect of the mutual coupling is to increase the time constants of the current decay in each of the coils.

Thus, it was concluded that induced currents will not cause any serious consequences if all coils are dumped simultaneously. However, the dump of a single coil should be investigated further and should not be ruled out as a possible past dump scenario on the basis of the preliminary analysis presented here. A more detailed analysis is required before the full consequences of the dump of one magnet can be evaluated.

3.4.3 Computer Control of Power Supplies

It is imperative that the power supplies (five or more for each half of the Yin-Yang pair) be computer controlled because of the problem that exists in trying to maintain a magnetic field which is the superposition of fields derived from coupled coils using separate current sources. The problem occurs when a given current source/coil combination senses a field perturbation in another flux-coupled coil. The source, in effect, then tries to regulate the current in all the coupled coils. Since there are multiple sources, this condition can cause positive feedback, or "hunting". among the multiple power supplies

A method for avoiding this instability is to use a computer or process controller in the feedback loop. As shown in Figure 3.4-19, a controller can provide simultaneous command signals to multiple supplies. Feedback signals to the controller may be in the form of individual signals representing supply current, magnetic field strength, or both. Use of the magnet current is probably the easiest and most effective signal to use. Figure 3.4-20 represents the signal conditioning required of the feedback signals by the controller. In essence, the various feedback signals are summed, divided, and integrated to provide an average error signal. The individual feedback signals are subtracted from this average to provide individual control signals to the power supplies. This type of control prevents instability and is in wide use in industry for such applications as autoclaves, in which many piece parts are cured at one time with multiple heaters.

3.4.4 Breakdown in Gaseous Helium and Insulation Flashover

In the emergency dump of a superconducting magnet, one of the most critical considerations is the possible electrical breakdown in the helium gas and/or flashover (tracking) along an

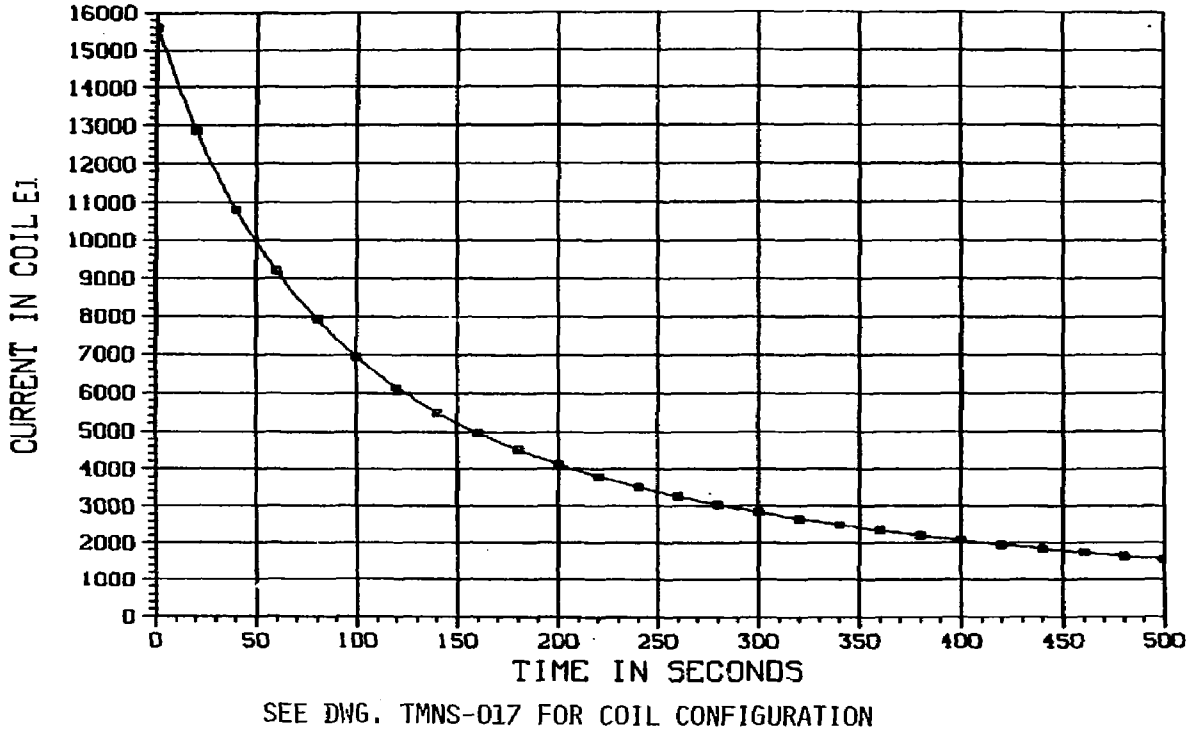

Figure 3.4-15. TMNS Induced Currents for Selected Configuration all Coils Dumped Simultaneously.

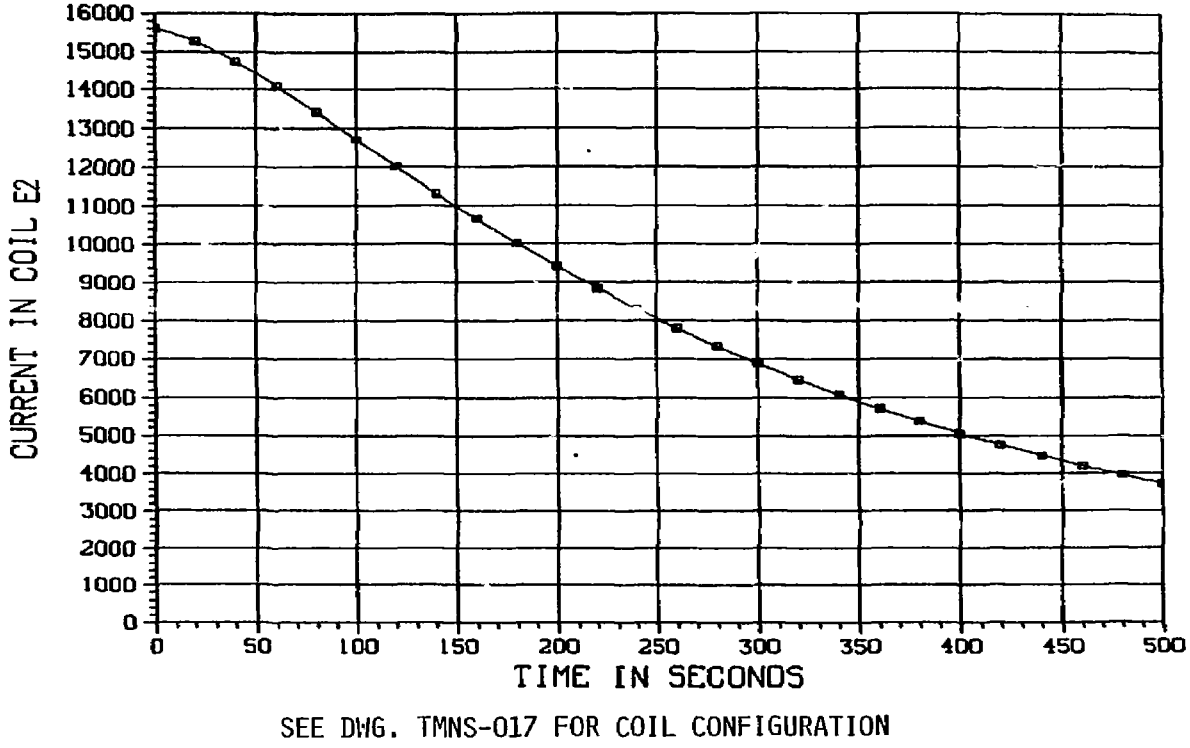

Figure 3.4-16. TMNS Induced Currents for Selected Configuration all Coils Dumped Simultaneously.

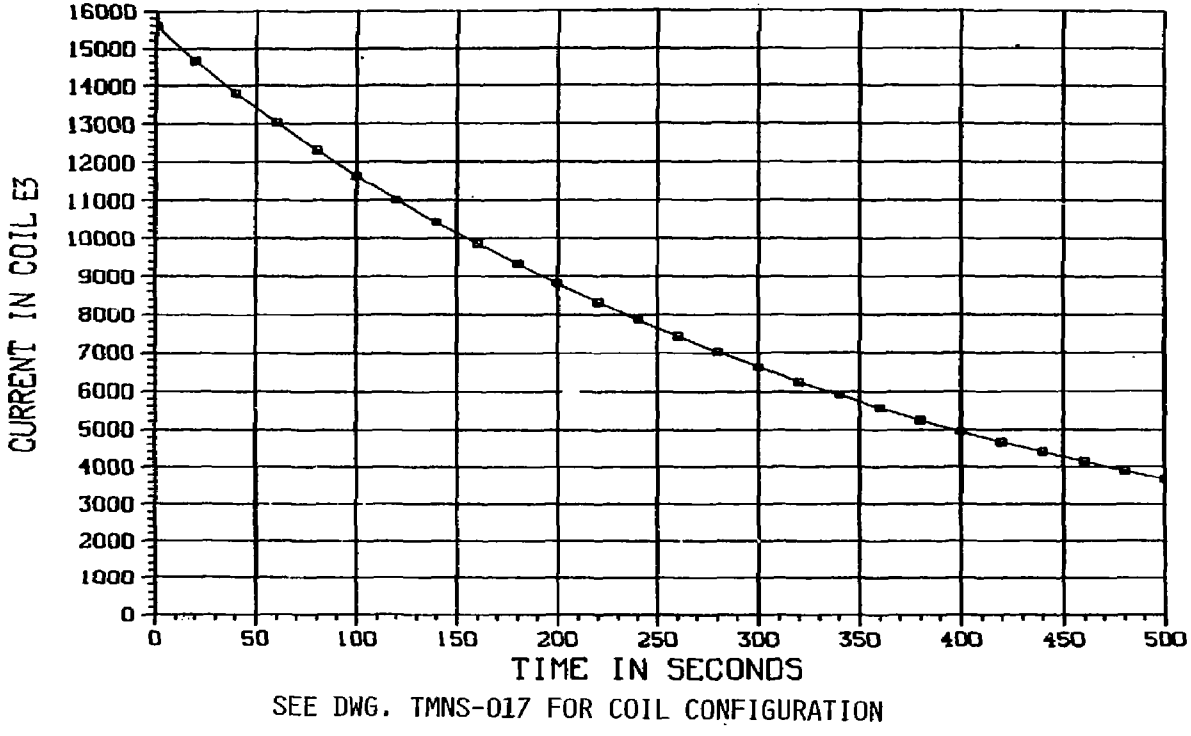

Figure 3.4-17. TMNS Induced Currents for Selected Configuration all Coils Dumped Simultaneously.

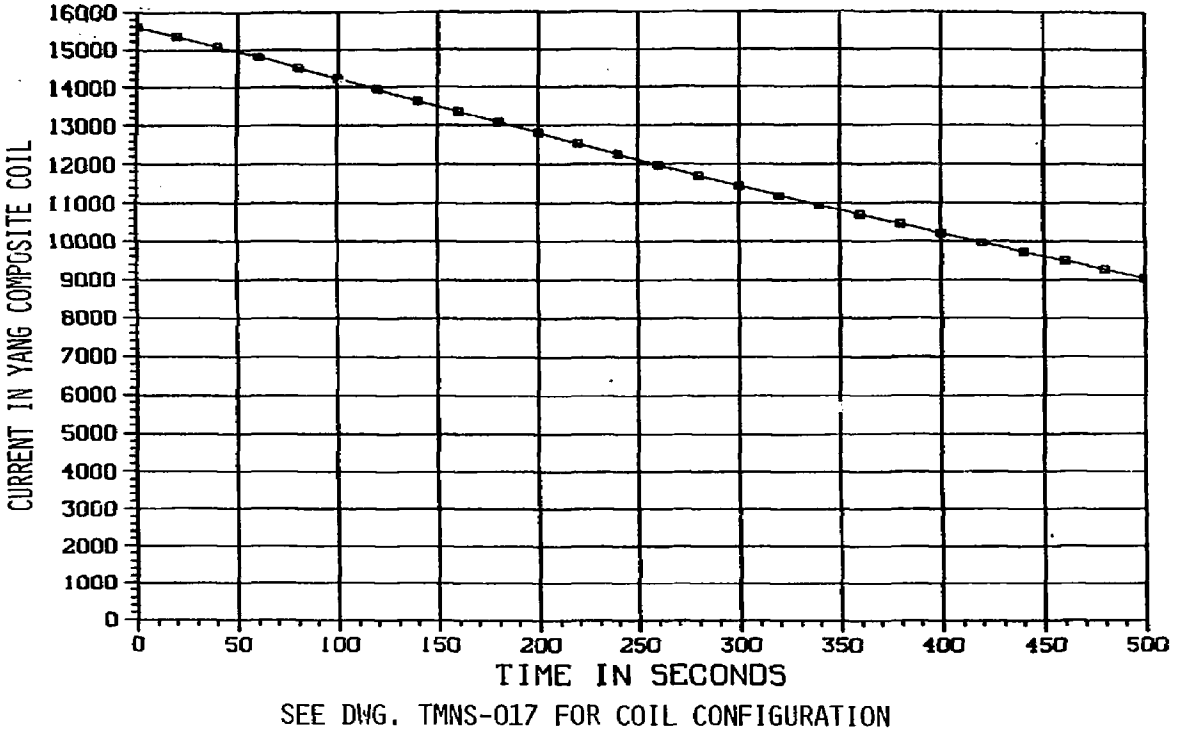

Figure 3.4-18. TMNS Induced Currents for Selected Configuration all Coils Dumped Simultaneously.

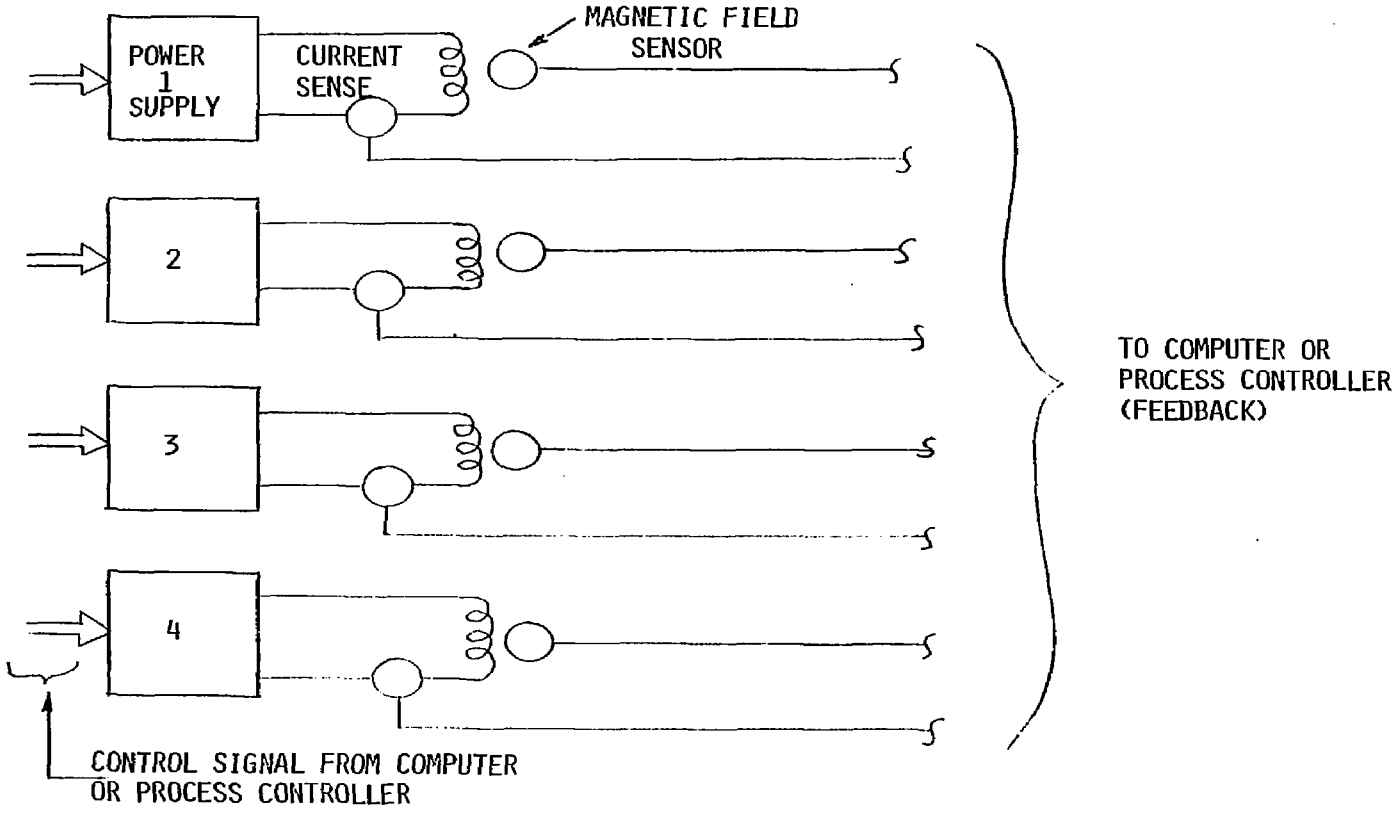

Figure 3.4-19. TMNS Multiple Power Supplies are Controlled with a Microprocessor Feedback Loop.

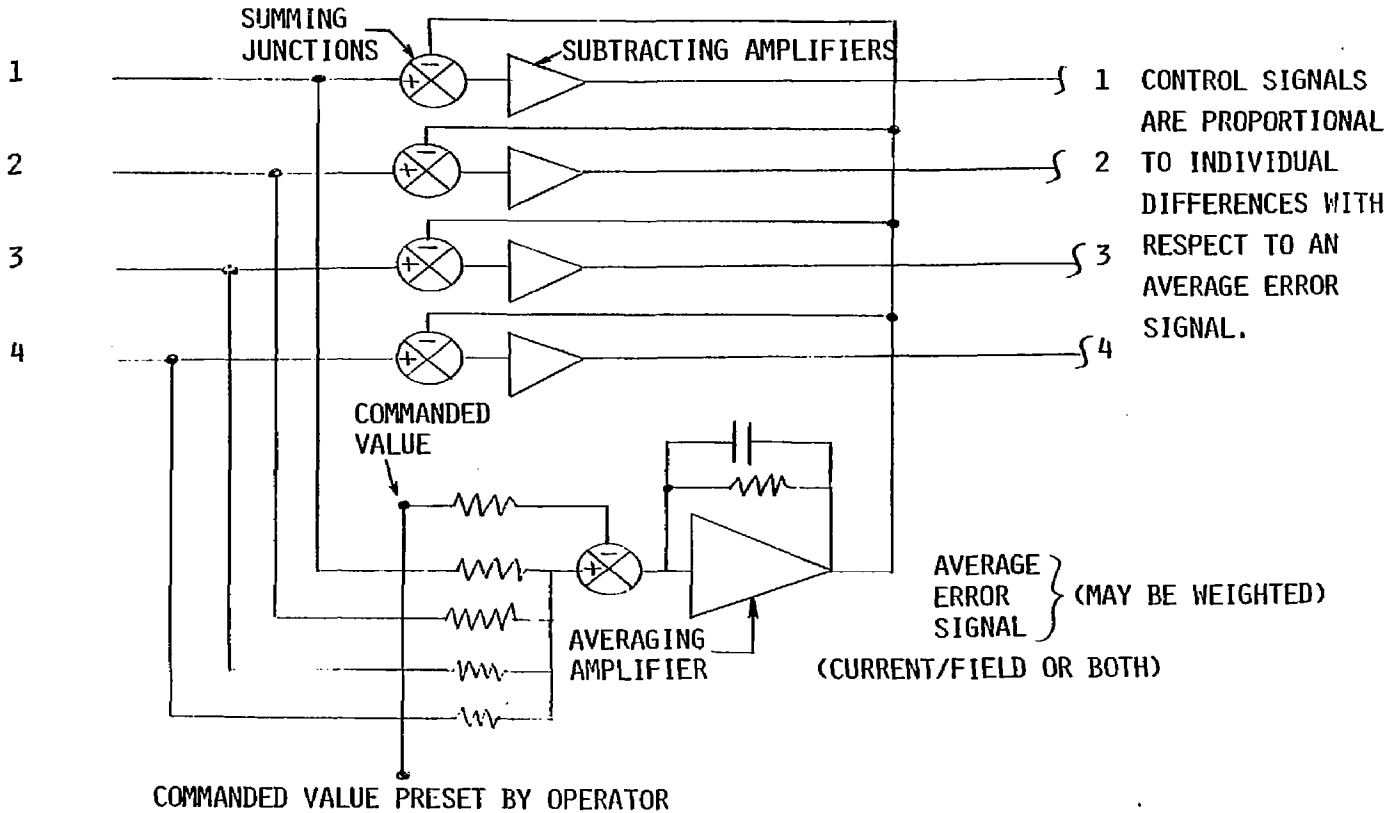

Figure 3.4-20. TMNS Process Controller for Multiple Power Supplies.

insulator due to the presence of high voltages. There should be no way to stop an arc initiated by either of these mechanisms, the results of which would be a catastrophic failure of the magnet. Therefore, the possibility of this occurrence in the TMNS magnet, and the precautions necessary to prevent it, should be carefully considered.

Unfortunately, the breakdown of gases across gaps and tracking along insulating surfaces is a subject of almost infinite variety. Such breakdown depends on many parameters such as:

- Impurities or contaminants in the gas or on the surface of the insulator.
- The pressure of the gas, temperature, electric field, electric field uniformity.
- Gap distance.
- The linear dimension of the insulator between electrodes.
- Mechanical strain at the surface of the insulator.
- Dielectric constant of the insulator.
- Gas species.
- Surface roughness.
- Surface charges.
- Non-uniform leakage currents.
- Uneven contact between the dielectric and the electrodes.

There exist reams of data on the breakdown of gases across gaps. Although these data show large variations, depending on the experimental conditions and the care of the investigator, a large enough body of data exists to obtain a reasonable estimate of breakdown in low temperature helium gas across gaps.

The same statement cannot be made for the flashover of high potentials along insulator surfaces at cryogenic temperatures. A fairly careful review of the literature uncovered only three references that contained any data at all on this subject at cryogenic temperatures and even these three papers provided no direct data that can be applied to the task at hand (References 8, 9 & 10). Other references that were found that treated the subject of potential tracking along insulator surfaces were primarily concerned with transmission lines and employed room temperature gases at or above atmospheric pressures.

All of the available data agrees in one essential point, namely, that the presence of a solid insulator decreases the voltage breakdown of a given gap. For example, the insertion of a smooth insulating surface, such as glass or porcelain across an otherwise uniform field air gap can reduce the flashover potential. This reduction is about 0.5 that of the air value alone for gaps of less than 1 cm, and falls to about 0.3 of the air value, for a gap of the order of 10 cms. (Reference 11.)

Corrugation of a solid surface increases the flashover potential in all cases, at least in room temperature air (References 11,12). The corrugation effectively increases the insulator length between electrodes for a given gap distance.

The small amount of data found implies that the tracking breakdown across insulator surfaces can be less than the breakdown potential by anywhere from a mere 10% (Reference 10) to a factor of 8 (Reference 9).

With the present lack of data of potential flashover along insulator surfaces at cryogenic temperatures, it seems that the most logical procedure to follow in the design of the ground insulation is to choose a thickness of insulation that will be able to withstand breakdown in the helium gas and then apply some reasonable factor to that value. On the basis of the available data, this factor should be between 1.1 and 8.0.

From a survey of many papers that deal with the subject of electrical breakdown of helium gas across gaps at cryogenic temperatures, a value of 1500 V/mm for the breakdown potential of helium gas in an inhomogeneous field at 4.2K has been selected. This appears to be a reasonable figure that is in agreement with many investigators.

SUPERQ calculates the minimum gap distance required to withstand breakdown in helium gas. This calculation is performed as follows: SUPERQ calculates the dump voltage as a function of time and the temperature of the conductor. The breakdown potential of the helium gas in contact with the conductor is then calculated from the relation (Reference 13),

$$V_{b2} = V_{b1} \left(\frac{T1}{T2} \right)^{0.9}$$

where V_{b1} and V_{b2} are the breakdown potentials of the helium gas at the temperatures T_1 and T_2, respectively, using V_{b1} of 1500 V/mm at T_1 = 4.2K. Then the minimum gap distance is calculated from the known breakdown potential at that temperature and the dump voltage at the same temperature. The result of this calculation is shown in Figure 3.4-9. Note that the largest minimum gap is 10 mm, at a conductor temperature of about 150K. This gap

distance contains no multiplicative safety factor. As indicated earlier in this section, no rational basis exists for selecting a thickness of insulation to prevent flashover. Therefore, a factor of 4 has been selected as a reasonable compromise and which implies 4 cm of ground insulation. However, since the dump resistor is center tapped to ground, 2 cm will suffice. Minimum layer-to-layer and turn-to-turn insulation thickness are shown in Table 3.4-III. These thicknesses also include a multiplicative factor of 4.

Table 3.4-III. Required Insulation Thicknesses to Prevent Helium Breakdown

NO. OF COILS	LAYER-TO-LAYER VOLTAGE	INS. THICKNESS MM	INS. THICKNESS INCHES
4	88.9 V	3.56	0.140
5	111 V	4.44	0.175
6	133 V	5.32	0.209

TURN-TO-TURN INSULATION

NO. OF COILS	TURN-TO-TURN VOLTAGE	INS. THICKNESS MM	INS. THICKNESS INCHES
4	1.35 V	0.054	0.003
5	1.68 V	0.067	0.003
6	2.02 V	0.081	0.004

3.5 THERMODYNAMIC ANALYSIS

3.5.1 Conductor Stability

Cryostability

The pertinent thermodynamic parameters needed for the stability calculations of the conductor are shown in Figure 3.5-1 and Table 3.5-I. Based on these parameters and the specified environment, the cryostability calculational procedure outlined in Section 2.5 was applied to the preferred conductor design to ensure that it meets the design goal of being unconditionally cryostable. Results of the above calculations indicate that the high field Nb_3Sn conductor will have a stability margin of +66%, while the NbTi grade will have a margin of +77%. The stability margin defined here is as follows:

$$\% \text{ margin} = \left[\frac{\dot{q}_c}{\dot{q}_g} - 1\right] * 100\%$$

Where

$\dot{q}_c$ = the heat conducted down the cooling channel - w/cm

$\dot{q}_g$ = the heat generated by the normal conductor that must be dissipated into the cooling channel under consideration - w/cm.

With these large positive margins, the optimum conductor design from a cryostability standpoint has not been realized. Several design changes could be made that would lower the stability margins and increase the structural margins of the conductor: (1) insulation voids could be decreased to provide greater structural footprint and thus possibly greater safety margins on the conductor; (2) the operating temperature of the coolant bath could be raised slightly to partially reduce operating costs; or (3) the residual resistivity ratio of the copper stabilizer could be lowered, increasing the load-carrying capability of the conductor by using a "harder" copper in its manufacture. Individually or collectively, the above design perturbations could be applied to the next iteration of the conductor. However, each has the effect of raising the conductor's generated joule heat flux, further re-enforcing the requirement that the winding pack be cooled with superfluid helium.

Kapitza Conductance

When a conductor is driven normal, it begins to generate heat. The joule heat produced is a function of temperature and other operating parameters. In helium II, the heat transfer through

Table 3.5-I. Operating Parameters Meet Design Requirements.

SUPERCONDUCTOR	Nb_3Sn	NbTi
B_{MAX}	~12T	~9T
T_{BATH}	1.8K	1.8K
ENHANCEMENT FACTOR	40%	25%
J_C	44192 A/CM^2	58354 A/CM^2
β	0.7	0.7
J_O	30934 A/CM^2	40848 A/CM^2
I_O	15.6 KA	15.6 KA

the bulk fluid was discussed in section 2.5. Another mode of heat transfer exists in this fluid known as the Kapitza conductance. This phenomena creates a temperature gradient of a few degrees across a thin boundary layer (on the order of microns), between the heated surface and the bulk fluid. As long as the Kapitza conductance and the bulk fluid can adequately allow dissipation of the joule heat flux, the normal zone created in the conductor should collapse. It has already been shown that the bulk fluid can dissipate the heat generated from a normal zone. Now it will be shown that the Kapitza conductance will not hinder the recovery of a fully normal section of the conductor.

From Reference 3, the relationship for the Kapitza resistance between a copper surface and helium II can be expressed as

$$\dot{q} = 0.02 \ (T_s^4 - T_b^4)$$

Where

$\dot{q}$ - heat transfer from the surface - w/cm^2

T_s = surface temperature - ^oK

T_b = bulk fluid temperature - ^oK

For a maximum generated heat flux of 0.77 w/cm^2 and a bulk fluid temperature of 1.8K, the conductor surface temperature is calculated to be 2.65K. Thus, as long as the heat generated in the conductor at this surface temperature is less than 0.77 w/cm^2, the conductor should be cryostable. This indeed is the case as 2.65K is less than either the current sharing temperature of 4.2K for Nb_3Sn (Reference 14) or 2.83K for NbTi (Reference 15), allowing no heat generation at all. Thus, the Kapitza conductance does not limit stability of the TMNS 15.6KA conductor.

In doing the stability analysis described above, the assumption was made that sufficient amounts of helium II were available to cool the conductor. This assumption was verified, and a detailed discussion of it is presented in Appendix A, along with discussions on transient and 'cold-end' stability.

3.5.2 Magnet Heat Loads

As part of this design study, ways of limiting the magnitude of the heat load to the superfluid helium II were to be considered. Specifically, this task considered two sources of heat loads as limitable: (1) those heat loads originating from sources exterior to the magnet such as support struts and radiation, from the LN_2 shield, and (2) those originating from the numerous splice joints in the coil itself. Interception

of the external heat loads will be discussed first.

Heat Intercepts

Early in the design study, it was decided that the best way to reduce the effects of the conductive heat loads from the support struts and the radiative loads from the LN_2 shields on the 1.8K windings, was to intercept them with normal liquid helium I. Two approaches evolved from this basic idea: (1) the outer surface of the structural case could be cooled to 4.5K using trace tubing, or (2) a liquid helium radiation shield could be placed in between the LN_2 shield and the magnet.

Trace Cooling Case

The structural case trace cooling scheme would intercept all heat at the outermost portions of the magnet. Flowing liquid helium in the trace tubing would then carry this heat away, leaving only conduction through the case as the primary external source of 1.8K heating. Since the surface area of the magnet is so large, even a 2.7K temperature difference can create a large heat load that must be dealt with. For the structural case concept shown in Figure 3.5-2, the total heat load to the 1.8K windings can be up to 1185 watts if only a five-inch structural case is assumed.

LHe Shield

When the LHe shield concept is considered, the primary heat source is conduction through the magnet and shield support struts. For this heat interception scheme, shown schematically in Figure 3.5-3, several assumptions were made: (1) the structural case is at 1.8K, (2) the magnet support struts have at most a 10K temperature maintained through them where they intercept the LHe shield, and (3) the shield support brackets are of the same design and thermal resistance as the MFTF-A LN_2 shield supports. Based on those assumptions, the total heat loads to the 1.8K environment from these sources is 201 watts. Table 3.5-II tabulates the heat loads to the 1.8K winding for these two concepts. From these calculations, the concept involving the LHe shield is obviously the preferred choice.

Conductor Splices

The proposed method for splicing together two superconductors was discussed in Section 3.1. Since these joints are not superconducting and are immersed in the helium II, they can represent a large part of the total heat load to the 1.8K helium. The important parameter in determining the heat generated in the joints is their electrical resistivity. Available data on the resistance of such joints is scarce, however some data were found (References 16,17).

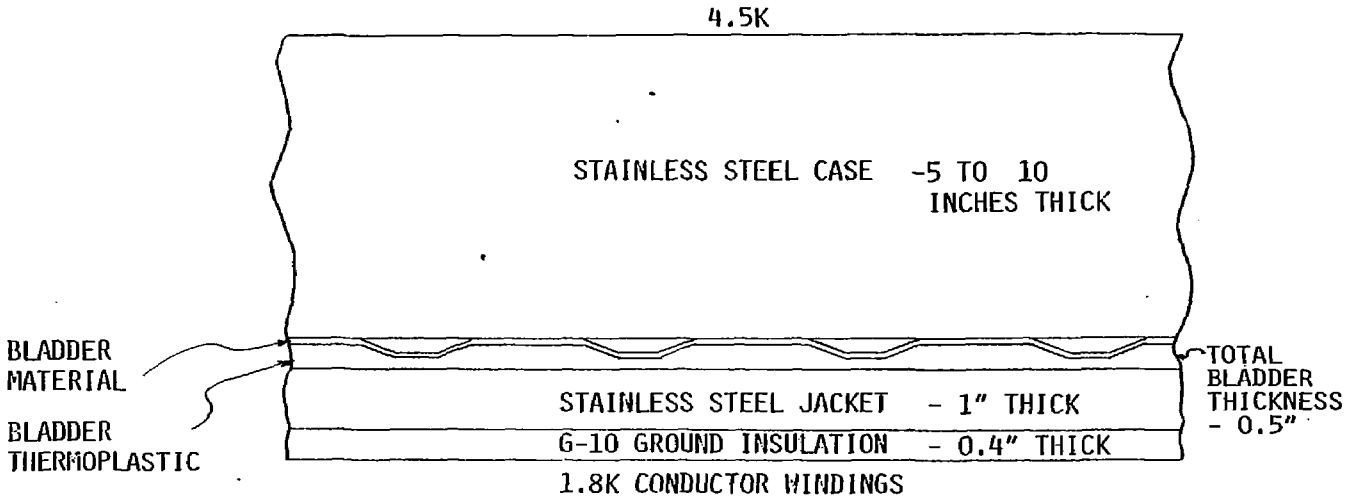

Figure 3.5-2. Steel Casing Dominates Thermal Resistance if Case is Cooled to 4.5K.

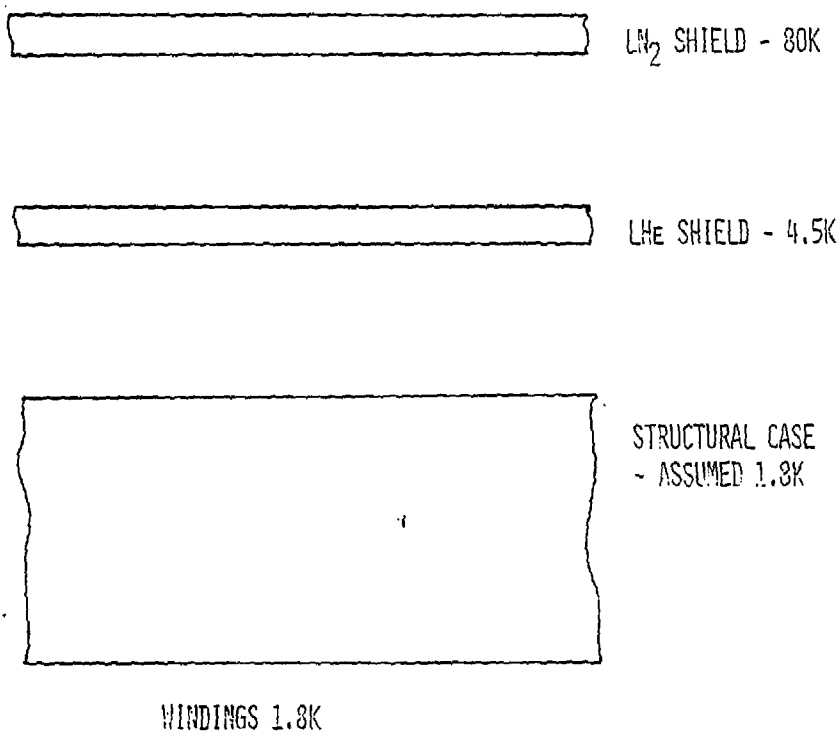

Figure 3.5-3. LHe Shield Effectively Reduces Heat Loads to the 1.8K Helium II.

Table 3.5-II. Utilizing the LHe Shield Approach Produces the Lowest Overall Heat Loads to the 1.8K Windings..

SOURCE	HEAT LOADS TO 1.8K TRACE COOLING (W)	 LHe SHIELD (W)
CONDUCTION THROUGH CASE	1185.5	0.0 (CASE @ 1.8K)
RADIATION FROM LHe SHIELD	NA	NEGLIGIBLE
CONDUCTION FROM SUPPORTS	NA	196.0
CONDUCTION FROM SHIELD SUPPORT BRACKETS	NA	5
TOTAL:	1185.5	201.0 *

*PREFERRED CONCEPT

These reports indicate that a wide range of values for the resistance of a lap joint have been measured with the TMNS type joint (48.5cm of soldered overlap), ranging from a low of $1* 10^{-9}\Omega$ to about $1* 10^{-8}\Omega$. For heat load calculations considered in this report, a medium value of $5* 10^{-9}\Omega$ was chosen as a representative, and probably achievable, joint resistance.

Currently, superconductor manufacturers can produce sufficient lengths of superconductor to limit the total number of conductor splices to 506 per Yin-Yang. A total of 616W would be generated using this number of joints. If the superconductor manufacturers could build longer lengths, the minimum number of joints in a Yin-Yang pair would be 326, generating a total of 397W. This reduction in generated heat does not greatly affect the amount of total refrigeration capacity required for the system. However, it does have a large impact on the total operating cost. If it is assumed that it takes 3KW of power to produce 1.0W of refrigeration at 1.8K, and that the reactor will operate for 24 hours per day for 10 months out of the year; if the life of the reactor is 10 years, and the average cost of power is $0.10/kWh, then the total savings for reducing the number of joints is $4.8 million. Thus, there is a large financial incentive to reduce the number of joints. Total heat loads for the TMNS Yin-Yang pair are summarized in Table 3.5-II.

3.5.3 Conclusions

Some further developmental work is needed to prove some of the concepts presented here. Stability and/or heat transfer tests of simulated conductor packs need to be conducted in helium II to prove out the stability theory used. Conductor splice joints need to be tested to verify the resistance assumed here. Also, a refrigeration system capable of producing between 3000 and 3500W will have to be developed to handle the heat loads from the Yin-Yang pair. Overall, however, the present concept is thermodynamically feasible.

Table 3.5-III. Total Heat Loads to the Cryogens are Manageable for Selected Concept.

SOURCE	4.5K (W)	1.8K (W)
LN_2 SHIELD RAD	84.4	-------
LN_2 SHIELD STRUTS	133.9	-------
LHE SHIELD RAD	-------	NEGLIGIBLE
LHE SHIELD STRUTS	-------	5.0
SUPPORTS	901.7	196.0
COIL SPLICES*	-------	616.0
INST LEADS	242.7	2.0
FLUID LEADS	420.0	-------
	1782.7 W	819.0

CURRENT LEADS
5 SETS @ 15.6 KA 182.0 L/HR

*CURRENTLY ACHIEVABLE

3.6 MANUFACTURING PLAN

In compliance with the TMNS study contract from Lawrence Livermore National Laboratory, the Convair Division of General Dynamics performed analysis and design of the conductor, conductor joint, and substructure for a 12 Tesla Yin-Yang Magnet System. A design concept was selected from this study.

This manufacturing plan presents a conductor fabrication and winding concept for this conductor that is similar to the fabrication method used by General Dynamics Convair Large Coil Program and a scaled up MFTF winding method.

3.6.1 Description of Product

The basic stabilizer and filler would be sized and shaped as shown in Figure 3.6-1. The superconductor configuration is illustrated in Figure 3.6-2.

Materials, Stabilizer and Conductor

The stabilizer and filler will be half hard OFHC (C10200) Copper. The "C" shaped channel would be extruded in twenty foot lengths and wound on large spools with the filler bar.

The superconductor is to be a monolith of Nb_3Sn (201,000 ft.) and NbTi (364,000 ft.) and delivered on reels greater than 13 ft. diameter. The large reels are desired to insure that the least amount of strain load is induced in the Nb_3Sn superconductor.

Materials, Insulation

All insulation will be fabricated from G-10CR Grade fiberglass material.

The turn-to-turn buttons will be procured from a subcontractor in the configuration shown in Figure 3.6-3. The design is such that large rolls would be procured.

Lateral Insulation, which is used to produce the layer-to-layer segments, will be procured with the cut out pattern shown in Figure 3.6-4.

Solder

Conductor fabrication will require 21,500 pounds of eutectic tin-lead solder (63% Sn, 37% Pb,) with complete liquefaction at $360^{o}F$.

Adhesive

Approximately 300 quarts of Loctite Superbonder # 414 would be procured to bond the insulation in place.

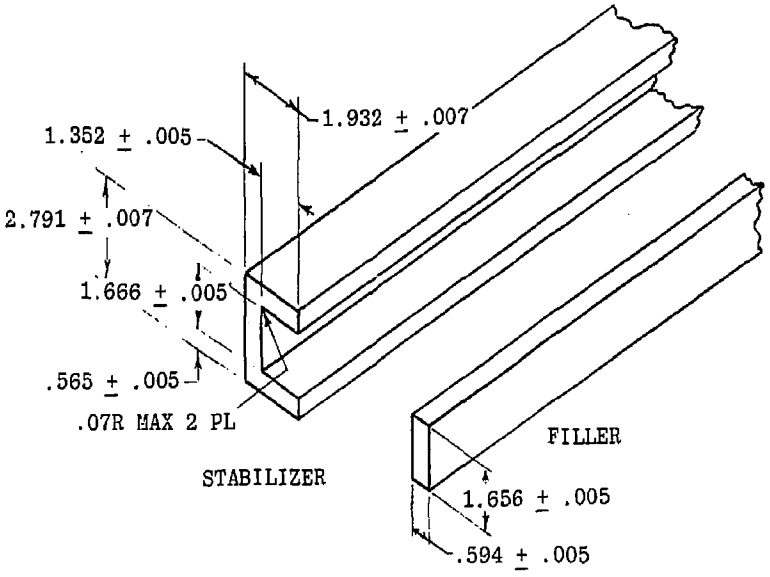

5. FILLER TO BE WOUND FLAT SIDE ON A SPOOL OF 13 FT. DIA. MIN. LENGTHS OPTIONAL.
4. STABILIZER TO BE DELIVERED IN 40 ± 2 FT. LENGTHS.
3. STABILIZER & FILLER TO BE DRAWN 1/2 HARD.
2. MATERIAL OFHC COPPER.
1. ALL DIM. IN CM.

Figure 3.6-1. Stabilizer and Filler.

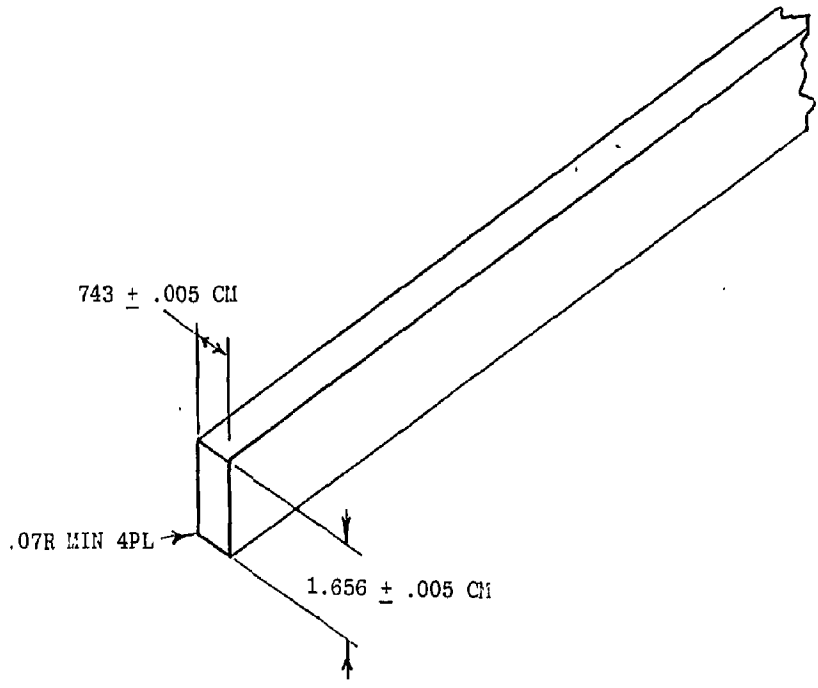

Figure 3.6-2. TMNS Conductor.

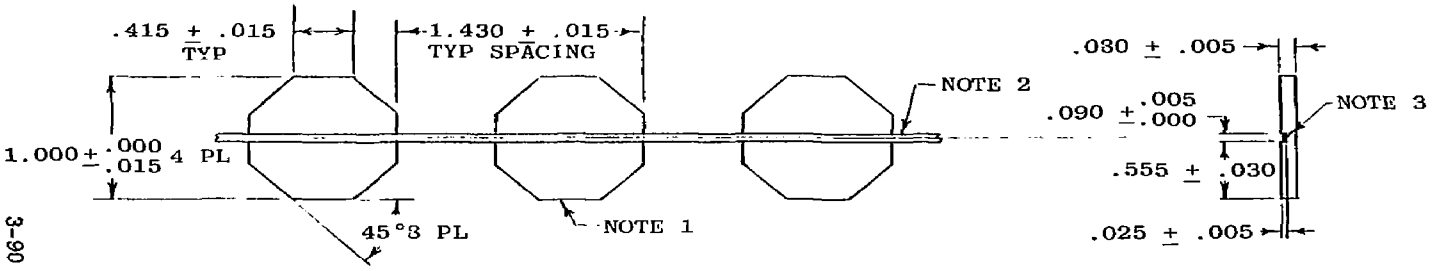

NOTES –

1. MATERIAL NEMA G-10CR
2. TAPE-LACING: TYPE IV, SIZE 3, FINISH A PER MIL-T-43435
3. BOND TAPE WITH LOCTITE SUPERBONDER 414
4. ALL DIM. IN INCHES

Figure 3.6-3. Button Insulation.

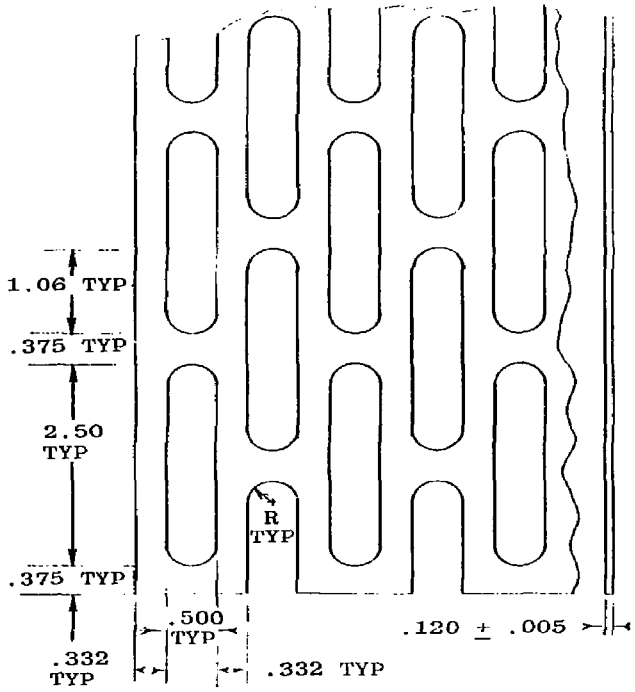

DETAIL A
FULL SIZE

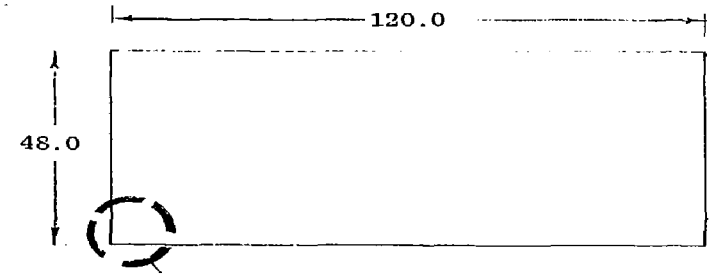

FOR TYPICAL CUTOUT
PATTERN SEE DETAIL A

NOTES:

1. MATERIAL: NEMA G-10CR
2. CUTOUT PATTERN TYPICAL OVER FULL SHEET
3. TOLERANCES: .X = +.03, .XXX = ±.010 OR AS NOTED
4. ALL DIM. IN INCHES

Figure 3.6-4. Lateral Insulation.

3.6.2 Ground Rules and Assumptions

Ground rules and instructions that provide boundaries for the general task description and ensure complete understanding of the proposed program have been established.

a. The coil is nominally defined as a superconducting Yin-Yang operating at a peak field of 12 Tesla.

b. Cooling medium for the coil shall be Helium II.

c. Convair would perform as prime contractor. The manufacturer of the superconductor would be a subcontractor responsible for design and production of the superconductor and for assisting Convair where required.

d. Fabrication and assembly would be accomplished in-plant.

e. Case fabrication is not included in this plan.

3.6.3 Make or Buy

A Make or Buy plan would be developed during a Phase I time frame and would become part of the final manufacturing plan. The plan would have two key objectives: 1) provide the lowest practical coil fabrication cost, regardless of Convair's inherent make capability, and 2) maximize the use of specialized skills and/or facilities from local industrial houses.

3.6.4 Subcontracting

Convair would enter into a subcontract agreement with a superconductor manufacturer who would be responsible for the design, development, test and delivery of the total superconductor requirements for the TMNS coil. In accordance with the subcontract provisions, and Convair approved manufacturing schedules, delivery of the superconductor monolith would be on reels with a suitable diameter to preclude mechanical stress.

Final Heat Treatment and Tinning

After the monolith is compacted, it will be given a final heat treatment and then tinned with 63-37 eutectic solder in preparation for the conductor to stabilizer association. This would be a subcontracted task.

3.6.5 Material Procurement

Convair will procure the C10200 OFHC copper in an extruded form. Convair will machine the final design configuration during the stabilizer assembly operation of superconductor to stabilizer. The stabilizer would be of one grade.

3.6.6 Manufacturing Facilities

Convair would select specific facilities that best satisfy the TMNS coil program objectives. In process handling of details and sub assemblies of the coil would be analyzed to minimize movement. The selected fabrication shops would be facilitized with adequate equipment to accomplish their assigned tasks. Handling of a completed coil would be accomplished by leased equipment as required.

Plant Layout

A TMNS sized coil could be assembled in Building 52, Lindbergh Field Ramp facility. Approximately 40,000 sq. ft. could be dedicated. See Figures 3.6-5 and 3.6-6 for building layout.

Significant features of this location are: building's structural configuration, i.e., floor load rating, free head room, and crane lift capabilities, it is in place and meets coil manufacturing requirements.

Facilities and Equipment

Specific company-owned facilities and government-owned facilities would be identified and included in the final draft of the manufacturing plan prepared during a Phase I time frame.

3.6.7 Manufacturing Analysis

The manufacturing policy as outlined herein discusses fabrication of the conductor and terminates with coil winding. Case structure buildup is not included.

Manufacturing Sequence and Flow

In support of the end-item deliverable date, Convair's Manufacturing Sequence and Flow Diagram (filed in pocket, inside back cover) provides a baseline for scheduling, facilities planning, material procurement, detail fabrication, assembly and installation planning, tool design and tool fabrication.

Conductor Fabrication

The term "conductor" used in this Manufacturing Plan includes both the superconducting monolith (Nb_3Sn and NbTi) and the stabilizer and filler bar, the structural housing of copper into which the superconducting monolith is soldered. This manufacturing description includes the operations for providing both the superconductor and the stabilizer and the task of soldering the two together to form the conductor. It is patterned after the General Dynamics Large Coil Program (LCP).

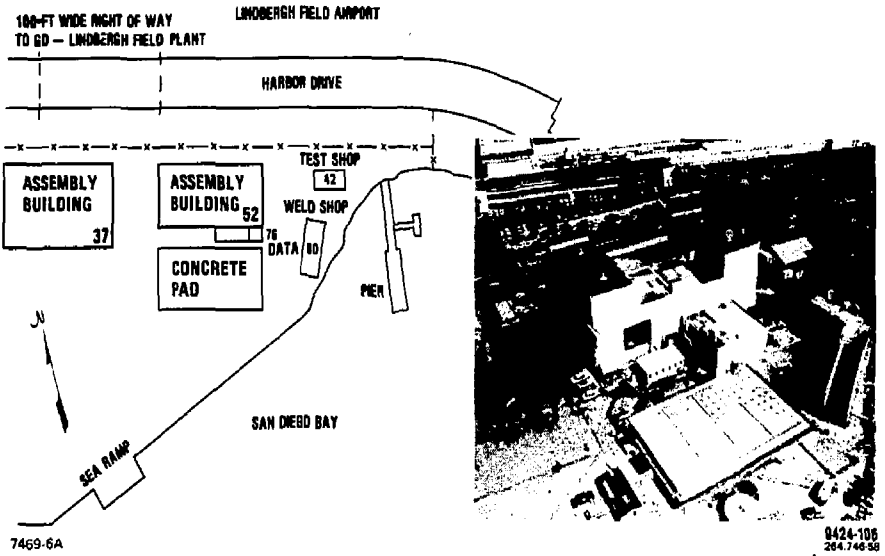

Figure 3.6-5. Harbor Drive Facility.

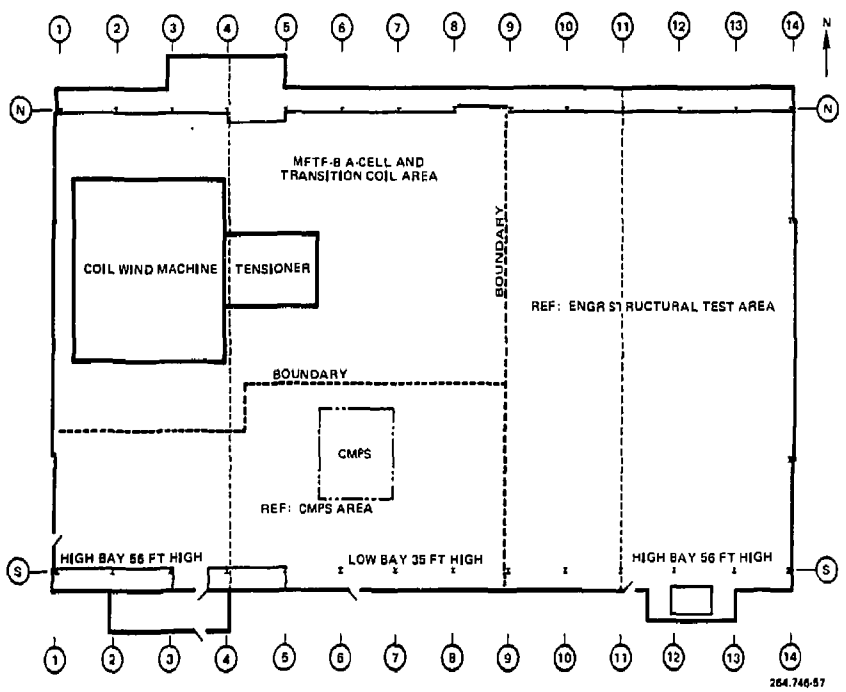

Figure 3.6-6. Building 52 Layout.

There are three separate lines shown in Figure 3.6-7 which illustrates the layout of the LCP production line. They are coldwelding, conductor assembly, and winding.

Coldwelding

A diffusion bonding process is used to make continuous quarter-hard copper stabilizer from 150-foot lengths for the LCP magnet. TMNS would use the same method to make continuous half hard copper stabilizer from 20 foot extruded lengths. Figure 3.6-8 shows the LCP weld press.

This joint would be annealed and then stretched back to the half hard condition, which also proof-tests the joint. This method is the same manner used by LCP, see Figure 3.6-9 for the LCP example of annealing coils, and Figure 3.6-10 shows the stretching jaws.

A stabilizer storage reel will receive the completed copper stabilizer, see Figure 3.6-11 for the reel used in the LCP line, TMNS would be similar.

Alternate Stabilizer Concepts

Two other stabilizer fabrication methods were considered in this study.

A rolled and formed stabilizer could be fabricated from 1/4 x 2-1/2 annealed bar. This bar stock would be milled with vee grooves at the bend lines, then rolled into the channel shape. A final draw operation would be required to bring the temper up to half hard. A final internal machining operation to control tolerances would be part of the stabilizer fabrication process, external final machining would still be part of the conductor to stabilizer production process. This method of manufacture would yield between 150 and 200 feet of stabilizer, reducing the coldweld operation.

Because of the discontinuity in the rolled corners of this stabilizer, it was considered structurally inadequate and was abandoned as a candidate manufacturing technique.

Alternate two would be to procure the stabilizer in a solid rectangular shape, rolled on coils of approximately 500 lbs. This bar would be power rolled from the reel into a milling operation that would have two cutting heads that would produce the slot in the bar in two steps. This milled bar would then be processed through the coldweld press. Based on a 500 lb. coil a 150 ft. yield of TMNS stabilizer could be expected, minimizing the butt weld operation.

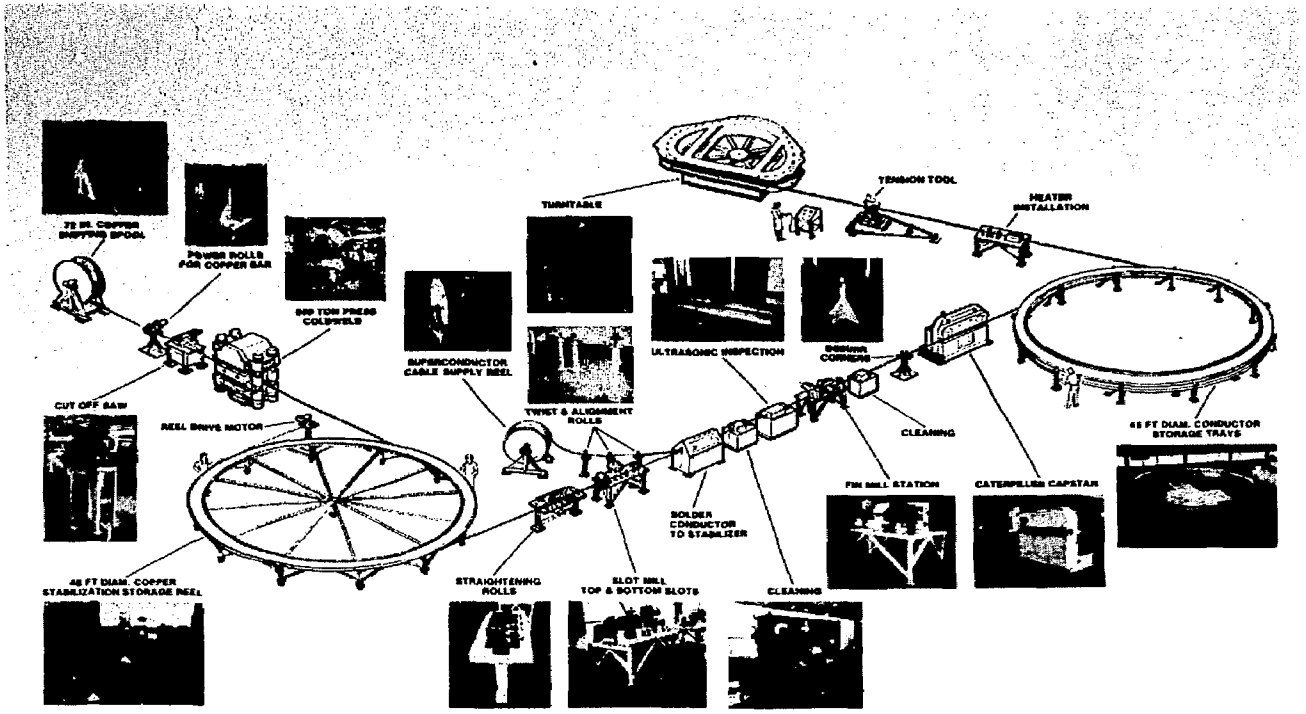

Figure 3.6-7. Large Coil Program Production Line.

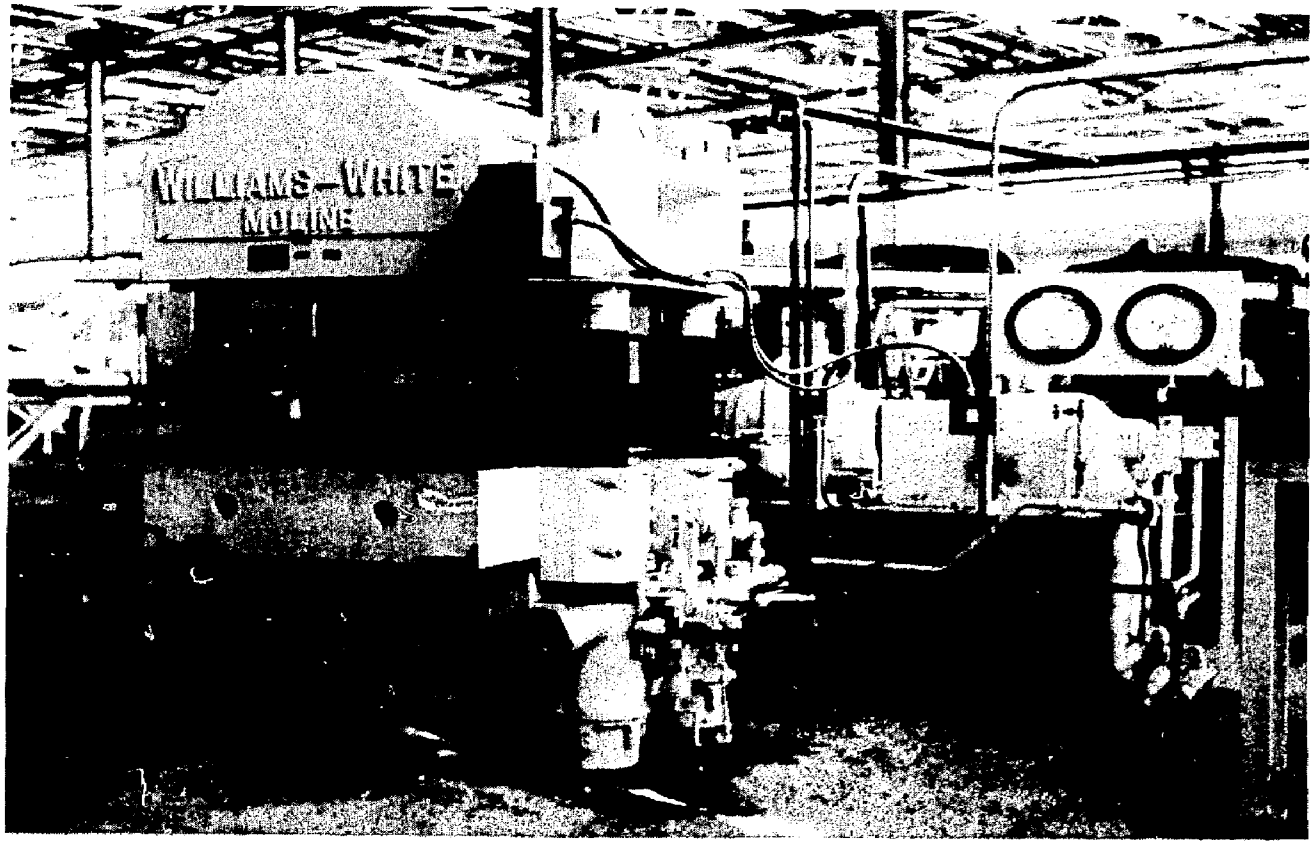

Figure 3.6-8. LCP Coldweld Press.

Figure 3.6-9. Annealing Coils on LCP Stabilizer.

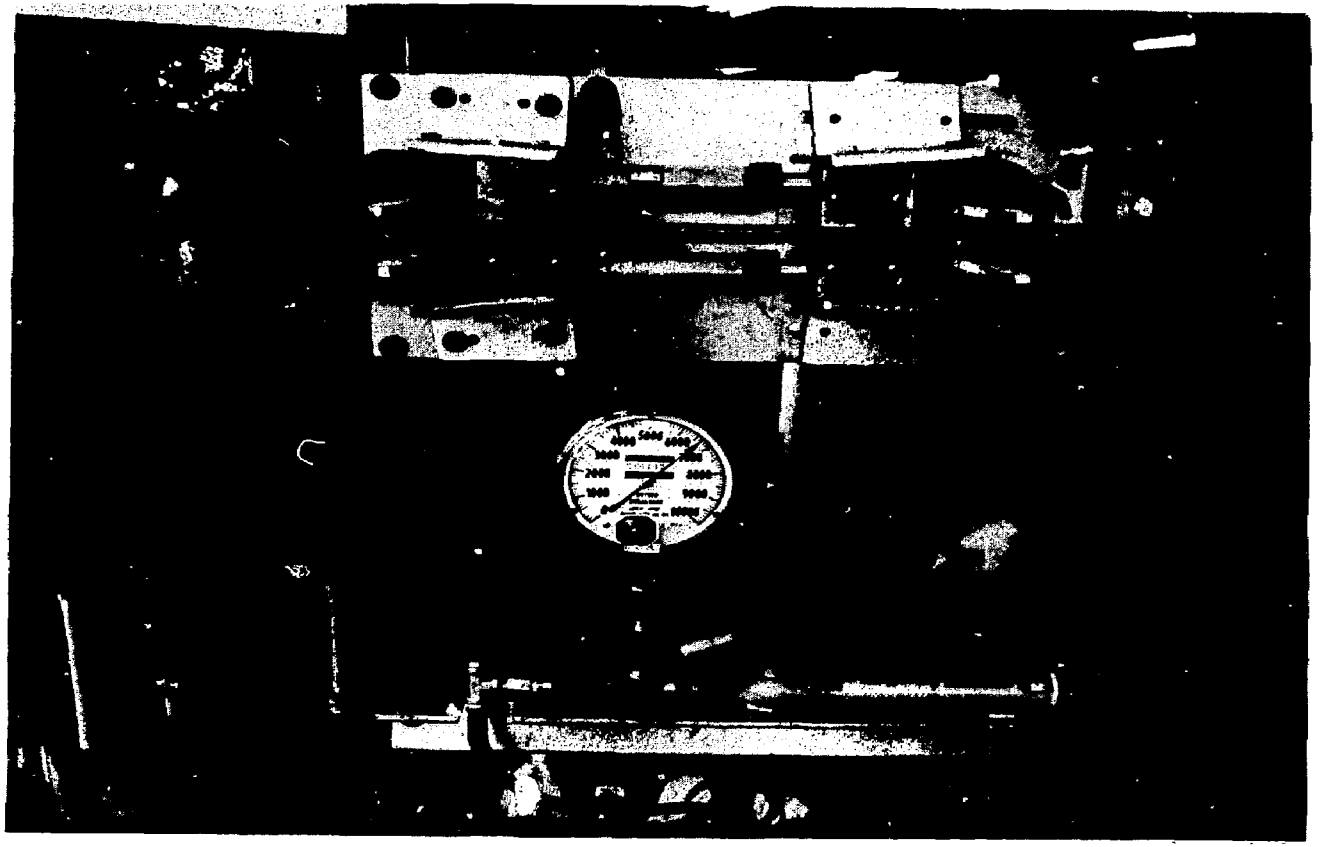

Figure 3.6-10. Stretching Operation LCP.

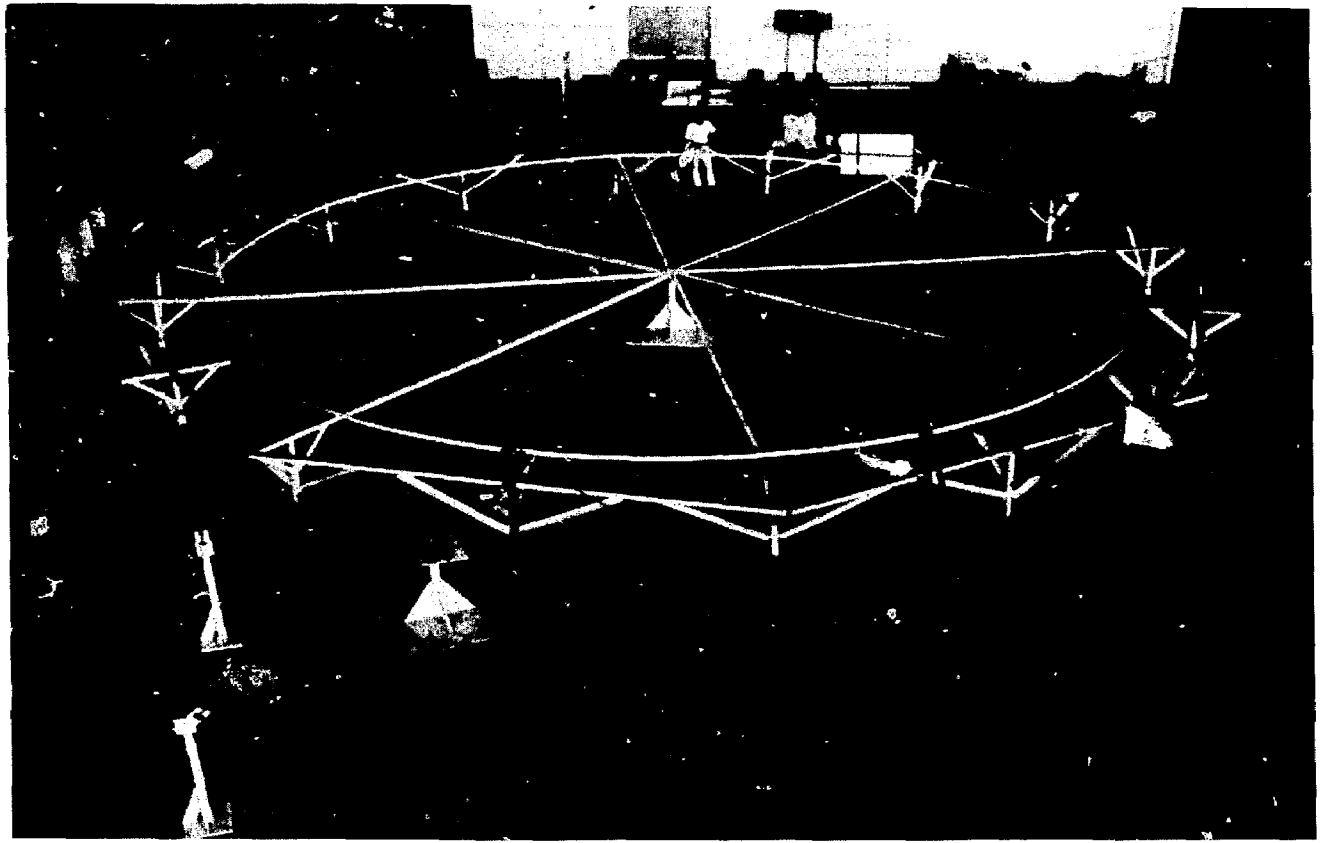

Figure 3.6-11. 48' Copper Stabilizer Storage Reel.

This process is viable, but the additional milling operation ahead of the coldweld operation does not appear to be the optimum fabrication technique. The length of the extruded shape could be extended by using longer draw benches. The 20 foot length discussed herein is used only because the capability exists throughout the industry today. Also the initial cost of the stabilizer becomes a consideration because the bar would weigh 75% more than the extrusion.

Conductor Assembly

The stabilizer is drawn from the storage reel and fed through straightening rolls. Using standard purchased components with rolls to fit the configuration of the stabilizer, the tool will be designed to remove uneveness of the extrusion in preparation for subsequent operations. A tool with several sets of idler rollers approximately 6 feet long is used by LCP, see Figure 3.6-12.

The coldwelded copper slot will be milled to final size and depth, this milling would be a clean up cut only. Discussions with copper manufacturers indicate the TMNS configuration is well suited to the extrusion process, but overall tolerance would be in the ± .010" range, which would be too large for good fit tolerances. The milling operation concept is well illustrated by the LCP production line which has four cutting and milling operations in its sequence, see Figure 3.6-13 for the LCP milling machine setup.

Both the stabilizer and the filler bar would be cleaned by a two-compartment tank with a detergent steam cleaning solution. This will be designed and fabricated to be placed in the conductor assembly line. The second tank will have steam jets for the rinsing agent. This ensures removal of all contaminants prior to the stabilizer and filler bar entering subsequent stations. A cleaning station designed and built for LCP is shown in Figure 3.6-14.

The TMNS superconductor, feeding directly from the supplier reel, on the order of fifteen feet diameter, will pass through a series of special slotted wheels laying the monolith into the precleaned and inspected slot of the stabilizer.

To ensure retention of the filler bar within the slot, a special "staking" wheel will place small indentations at the slot edge, forcing the copper into the filler bar. Paste solder will be applied to the superconductor by forced flow prior to laying the filler bar.

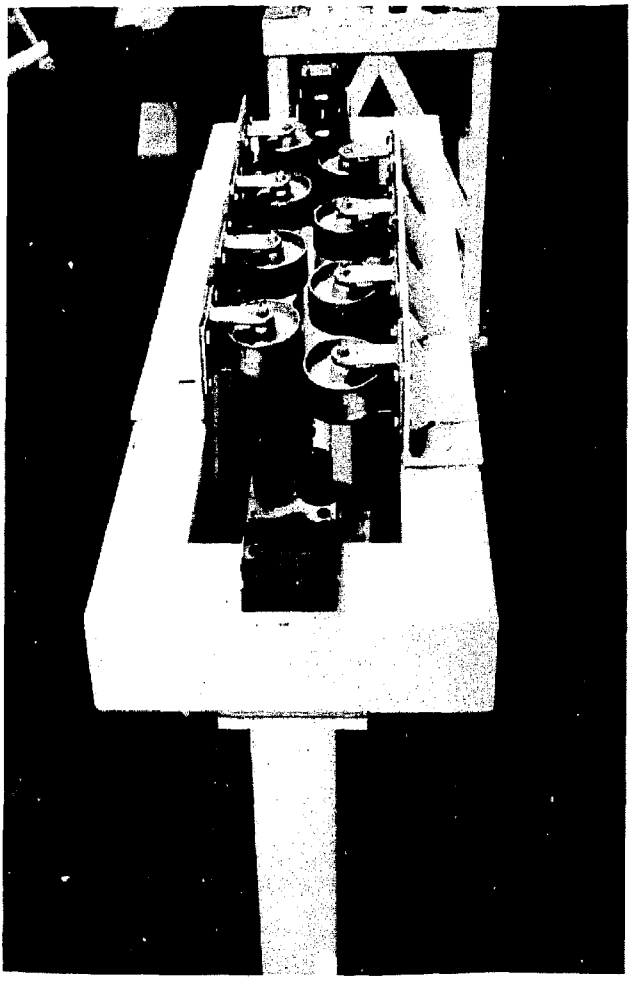

Figure 3.6-12. Straightening Rolls.

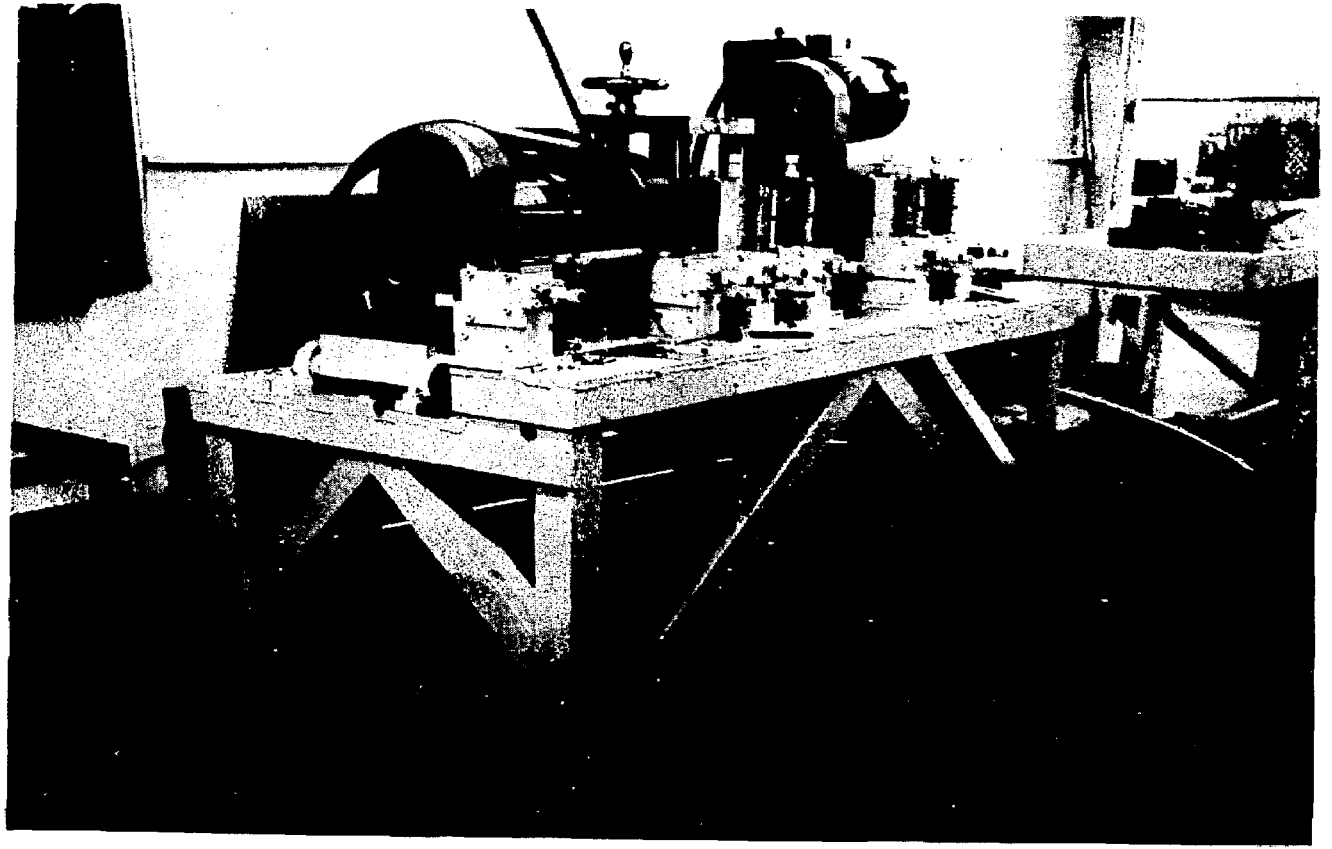

Figure 3.6-13. Slot Milling Machine Setup.

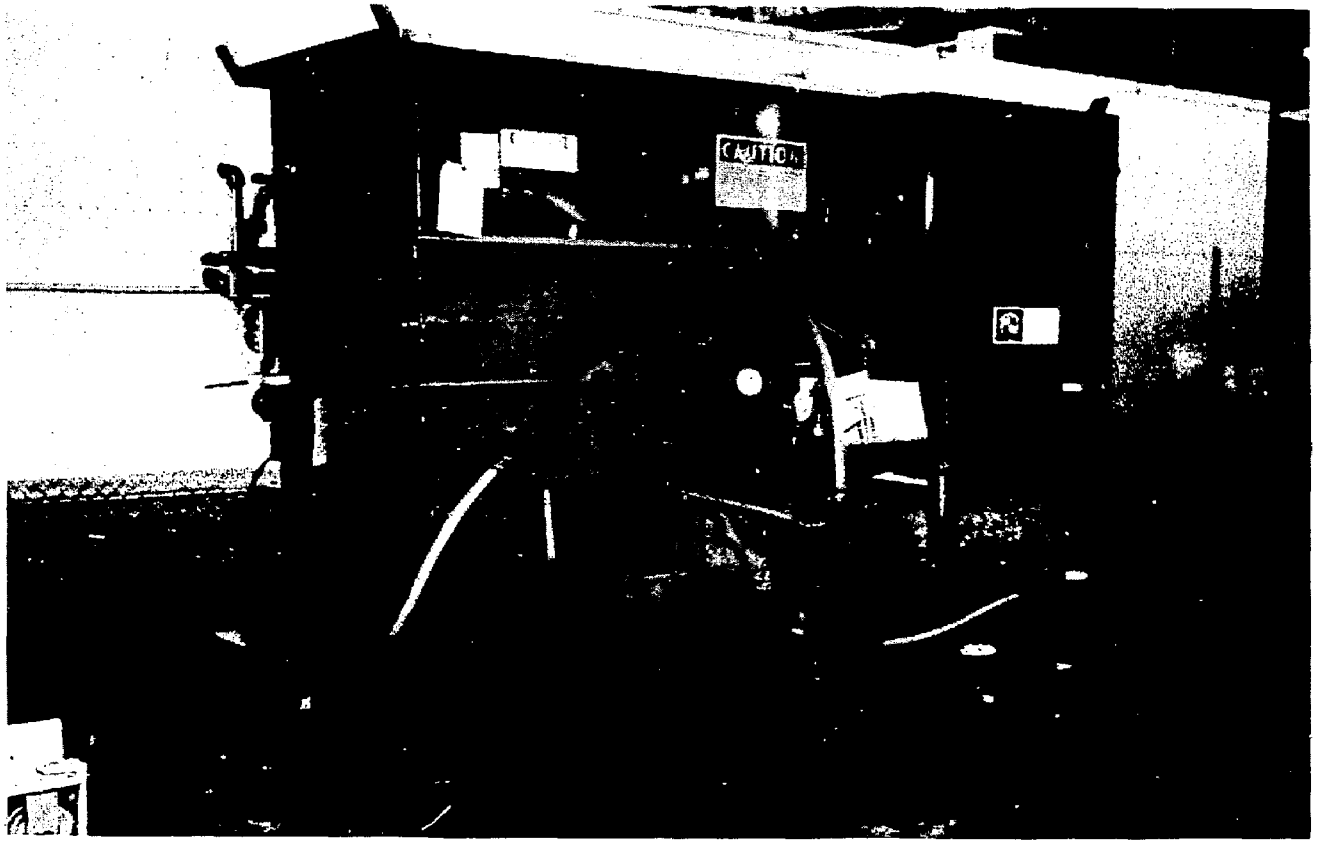

Figure 3.6-14 Degreasing & Cleaning Station.

Two views of the LCP solder line are shown in Figures 3.6-15 and 3.6-16. Figure 3.6-15 shows feeding rolls, solder and heating elements in an overall view. Figure 3.6-16 shows the conductor height sensor and the solder metering system, all of which could be scaled to TMNS.

As the conductor passes through the solder station, Selas burners on all four sides will raise the conductor temperature to a precisely controlled value, established by testing. The controlled heat will ensure the integrity of the solder bond between the monolith and stabilizer. As the conductor leaves the solder station, water will cool the conductor to ambient temperature for inspection purposes.

Inspection of the completed conductor will include monitoring of the process elements, visual inspection of each work station, and samples from the start and completion of a production lot. An ultrasonic scanning station would be incorporated in the process line to determine percent of solder bond between the superconductor and the copper stabilizer. An automatic marking device and a line stoppage switch would be included in this equipment. The line equipment could be stopped with all systems immediately returning to a neutral state, including the slot milling machines and solder station if a defect or problem was noticed. Reactivation of the line would start when the switch is turned to the "ON" position and all systems have reached their operating speeds and temperatures. This is patterned after the LCP method.

Final sizing will be done by a milling station using commercially available milling heads and support rollers. Again it is assumed that this would be cleanup cutting on three sides to maintain a tight pack buildup. LCP uses a similar cleanup cut when they remove their solder reservoir and machine the cooling fins.

After this mill operation the conductor would have a final cleaning prior to storage on the 50 foot diameter storage tray. Figure 3.6-17 shows a bead cleaning station and the Caterpillar Capstan used to pull the LCP conductor through the assembly line.

The LCP tooling for fabrication of the conductor includes a storage reel station incorporating separate positions for the storage of completed conductor requirements awaiting their use at the coil winding line. As the finished and accepted conductor leaves the final clean station in the conductor fabrication line, it is fed onto and secured to one of the shelves of the storage fixture. These shelves, 32 inches wide and 45 feet in diameter, are powered by an electric motor/gear box. Twelve welded pipe supports, equally spaced under the storage shelves, provide for the support and radial movement of the shelves. Each shelf carries the conductor requirements for a complete grade.

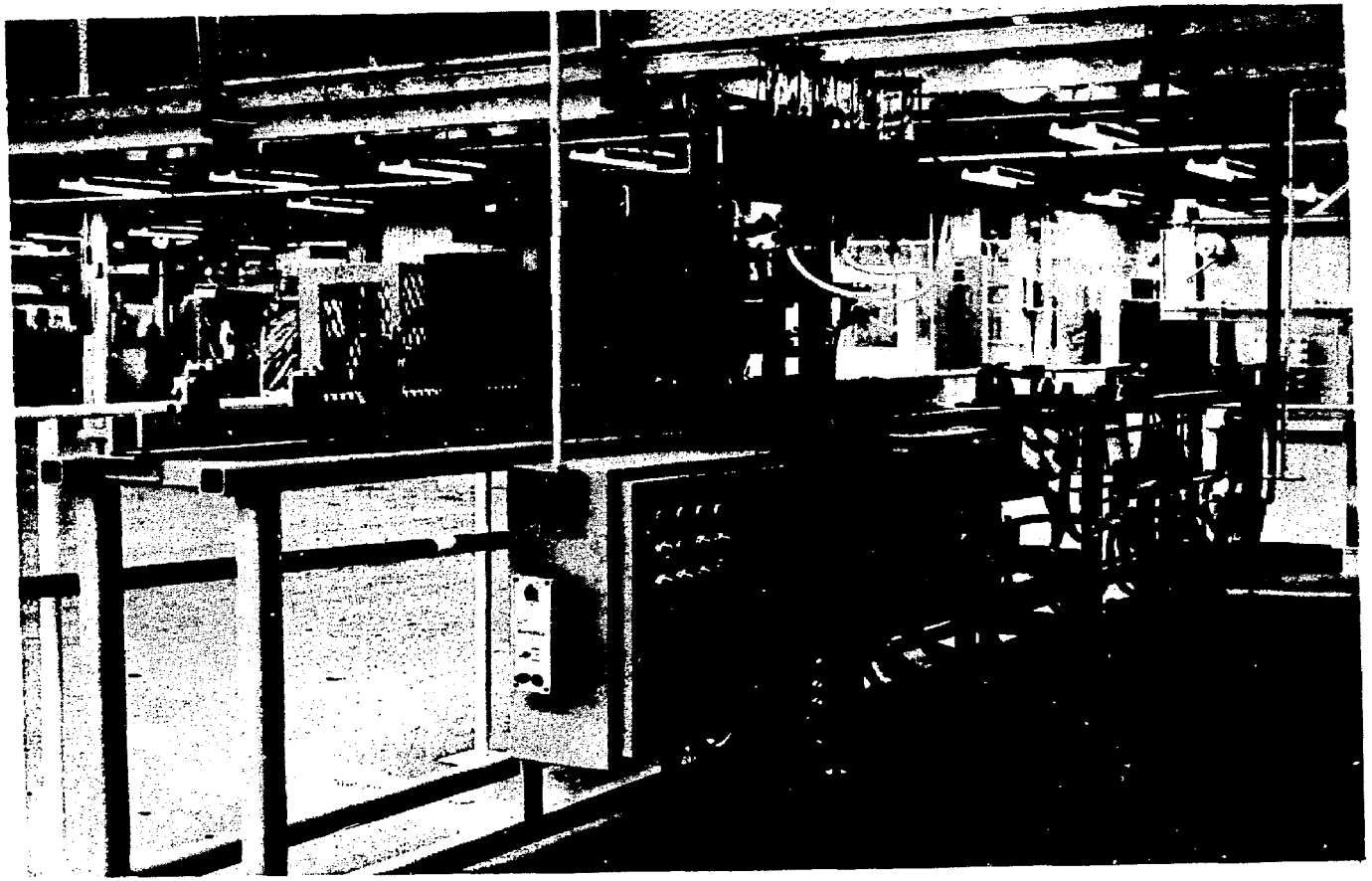

Figure 3.6-15. Conductor Association & Heating Station.

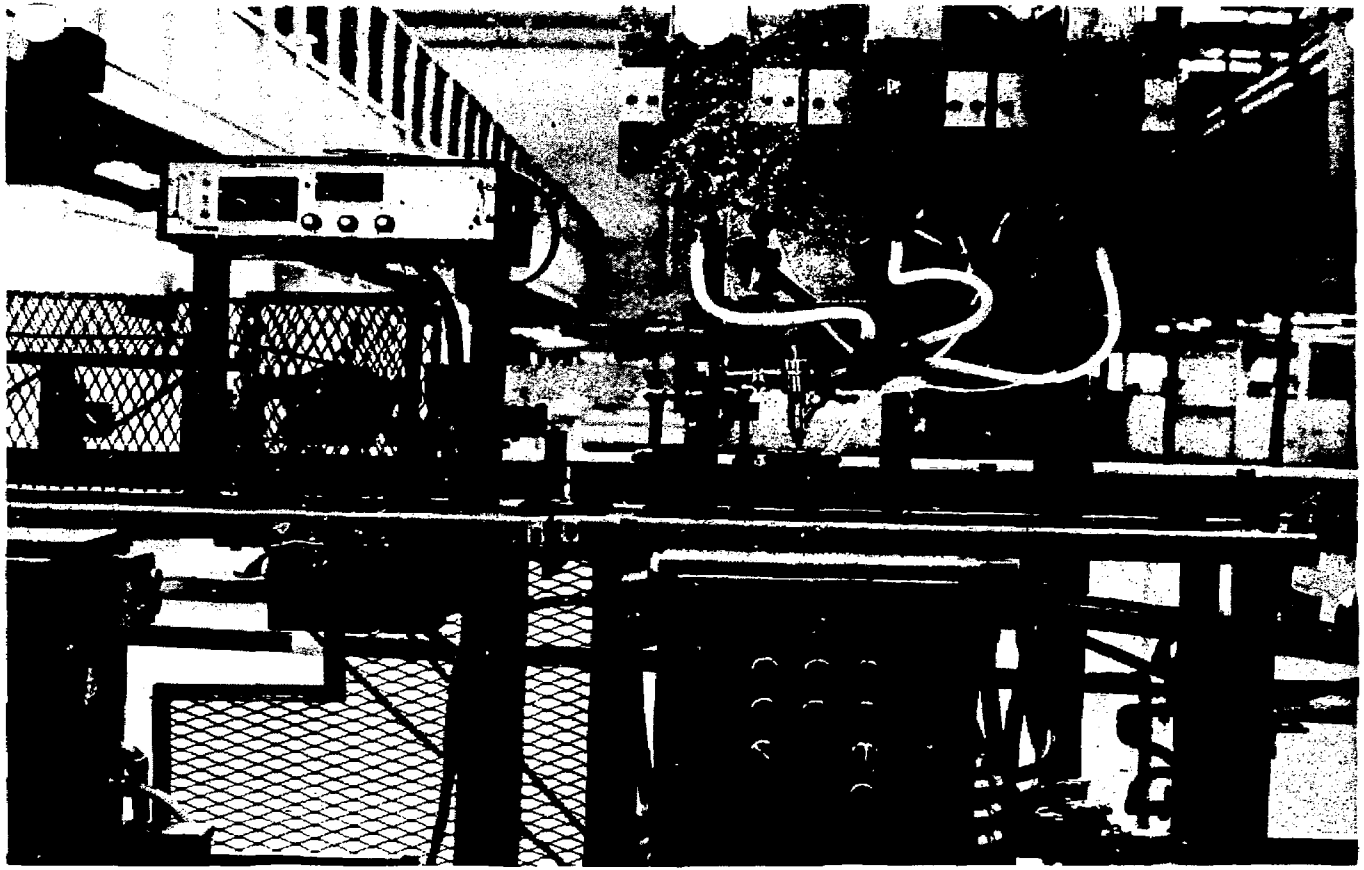

Figure 3.6-16. LCP Solder Metering Equipment.

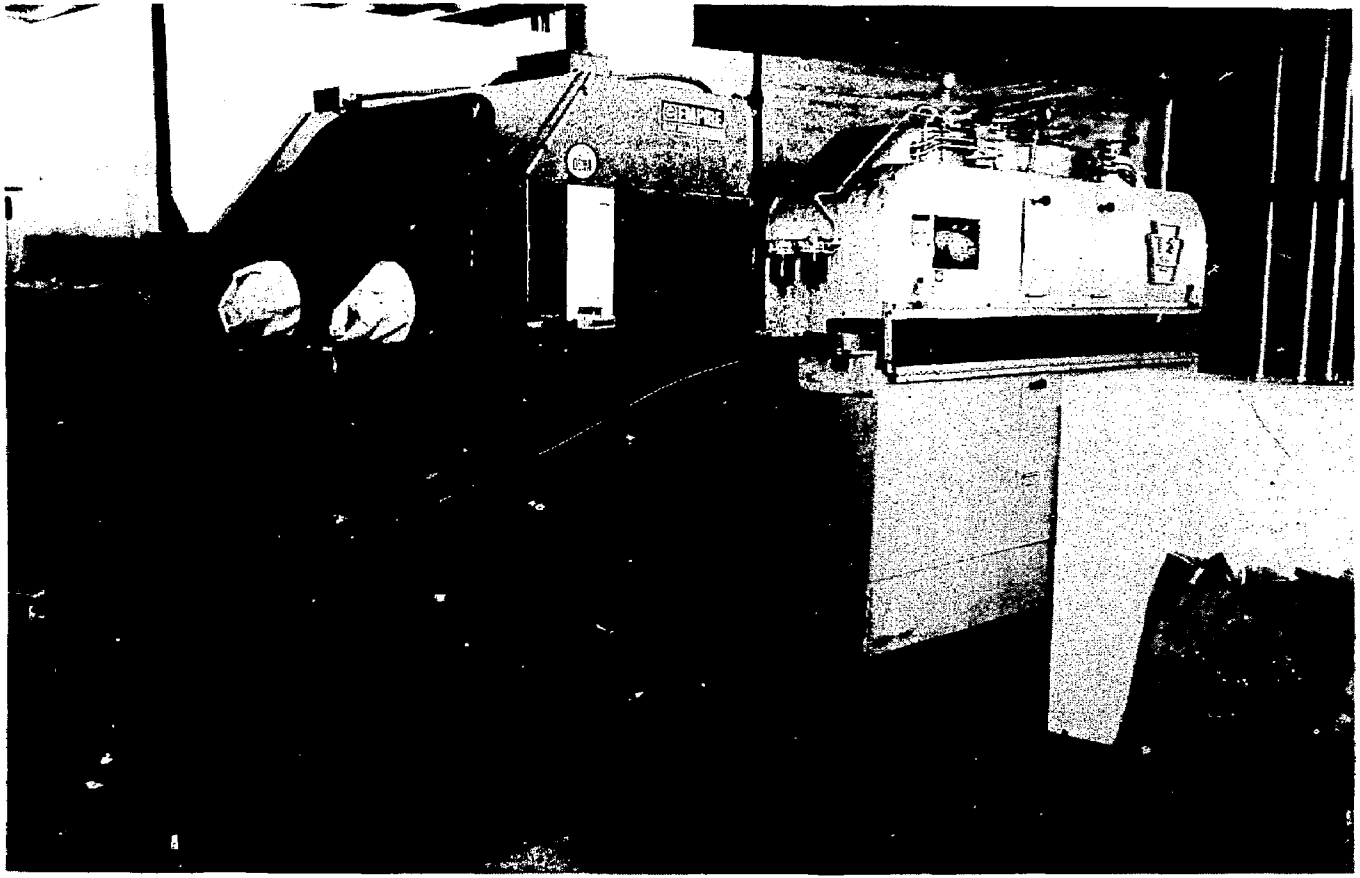

Figure 3.6-17. Final Cleaning and Assembly Line Capstan.

This concept is directly applicable to the manufacture of conductor requirements for TMNS and allows for the independent operation of the two lines while minimizing space requirements.

When the coil conductor grade requirements have been fully wound on a specific shelf, the drive motor is released from that shelf and moved to supply rotation power to the next shelf. The previous shelf is now allowed to free-wheel in the opposite direction as the conductor is unwound, pulled by the coil winding tool. See Figure 3.6-18. For TMNS the conductor would be processed in a like manner.

Conductor Winding

The winder would be contained in a specially constructed dust resistant enclosure, this enclosure will contain the ancillary equipment for cutting, trimming, splicing and testing of the conductor.

At the end of each layer a conductor splice would be accomplished. After locating and marking the splice area, the conductor on the coil would be securely clamped and the tension relaxed. The end would be trimmed and prepared for splice at the pre-located point. The splice plate would be brought to the end region which will have been prepared by hand routing the insulation. The two splice ends are clamped in proper location and Indium solder used with low temperature induction coils. Figure 3.6-19 shows the LCP capstan.

Conductor Fabrication Tools

Convair would propose to procure the total stabilizer requirement for this program in the extruded "C" shape in twenty foot lengths. Preparation of the stabilizer extrusion and its subsequent bonding with the superconducting monolith would require several specific and critical operations, listed in Table 3.6-1.

3.6.8 Program Schedule

A schedule has been layed out for the TMNS coil, it is based on experience factors from the MFTF, LCP and PMS programs.

These experience factors enabled the use of a conductor fabrication time and winding time of one to one and half feet per minute. To bring the time span down to a reasonable time frame, the conductor fabrication and winding time was spread over three shifts, which seems feasible for these operations. The schedule is presented in Figure 3.6-20

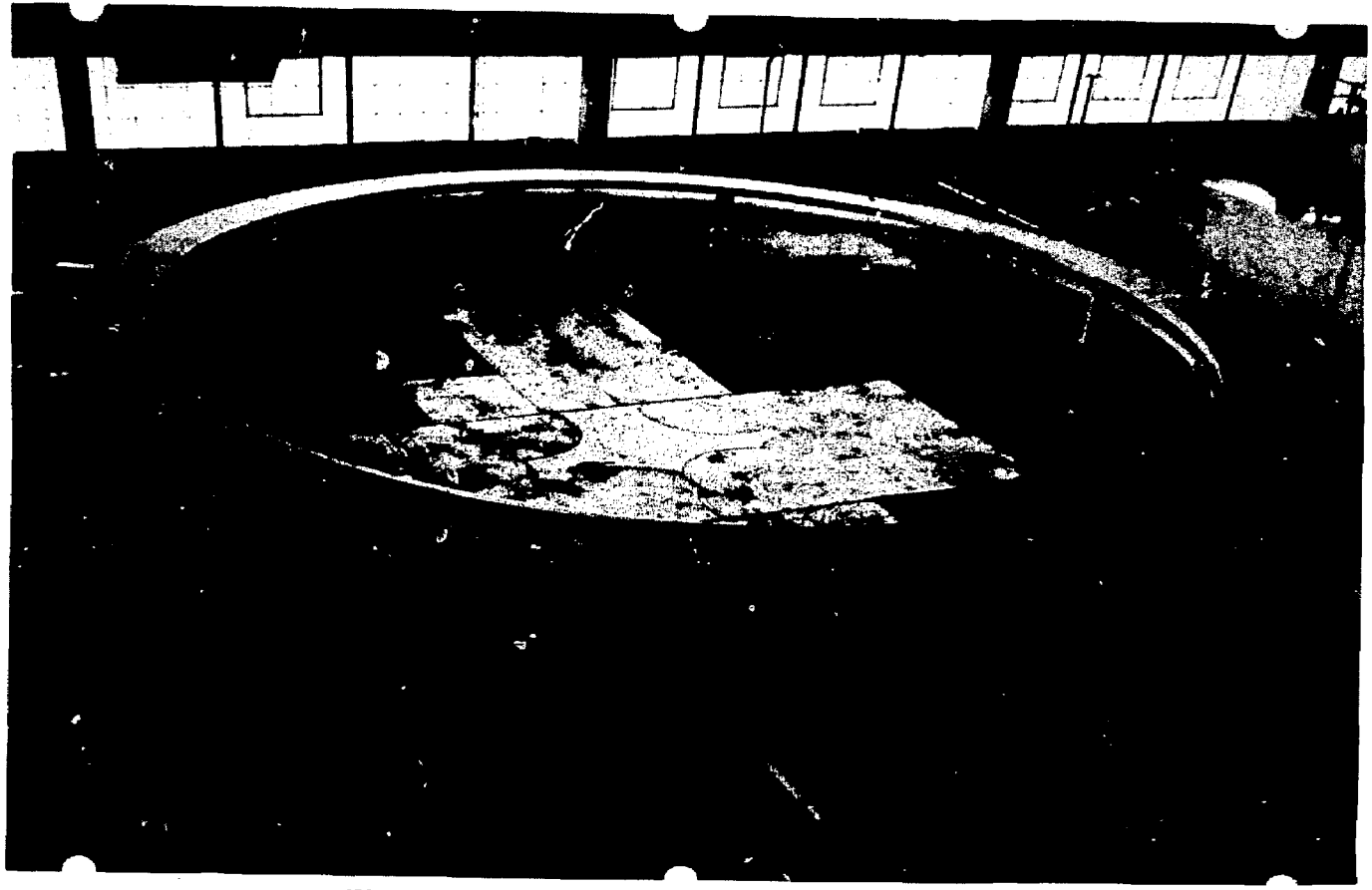

Figure 3.6-18. Conductor Storage Reel Station.

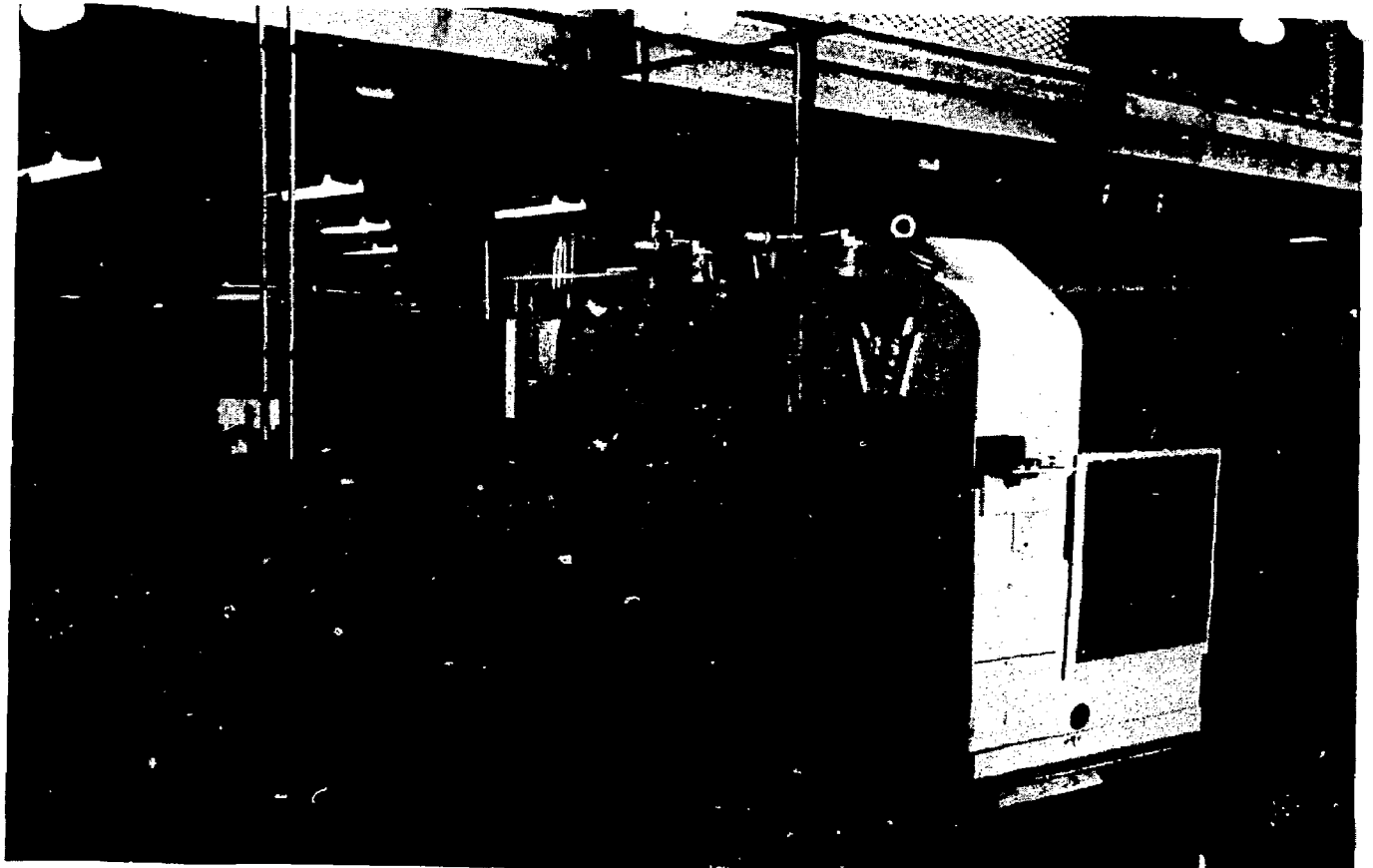

Figure 3.6-19. LCP Winding Caterpillar Capstan

Table 3.6-I. Tool/Equipment Table.

- Power Rolls for Feeding Stabilizer
- Cut Off Saw
- 800 Ton Press for Coldwelding
- 50 ft. diameter Stabilizer Storage Reel
- Straightening Rolls
- Slot Mill
- Heating Elements for Soldering
- Solder Feeding Equipment
- Vapor Degreaser
- Milling Machine for Final Sizing
- Sand Blaster/Cleaner
- Caterpillar Capstan
- 50 ft. diameter Conductor Storage Reel
- Tensioning Machine
- Insulation Applicator
- Winding Machine
- Ultrasonic Inspection Equipment

3.7 QUALITY ASSURANCE

3.7.1 Inspection of Conductor/Stabilizer Solder Bond

The use of a rectangular cross-section superconductor (solid matrix) soldered into a rectangular cross-section copper stabilizer (including copper filler) is readily inspectable with ultrasonics. The inspection system proposed is greatly simplified over similar systems by the use of through-transmission techniques, transducer arrays and direct digital positioning. Through-transmission signals are positive indications of solder bond quality while pulse echo signals require close time discrimination and are more prone to spurious signal interference. If, for any reason, it is determined that pulse echo techniques are required, minor changes in circuit hookup and the addition of manually-operated calibration masks are all that would be required. In this system, four transducer arrays would be utilized eliminating the necessity to mechanically scan the width of the solder bond (Figure 3.7-1). The rectangular nature of the solder bond to be inspected does not require the use of a phased array further simplifying the system. The conductor position is indicated by a digital encoder which the computer accepts directly eliminating any analog to digital conversion or servo loop systems.

The inspection system consists of four transducer arrays positioned around the superconductor. Two of the arrays will act as transmitters for ultrasonic signals which will be received by the arrays on the opposite side of the stabilizer if the solder bond is good. The input and output of these arrays will be handled by the ultrasonic instrumentation which will also select the element for interrogation, determine if the signal timing is correct, convert the signal to digital form and relay it to the computer (Figure 3.7-2). The computer will collect the information required to determine if the solder bond specifications have been met and output the appropriate commands or data. The CRT terminal will present the data in real time and provide for hard copy printout if required.

3.7.2 Inspection of Conductor Splice Solder Bond

Review of trade-offs indicate that a semi-automated system for inspection of the splice solder bond would be the most cost-effective when compared with manual or fully-automated inspection of the 506 (or less) joints.

A manual inspection system would consist of a pair of transducers used for through-transmission testing. These transducers would be held in a fixed orientation by a yoke positioned to scan the splice in two directions perpendicular to the centerline. In this setup, the operator depends on the instrument alarm to indicate any lack of bond in the solder interfaces. No permanent record is available when using this type of system.

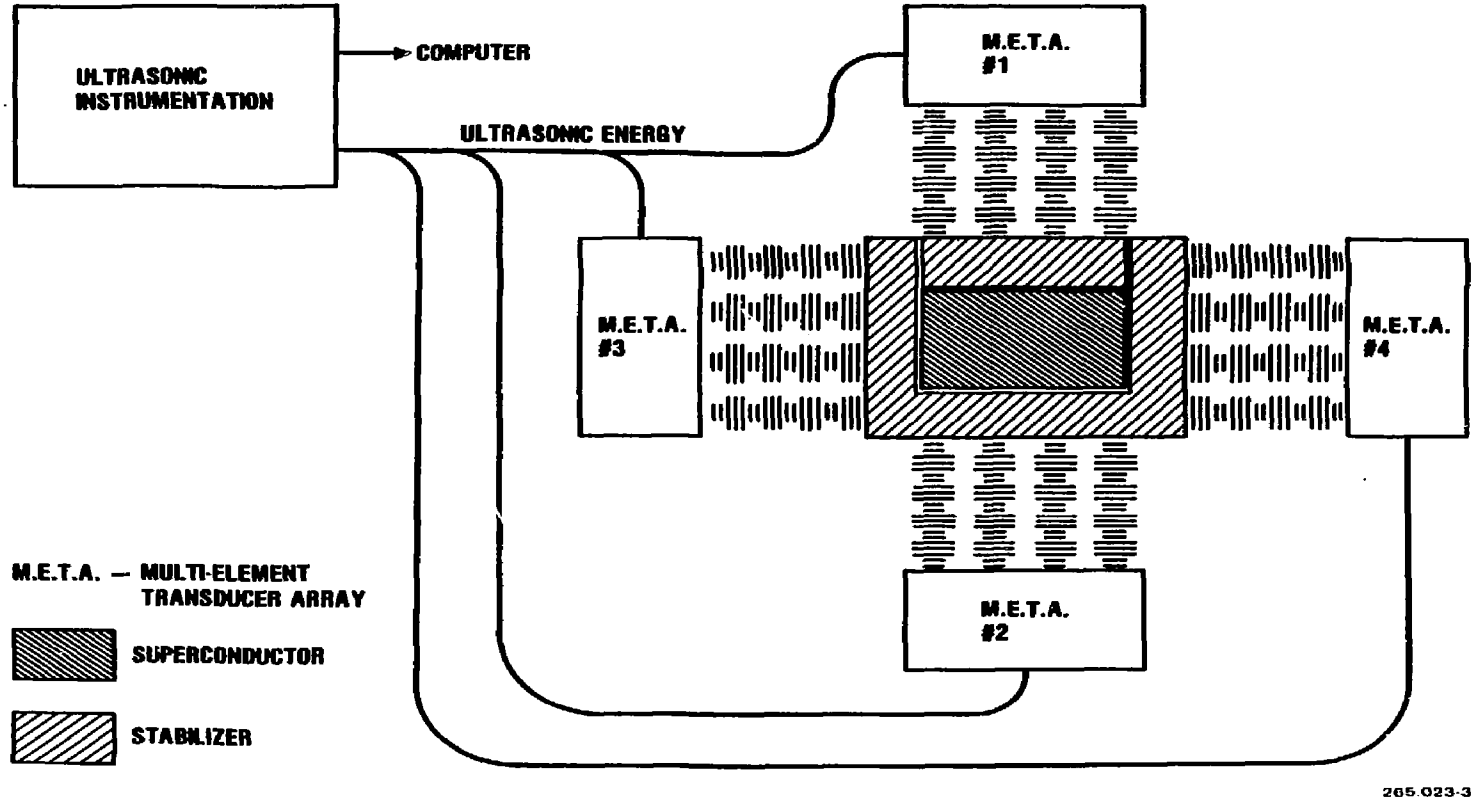

Figure 3.7-1. TMNS Solder-Bond Inspection System Ultrasonic Transducer Orientation.

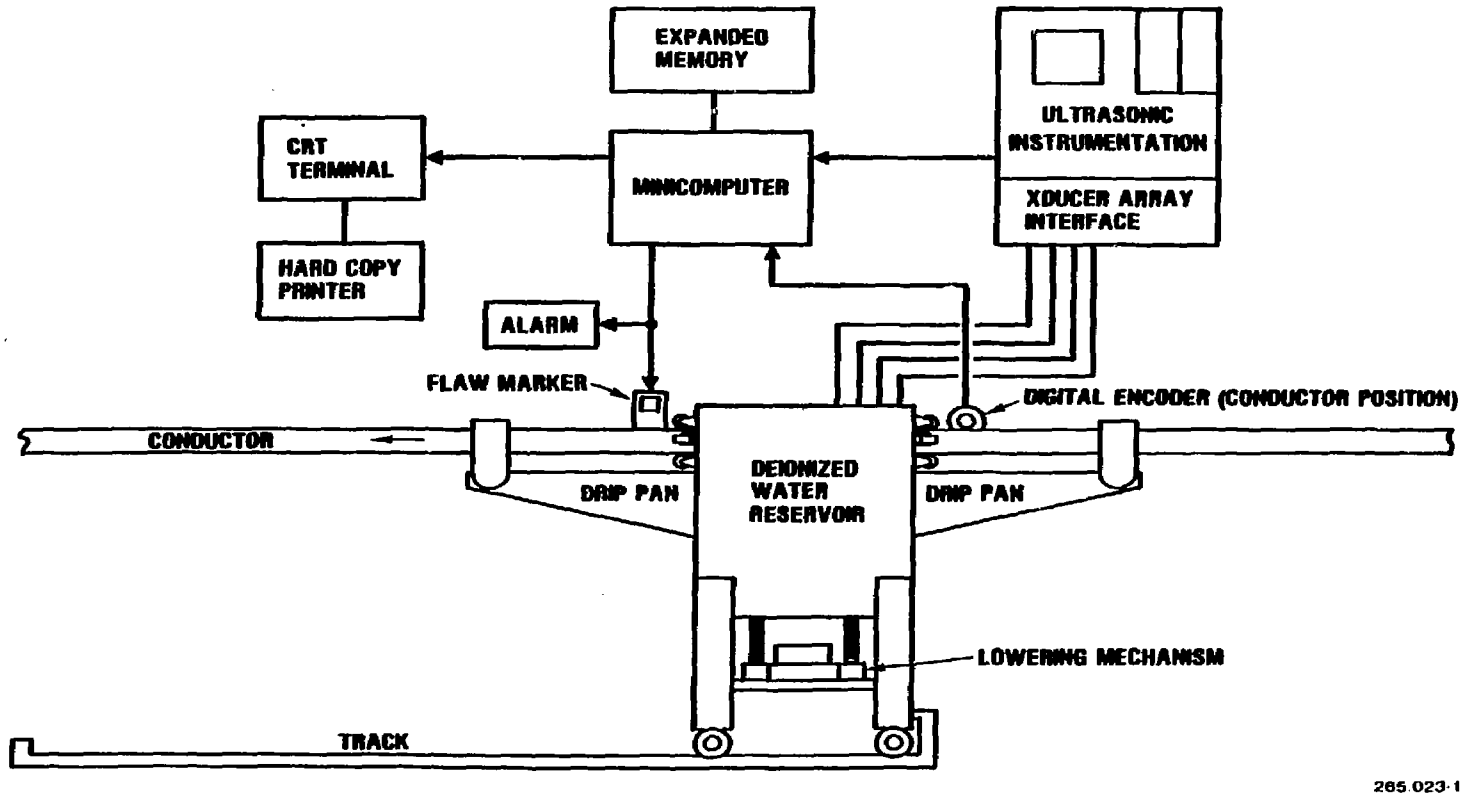

Figure 3.7-2. TMNS Automated Ultrasonic Solder-Bond Inspection System.

If an automated system were used, it would entail the use of equipment similar to that used for the inspection of the conductor/stabilizer solder bond. This requires an extensive capital investment as schedules would not permit the sharing of equipment. It would also entail extensive software development.

A semi-automated system configuration (Figure 3.7-3) provides a framework in which the transducers (2) are constrained. Manual scanning of the entire surface to be inspected is possible and the transducer yoke position is a continuous output. The transducers are moved over the part in any pattern including random and at the same time the solder bond condition is recorded on a CRT at the appropriate position. A complete picture of the solder bond is generated in this fashion and hard copy printout can be obtained if required.

4.0 COST ESTIMATE

4.1 INTRODUCTION AND GROUND RULES (WINDING)

The total cost (including contingency and including fee) for the coil winding is $64,869,248. A breakdown of this cost is provided in Table 4.1-I. This cost is based on the following groundrules:

- Costs are computed in constant 1981 dollars.
- Escalation costs are not included.
- The cost estimate assumes that a completely facilitized site will perform the winding, thus no facility costs are included.
- Tool design and manufacturing costs are excluded.
- Shipping costs are excluded.
- Instrumentation costs are excluded.
- Quality Assurance and Manufacturing Plan costs are excluded.
- Expense for liquid helium is excluded.
- All progress reviews will be held in San Diego, California.

4.2 DETAILED COST ESTIMATE (WINDING)

The cost estimate was done for the task of winding a 12T Yin-Yang coil, which was considered to be composed of the following tasks:

- Material Procurement
- Setup & Checkout the Conductor Production Line
- Conductor Fabrication
- Insulation Fabrication
- Conductor Practice Winding
- Coil Winding Operation
- Program Management

4.2.1 Material Procurement

The estimated cost of this task is $37,114,595 (Table 4.2-I). This is the cost of procuring all the items in Table 4.2-I which are necessary for the TMNS coil winding task. In addition to the

Table 4.1-I. TMNS Cost Estimate

Task #	Description	Cost (1981 $)
1	Material Procurement	$37,114,595
2	Conductor Production Line	373,603
3	Conductor Fabrication	3,474,276
4	Insulation Fabrication	164,969
5	Conductor Practice Winding	235,994
6	Coil Winding Operation	4,181,076
7	Program Management/Engineering	1,633,122
		$47,177,635
	Contingency (25%)	11,794,409
		$58,972,044
	Profit (10%)	5,897,204
	TOTAL PRICE	$64,869,248

Table 4.2-I. Major Construction Material Quantities and Cost

Item	Qty		Cost
Superconductor Nb3 Sn Monolith	201,000 ft		$17,002,188
Superconductor NbTi Monolith	364,000 ft		12,820,080
Copper			5,140,644
Stabilizer & Filler Bar	565,000 ft	$5,118,900	
Practice Winding	2,400 ft	21,744	
Insulation			1,860,107
Button Insulation	565,000 ft	$1,328,880	
Lateral Insulation	944 Sheets	334,006	
Side Insulation (incl. Practice)	181 Sheets	197,221	
Solder	21,500 Lb		178,020
Adhesive	293 Qts		51,643
Indium	3,279 ft		52,648
Material Receiving/Inspection			9,265
		TOTAL	$37,114,595

material cost, this task includes the value for Quality Assurance to perform inspection on materials received.

4.2.2 Setup and Checkout the Conductor Production Line

The estimated cost of this task is $373,603.

Manufacturing	-	$128,035
Tooling	-	$127,368
Quality Assurance	-	$118,200
Total		$373,603

Facilities Engineering will clear a work area and provide utilities to tools, equipment, and machines on the conductor assembly line. Tooling will install, level, and checkout all tools and machines needed on the assembly line. A final checkout and validation will be performed by the Program's Operations Department. Crane and rigging will provide support as needed. The Manufacturing Engineering Project Office (MEPO) will monitor all tooling and factory activity. Quality Engineering will provide inspection support.

4.2.3 Conductor Fabrication

The estimated cost of this task is $3,474,276.

Manufacturing	-	$2,659,096
Tooling	-	45,086
Quality Assurance	-	464,650
Engineering	-	305,444
		$3,474,276

Costs associated with the manufacture of 565,000 feet of conductor are presented in this task. A 5 man crew will be required to support the fabrication of the conductor. The crew will consist of 1 leadman, 3 mechanics and 1 helper. The manufacturing costs include cold welding the copper stabilizer and filler bar to the required length per grade as well as roll straightening to remove irregularities from the copper bar. In addition, factory hours include milling of the stabilizer slot to final specs in preparation for insertion of the superconductor. Labor costs also consist of cleaning, inspection, soldering the conductor, stabilizer and filler bar, and winding the finished conductor onto a storage reel. Quality Assurance will perform an ultrasonic inspection on the soldered conductor, as well as providing inspection to each operation. The MEPO will act as a coordinator for any other departmental support required. They will provide the instructions for conductor fabrication and check progress for the Program Manager. Tool Planning will provide work instructions.

Engineering costs are for the test lab to perform 1,020 conductor short sample tests and 1,165 electrical checks. Finally, Plant

Engineering will provide transportation and handling for the superconductors, stabilizer and filler bar.

4.2.4 Insulation Fabrication

The estimated cost for this task is $164,969.

Manufacturing	-	$143,461
Tooling	-	8,290
Quality Assurance	-	13,218
Total		$164,969

This is the required cost to fabricate insulation necessary for the coil winding operation. Vendor provided details and details cut from sheet material will be fabricated into layer-to-layer insulation. Tooling costs contain coordination efforts by the MEPO to monitor and report the progress of the fabrication. Tooling costs also provide work instructions to make the insulation. Inspection support is provided by Quality Assurance during the insulation fabrication.

4.2.5 Conductor Practice Winding

The estimated cost of this task is $235,994.

Manufacturing	-	$191,279
Tooling	-	11,635
Quality Assurance	-	33,080
Total	-	$235,994

In order to check out and verify all operations and equipment, 2400 feet of simulated superconductor and stabilizer will be practice wound, including insulation. This cost consists of factory efforts needed for the winding, including coldwelding the stabilizer and filler bar, roll straightening of the copper bar, milling of the slot in preparation for insertion of the superconductor. This task also includes cleaning of the bar and prep for solder adhesion, bonding the filler bar, superconductor and stabilizer together, and providing support during inspection and checkout of the wound conductor. Crane and rigging will provide transportation and handling for the conductor. Tooling costs cover support by the MEPO to coordinate overall operations. Quality Control will perform conductor electrical checks and other inspection support. Material costs are covered in Paragraph 4.2.1.

4.2.6 Coil Winding Operation

The estimated cost of this task is $4,181,076.

Manufacturing	-	$3,570,206
Tooling	-	62,103
Quality Assurance	-	548,767
Total Cost		$4,181,076

This is the cost to conduct winding operations to pancake wind 201,000 ft. of Nb_3Sn and 364,000 ft. of NbTi. The factory task includes the following:

- Installing electrical insulation.
- Performing various electrical checks on the wound layers, the complete power lead circuits, and the complete coil.
- Fabrication conductor joint components.
- Assembling splice joints in the coil pack.
- Assisting in the electrical checks of the joints.

Transportation and handling assist will be supplied by Plant Engineering (crane and riggers). The fabrication crew size will consist of four mechanics and one instrumentation technician. All support for the coil winding will be coordinated by the MEPO. They will monitor progress and report status of the operation. Tooling will also provide coil winding work instructions. Quality Control will provide inspection support.

4.2.7 Program Management

The estimated cost of this task is $1,633,122.

Tooling	-	$267,610
Quality Assurance	-	289,984
Engineering	-	767,528
Program/Financial Mgt.	-	302,890
Travel	-	5,110
Total		$1,633,122

The tooling costs consist of a full time Operations Manager to oversee tooling and factory throughout the winding task. Similarly, there will be a Quality Assurance Manager for the program. Engineering liaison will be provided during conductor fabrication, insulation fabrication, coil winding and coil checkout. Engineering will monitor and evaluate in-process verification tests during conductor fabrication. Analysis will be provided during coil winding to ensure functional integrity. Also, engineering will provide liaison and coordination support to solve day-to-day fabrication problems. Checking and release assist will be provided during conductor fabrication. Also, parts and data record support.

To handle design changes and manufacturing variances, test procedures will be prepared and checkout testing will be conducted on the coils. Engineering will also provide vendor coordination and participate in vendor reviews. In addition, a Chief Engineer

will provide functional direction throughout the winding task. Finally, a Program Manager will be provided, as well as financial management support for financial reports.

4.3 ROUGH COST ESTIMATE YIN-YANG

Our survey of existing and proposed superconducting magnet designs has shown that overall magnet weight and hence magnet cost can be estimated based on the magnet's stored energy. The following information was obtained from the MFTF-A and CASK CDP programs.

MAGNET	WEIGHT (lbs)	STORED ENERGY (MJ)	#/MJ
• MFTF-A	700,000	500	1400
• CASK CDP*	5,068,163	5000	1013

* excluding vacuum vessel

Based on this information, a weight to stored energy ratio of 1,000 lbs/MJ was assumed for TMNS. This assumption includes the projection that larger magnets are more structurally efficient than smaller magnets. The estimated stored energy for TMNS is 13.34 GJ, leading to a projected total weight of:

13340 MJ * 1000 #/MJ = 13,340,000 lbs.

To find the weight of just the structural case by itself, subtract out the estimated weight of the winding.

Total Magnet estimated weight	-	13,340,000 lbs.
Computed weight of winding	-	1,828,000 lbs.
Balance (Case Structure)		11,512,000 lbs.

The cost estimate for the TMNS structural case is based on the actual costs of MFTF as structural case. Those costs are:

Material	$1.07/lb.
Labor	6.75/lb.
Misc. (Management, Shipping, Weld Rod, etc.)	0.40
	$8.22/lb (1979 dollars)

If an annual inflation rate of 12% is used, then the estimated cost for the structural case of TMNS is $10.30/lb. in constant 1981 dollars.

5.0 CONCLUSIONS

The TMNS Yin-Yang magnet winding conceptual design meets all functional requirements. During the course of this study, a variety of important design considerations were concluded regarding a coil of this size and 12T field magnitude. The following paragraphs summarize these features.

Conductor ability to meet current density requirements lies mainly in the usage of helium II as the cryogenic coolant. With a generated heat flux of 0.77 w/cm^2, the conductor far exceeds the capability of helium I to render it steady-state cryostable. Thus, the design is forced to use helium II as the coolant, even though a large amount of its cooling capacity is unused. Since the cooling capacity of the helium II is not fully utilized, conductor cryostability was easily achieved and it was not a major design driver for this magnet.

Heat loads to the 1.8K Helium II are best limited with the use of an LHe shield placed between the magnet and the LN_2 shield. These heat loads can be further limited by reducing the number of superconductor joints and/or lowering the resistivity of the joint itself. Overall, the magnet heat loads are manageable and within the capacity of existing refrigeration systems.

Structural integrity proved to be the most challenging aspect of this design study. However, our studies have shown that a TMNS size 12 Tesla Yin-Yang magnet pair using Nb_3Sn superconductor can have acceptable conductor stress and strain levels. The structural integrity is derived from efficient utilization of the magnet structural case. The substructure arrangement envisioned for this coil effectively reduces the forces acting on the conductors by regionalizing the magnetic pressures, thereby inhibiting their ability to accumulate. The half-hard copper stabilizer surrounding the superconductor further limits the strain on the brittle Nb_3Sn superconductor. The divided structure and half-hard stabilizer limit the strains in the Nb_3Sn within a favorable current carrying region.

The operation and control of the nested coils making up the Yin-Yang can be accomplished effectively and safely by use of present day technology. Using five or more nested coils per Yin-Yang, the adiabatic temperature rise of the conductor can be kept below 200K while maintaining the dump voltage for each coil at 1000 volts or less. Further, the computer control of the coil currents can be accomplished using existing off-the-shelf hardware.

Fabrication of the conductor is feasible with reasonable extrapolations of existing technology and procedures. Proposed construction materials have proven properties and are readily available. Quality assurance techniques proposed for the construction have been successfully used on other magnet programs.

In summary, the major design drivers for a coil of this size are the structural and electrical integrity of the winding. The design presented in this report successfully meets these challenging technical requirements as well as providing a readily producible coil design.

6.0 REFERENCES

1. Baldi, R.W., et al, "Cask Commercial Demo Plant Superconducting Magnet System - Conceptual Design Final Report," Report No. CASK-GDC-031, December 1979.

2. EFFI Calculations for TMNS Model 05R, per Dwg. AAA80-103415-OB, from R. W. Hoard, Lawrence Livermore National Laboratory, May 5, 1981.

3. Hoard, R. W., "Heat Transfer and Stability of TMNS Coils in Superfluid He-II," LLNL Interdepartmental memo, 6 February 1981.

4. "The Structural Analysis of Non-Homogeneous Solenoids Using the Stansol Computer Program," Mechanics Research Inc., Report No. MRI-C2754-TR-3, September 30, 1975.

5. "TMNS Preliminary Statement of Work," September 1979.

6. Deis, D.W., et al, "Strain-Critical Current Data for Large Multifilament Nb_3Sn Conductors," UCRL-79724 Preprint, Lawrence Livermore National Laboratory, October 5, 1977.

7. Scanlan, R.M., et al., "Mechanical Properties of High Current Multifilamentary Nb_3Sn Conductors," UCRL-84040 Preprint, Lawrence Livermore National Laboratory, May 23, 1980.

8. Milgilori, R.I., et. al., "Dielectric Tracking in Liquid Helium," Cryogenics, July 1978.

9. Haarman, R. A. and K. D. Williamson, Jr., "Electrical Breakdown and Tracking Characteristics of Pulsed High Voltages in Cryogenic Helium and Nitrogen," Advances in Cryogenic Engineering. Vol. 21, 1976.

10. Hwang, K.F. and S.O. Hong, "Dielectric Breakdown of Liquid and Vapor Helium in Bulk and Across Epoxy Insulation," 7th Symposium on the Engineering Problems of Fusion Research, October 1977.

11. Maxstadt, F.W., Electrical Engineering 53 (1934) Quoted in Reference 12.

12. "An Introduction to Discharge and Plasma Physics," Edited by S.C. Haydon.

13. Gerhold, J., "Dielectric Breakdown of Helium at Low Temperatures," Cryogenics December 1972.

14. "Conceptual Design of a 12 TESLA Model Magnet for Testing in the High Field Test Facility - Part II, Phase I Final Report," General Dynamics Convair Report No. GDC-ORWL-80-002, June 1980.

15. O'Neill, R.F. and D.H. Riemer," Thermodynamic Analysis of the Magnet System for Mirror Fusion Test Facility," General Dynamics Convair Report No. CASD-LLL-78-002, October 1978.

16. Rackov, P.M. and C.D. Henning, "Superconductor Joining Methods for Large CTR Magnets," Sixth Symposium on Engineering Problems of Fusion Research, San Diego, California, 1975.

17. Hilal, M.A., "Thermal Contact Resistance and Cryogenic Stability of Large Conductors," to be published in the proceedings of the 1981 Cryogenic Engineering Conference.

APPENDIX: HEAT TRANSFER AND STABILITY OF TMNS COILS IN SUPERFLUID He-II

Purpose

The purpose of this appendix is to document our conclusions concerning heat transfer calculations necessary for the design of the 12-T, Nb_3Sn A-cell coils for the LLNL TMNS fusion program. The present interest is in incorporating into the magnet design He-II coolant flow channels that permit steady-state stabilization of a single turn of superconducting composite conductor. This problem is best solved by reviewing the heat generation in the conductor in the event of a possible superconducting-to-normal quench and understanding the heat transfer (or removal) properties of the He-II coolant.

Heat Generation in the Conductor

Please refer to Fig. 1, which shows a plot of the heat generated in the conductor turn as a function of its temperature. This curve is made by flowing a constant current through the conductor in the presence of a transverse constant magnetic field (I and H_a). The temperature of the conductor length is slowly increased by external means, and the heat generated by the current flow is plotted as a function of the conductor temperature. The resultant heat production (watts/cm^2) can be summarized as:[1]

$$
\begin{aligned}
G &= 0 && T_b \leq T < T_{cs} \\
G &= I\left[I - I_c\left(\frac{T_c - T}{T_c - T_b}\right)\right]\frac{\rho}{PA_c} && T_{cs} \leq T < T_c \qquad (1) \\
G &= \frac{I^2\rho}{P_s A_c} && T_c < T
\end{aligned}
$$

where I_c and T_c are the critical values obtained at 1.8 K and at applied field H_a, T_b is the starting bulk temperature of the coolant bath, ρ and A_c are the resistivity and area of the nonsuperconducting composite component (usually the copper matrix), P_s is the conductor perimeter, and T_{cs} is the temperature at which current sharing begins between the superconducting filaments, composite matrix, and copper stabilizer. T_{cs} is given by:

$$
T_{cs} = T_b + \left(1 - \frac{I}{I_c}\right)\left(T_c - T_b\right) \qquad (2)
$$

Once again I_c and T_c are evaluated at 1.8 K and at H_a.

In words, Fig. 1 states that no heat is generated by the conductor until a portion of the current I starts to spill into the copper matrix at T_{cs}. Then the heat production increases linearly until all the current flows into the copper at T_c and beyond. The three heat generation regions depicted in Fig. 1 are summarized by equations 1 and 2.

Heat Transfer to He-II

Fig. 2 shows the heat transfer curve of an open coolant channel immerged in superfluid He-II. The channel is heated with known power inputs, and the resulting temperature rise is plotted as shown.[2] The low flux region is determined by the Kapitza conductance, a little understood phenomenon in which heat is conducted by an apparent radiant transport of phonons between the conductor surface and the He-II. For copper to He-II, it takes the form of:[3]

$$q_k = \frac{Q}{P_s} = 0.02\left(T^4 - T_b^4\right) \frac{\text{watts}}{\text{cm}^2} \qquad T_b \leq T < T_m \tag{3}$$

Beyond the Kapitza region, the heat transfer becomes constant (with respect to temperature) taking upon a value which appears to be a function of channel length only:[4]

$$q_c = \frac{\alpha}{L^{1/3}} \tag{4}$$

where α has been reported to assume values from 7.0 to 7.4. Here q_c represents the heat flux in the channel, the actual conductor wetted surface heat flux is:

$$\bar{q}_c = \frac{q_c n_c f W}{P_s} \quad \text{per unit conductor length.} \tag{4.a}$$

where n_c is the number of channels, f the channel void fraction, and W is the channel width.

This flat region on the heat transfer curve has the most impact on magnet design because if $\bar{q}_c$ is never exceeded during a superconducting-to-normal transition the conductor will always recover. Heat transfer is accomplished by the outward flow of He-I fluid (away from the heat source) with an inward motion of the He-II fluid component (towards the heat source). The He-II fluid components then undergo transitions to normal He-I fluid at the conductor surface. At the temperature T^*, all of the liquid helium has been converted to normal He-I and film boiling commences.

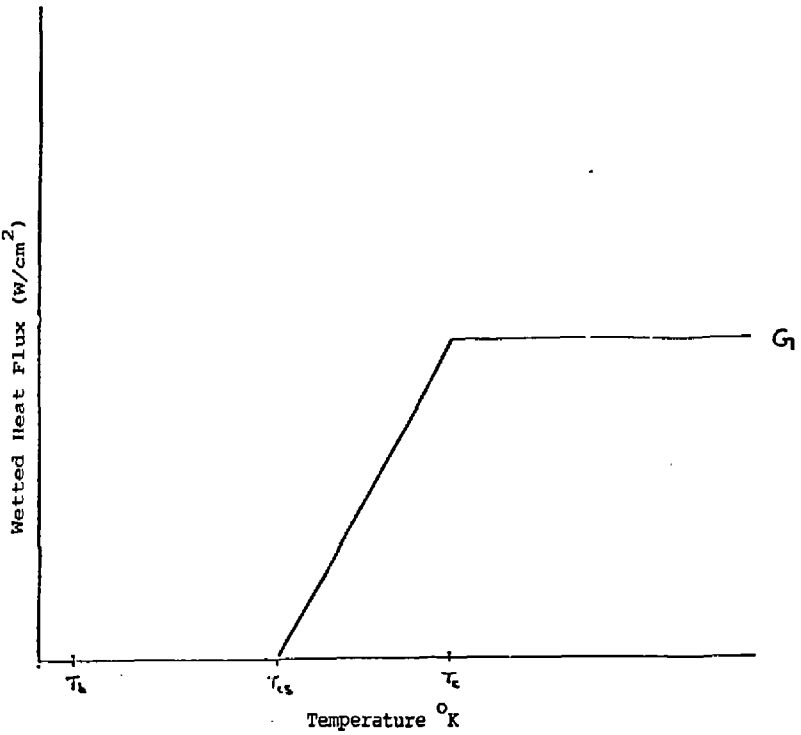

Figure A-1 TMNS Conductor Heat Generation Curve

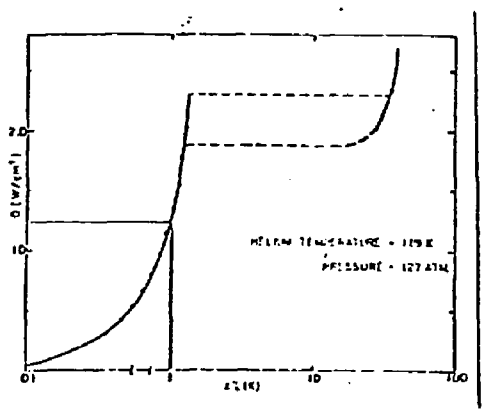

Figure A-2 He II Heat Transfer Curve

These heat transfer and generation regions are graphically depicted in Fig. 3 with the corresponding transitional temperatures. T_m is defined when the Kapitza heat transfer equals the flat critical value of equation 4.

$$T_m = \left[\frac{\bar{q}_c}{0.02} + T_b^4 \right]^{1/4} \tag{5}$$

assuming that in the film boiling region q is linear with temperature; T* is the temperature at which $\bar{q}_c$ intercepts the film boiling line.

$$T^* = T_b + \frac{\bar{q}_c}{h} \tag{6}$$

since:

$$q_f = h(T - T_b) \text{ with } h \approx 0.1 \frac{\text{watts}}{\text{cm}^2\ \text{K}} \tag{7}$$

for the film boiling region.

T_f is defined by the interception of the I^2R heating curve with the film boiling region:

$$T_f = T_b + \frac{I^2 \rho}{A_c P_s h} \tag{8}$$

These heat transfer and generation curves will be used in magnet design considerations in the next sections.

Application to the Design of the TMNS 12-T Magnets

This section concerns the design of He-II coolant channels for the 12-T Nb_3Sn TMNS yin-yang magnets. Figure 4 shows the conductor, layer, and interturn G-10 insulation. The problem entails designing adequate He-II cooling channels within the G-10 insulation spaces. The various calculated steps are summarized and tabulated below.

Cross-sectional area of the total conductor copper A_{cu}:

$$A_{cu} = 4.897 \text{ cm}^2$$

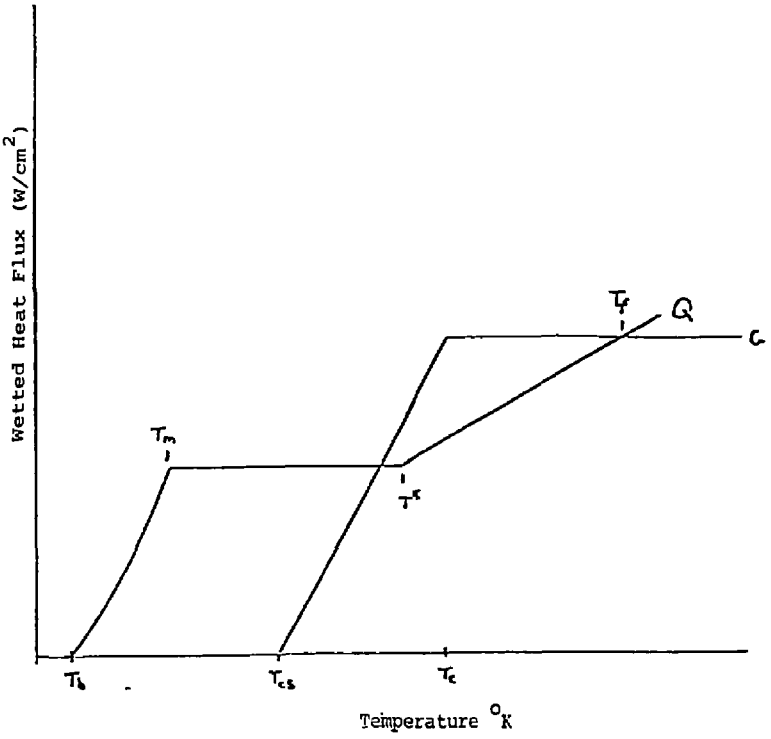

Figure A-3 Heat Transfer and Generation Curves
TMNS Conductor in He II

THE SELECTED TMNS CONDUCTOR DESIGN IS
THE RESULT OF EXTENSIVE TRADE STUDIES

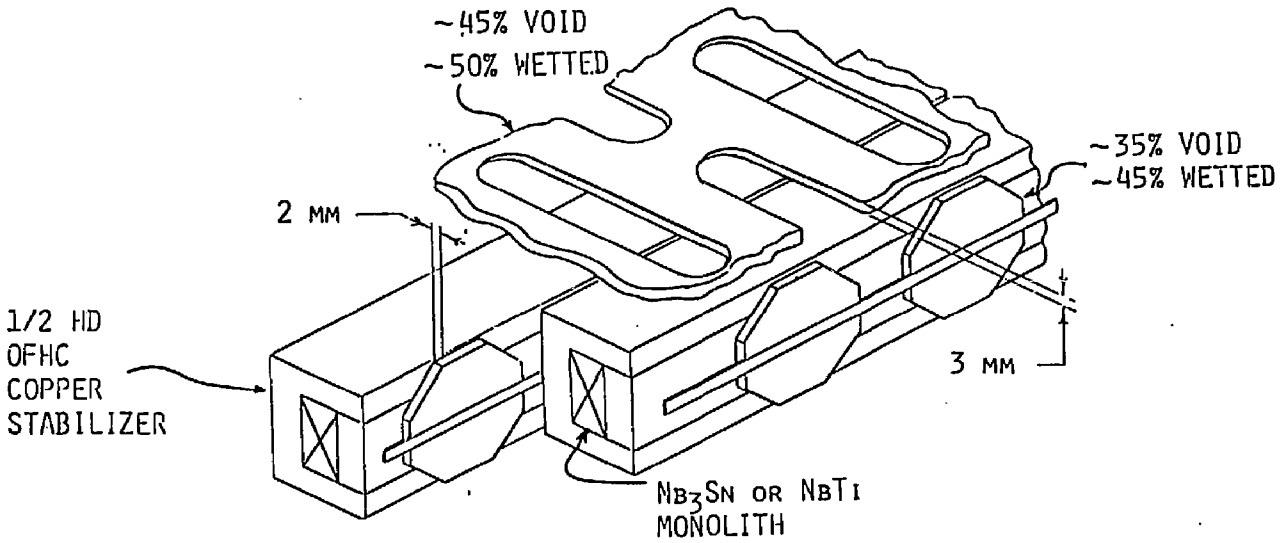

Figure A-4

Effective copper resistivity P:

$$\rho = 6.802 \times 10^{-8}\ \Omega - \text{cm}$$

Normal conductor generated power per unit length:

$$P/l = Q = \frac{I^2\rho}{A_{cu}} = 3.380 \text{ watts/cm}$$

Volume of He-II surrounding each conductor per unit length:

$$V_{He\text{-}II}/l = 1.058 \text{ cm}^3/\text{cm}$$

Conductor wetted surface area per unit length A_{ws}:

$$A_{ws} = 4.119 \text{ cm}^2/\text{cm}$$

Conductor wetted heat flux $\bar{q}_c$:

$$\bar{q}_c = \frac{P/l}{A_{ws}} = 0.821 \text{ watts/cm}^2$$

Figure 5 shows a schematic cross section of bundle of conductors and their associated He-II cooling channels. Notice that there are actually eight cooling channels that surround each conductor length (four horizontal and four vertical). In general, the heat flux will not flow equally through each, but will predominately travel through the channel having the smallest resistance for heat transport to an additional volume of He-II. This concept defines a He-II coolant channel conductance given below for the horizontal and vertical channels:

$$\text{From equation 4, } \frac{Q}{A} = F\nabla T^{1/3} = F\frac{\bar{\Delta T}^{2/3}}{\Delta L^{1/3}}\Delta T = C\Delta T$$

where C is the channel conductance.

Horizontal:

$$q_h = \frac{Q}{4}\left(\frac{C_h}{C_h + C_v}\right) \text{ will flow into each horizontal channel}$$

COOLING CHANNELS ACCESSIBLE TO NORMAL
TURN X VIA NEAREST NEIGHBORS IN ZONE 1

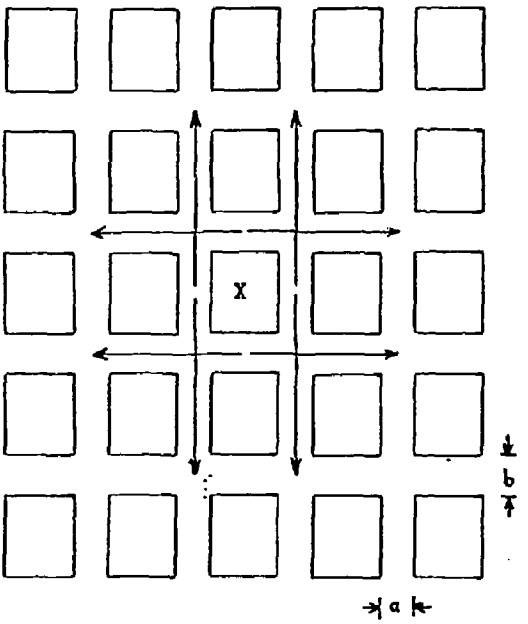

Figure A-5

with $C_h \approx A_h / L_n^{1/3}$ and $C_v \approx A_v / L_v^{1/3}$

$$q_h = \frac{Q}{4}\left[\frac{1}{1 + \frac{A_v}{A_h}\left(\frac{L_h}{L_v}\right)^{1/3}}\right] \tag{9}$$

Vertical:

$$q_v = \frac{Q}{4}\left[\frac{1}{1 + \frac{A_h}{A_v}\left(\frac{L_v}{L_h}\right)^{1/3}}\right] \tag{10}$$

will flow into each vertical channel in which A_v, A_h, L_v, and L_h are the vertical and horizontal coolant channel cross-sectional areas and channel lengths. An important observation is that effectively there are many interconnecting cooling channels surrounding each conductor length, as shown in Fig. 5. After the heat fluxes leave the first zone of nearest neighbors, they are each split into two channels (one horizontal and one vertical). As shown in Fig. 6, the fluxes are further reduced as they diffuse pass each successive zone of neighboring conductors. In a large magnet system, an initial coolant channel carrying a heat flux of 1 W/cm^2 can rapidly split into 100 channels carrying a flux of 0.01 W/cm^2 each after migrating a distance several conductors away from the normal turn. However, the maximum heat allowed to leave the conductor has to first propagate through the original eight cooling channels adjacent to the normal turn. The initial horizontal and vertical channel lengths are those transversed by the fluxes before they are divided at the intersections. Ideally, the maximum full recovery current is that which produces the maximum heat flux that can propagate down a channel of length L_c without initiating breakdown of superfluid in the channel. The inlet and outlet temperatures within the channel vary from approximately 2.17 to 1.8 K. If the heat flux is too large for a given channel length, the inlet temperature can rise above T_λ (2.17), converting the He II to He I throughout the channel. In this study, L_c is defined as the maximum length that a given heat flux travels before it is split or subdivided by flowing into a connecting cooling channel. From Fig. 5, this is shown by the arrows to be the distance from the middle of the normal conductor to just beyond the first zone of nearest neighboring conductors (this definition of L_c is slightly more conservative than that given in Section 2.5.1, but the additional channel lengths are only a few centimeters longer). For the TMNS conductor design, these are defined as shown in Fig. 5. These distances are:

L_v = 4.586 cm and L_h = 3.198 cm

also (11)

COOLING CHANNELS ACCESSIBLE TO NORMAL
TURN X VIA NEAREST NEIGHBORS OF ZONES 1-3

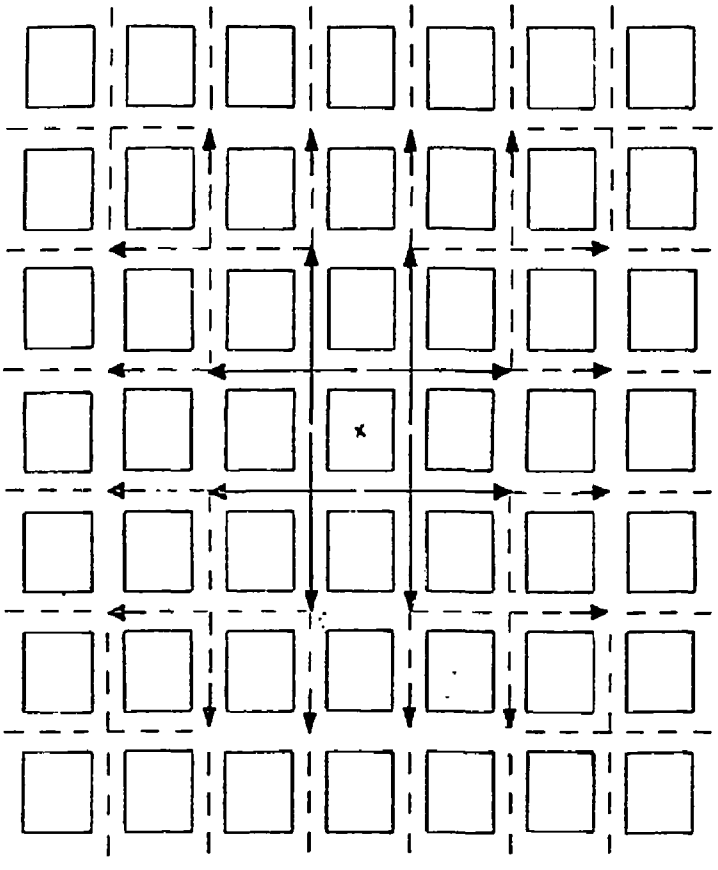

Figure A-6

$A_v = 0.222\ cm^2$ and $A_h = 0.577\ cm^2$

Utilizing equations 9, 10, and 11, yield:

$$q_h = 3.97\ watts/cm^2$$
$$q_v = 3.52\ watts/cm^2 \qquad (12)$$

flow thru each horizontal and vertical channel due to power production of 3.380 watts/cm length of normal conductor turn. While using equation 4 indicates that the maximum permissible heat fluxes are:

$$q_{hmax} = 7.4/L_h^{1/3} = 4.45\ watts/cm^2$$
$$q_{vmax} = 7.4/L_v^{1/3} = 5.02\ watts/cm^2 \qquad (13)$$

Comparing equations 12 and 13, we see that $q_{h,vmax} > q_{n,v}$, which implies that the designed insulation cooling channels are adequate to provide thermal stability to the TMNS conductor configuration operating at 15.6 kA current. In fact, since the maximum full recovery current scales as the square root of the maximum transmitted heat flux:

$$\frac{I_{max}}{I} \approx \left(\frac{q_{max}}{q}\right)^{1/2} = \left(\frac{9.47}{7.49}\right)^{1/2} = 1.124$$

which implies that the maximum full recovery current in the TMNS is 17.5 kA or 12.4 percent higher than the operating current (15.6 kA).

The above analysis has ignored the effects of cold ends on the heat transfer stability. If a given length of conductor becomes normal and experiences a temperature rise while its ends are maintained at the coolant bath temperature, the colder ends act together with the channel coolant to enhance the conductor stability via "cold-end recovery."[1] The Maddock criterion for cold-end recovery states that the maximum current that will yield recovery is determined from equating the areas of the heat transfer and heat generation curves of Fig. 3. This requires that

$$\int_{T_b}^{T_f} \left[G(H_a, I, T) - Q(T)\right] dT = 0 \qquad (14)$$

Integrating equations 1, 3, 4, and 7 between the temperature ranges depicted by equations 2, 5, 6, and 8 yields an equation for the maximum cold-end recovery current:

$$\left\{ 0.02\left(\frac{T_m^5}{5} - T_m T_b^4 + \frac{4}{5} T_b^5\right) + \bar{q}_c(T^* - T_m) + h\left(\frac{T_f^2}{2} - T_f T_b + T^* T_b^2 - \frac{T^{*2}}{2}\right) \right.$$

$$\left. \frac{-\rho}{P_s A_c}\left[I^2(T_c - T_s) - \frac{II_c T_c (T_c - T_s)}{T_c - T_b} + \frac{II_c\left(T_c^2 - T_s^2\right)}{2(T_c - T_b)} + I^2(T_f - T_c)\right]\right\} = 0 \qquad (15)$$

with

$$T_b = 1.8 \text{ K}$$

$$T_{in} = \left[\frac{\bar{q}_c}{0.02} + T_b^4\right]^{1/4} \qquad \text{with } \bar{q}_c = \frac{q_c \eta_c f W}{P_s}$$

$$T_s = T_b + \left(1 - \frac{I}{I_c}\right)(T_c - T_b)$$

$$T^* = \frac{\bar{q}_c}{h} + T_b \qquad (16)$$

$$T_c = T_c(H_a) \approx 10 \text{ K at } H_a = 12 \text{ T}$$

$$T_f = T_b + \frac{I^2 \rho}{APh}$$

Notice that equations 15 and 16 require solving a fourth degree equation for the current. This is best done by a small computer program into which initial guesses for I are input and the integral in equation 14 is output. The output of equation 14 is plotted against the current, and the maximum recovery current is determined by extrapolation through the function zero. The required computer program and a sample extrapolation plot are shown in Figs. 7 and 8. Notice that for the TMNS coil the fully stable recovery current is 17,500 amps, while the cold-end recovery current is 19,850 amps.

```
* HEAT EXCHANGER COIL COLD END RECOVERY IN HE-II
FUNCTION FN(A)
DATA TE/1.8/,PM/0.821/,CC/22296./,TC/9.8/,H/0.1/
DATA PHO/6.802E-8/,E/4.119/,AE/4.897/
TM1=SQRT((PM/0.02) + TE**4)
TM=SQRT(TM1)
TE=TE+(1.0-(A/CC))*(TC-TE)
TM=PM/H + TE
T=TE + (A**2)*PHO/(AE*E*H)
HT1=0.02*(.2*TM**5-TM*TE**4+.8*TE**5)
HT2=PM*(TM-TM)
HT3=H*(.5*TE**2-TE*TE-.5*TM**2+TM*TE)
FAC=PHO*(E*AE)
HS1=-A**2*(TC-TE)
HS2=FA*CC*TC*(TC-TE)/(TC-TE)
HS3=-A*CC*(TC**2-TE**2)/(2.0*TC-2.0*TE)
HS4=-A**2*(TE-TC)
HT=HT1 + HT2 + HT3
HS=FAC*( HS1 + HS2 + HS3 + HS4 )
FN = HT + HS
RETURN
END
```

Figure A-7 Sample Computer Program Used To Calculate the Cold-End Recovery Current

TMNS COLD END RECOVERY CURRENT

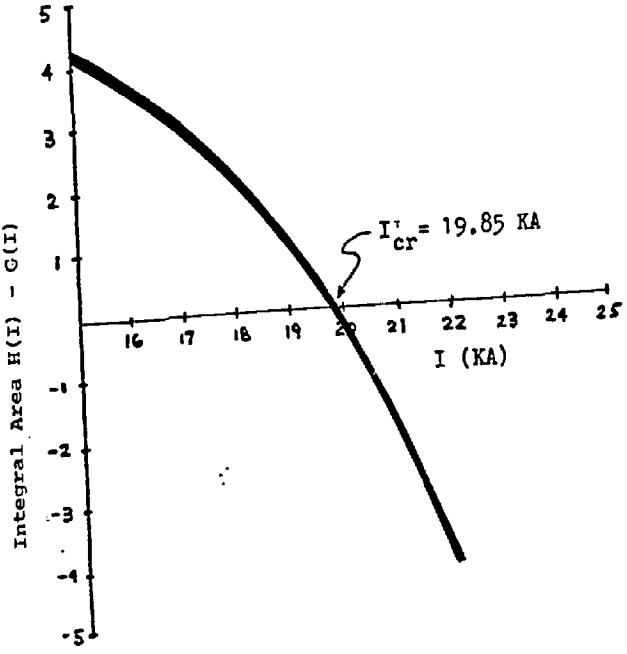

Figure A-8

Transient Stability Analysis

The TMNS conductor-cooling channel configuration, shown in Figs. 4 through 6, has been shown to be remarkable stable under steady-state operation in subcooled superfluid He-II. The enhanced behavior over that of normal liquid He-I coolant can be attributed to two factors: the unique thermophysical properties of He-II, and the selection of either "ladder or button-snowfence" insulation, which produces a network of multiple branching coolant channel networks. Another important issue is to consider the effect of transient phenomenon on the coil stability. Suppose 10 m of turn X in Fig. 6 goes normal. Since the single turn produces 3.38 watts per cm length, this corresponds to a total power production of 3380 watts, a value greater than the refrigeration capacity at 1.8 K. How long can the conductor remain normal before the He-II in thermal contact converts to He-I and film boiling is initiated, or before the electronic protection system can engage a magnet quench? Investigations are continuing to answer this question. It is known that the He-II surrounding the normal turn must absorb enough energy, equal to its enthalpy between 1.8 to 2.17 K before changing phase to He-I.[5] Therefore, the time before film boiling can be represented as:

$$\Delta t = \Delta E_{II} \, V_{II} / Q, \; \Delta E_{II} = 270 \text{ mJ/cm}^3 \tag{17}$$

Where ΔE_{II} is the enthalpy difference between 1.8 and 2.17 K, V_{II} is the effective He-II volume in thermal contact with the conductor, and Q is the power produced by the normal turn. Claudet, et al. have shown that the effective volume of He-II is dependent on the cooling channel heat flux and length. This functional dependence is shown graphically in Fig. 9, which was obtained from experiments performed in Gorter-Mellink tubes.[6] A possible means of extrapolating these results to encompass multiple branching cooling channel networks is to follow the diffusion of horizontal and vertical heat fluxes emanating from normal turn X in Fig. 6. Eight coolant channels leave the conductor surface, these are increased to 16 after passing zone 1, 24 after zone 2, 32 after zone 3, ... In general, the evolution of the fluxes can be represented as:

$$q_{h,v} = q_{oh,v}/N \tag{18}$$

where $q_{h,v}$ are the horizontal and vertical heat fluxes after spreading through zone N and $q_{oh,v}$ are their starting values at the conductor surface (equation 12). The zone number N can also be defined as a distance from the normal turn by

$$N = L_t/L_{h,v} \tag{19}$$

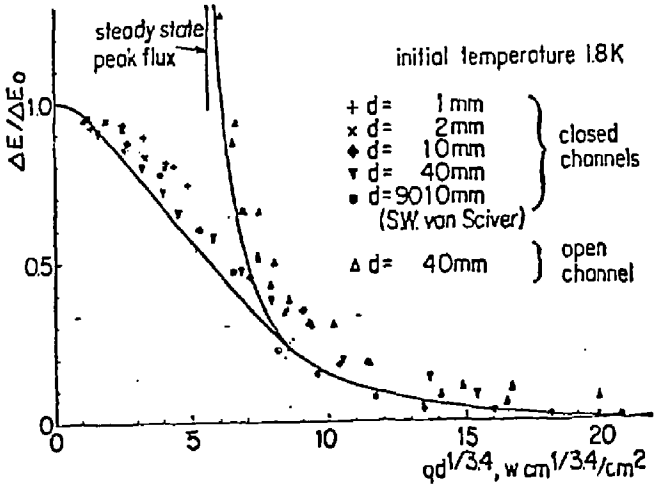

Fraction of enthalpy used during transient heat transfer

Figure A-9

where L_t is the total distance from conductor X and $L_{h,v}$ are the original horizontal and vertical channel distances of equation 11. As the heat spreads outward from the turn, we can describe an average heat flux between the conductor and the wave front as it passes the N_{th} zone.

$$\langle q_{h,v} \rangle = \frac{\int_1^{N_{th}} \frac{q_{oh,v}}{N} dN}{\int_1^{N_{th}} dN} = \frac{q_{oh,v} \ln (N_{th})}{N_{th} - 1} \qquad (20)$$

This function, which shows how an initial single channel heat flux is reduced due to branching into other channels, is shown plotted in Fig. 10, using the parameters of the TMNS design. The product of:

$$\langle q_{h,v} \rangle L_{h,v}^{1/3-4}$$

when compared with Fig. 9, gives the fraction of the total volume of He-II, f, which can absorb energy $\Delta E_{II} V_{II}$ from the conductor. Equation 17 then becomes

$$\Delta t = \frac{270 \text{ mJ } V_{oII} f (2N+1)^2}{Q} \qquad (21)$$

where V_{oII} is the volume of He-II surrounding each unit length of conductor and the $(2N + 1)^2$ factor is the number of conductors enclosed in the N_{th} zone. Equation 21 is plotted for the TMNS parameters in Fig. 11, in which N = 16 corresponds to a 33 x 33 turn conductor pack subcoil. If each subcoil is refrigerated separately at 1.8 K, we may expect a normal turn at 15.6 kA to take up to 87 seconds before the unset of film boiling.

Summary

Following the steady-state and transient stability analysis, several summary parameters of the TMNS design are tabulated below:

Normal Conductor Kapitza Temperature = 2.65 K at 15.6 kA

Conductor Current Sharing Temperature = 4.2 K (Nb_3Sn)

= 2.83 K (Nb-Ti)

Conductor Operating Current = 15.6 kA

CHANNEL HEAT FLUX VERSUS CHANNEL LENGTH

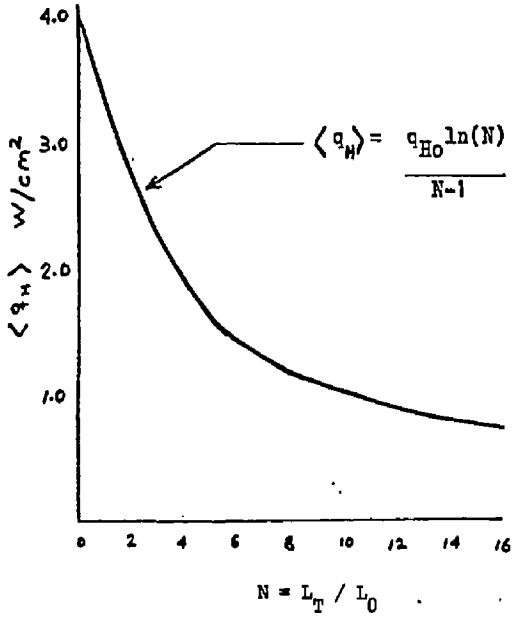

Figure A-10

TIME TO FILM BOILING CURVE

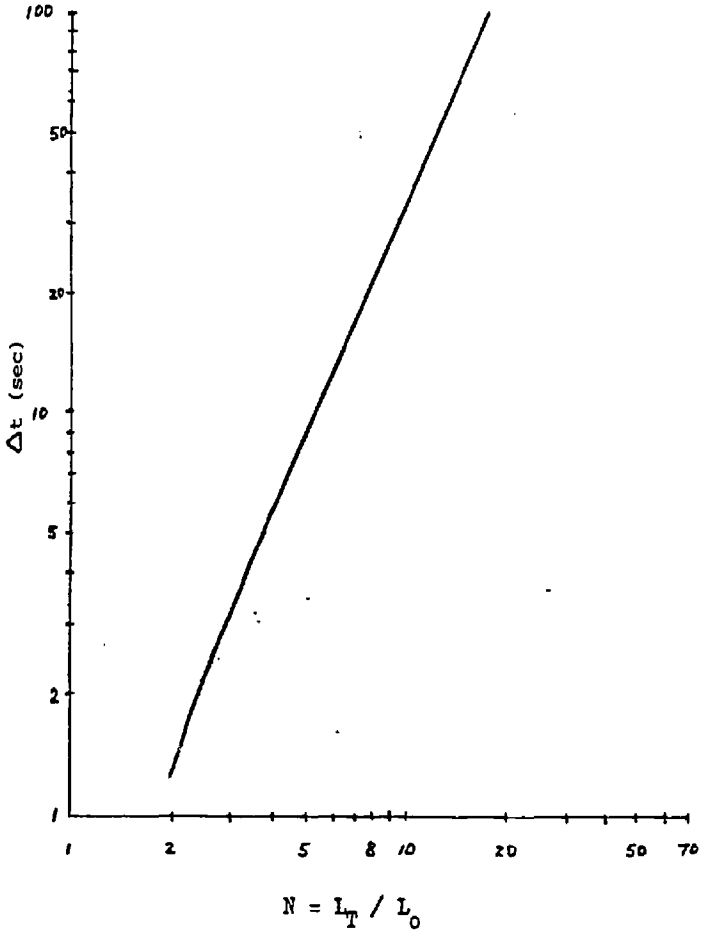

Figure A-11

Conductor Full Recovery Current = 17.5 kA

Conductor Cold End Recovery Current = 19.85 kA

Conductor Critical Current = 22.29 kA

References

1. B. J. Maddock, G. B. James, and W. T. Norris, "Superconductive Composites: Heat Transfer and Steady-State Stabilization," Cryogenics (August, 1969), pp. 261-273.

2. S. W. Van Sciver, "Cryostabilization of Large Superconducting Magnets Using Pool Boiled Helium II," 6th Symposium on Engineering Problems of Fusion (1977), pp. 690-694.

3. G. Bon Mardion, G. Claudet, P. Seyfert, and J. Verdier, "Helium II in Low-Temperature and Superconductive Magnet Engineering," 7th International Cryogenic Engineering Conference (1978), pp. 358-362.

4. N. S. Snyder, "Heat Transport Through Helium II: Kapitza Conductance," Cryogenics (April, 1970), pp. 89-95.

5. S. W. VanSciver, "Heat Transfer in Superfluid Helium II," Proc. 8th International Cryogenic Eng. Conference, Genova, Italy (June 1980), pp. 228-237.

6. G. Claudet, P. Seyfert, "Bath Cooling with Subcooled Superfluid Helium," Adv. in Cryogenic Eng., Vol. 27, Paper KA-3 (1981).

vz/0156v

TANDEM MIRROR NEXT STEP

STATEMENT OF WORK

1.0 GENERAL DESCRIPTION OF ARTICLES AND SERVICES

1.1 The Convair Division of General Dynamics proposes to perform the winding of a 12T yin yang coil. This task will include setup of the line, fabrication of G-10CR insulation and practice winding.

2.0 GROUND RULES, CONDITIONS AND ASSUMPTIONS

2.1 All tools required for the winding task such as winders, cold-welders, storage reels, coil forms and coil case will be identified but not included in the cost estimate.

2.2 Cost estimate assumes a completely facilitized site will perform the winding, however no facility costs are included.

2.3 The winding will be done at Convair and the completed winding will be shipped to the assembly site of the magnet. No shipping costs will be included.

2.4 Quality Assurance and Manufacturing plans are assumed to be part of the detail design phase. All costs associated with these plans are excluded.

2.5 Instrumentation costs are excluded from this estimate.

2.6 All progress reviews will be held in San Diego.

2.7 All costs are in constant 1981 year dollars.

2.8 Liquid helium expense is not included.

3.0 SPECIFICATIONS, REFERENCES AND DESCRIPTIVE DATA

3.1 PIN 80-305

3.2 PIN 80-305-1

4.0 PRODUCT DEFINITION

4.1 The product of this proposal will be the winding of a 12T yin yang coil which will include the following tasks:

Task 1 - Material Procurement
Task 2 - Conductor Production Line
Task 3 - Conductor Fabrication
Task 4 - Insulation Fabrication
Task 5 - Conductor Practice Winding
Task 6 - Coil Winding Operations
Task 7 - Program Management/Financial Management

5.0 DETAILED TASK DESCRIPTION

5.1 TASK 1 - MATERIAL PROCUREMENT

5.1.2 D/810-0 OPERATIONS PROCUREMENT

Prepare and arrange subcontract. Provide contractual interface with the subcontractor. Procure materials listed in Attachment I.

5.1.3 D/358-0 RECEIVING INSPECTION

Receive and inspect material.

5.1.4 D/831-0 MATERIAL STORERS RECEIVING TRAFFIC

Receive and stage material at work site.

5.2 TASK 2 - CONDUCTOR PRODUCTION LINE

5.2.1 D/427-0 MANUFACTURING ENGINEERING PROJECT OFFICE (MEPO) SUPPORT

Coordinate overall operations; monitor all tooling and factory activity.

5.2.2 D/250-0 FACILIITES ENGINEERING

Clear area and provide utilities to tools and equipment and machines on assembly line.

5.2.3 D/455-0 TOOL MANUFACTURING - JIGS AND FIXTURES

Install, level & check out all tools and machines on the assembly line.

5.2.4 D/064-0 OPERATIONS - ENERGY PROGRAM

Perform conductor assembly line checkout and validation. The checkout applies to all operations and equipment shown in conductor fabrication (Task 4).

5.3 TASK 3 CONDUCTOR FABRICATION

5.3.1 D/064-0 OPERATIONS - ENERGY PROGRAM

Manufacture 565,000 feet of conductor to include the following tasks:

Cold weld copper stabilizer and filler bar to required length per grade.

Roll straightening to remove irregularities in the straightness of the copper bar caused by manufacturing operations and rolling on the supply spool.

Mill to final size the slot in preparation for the insertion of the super conductor.

Clean to remove oil, dirt of other contaminants accumulated during manufacturing and shipping.

Prepare the slot and filler bar to assure all solder adhesion.

Insert the superconductor in the stabilizer and add filler bar on top of solder.

Heat the conductor to melt the solder bond the filler bar, superconductor and stabilizer together.

Operate conductor fabrication to support ultrasonic inspection. Perform final size machining.

Perform final cleaning prior to storage. Support electrical shock and tools. Wind the conductor onto storage reel.

5.3.2 D/346-0 QUALITY CONTROL

Provide inspection to each operation. Perform ultrasonic inspection on soldered conductor.

5.3.3 D/427-0 MEPO SUPPORT

Support conductor fabrication by integrating other departmental support required. Monitor, progress and report status to Project Manager.

Provide conductor fabrication work instructions.

5.3.4 D/661 TEST LABORATORIES

Perform 1,020 conductor short sample tests and 1,165 electrical checks.

5.3.5 D/250-0 TRANSPORTATION

Provide transportation and handling for filler bar, superconductor and stablizer.

5.4 TASK 4 - INSULATION FABRICATION

5.4.1 D/064 OPERATIONS - ENERGY PROGRAM

Cut layer to layer details from 4' x 8' sheet material using pin router or saw.

Cut ground insulation details from 6' x 12' sheet material with pin routers and saws.

Fabricate layer to layer insulation from vendor provided details.

5.4.2 D/346-0 QUALITY CONTROL

Provide inspection support.

5.4.3 D/427-0 MEPO SUPPORT

Support insulation fabrication by integrating other departmental support monitor progress and report progress. Provide planning.

5.4.5 D/230-0 MANUFACTURING CONTROL

Stage insulation details.

5.5 TASK 5 - CONDUCTOR PRACTICE WINDING

5.5.1 D/064-0 OPERATIONS - ENERGY PROGRAM

Perform practice wind (2,400 feet) including insulation to consist of:

- pancake tiers clockwise
- pancake tiers counterclockwise
- layer turns clockwise
- layer turns counterclockwise
- conductor splice joints

Cold weld copper stabilizer and filler bar to required length.

Roll straightening to remove irregularties to the straightness of the copper bar caused by manufacturing operations and rolling on the supply spool.

Mill to clean up the slot in preparation for the insertion of the superconductor.

Clean to remove oil, dirt and other contaminants accumulated during manufacturing and shipping stage.

Prepare the slot on a filler bar to ensure the solder adhesion.
Insert simulated superconductor (i.e., OFHC copper bar) in the stabilizer and add filler bar on top of solder. Heat the conductor to melt the solder, bond the filler bar, superconductor and stabilizer together.

Operate conductor practice line to support ultrasonic inspection. Perform final size machining.

Perform final cleaning prior to storing. Support electrical checks and tests and NDT. Wind the conductor onto storage reel.

5.5.2 D/427-0 MEPO SUPPORT

Coordinate overall operations.

5.5.3 D/340-0 QUALITY CONTROL

Perform conductor electrical checks and tests. Conduct NDT on practice conductor.

5.5.4 D/250-0 TRANSPORTATION

Provide transportation and handling for filler bar, simulated superconductor and stabilizer.

This winding would involve all the operations and equipment shown in conductor fabrication.

5.6 TASK 6 COIL WINDING OPERATIONS

5.6.1 D/064 OPERATIONS - ENERGY PROGRAM

Conduct winding operations to pancake wind 201,000 feet of Nb_3Sn and 364,000 feet of NbTi.

Install electrical insulation.

Perform electrical checks as follows:

Wind layers (32 wide x 91 high)
- layer to layer resistance
- layer to ground resistance
- continuity
- inter turn resistance

Complete (power lead) circuits (3 per coil)
- circuit to ground resistance
- circuit to other coil resistance
- continuity

Complete Coil
- coil to ground resistance
- coil continuity

Fabricate conductor joint components.

Assemble splice joints in coil pack. (Approximately 508 conductor joints).

Support electrical checks of joints.

5.6.2 D/427-0 MEPO SUPPORT

Support coil winding operations by integrating other departmental support required. Monitor progress and report status.

5.6.3 D/431-0 PLANNING

Prepare coil winding operations work instructions.

5.6.4 D/346-0 QUALITY CONTROL

Provide inspection support during coil winding operations.

5.6.5 D/230-0 MANUFACTURING CONTROL

Support coil winding operations by scheduling and controlling details and material delivered to fabrication site.

5.6.6 D/250-0 TRANSPORTATION

Provide transportation and handling support.

5.6.7 D/346-0 QUALITY CONTROL

Provide inspection support.

5.7 TASK 7 PROGRAM MANAGEMENT/FINANCIAL MANAGEMENT

5.7.1 D/107-0 PROGRAM MANAGEMENT

Provide full-time program management direction and other tasks associated thereof throughout the winding task.

5.7.2 D/681-0 ENERGY SYSTEM TECHNICAL MANAGEMENT

Provide full-time functional direction as Chief Engineer throughout the winding task.

5.7.3 D/427-0 OPERATIONS MANAGEMENT

Provide full-time functional direction of an operations manager and a manufacturing engineer for the tooling and factory tasks throughout the winding task.

5.7.4 D/673-0 ADVANCED DESIGN
D/643-0 CHECKING AND RELEASE
D/621-0 GUIDANCE TECHNOLOGY (ELECTRICAL ANALYSIS)
D/800-0 SUPERCONDUCTOR ANALYSIS AND DESIGN (SUBCONTRACT)
D/696-0 THERMODYNAMICS ANALYSIS
D/681-0 ADVANCED STRUCTURES ANALYSIS
D/630-0 MATERIALS AND PROCESSES
D/264-0 TECHNICAL PUBLICATIONS

Provide sustaining engineering activities consisting of the following tasks:

Provide liaison and coordination support to resolve day-to-day problems as fabrication progresses.

Provide analysis support to ensure functional integrity is maintained in disposition of discrepancies.

Monitor and evaluate in-process verification tests.

Provide vendor coordination and participate in vendor reviews.

Participate in component reviews leading to certification and turnover of the magnet winding to the customer.

Update technical specifications and manuals.

5.7.5 D/194-5 ADVANCED PROGRAMS AND ENERGY BUSINESS MANAGEMENT

Provide financial management support for financial reports.

5.7.6 D/311-0 QUALITY ASSURANCE MANAGEMENT

Provide direction as quality assurance manager throughout the winding task.

APPENDIX C

12 TESLA YIN-YANG SUPERCONDUCTING MAGNET

DRAWINGS FOR TMNS

APPENDIX

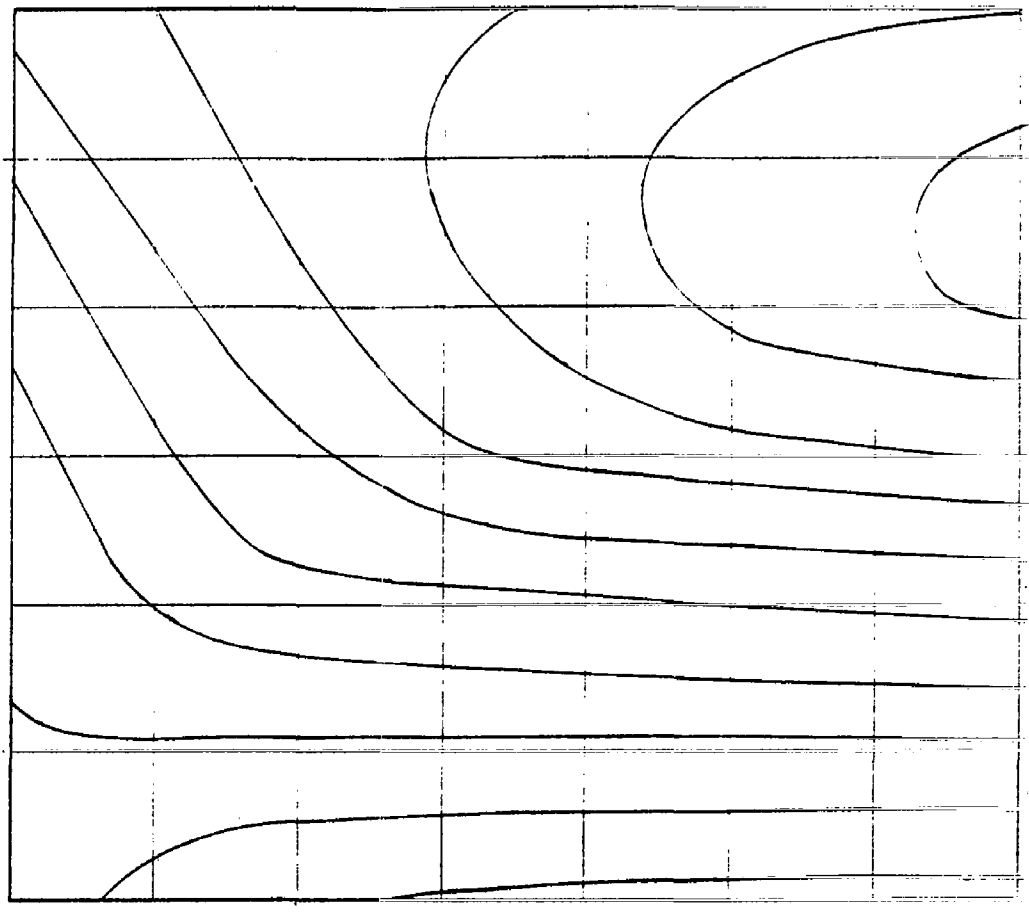

INSIDE CORNER

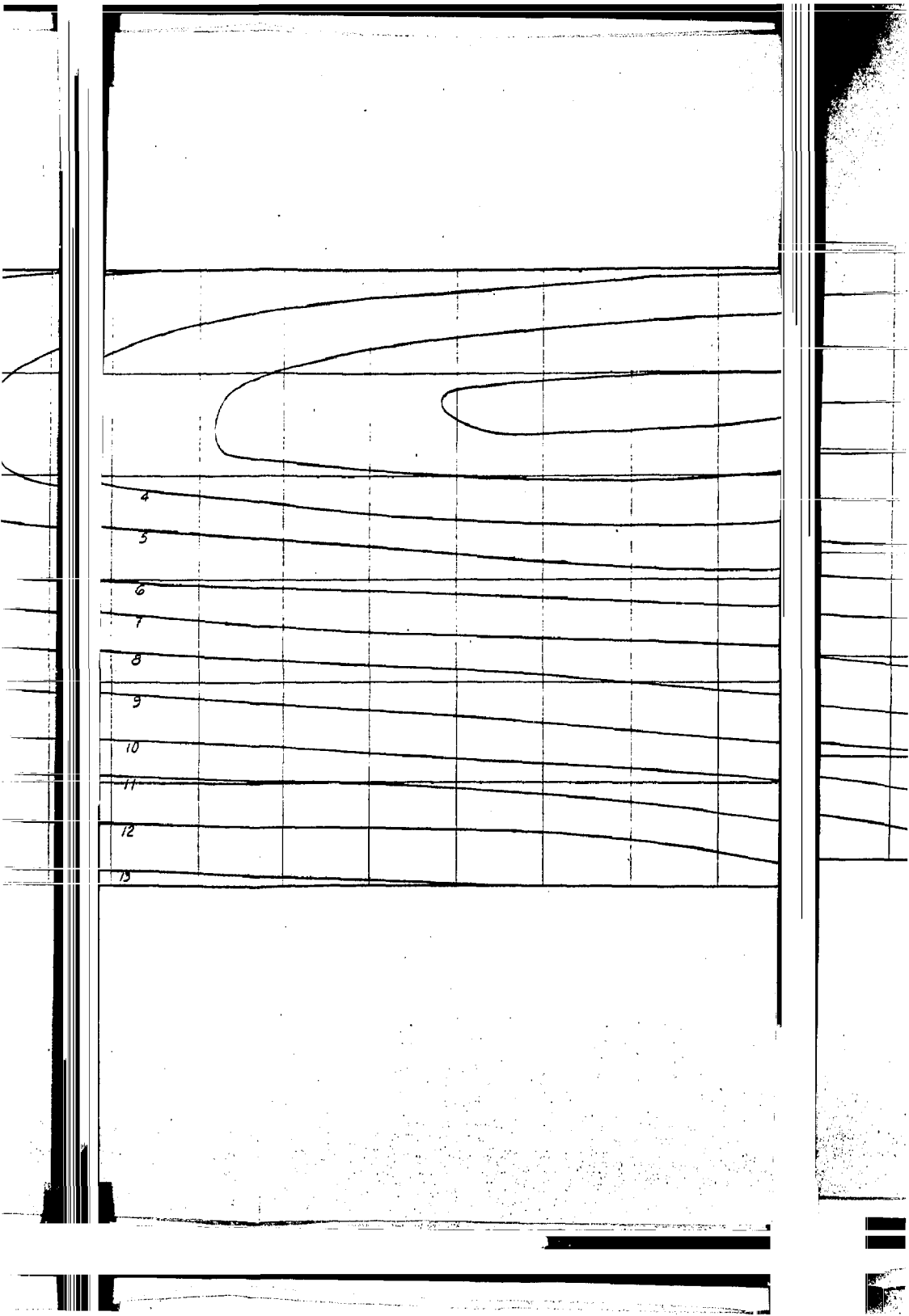
4
5
6
7
8
9
10
11
12
13

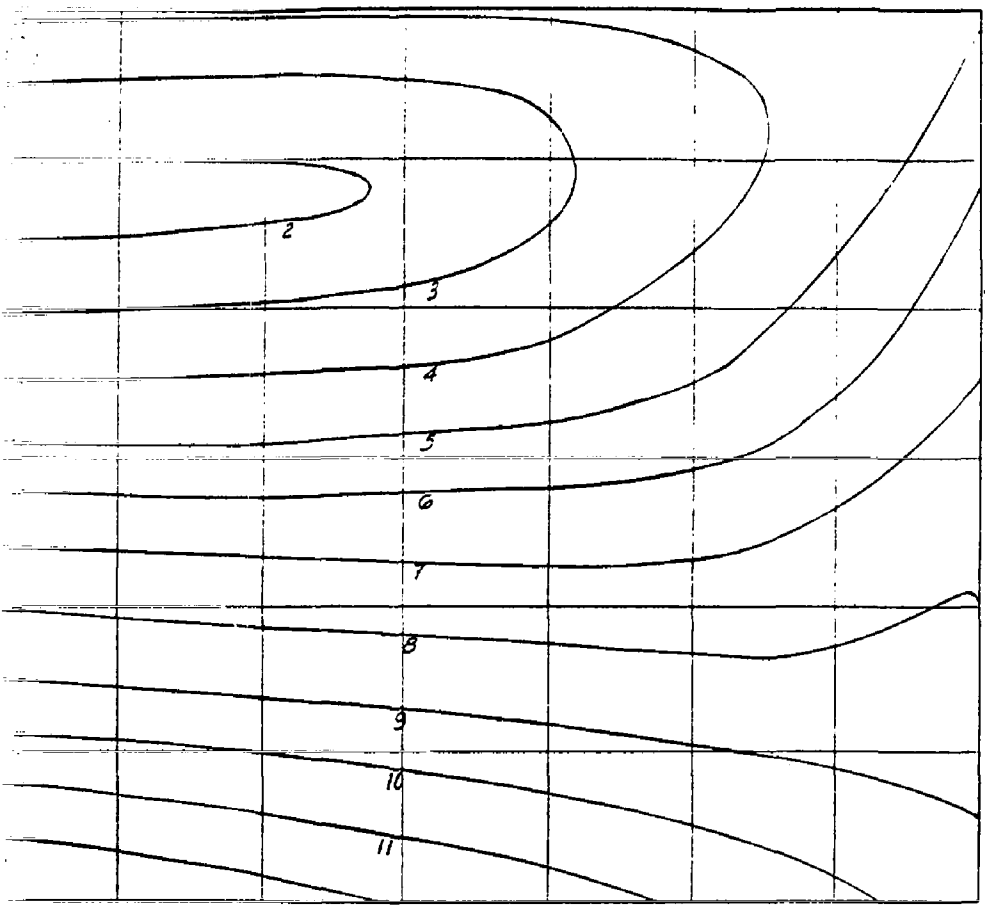
2
3
4
5
6
7
8
9
10
11

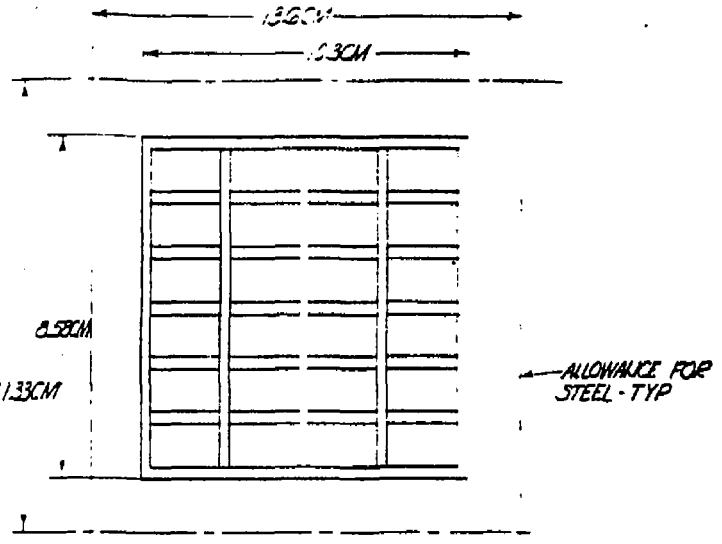

TYPICAL 6 WIDE x 4 HIGH CONDUCTOR BOX

2. CONTOURS ARE MAX. OF LLL PLOTS FOR MAJOR & MINOR RADII.
1. FIELD STRENGTH IN TESLA.

NOTES:

GENERAL DYNAMICS Convair Division SAN DIEGO, CALIFORNIA	PRELIMINARY DESIGN DRAWING	
	MAXIMUM FIELD INTENSITY TMMJS CROSS SECTION	
	14170	TMMJS-010
	SCALE NONE	SHEET 1 OF 1

TMNS CONDUCTOR

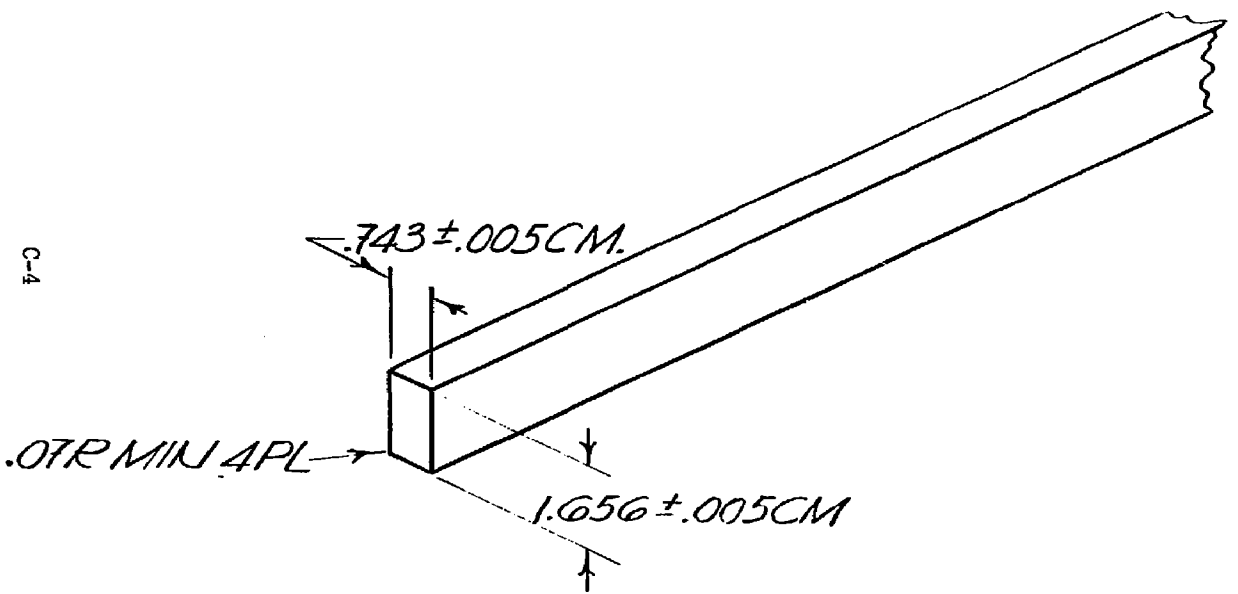

C-4

TMNS-011
SCALE-FULL 6-26-81

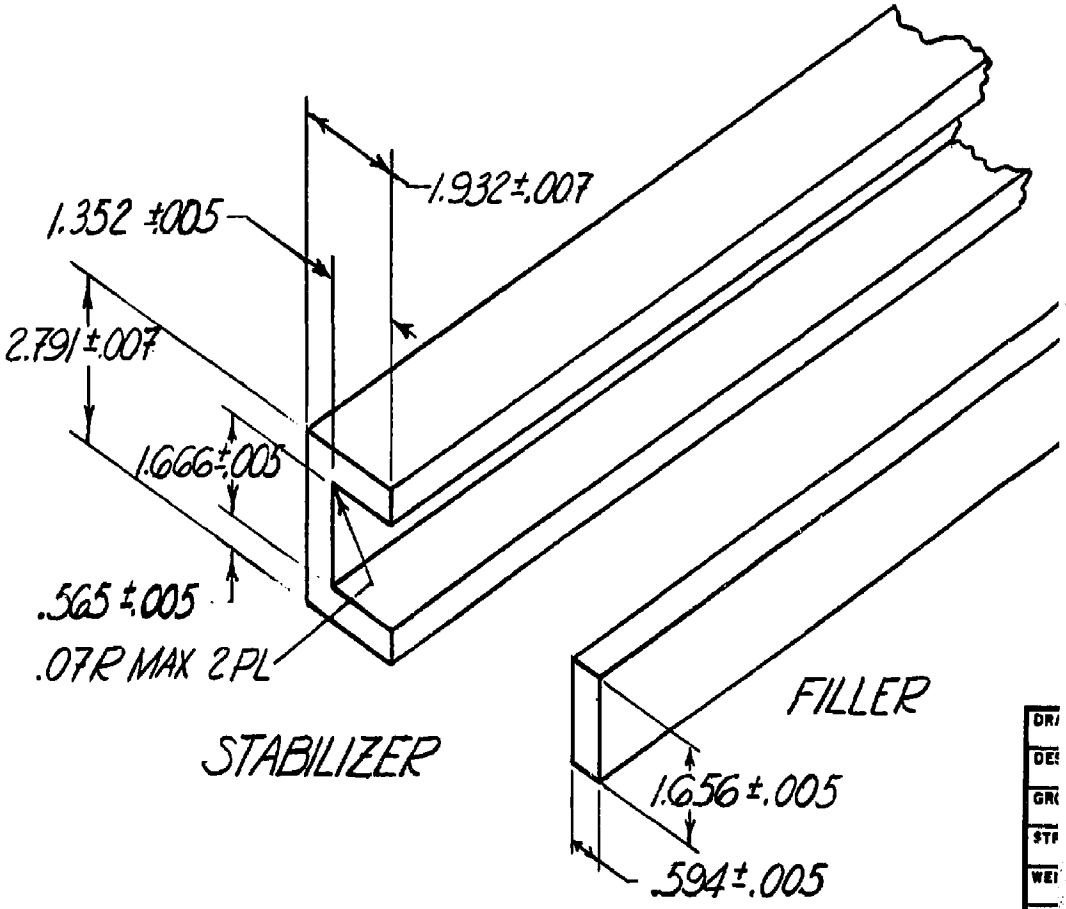
1.352 ±.005
1.932±.007
2.791±.007
1.666±.005
.565 ±.005
.07R MAX 2PL
STABILIZER
FILLER
1.656 ±.005
.594±.005

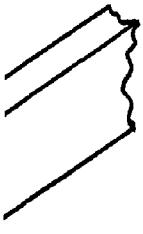

5. FILLER TO BE WOUND FLAT SIDE ON A SPOOL OF 13 FT. DIA. MIN. LENGTHS OPTIONAL.
4. STABILIZER TO BE DELIVERED IN 40 ± 2 FT. LENGTHS
3. STABILIZER & FILLER TO BE DRAWN ½ HARD.
2. MATERIAL OFHC COPPER.
1. ALL DIM. IN CM.

NOTES-

DRAWN BY R. A. SUTTON 6/26/81	PRELIMINARY DESIGN DRAWING	
DESIGN ENGR		
GROUP ENGR	STABILIZER & FILLER TMNS	
STRESS		
WEIGHTS		
MATERIAL		
OPERATIONS		
PROJECT		
GENERAL DYNAMICS Convair Division SAN DIEGO, CALIFORNIA	CODE IDENT. 14170	DRAWING NO. TMNS-012 C-5
	SCALE FULL	SHEET 1 OF 1

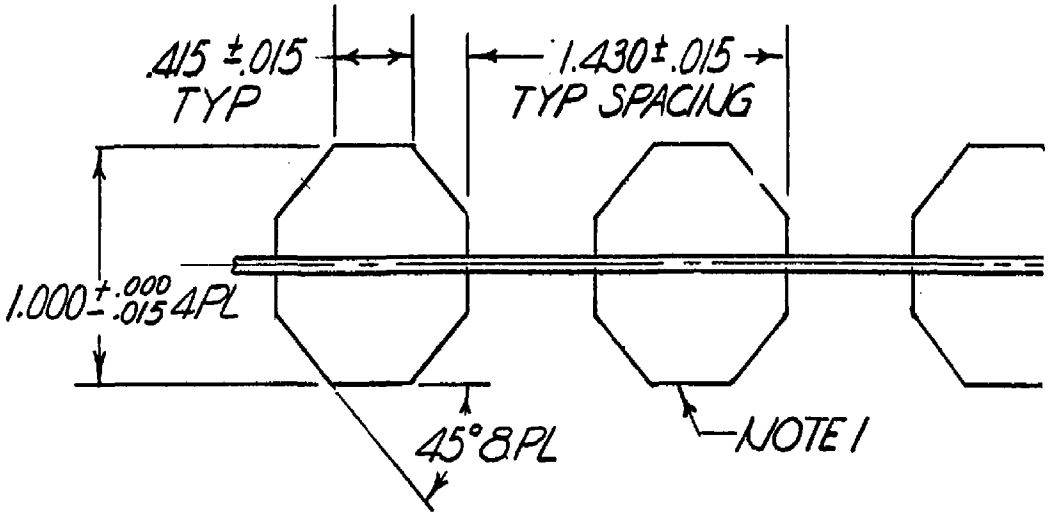

NOTES -

1. MATERIAL NEMA G-10 CR.
2. TAPE - LACING; TYPE IV, SIZE 3, FINISH A PER MIL-T-43435.
3. BOND TAPE WITH LOCTITE SUPERBONDER 414.
4. ALL DIM. IN INCHES.

DR
DE
GR
ST
WE
MA
OP
PR

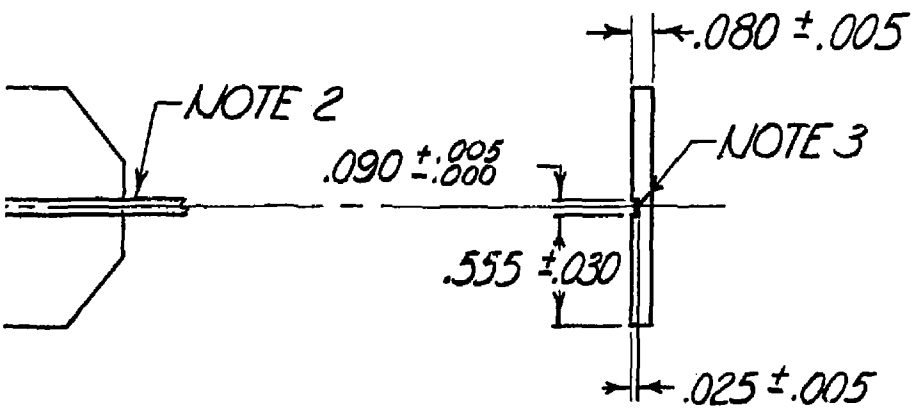

REV A - CHANGED OVERALL DIM. 5/15/81

DRAWN BY R.A. SUTTON	6/26/81	PRELIMINARY DESIGN DRAWING
DESIGN ENGR		BUTTON INSULATION TMNS
GROUP ENGR		
STRESS		
WEIGHTS		
MATERIAL		
OPERATIONS		
PROJECT		

GENERAL DYNAMICS Convair Division SAN DIEGO, CALIFORNIA	CODE IDENT. 14170	DRAWING NO. TMNS-013	C-6
	SCALE NTS	SHEET 1 OF 1	

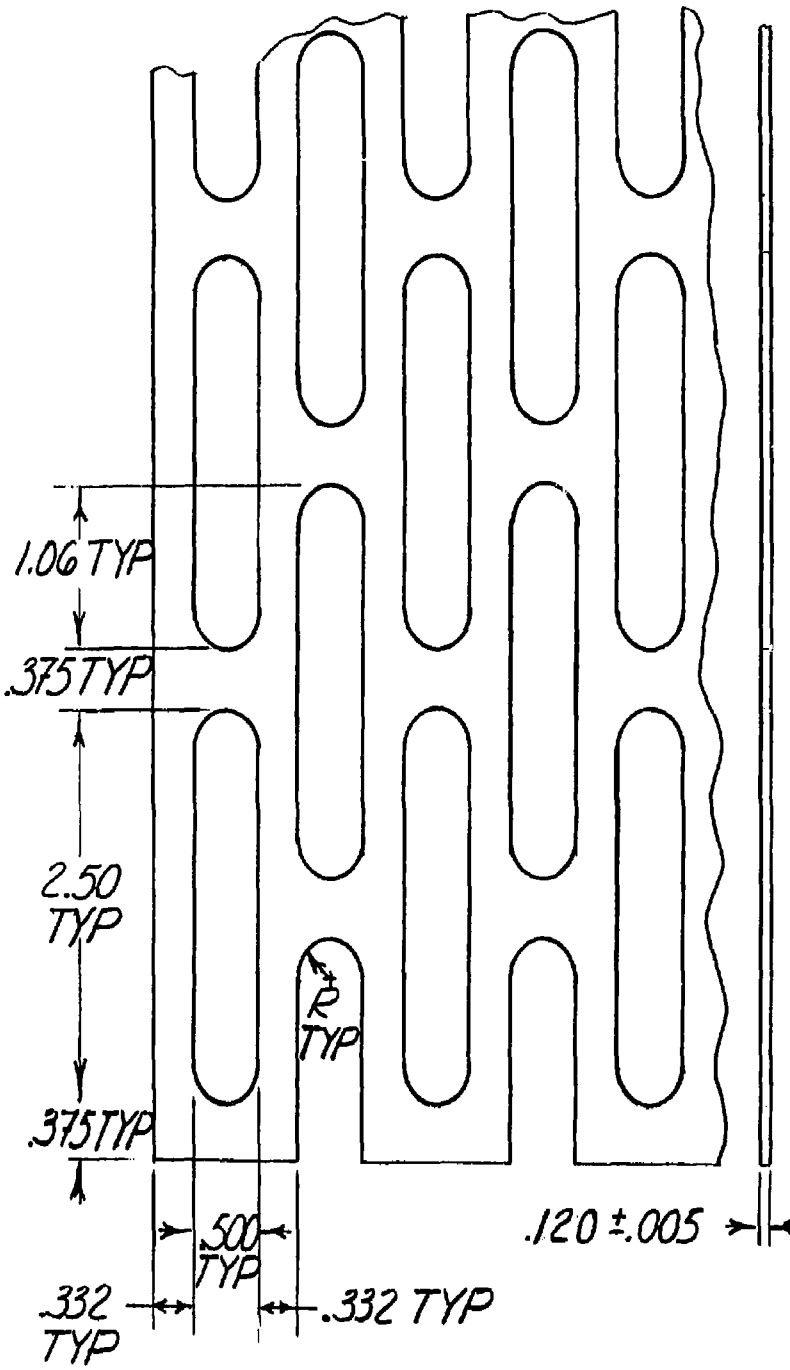

DETAIL A
FULL SIZE

48.0

4. ALL
3. TOLE
2. CUT
1. MAT

NOTES:

REV A - THICKNESS WAS .080 8/10/81

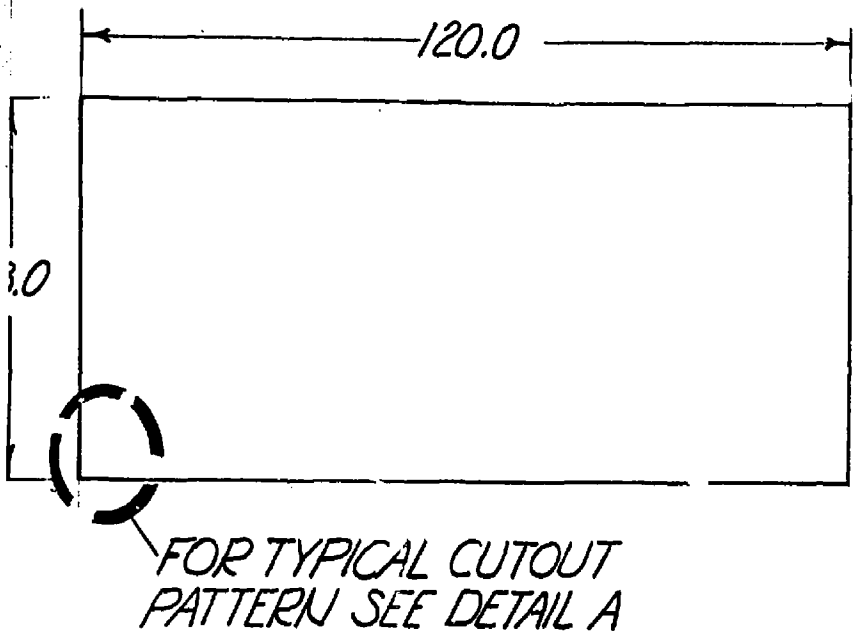

LL DIM. IN INCHES.
OLERANCES: .X=±.1, .XX=±.03, .XXX=±.010 OR AS NOTED.
UTOUT PATTERN TYPICAL OVER FULL SHEET.
IATERIAL: NEMA G-10CR.

DRAWN BY R.A. SUTTON 6/30/61	PRELIMINARY DESIGN DRAWING	
DESIGN ENGR		
GROUP ENGR	LATERAL INSULATION TMNS	
STRESS		
WEIGHTS		
MATERIAL		
OPERATIONS		
PROJECT		
GENERAL DYNAMICS Convair Division SAN DIEGO, CALIFORNIA	CODE IDENT. 14170	DRAWING NO. TMNS-014 C-7
	SCALE	SHEET OF

/81

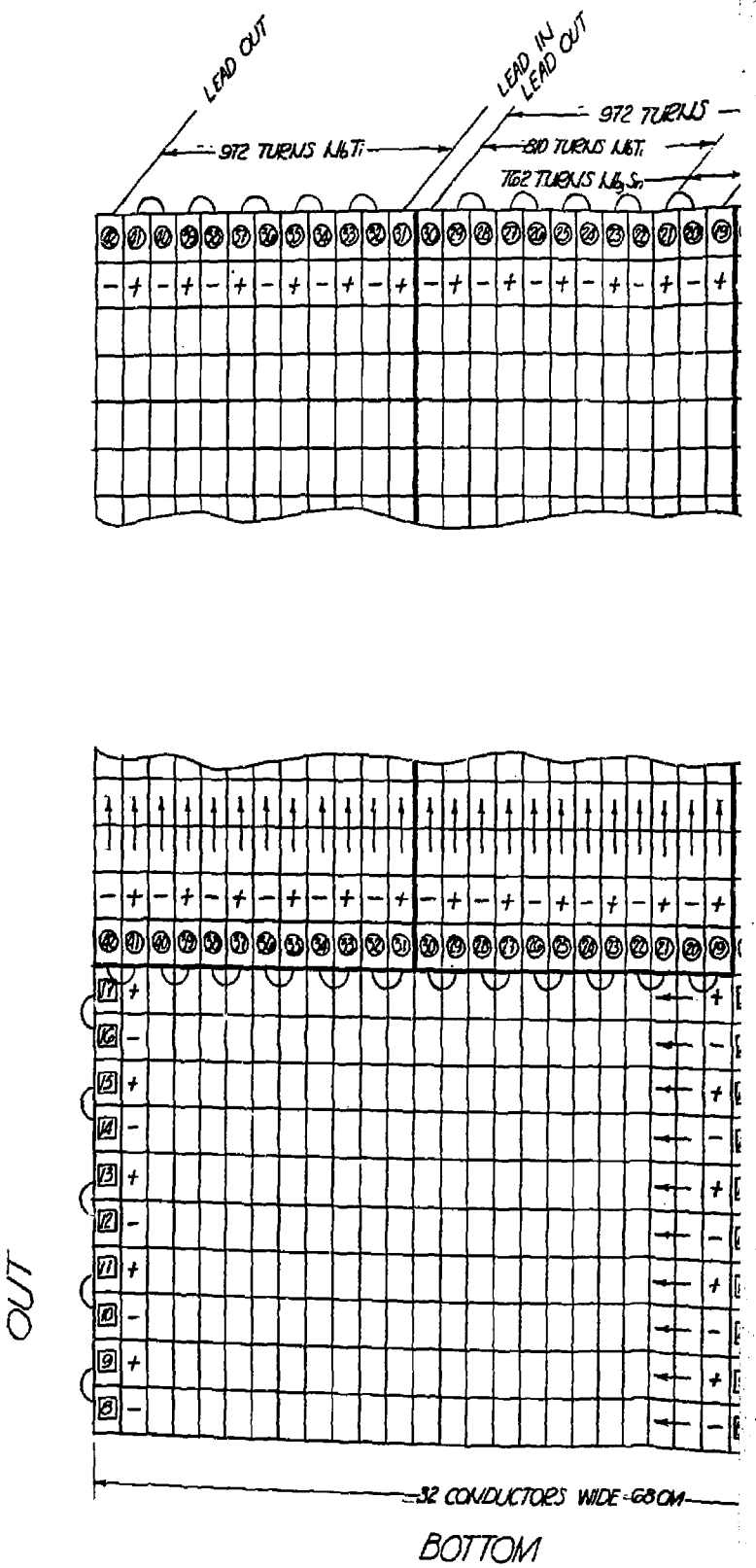
LEAD OUT
LEAD IN
LEAD OUT
972 TURNS
972 TURNS MGT.
810 TURNS MGT.
762 TURNS MGS.
OUT
32 CONDUCTORS WIDE - 68 CM
BOTTOM

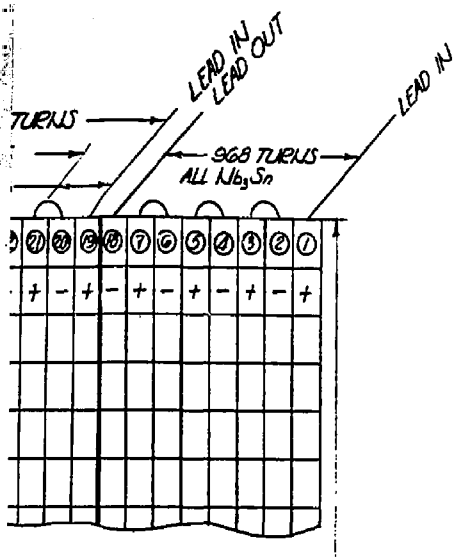

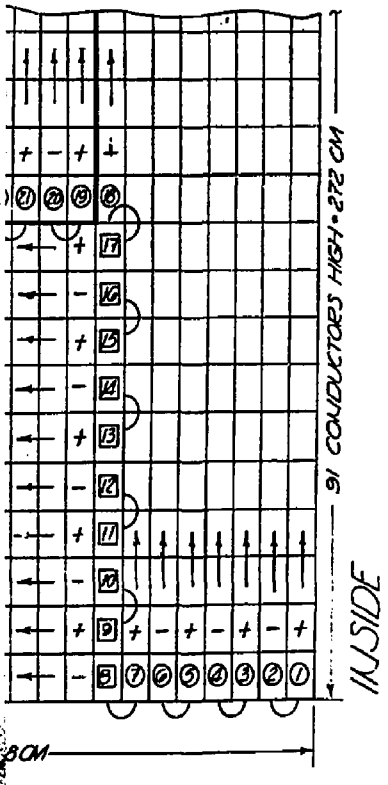

6. SPLICES IN MINOR RADIUS REGION.
5. ⌒ = CONDUCTOR SPLICE.
4. + = CONDUCTOR WOUND CLOCKWISE LOOKING FROM INSIDE TO OUT; − = C'CLOCKWISE.
3. BRACKETED NO'S GIVE WINDING SEQUENCE; ○ = PANCAKE, □ = LAYER WINDING.
2. LAYER WINDINGS START FROM INSIDE.
1. PANCAKE WINDINGS START FROM BOTTOM.

NOTES-

GENERAL DYNAMICS	PRELIMINARY DESIGN DRAWING	
	WINDING SEQUENCE TMNS	
	14170	TMNS-015

C-8

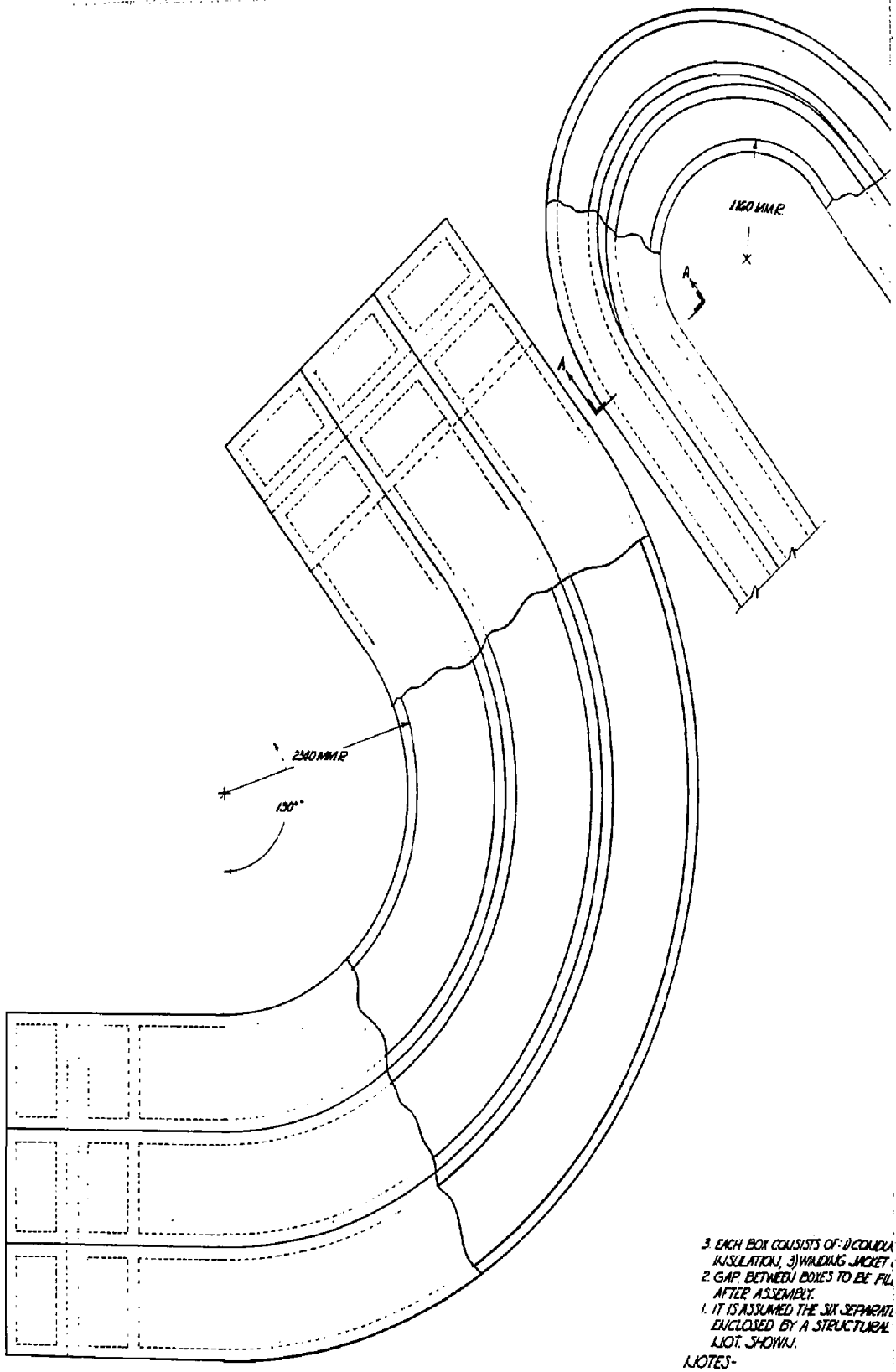

NOTES-

1. IT IS ASSUMED THE SIX SEPARATE
ENCLOSED BY A STRUCTURAL
NOT SHOWN.
2. GAP BETWEEN BOXES TO BE FIL
AFTER ASSEMBLY.
3. EACH BOX CONSISTS OF: 1) CONDU
2) INSULATION, 3) WALKING JACKET

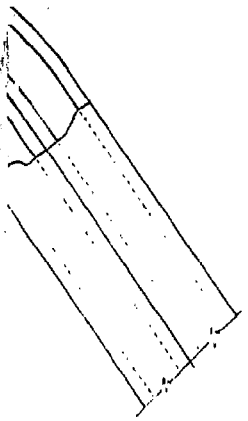

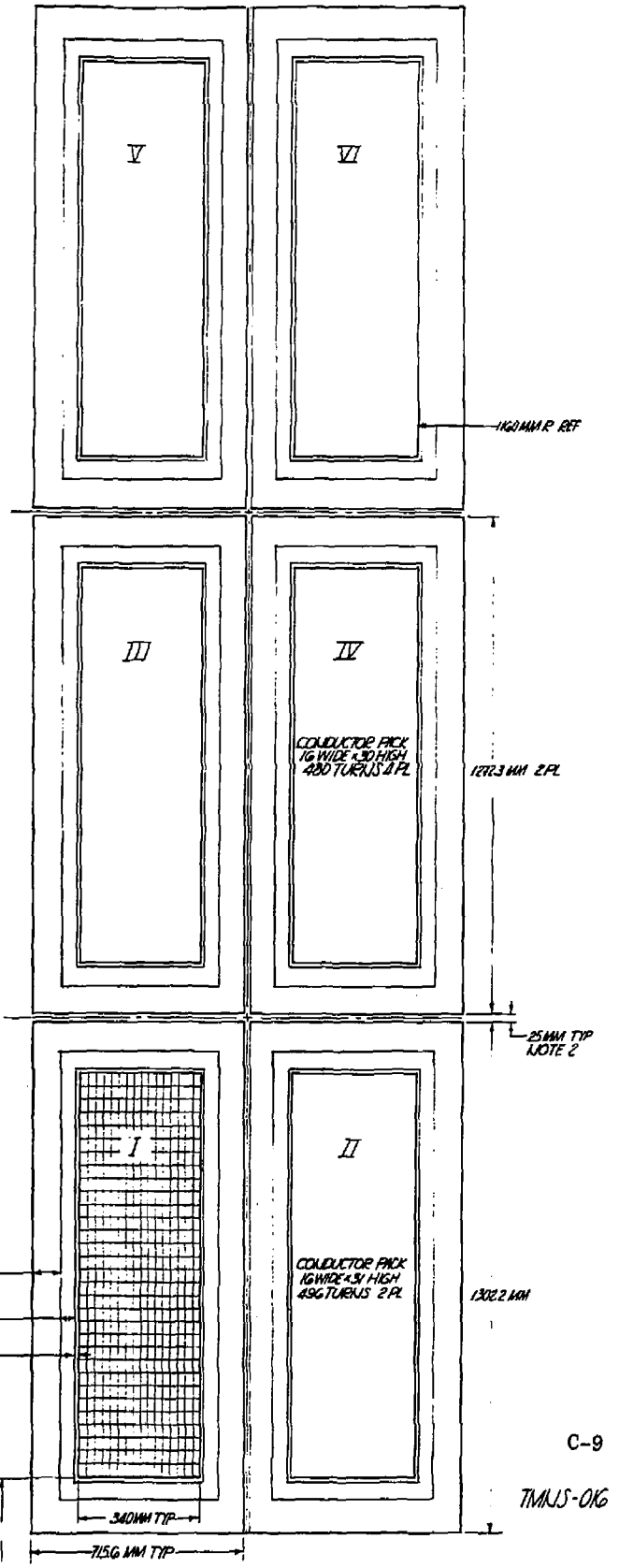

Discarded concept used in tradeoff studies

DISCARDED CONCEPT

0 CONDUCTOR PACK, 2) GEOLAID
S JACKET & 4) STRUCTURAL SHELL.
TO BE FILLED WITH URETHANE

SEPARATE BOXES WILL BE
CTURAL CASE WHICH IS

SECTION A-A
ROTATED 40° CW
SCALE: NONE

TMMS-0K6

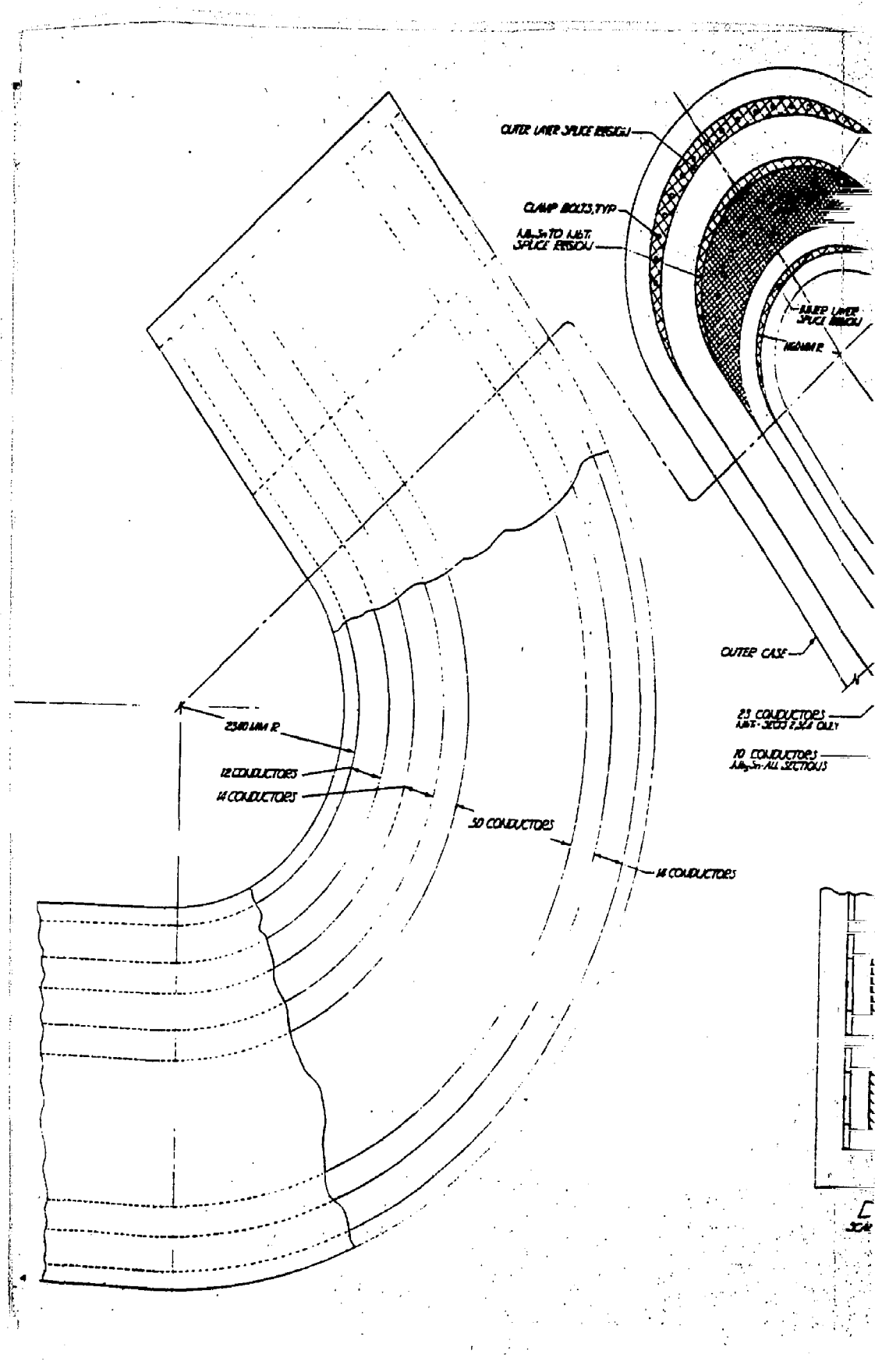
OUTER LAYER SPLICE BRIDGE
CLAMP BOLTS, TYP.
SPLICE BRIDGE
OUTER CASE
2340 MM R
12 CONDUCTORS
14 CONDUCTORS
50 CONDUCTORS
16 CONDUCTORS
23 CONDUCTORS
10 CONDUCTORS

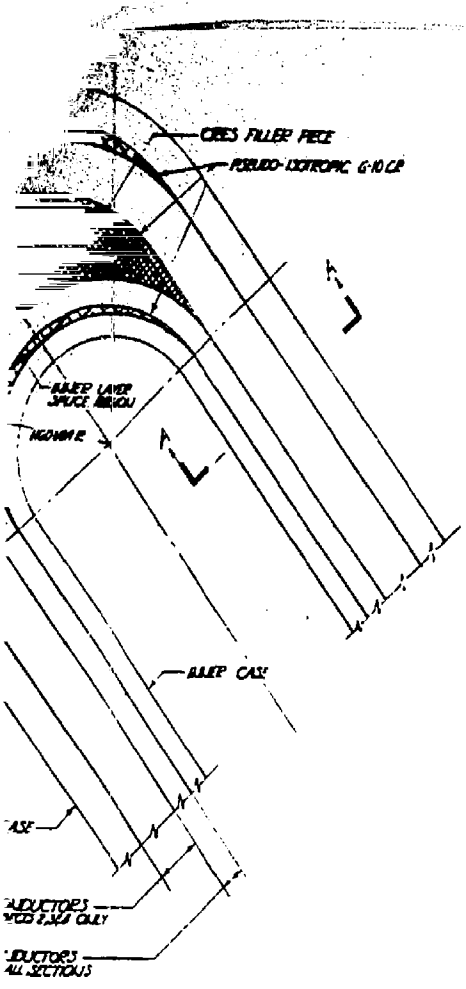
CREES FILLER PIECE
PSEUDO-ISOTROPIC G-10 CR
A
A
FILLER CASE

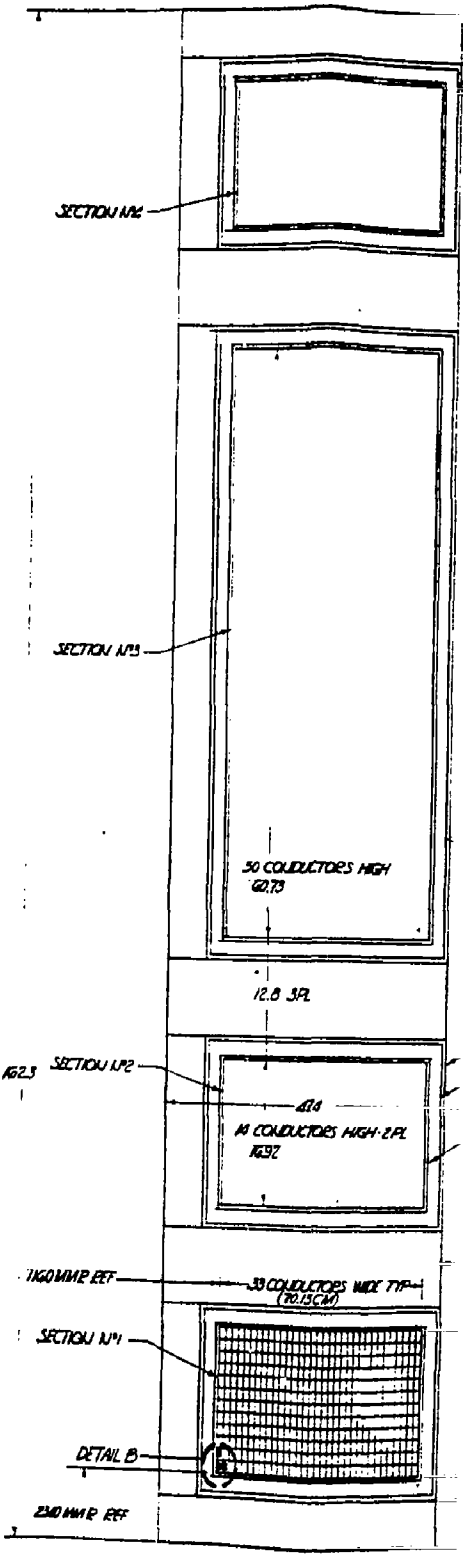
SECTION N°2
SECTION N°3
50 CONDUCTORS HIGH
12.8 SPL
SECTION N°2
44 CONDUCTORS HIGH-2 PL
SECTION N°1
39 CONDUCTORS WIDE TYP
DETAIL B
SECTION A-A
SCALE: NONE

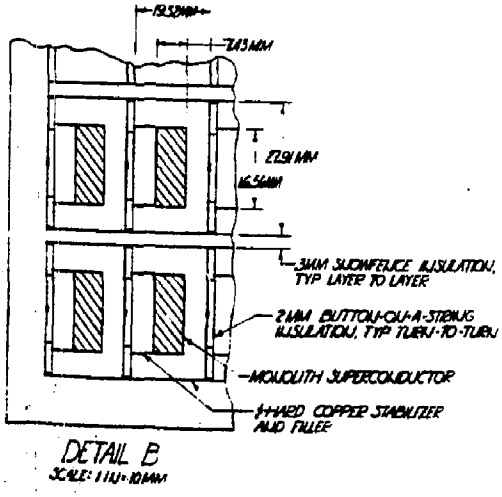
7.43 MM
2.91 MM
3 MM SILICONE RUBBER INSULATION, TYP LAYER TO LAYER
2 MM BUTTON-ON-A-STRING INSULATION, TYP TURN-TO-TURN
MONOLITH SUPERCONDUCTOR
4 HARD COPPER STABILIZER AND FILLER
DETAIL B
SCALE: 1 IN = 10 MM

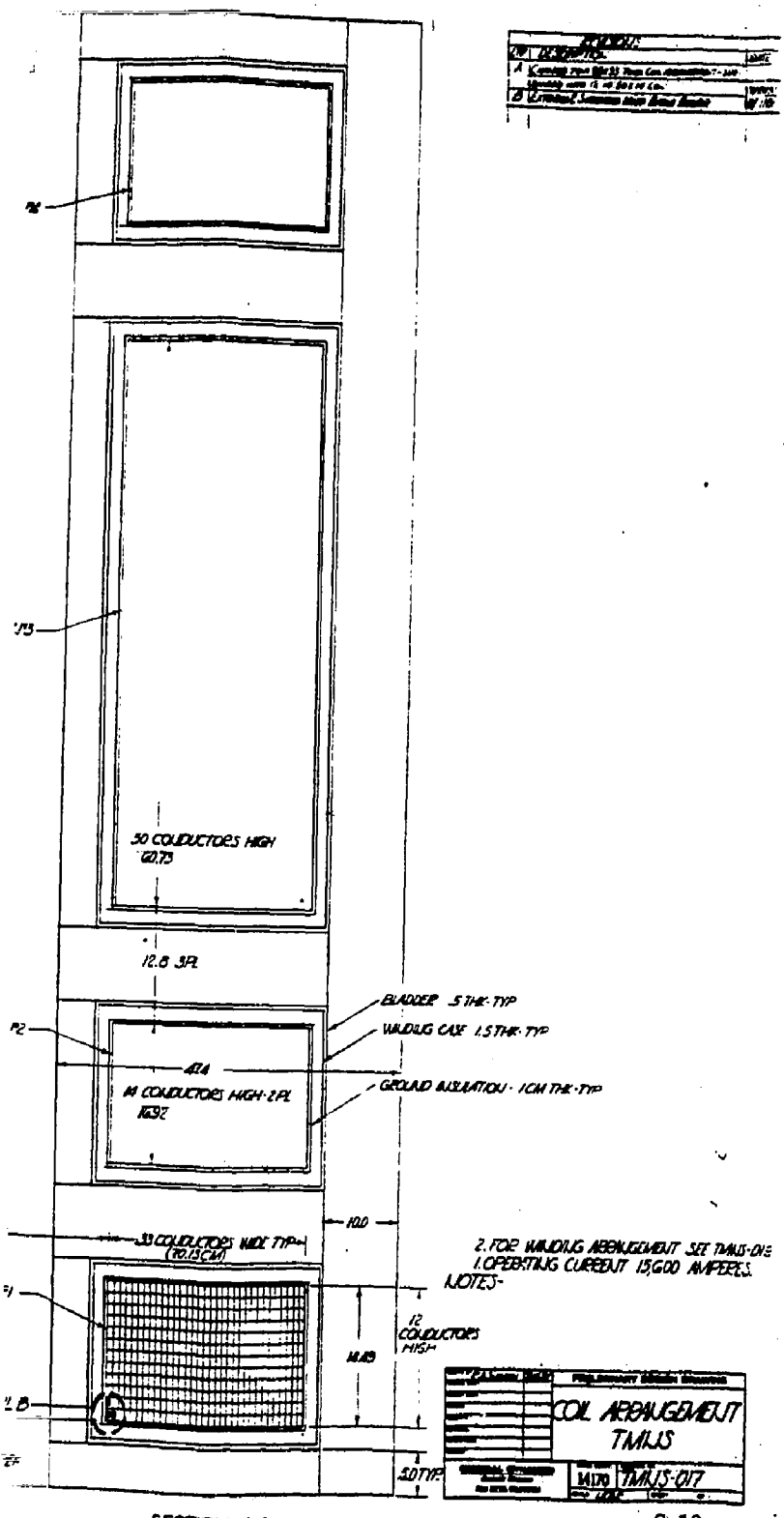

2. FOR WINDING ARRANGEMENT SEE TMJS-DWG
1. OPERATING CURRENT 15,000 AMPERES.

NOTES-

COIL ARRANGEMENT
TMJS

TMJS-017

SECTION A-A
SCALE - NONE

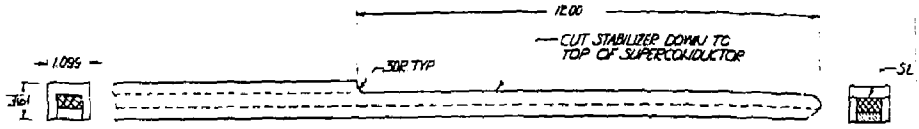

PREPARE

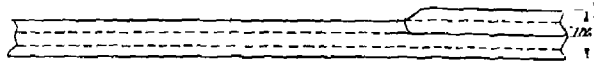

LA

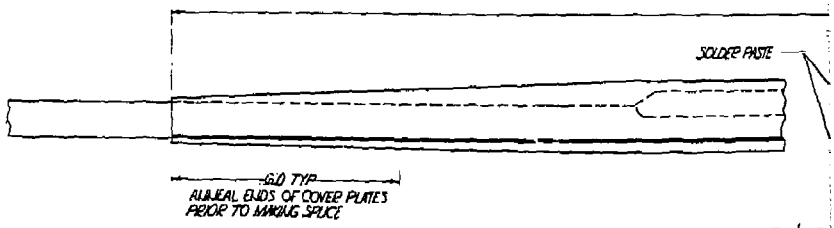

ADD SOLDER PASTE & C

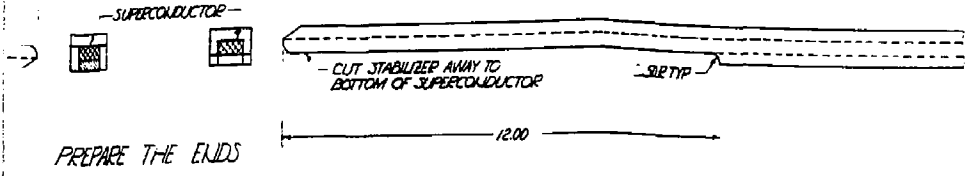

PREPARE THE ENDS

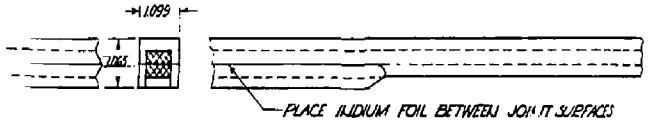

LAP THE ENDS

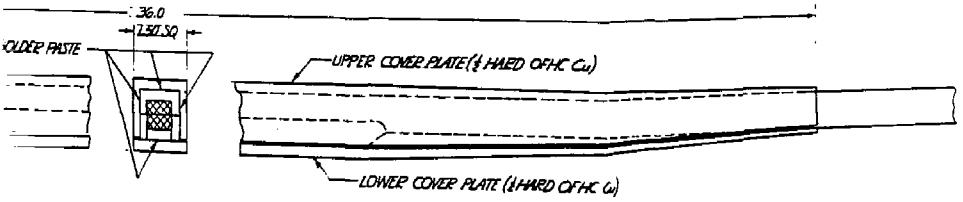

'R PASTE & COVER PLATES, CLAMP & HEAT

NOTES-
1. ACTUAL SPLICES WILL BE MADE ON A RADIUS IN MINOR RADIUS REGION - THEY ARE SHOWN STRAIGHT FOR EASE IN DRAFTING.
2. EUTECTIC TIN-LEAD SOLDER TO BE USED
3. CLAMPS NOT SHOWN

	PRELIMINARY DESIGN DRAWING	
	SPLICE TMNJS	
	14170	TMNJS-018

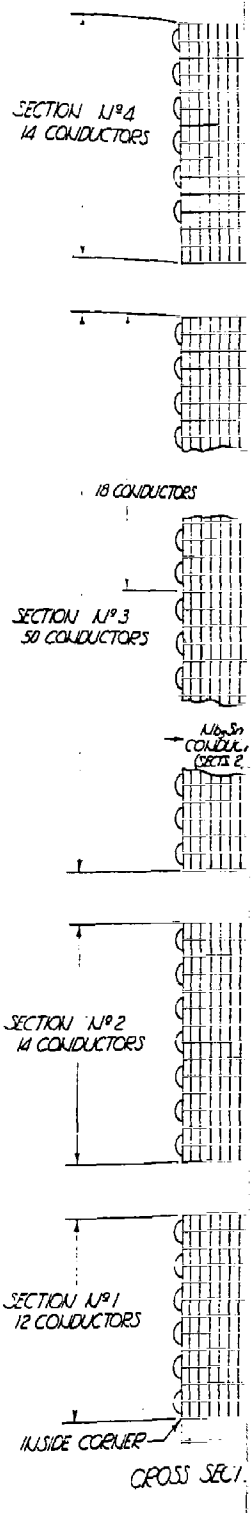
SECTION N°4
14 CONDUCTORS
18 CONDUCTORS
SECTION N°3
50 CONDUCTORS
SECTION N°2
14 CONDUCTORS
SECTION N°1
12 CONDUCTORS
INSIDE CORNER

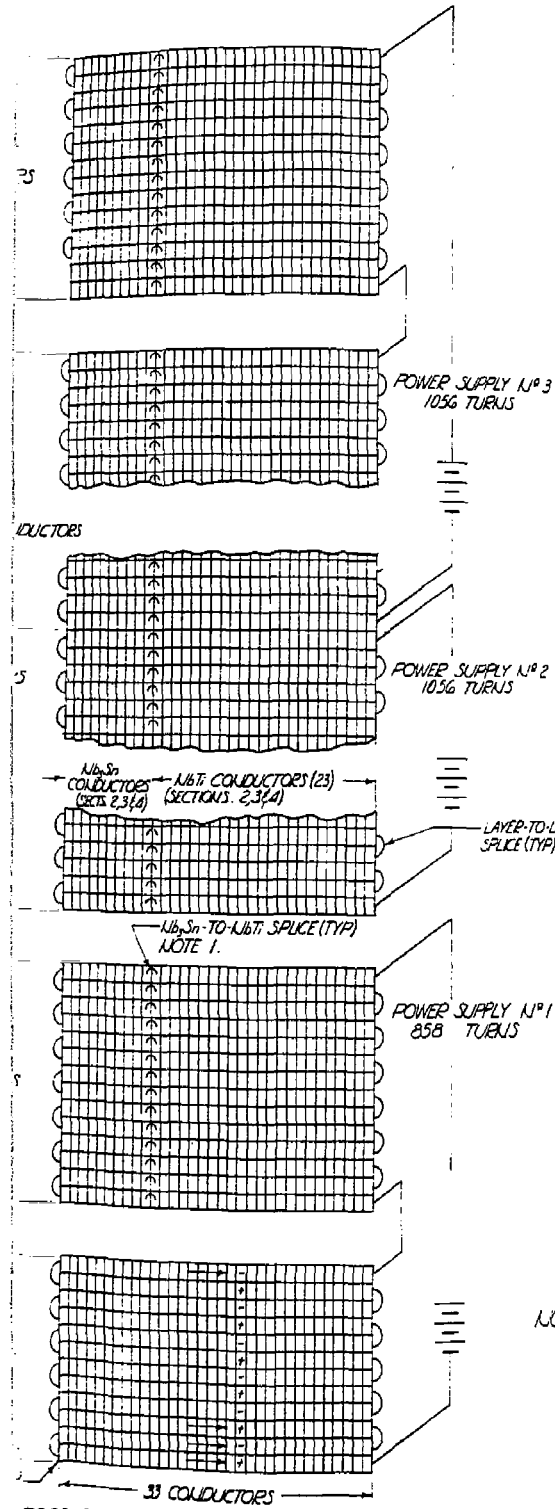

CROSS SECTION THROUGH MAJOR RADIUS

NOTES-

1. SEE TMNS-018 FOR SPLICE DETAILS.
6. 163 SPLICES REQUIRED PER YIN BASED ON 2600-FOOT LENGTHS OF CONDUCTOR. FOR 1300-FOOT LENGTHS THE NO OF SPLICES INCREASES TO 253.
5. ALL LAYERS START FROM THE INSIDE; FIRST LAYER STARTS AT BOTTOM OF SECTION NO 1.
4. ALL TURNS ARE LAYER WOUND IN THE MAJOR RADIUS REGION, PANCAKE IN MINOR RADIUS.
3. + = WIND CLOCKWISE; - = WIND COUNTERCLOCKWISE.
2. SEE TMNS-017 FOR COIL ARRANGEMENT.
1. ALL SPLICES PERFORMED IN MINOR RADIUS REGION.

PRELIMINARY DESIGN DRAWING

WINDING ARRANGEMENT TMNS

14170 TMNS-019

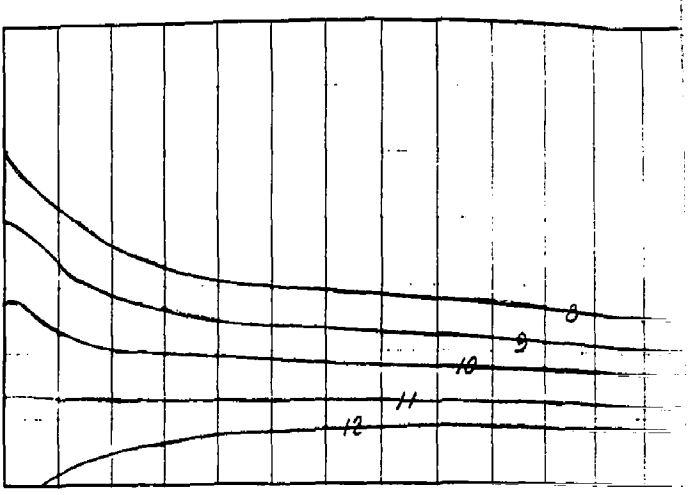

INSIDE CORNER

YZ

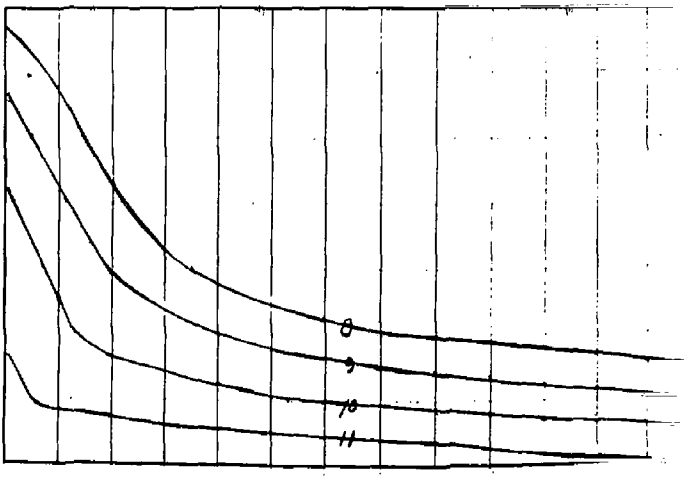

INSIDE CORNER

X-Z

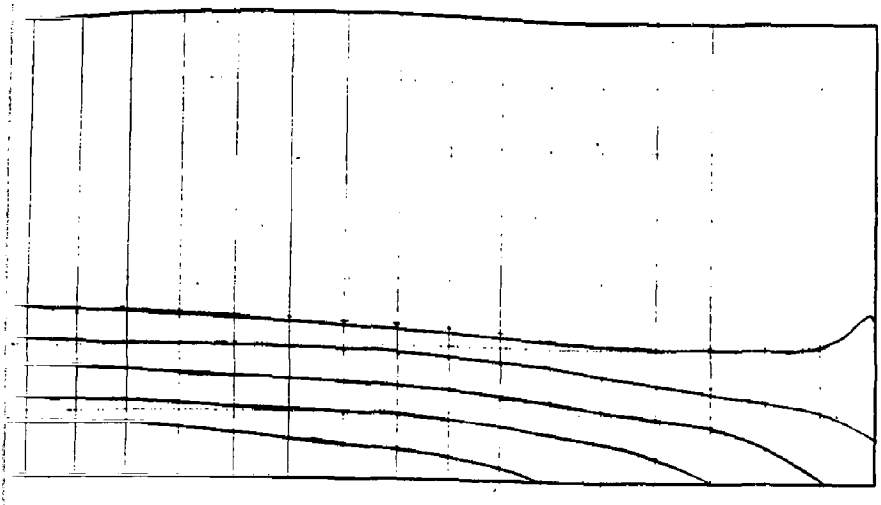

YZ PLANE - MINOR RADIUS

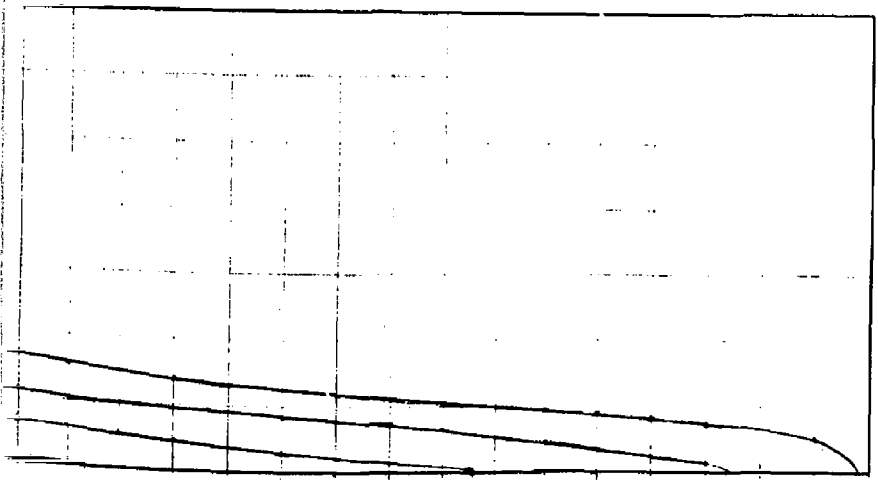

X-Z PLANE - MAJOR RADIUS

CROSS SECTION FIELD STRENGTH
TMNS SCALE: 1"=15CM

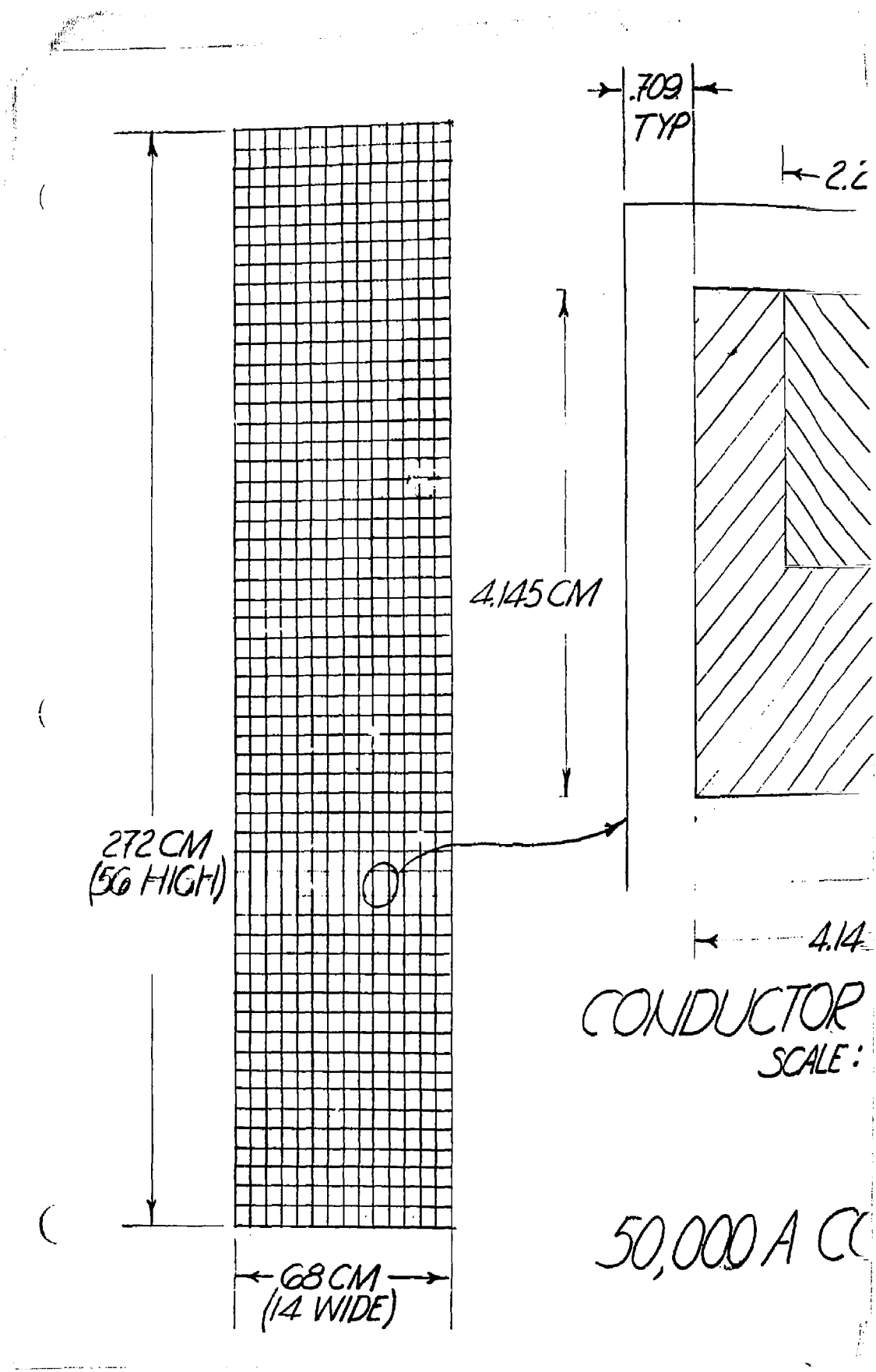
.709
TYP
2.2
4.145 CM
272 CM
(56 HIGH)
4.14
CONDUCTOR
SCALE:
50,000 A C
68 CM
(14 WIDE)

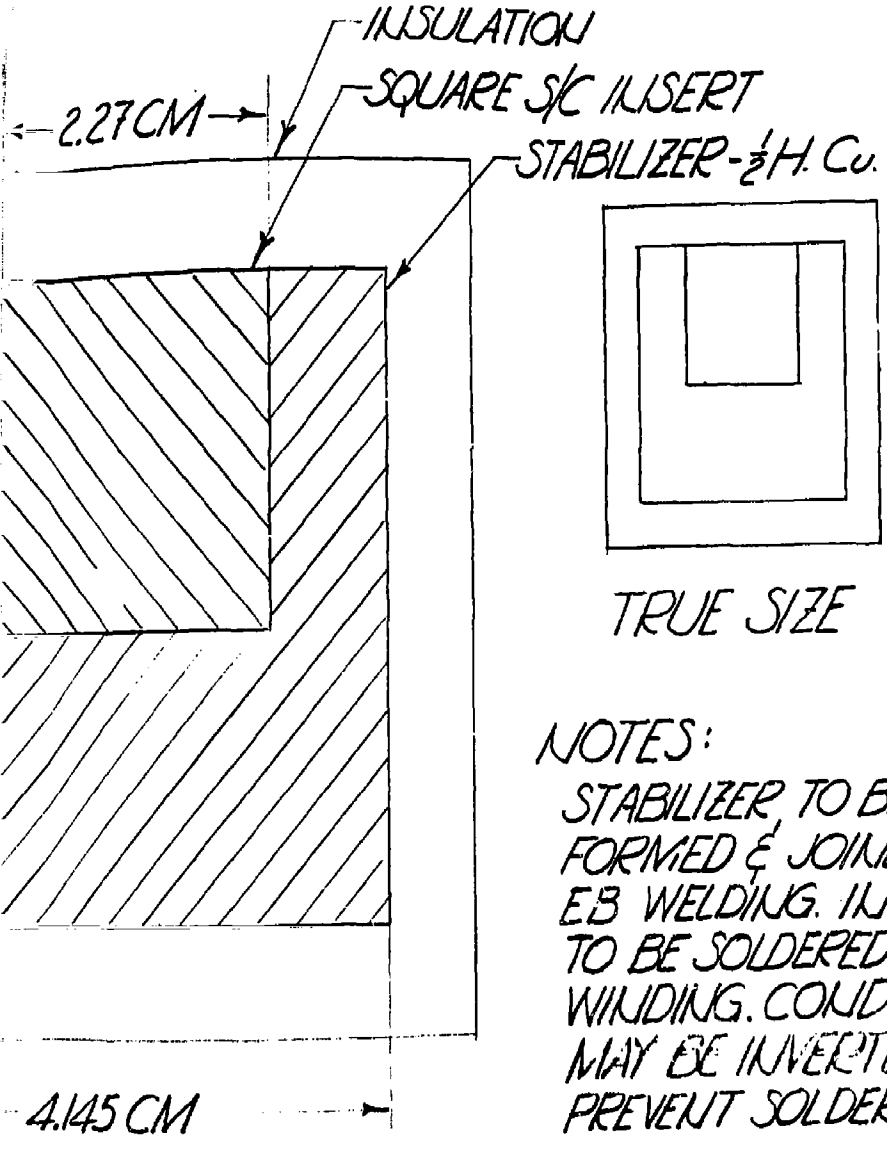

TRUE SIZE

NOTES:

STABILIZER TO BE PRE-FORMED & JOINED BY EB WELDING. INSERT TO BE SOLDERED DURING WINDING. CONDUCTOR MAY BE INVERTED TO PREVENT SOLDER SPILLS.

'OR CROSS SECTION

CALE: 1IN = 1CM

Discarded concept -- used in tradeoff studies

1 CONDUCTOR - TMNS

C-14

R.A. SUTTON 5/27/81

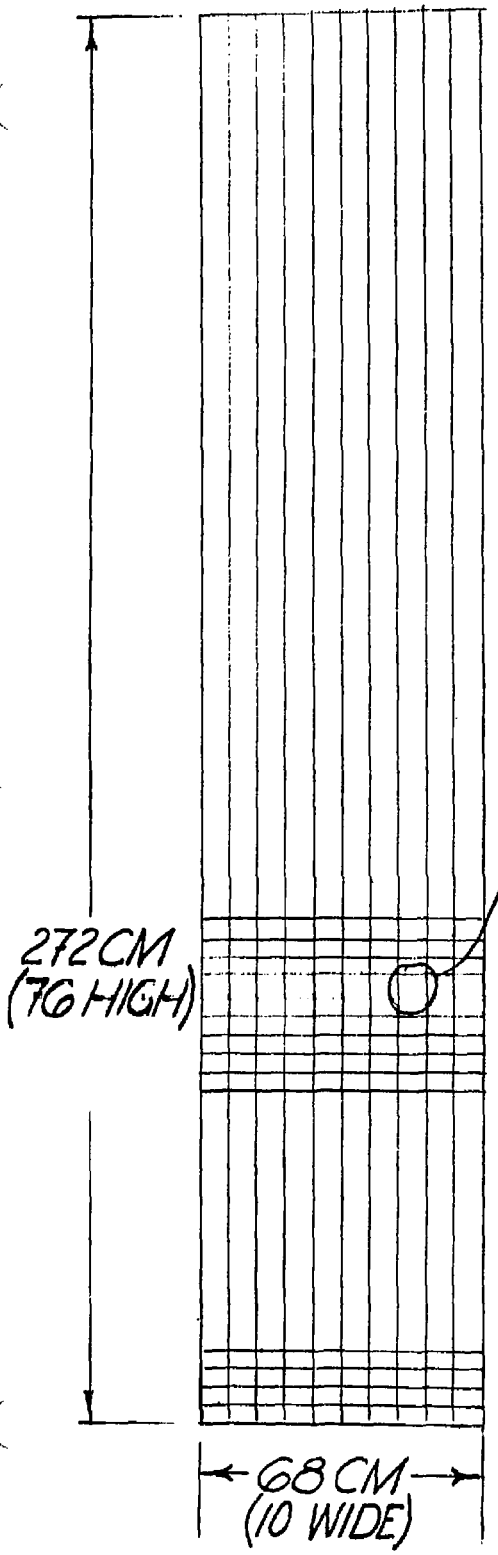

CONDUCTOR (
SCALE :

NOTES-
STABILIZER TO BE PR
INSERT TO BE SOLDE
CONDUCTOR MAY BE

50,000 A. CO

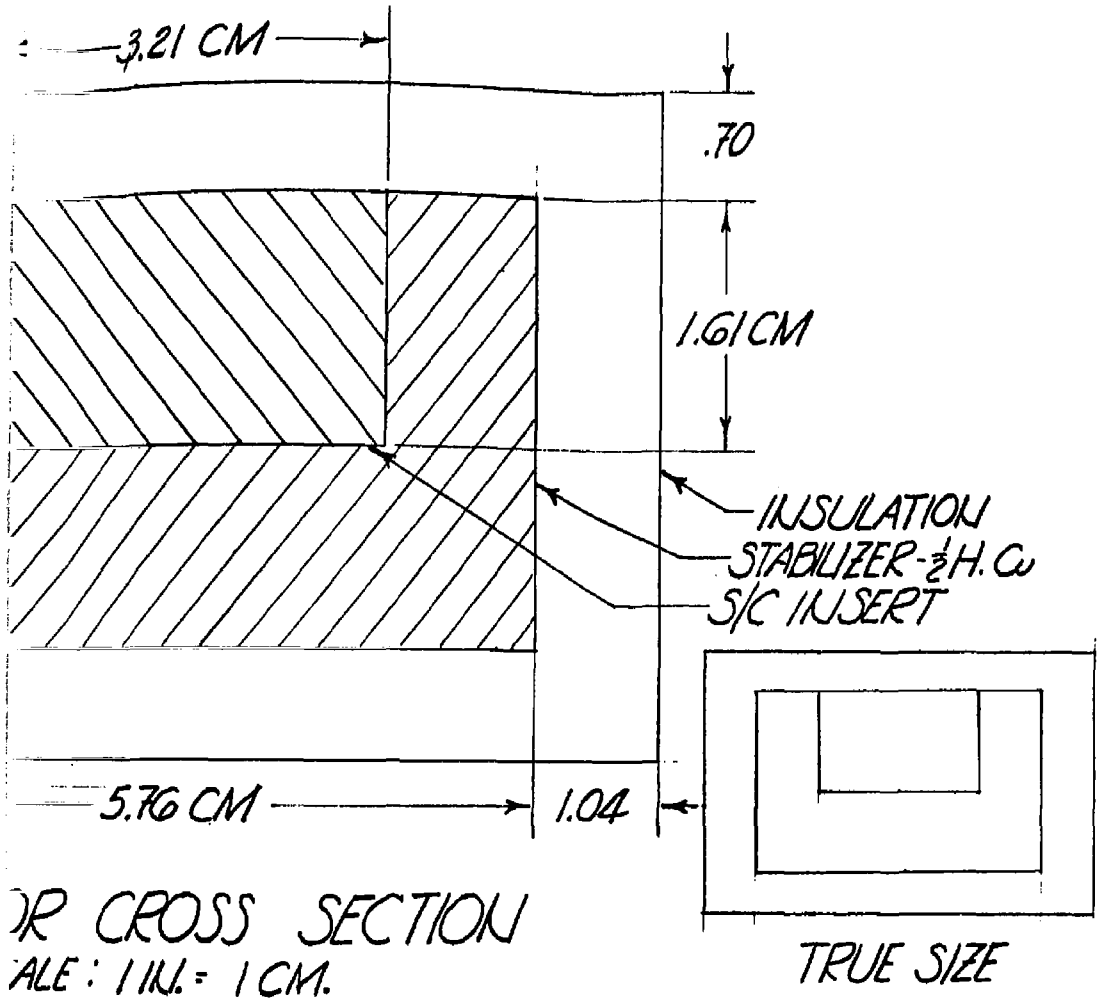

OR CROSS SECTION
ALE: 1 IN. = 1 CM.

E PRE-FORMED & JOINED BY E.B WELDING.
OLDERED DURING WINDING.
AY BE INVERTED TO PREVENT SOLDER SPILLS.

Discarded concept -- used in tradeoff studies

CONDUCTOR- TMNS

R.A.SUTTON 5/27/81

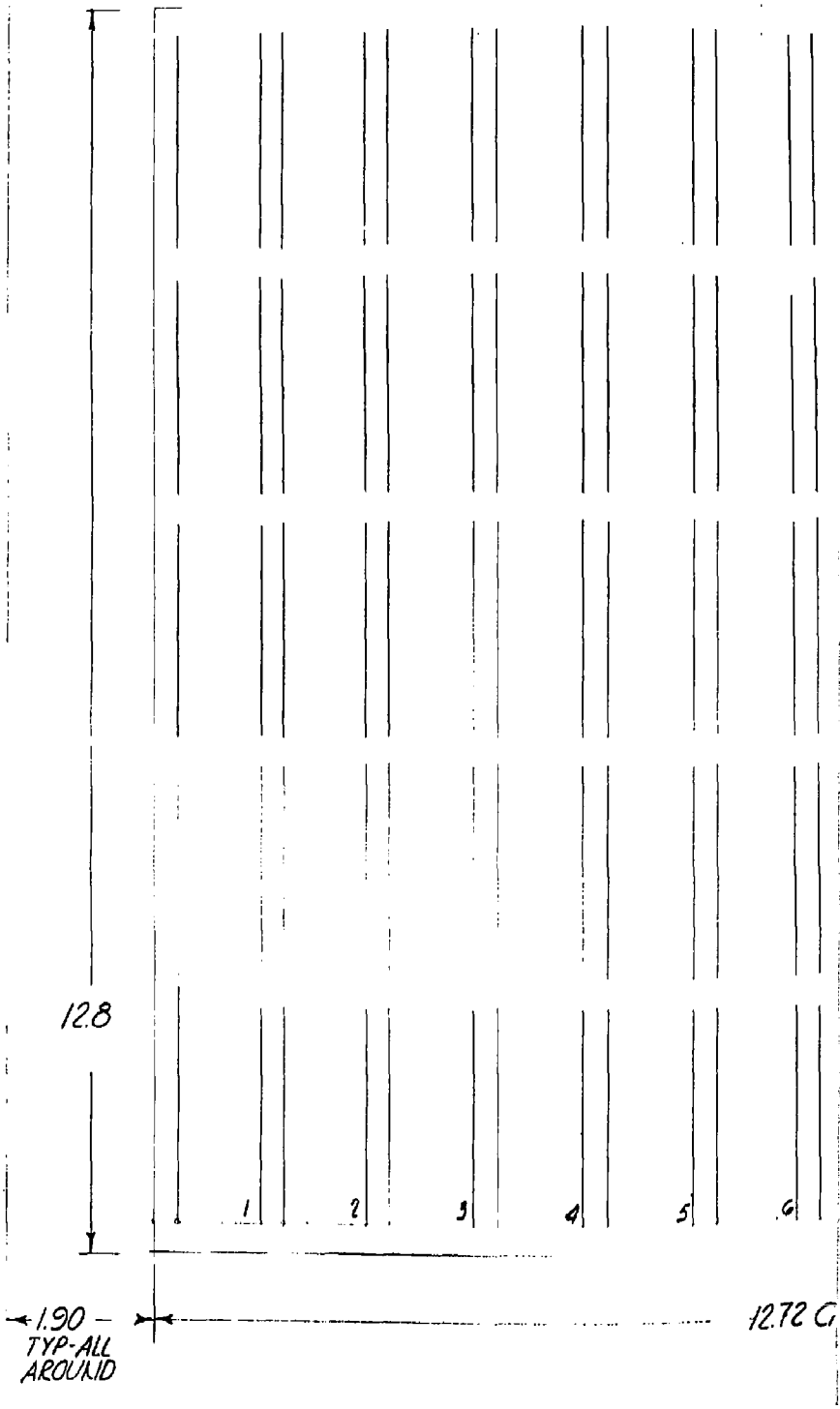
12.8
1
2
3
4
5
6
1.90 –
TYP-ALL
AROUND
12.72 C

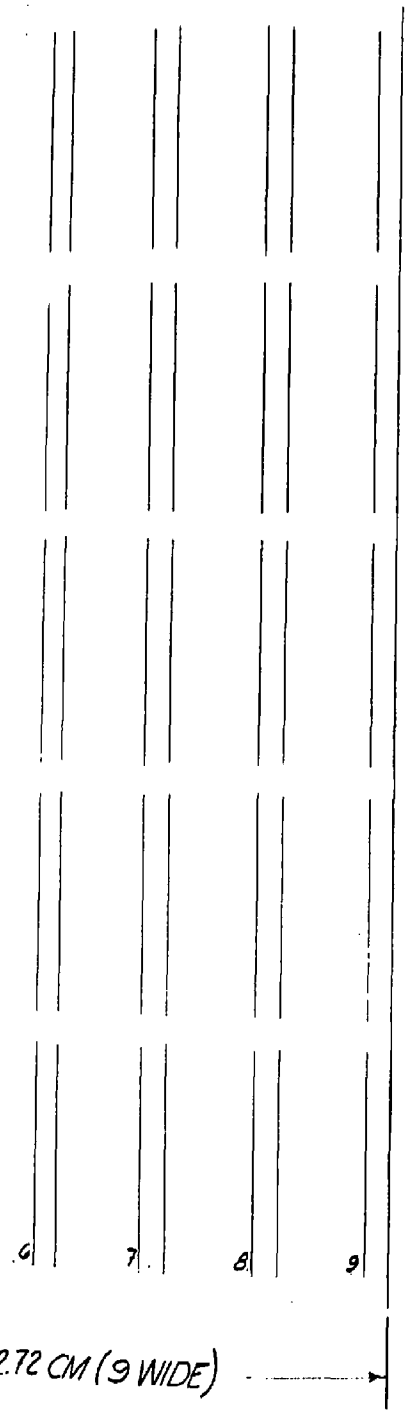

Discarded concept -- used in tradeoff studies

9×5 BOX
12.72 CM × 12.7 CM

SCALE: 1 IN = 1 CM

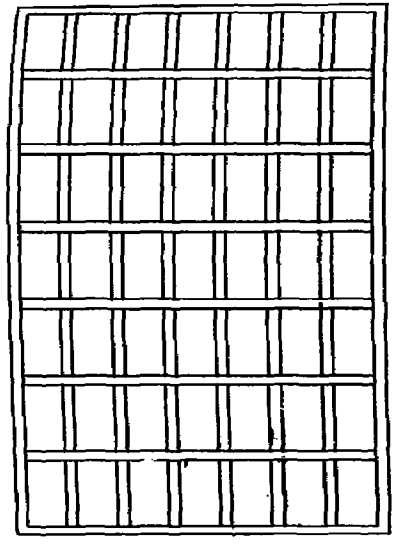
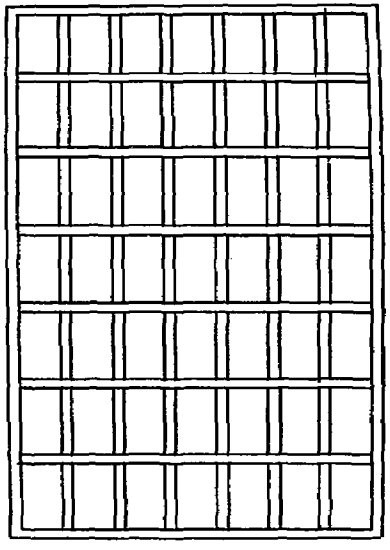
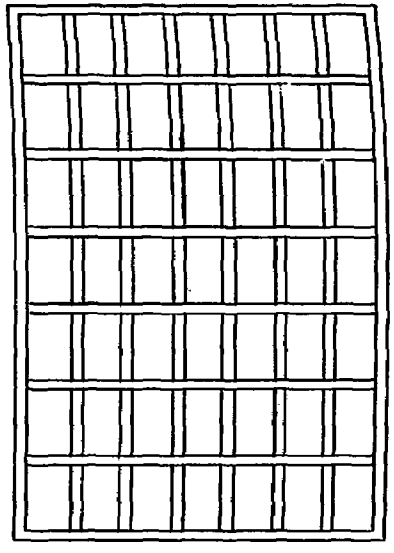

7×7 BOXES
FULL SIZE

Discarded concept -- used in tradeoff studies

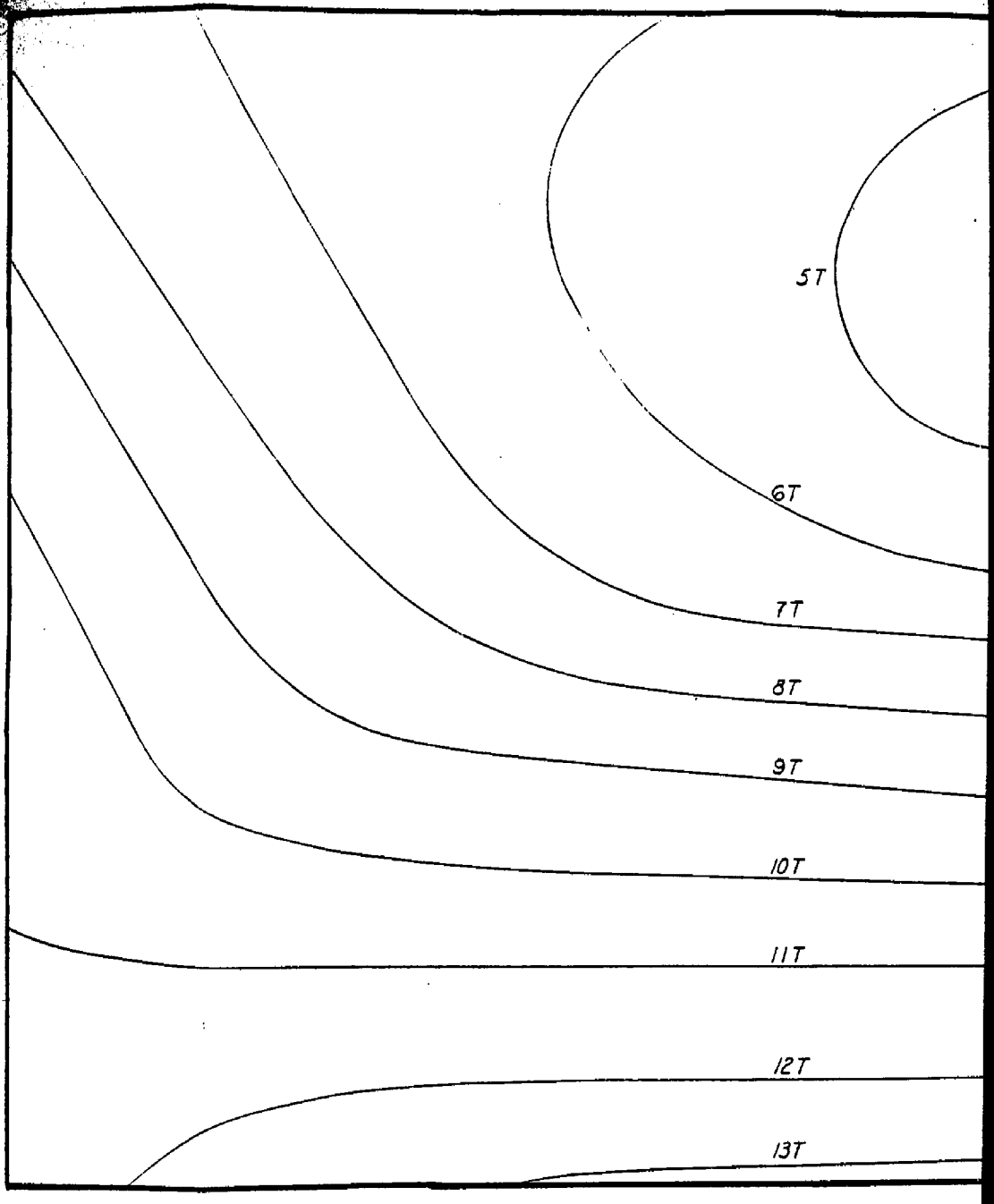
5T
6T
7T
8T
9T
10T
11T
12T
13T

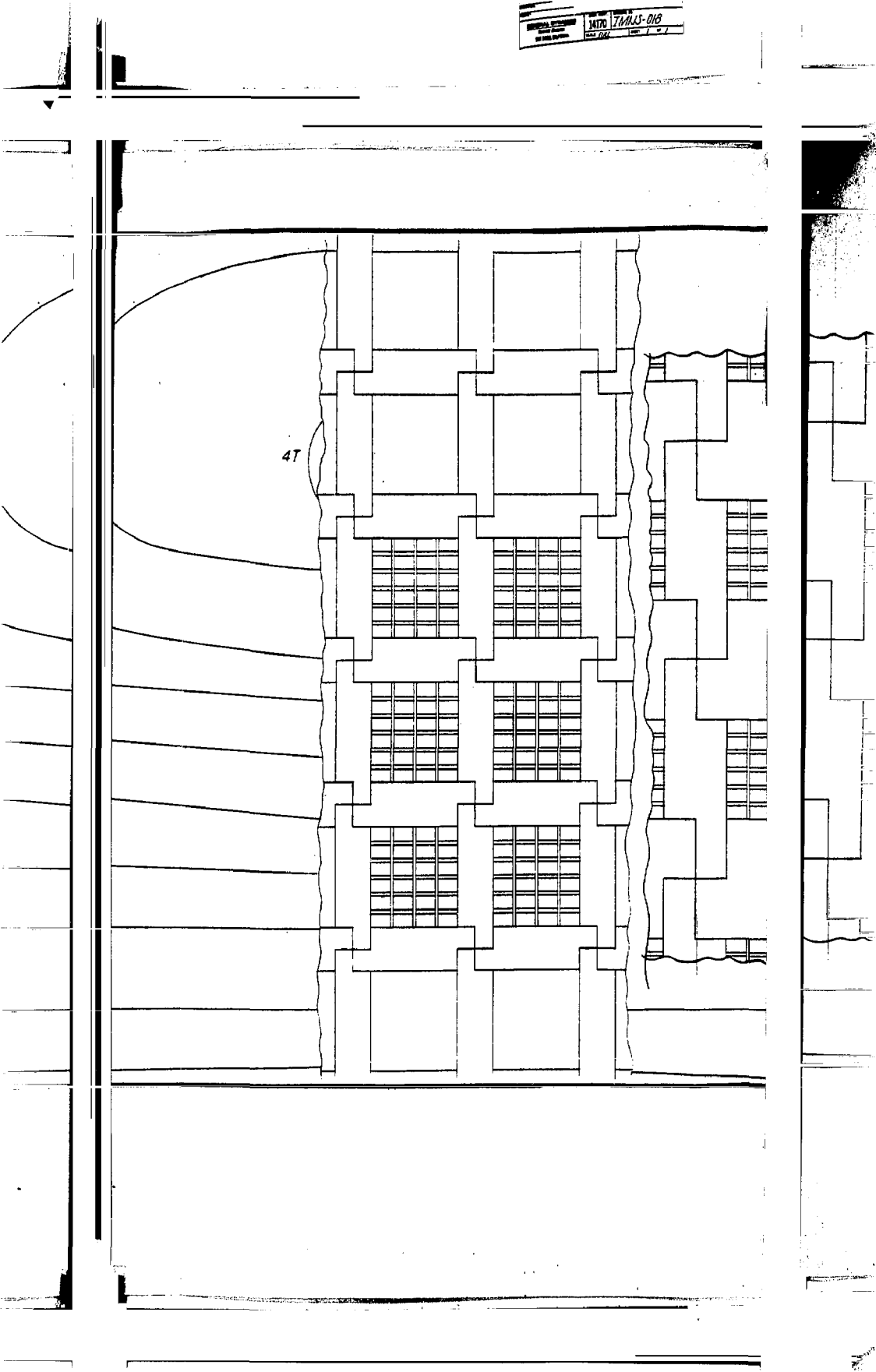

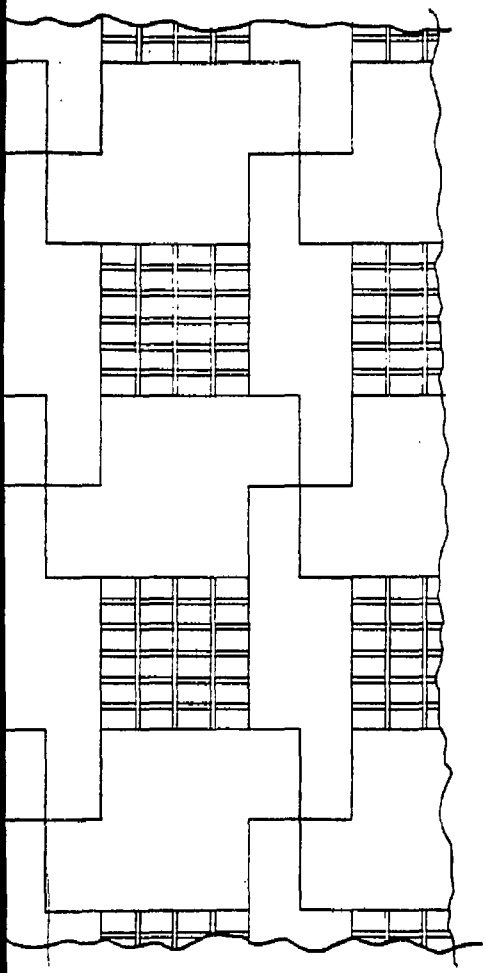

4T

3T

2T

2T

3T

5T

6T

7T

8T

9T

10T

11T

12T

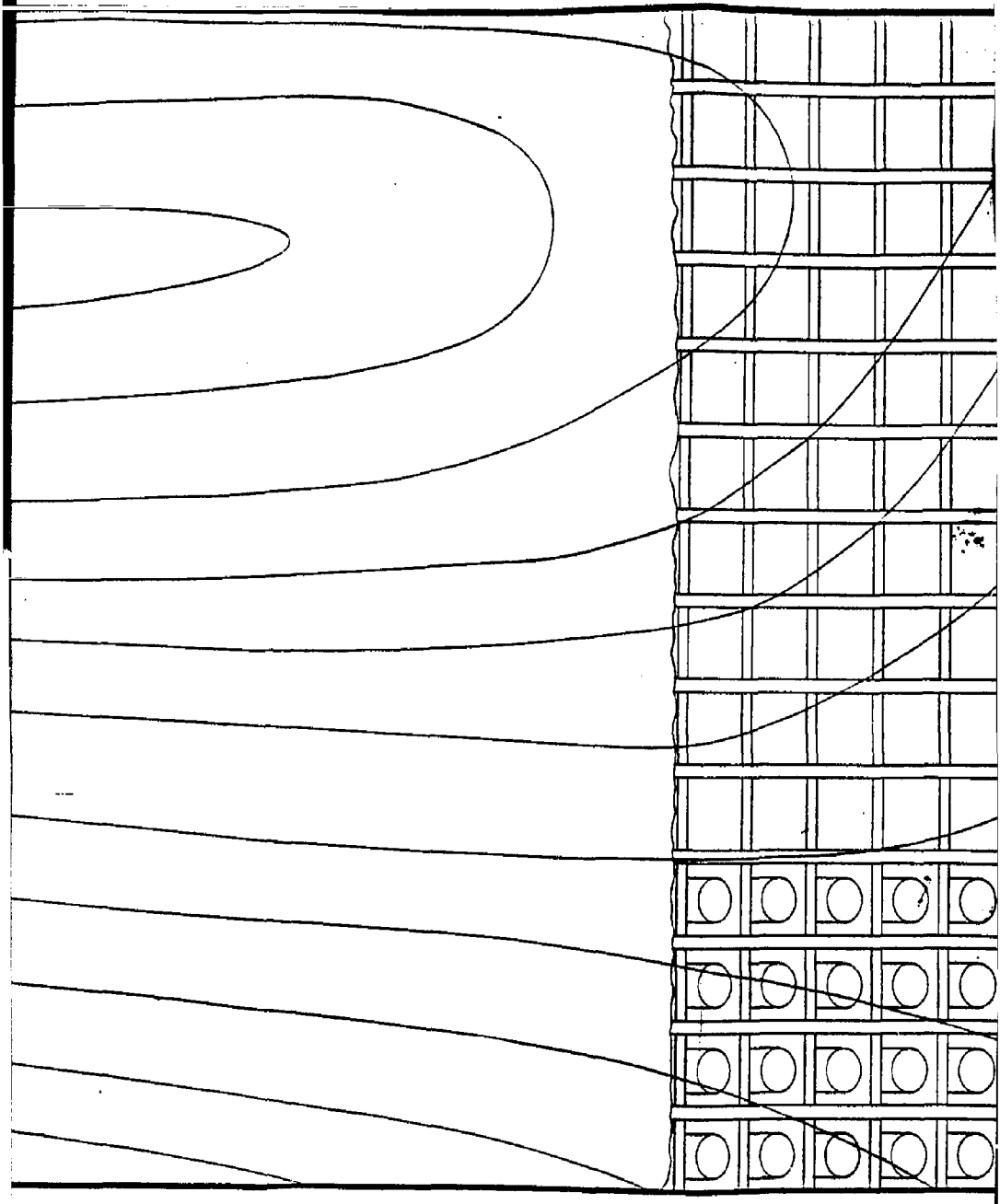

50,000-AMP COND.
PACK CROSS SECT

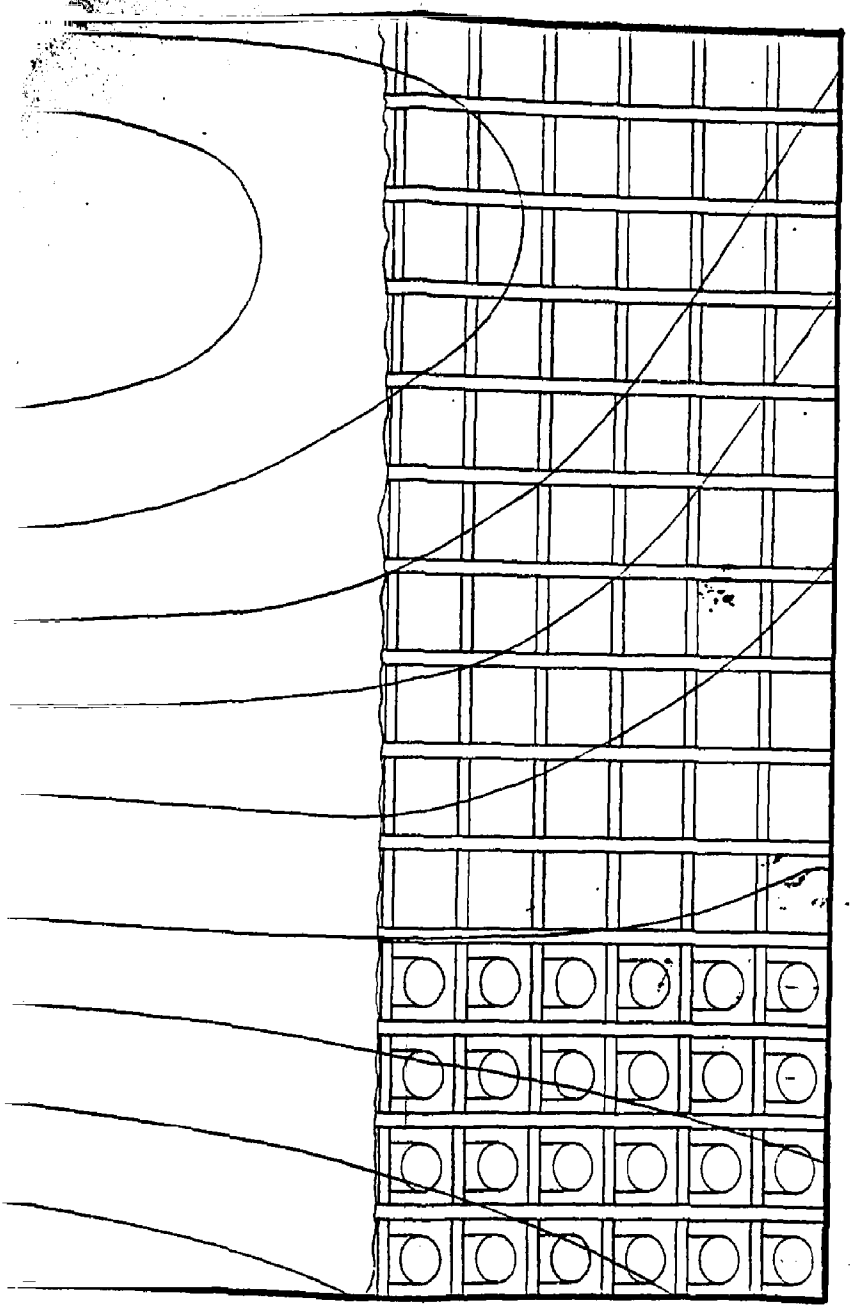

Discarded concept — used in tradeoff studies

50,000-AMP COND. PACK CROSS SECTION

DISCARDED CONCEPT

APPENDIX D

A BRIEF DESCRIPTION OF THE COMPUTER CODES

SUPERQ AND SPICE

D.1 SUPERQ

To calculate the adiabatic temperature rise of the conductor, the GDC computer program SUPERQ was used. SUPERQ calculates the time and temperature evolution of system parameters by numerically integrating the basic equations governing the power balance and voltages during a quench condition. The actual integration is performed using temperature steps, calculating the current from the temperature, and the time from the current. The magnetic field is allowed to vary with the current.

The program commences with a segment of the conductor going normal. It is assumed that this normal region remains constant in length. The joule heat generated causes a rise in the zone temperature and the resistive voltage drop across the normal zone exceeds the inductive. The resistive voltage drop across the normal zone is calculated at each temperature step and compared to the dump initiation voltage. The emergency discharge is initiated by introducing an appropriate dump resistor in the circuit (d termined by the desired dump voltage) a given time after the normal zone voltage equals or exceeds the dump initiation voltage. The integration is terminated when the stored energy in the magnet has been dissipated. SUPERQ is very conservative in that the temperature rise of the conductor is calculated using only the specific heat of the conductor and superconductor. The specific heats of the insulation and helium are ignored.

D.2 SPICE

SPICE is a general purpose circuit simulation program for nonlinear DC, nonlinear transient, and linear AC analyses. Circuits may contain resistors, capacitors, inductors, mutual inductors, independent voltage and current sources, four types of dependent sources, transmission lines, and the four most common semiconductor devices: diodes, BJTS, JFETS, and MOSFETS. SPICE uses dynamic memory management to store elements, models, and output values. Thus, the only limitation imposed by the program on the size or the complexity of the circuit to be simulated is that all necessary data fit in memory.

The transient analysis portion of SPICE, used for TMNS, computes the transient output variables as a function of time over a user-specified time interval. The initial conditions are automatically determined by a DC analysis. All sources which are not time dependent (for example, power supplies) are set to their DC value.

For large-signal sinusoidal simulations, a Fourier analysis of the output waveform can be specified to obtain the frequency domain Fourier coefficients.

INTRODUCTION

In addition to those studies undertaken to meet the criteria related to thermal stability, quench protection, mechanical structural integrity, and manufacturability, several iterations were necessary to satisfy magnetic field considerations, such as: the central field strength on the plasma, the magnetic mirror ratio, and the maximum field impending upon the Nb_3Sn conductor windings. The purpose of this section is to review the magnetic field requirements of the TMNS 12-T yin-yang superconducting magnets and to document their impact upon the final design recommendation.

GEOMETRY OF THE 12-T YIN-YANG COILS

A cross section of the TMNS 12-T yin-yang coils is shown in Figure 1, which includes the internal stainless-steel substructure and conductor pack. Electrical quench protection considerations warranted subdividing the coil into three subcoils, each energized by a separate power supply. Coils 1a - 1b and 3a - 3b are further split by stainless-steel substructural pieces. Coil 1a has 33 x 12 turns; 1b has 33 x 14, 2 has 33 x 52, 3a has 33 x 18, and 3b has 33 x 14 turns. The geometry of this coil pack was modeled on the EFFI computer program which generated an equivalent yin-yang pair. Various three-dimensional projective views of the yin-yang pairs are shown in Figures 2 - 4. Notice that the stainless steel substructure is excluded and is modeled by blank spaces between the subcoils.

INDUCTANCE CALCULATIONS

Each subcoil of Figure 1 is modeled as a single filament in the EFFI code. Therefore, coil 1 has two filaments (1a and 1b) along with coil 3 (3a and 3b). The fourth coil is composed of the entire opposing yang

magnet, which is represented by five filaments. The resulting filament unit inductances (self and mutual) are displayed in the lower diagonal of a 4 x 4 matrix tabulated below:

ltmnsgd 07248120+ Configuration No. 3

Inductance matrix for coils one through four (in Henrys):

2.997e-05

7.353e-06 1.083e-05

7.320e-06 1.171e-05 4.678e-05

7.797e-06 2.957 J6 4.660e-06 1.403e-04

Total inductance for these coils is 3.115e-04

MAGNETIC FIELD CALCULATIONS:

Figure 5 shows a cross-sectioned slice through the minor radii of the left yin coil and a slice through the middle of the major radius of its right yang magnet counterpart. Magnetic-field calculations produced the field contours for the 13 kA conductor at the minor radius shown in Figure 6, while Figure 7 displays the field magnitude as a function of the "z" coordinate at the center of the yin-yang pair. The plasma physics requirements include a mirror ratio of 1.5 $\pm$ 10% and a minimum saddle point field of 6 T at the center of the magnet pair. The latter consideration prompted an increment in the conductor current by 20 percent to a new value of 15.6 kA. Since the field scales linearly with current, the maximum field exposed to the conductor at the minor radius has increased to 14.6 T, as shown in Figure 8, for the 15.6 kA conductor. Such a high transverse field value enhances the difficulty of fabricating a Nb_3Sn composite conductor. Figure 9 displays the field contours for coils 2 and 3a at the major radius cross section also for

the 15.6 kA conductor. Since its peak field is only 11.8 T, it suggests that the problem may be obviated by spreading out the coils at the minor radius. Figure 10 shows a successful iteration which reduced the maximum minor radius field from 14.6 T to 12.0 T. In the figure, the 12 T field permeates through four turns of conductor, which are separated with 50 cm of G-10 insulation from seven turns, which have a peak field of 11 T. Thirty centimeters of G-10 are spaced between the inner 7 turns and the outer 22 turns of the coil cross section. The G-10 inserts can be visualized as crescent-shaped pieces, that have maximum thicknesses of 50 and 30 cm, respectively, at the minor radii. It is important to realize that the EFFI program cannot model the minor radii distortions produced by the insulation inserts. The iterative procedure was to generate complete yin-yang pairs from the coil cross sections shown in Figures 8 and 10, compute the resulting field distributions, and use the principle of superposition to approximate the actual fields of the final yin-yang geometry.

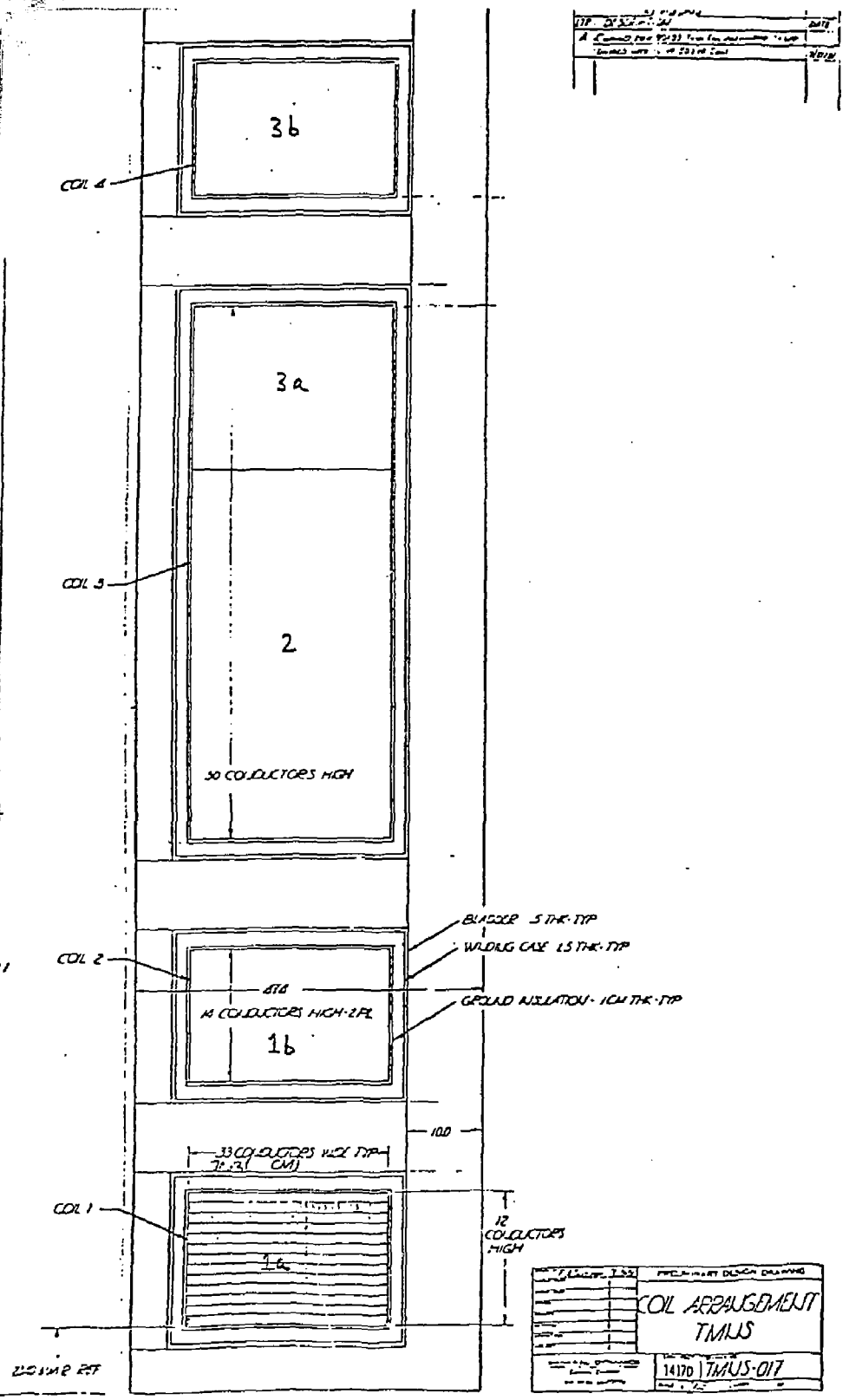
3b
COIL 4
3a
COIL 3
2
30 CONDUCTORS HIGH
BLANKET 5 THK. TYP
WELDED CASE 1.5 THK. TYP
COIL 2
GAP
14 CONDUCTORS HIGH-2 PL
1b
GROUND INSULATION - 1CM THK. TYP
10.0
33 CONDUCTORS WIDE TYP
COIL 1
1a
12 CONDUCTORS HIGH
COIL ARRANGEMENT
TMUS
14170 TMUS-017
SECTION A-A
SCALE NONE

FIGURE E-1

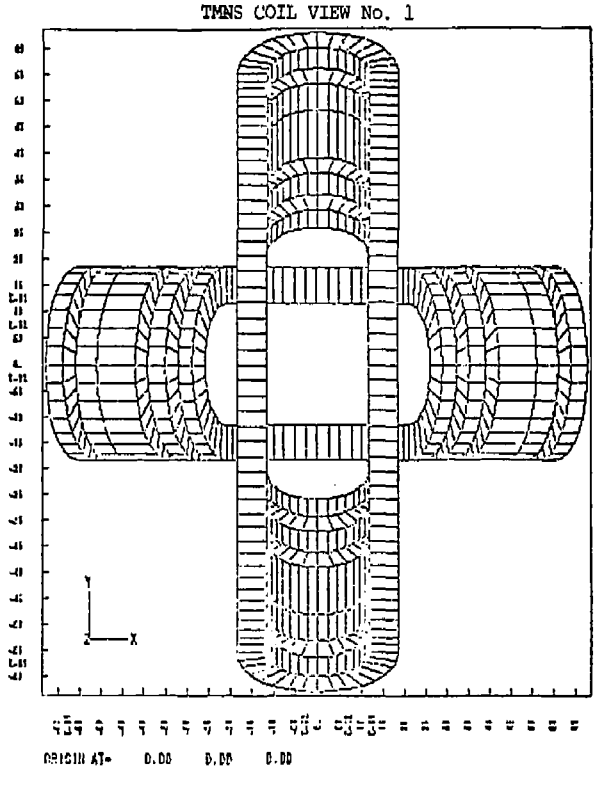

FIGURE E-2

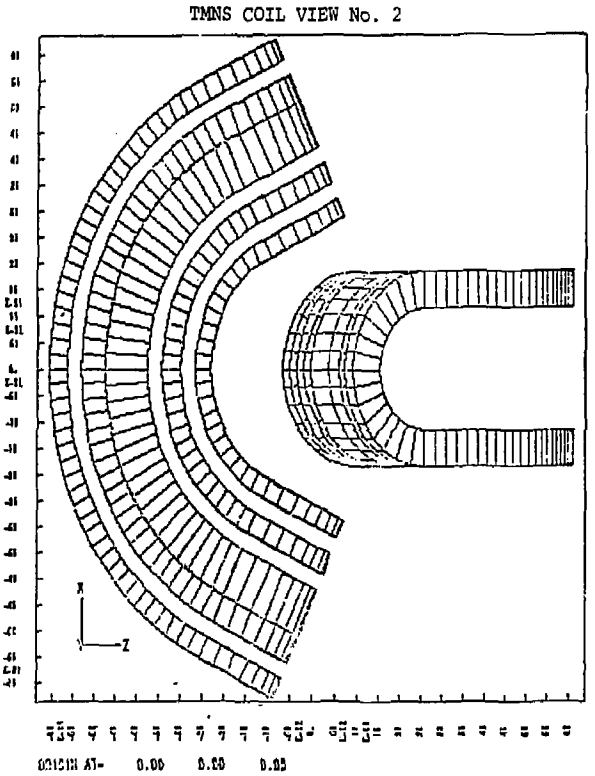

FIGURE E-3

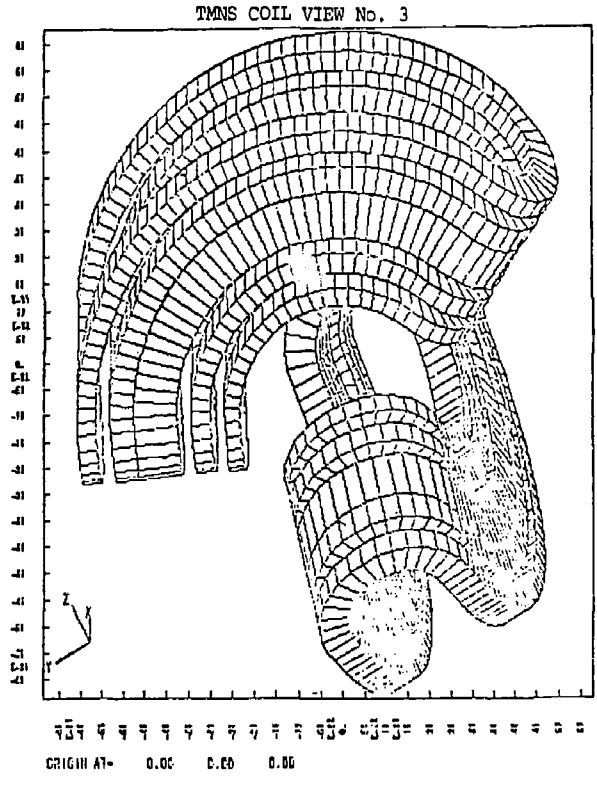

FIGURE E-4

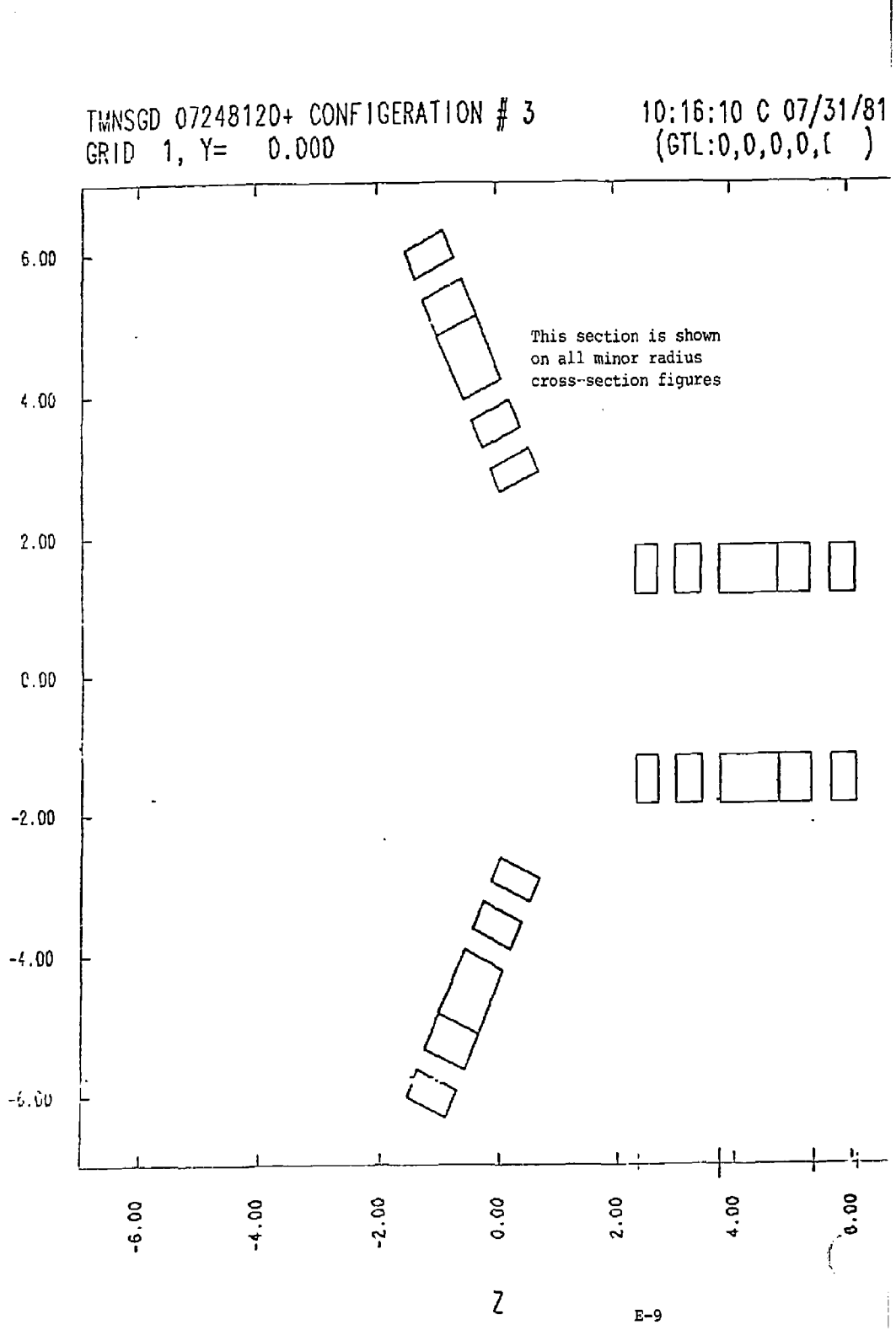
TMNSGD 07248120+ CONFIGERATION # 3
GRID 1, Y= 0.000
10:16:10 C 07/31/81
(GTL:0,0,0,0,( )
This section is shown
on all minor radius
cross-section figures
6.00
4.00
2.00
0.00
-2.00
-4.00
-6.00
-6.00
-4.00
-2.00
0.00
2.00
4.00
6.00
Z

FIGURE E-5

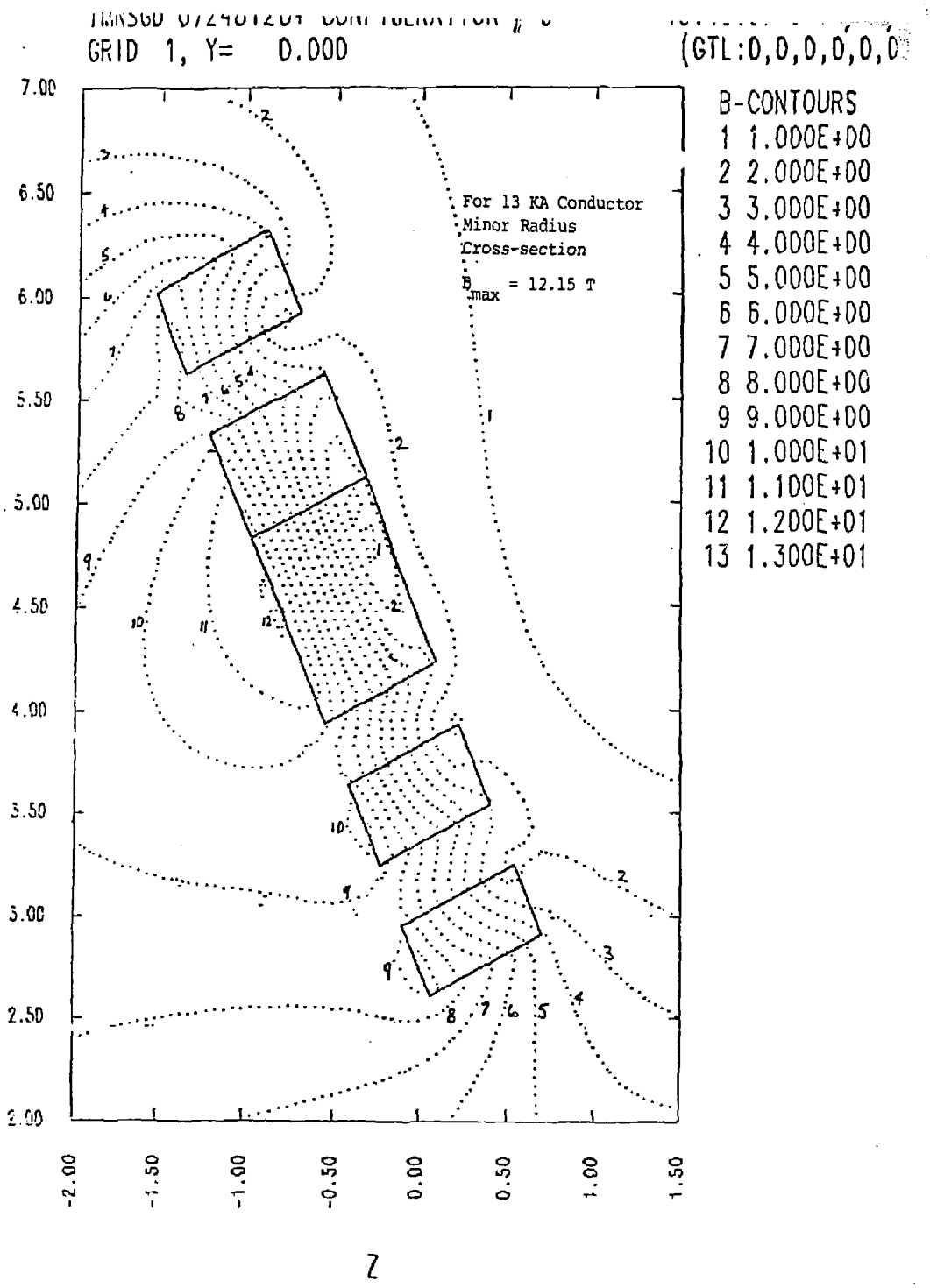
TRNSGD 07240120? CONFIGURATION # 0
GRID 1, Y= 0.000
(GTL:0,0,0,0,0,0
B-CONTOURS
1 1.000E+00
2 2.000E+00
3 3.000E+00
4 4.000E+00
5 5.000E+00
6 6.000E+00
7 7.000E+00
8 8.000E+00
9 9.000E+00
10 1.000E+01
11 1.100E+01
12 1.200E+01
13 1.300E+01
For 13 KA Conductor
Minor Radius
Cross-section
B max = 12.15 T
7.00
6.50
6.00
5.50
5.00
4.50
4.00
3.50
3.00
2.50
2.00
-2.00
-1.50
-1.00
-0.50
0.00
0.50
1.00
1.50
X
Z

FIGURE E-6

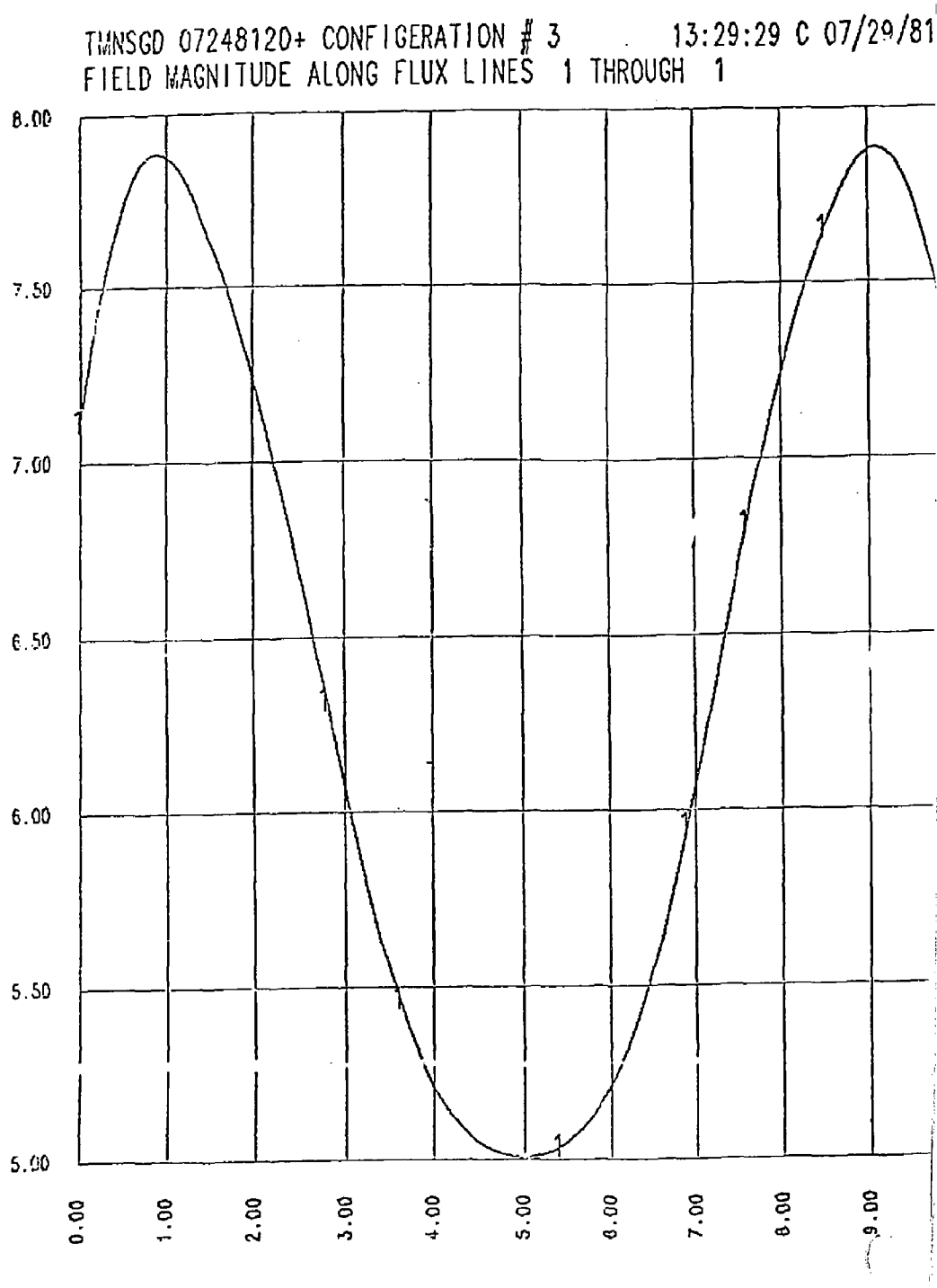
TMNSGD 07248120+ CONFIGERATION # 3 13:29:29 C 07/29/81
FIELD MAGNITUDE ALONG FLUX LINES 1 THROUGH 1
8.00
7.50
7.00
6.50
6.00
5.50
5.00
0.00
1.00
2.00
3.00
4.00
5.00
6.00
7.00
8.00
9.00
S

FIGURE E-7

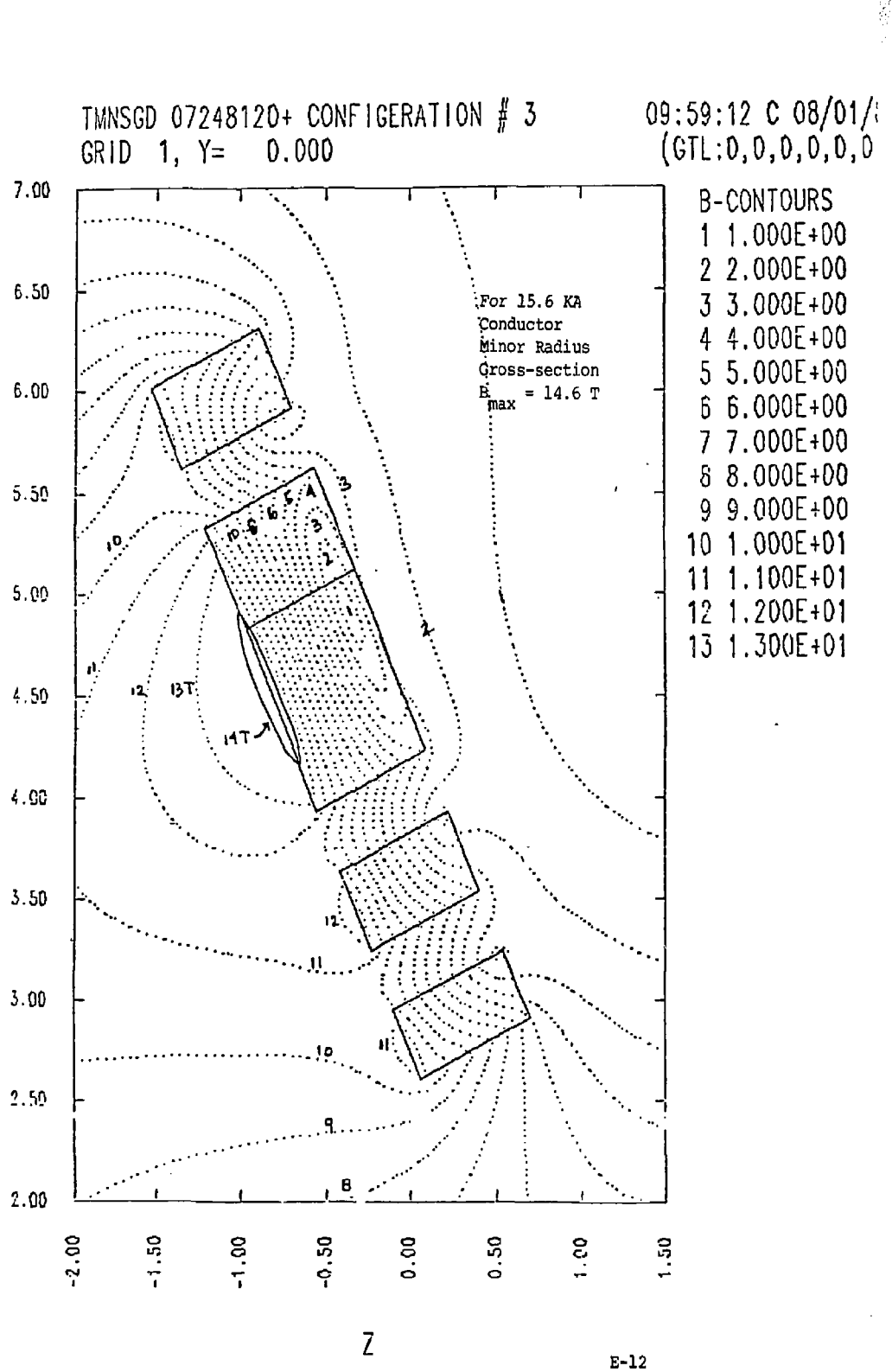
TMNSGD 07248120+ CONFIGERATION # 3
09:59:12 C 08/01/
GRID 1, Y= 0.000
(GTL:0,0,0,0,0,0
B-CONTOURS
1 1.000E+00
2 2.000E+00
3 3.000E+00
4 4.000E+00
5 5.000E+00
6 6.000E+00
7 7.000E+00
8 8.000E+00
9 9.000E+00
10 1.000E+01
11 1.100E+01
12 1.200E+01
13 1.300E+01
For 15.6 KA
Conductor
Minor Radius
Cross-section
B max = 14.6 T
13T
14T
7.00
6.50
6.00
5.50
5.00
4.50
4.00
3.50
3.00
2.50
2.00
-2.00
-1.50
-1.00
-0.50
0.00
0.50
1.00
1.50
X
Z

FIGURE E-8

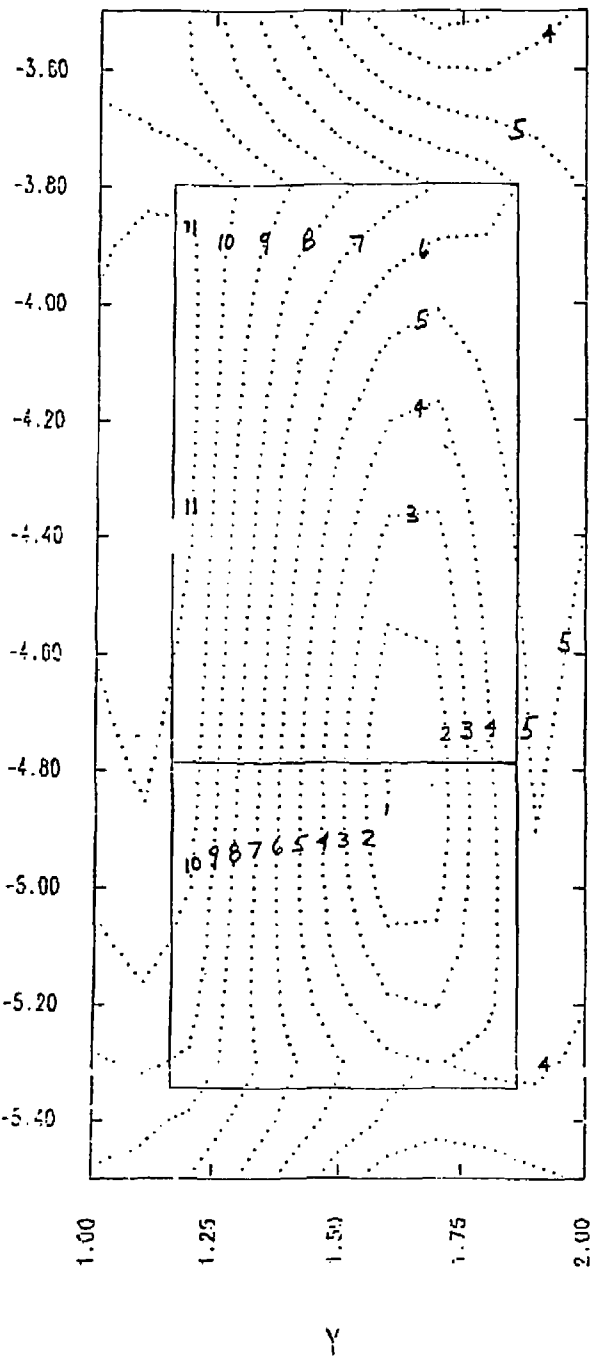

Major Radius
Cross-section
For 15.6 KA Conductor
B_{max} = 11.8 T

Figure E-9

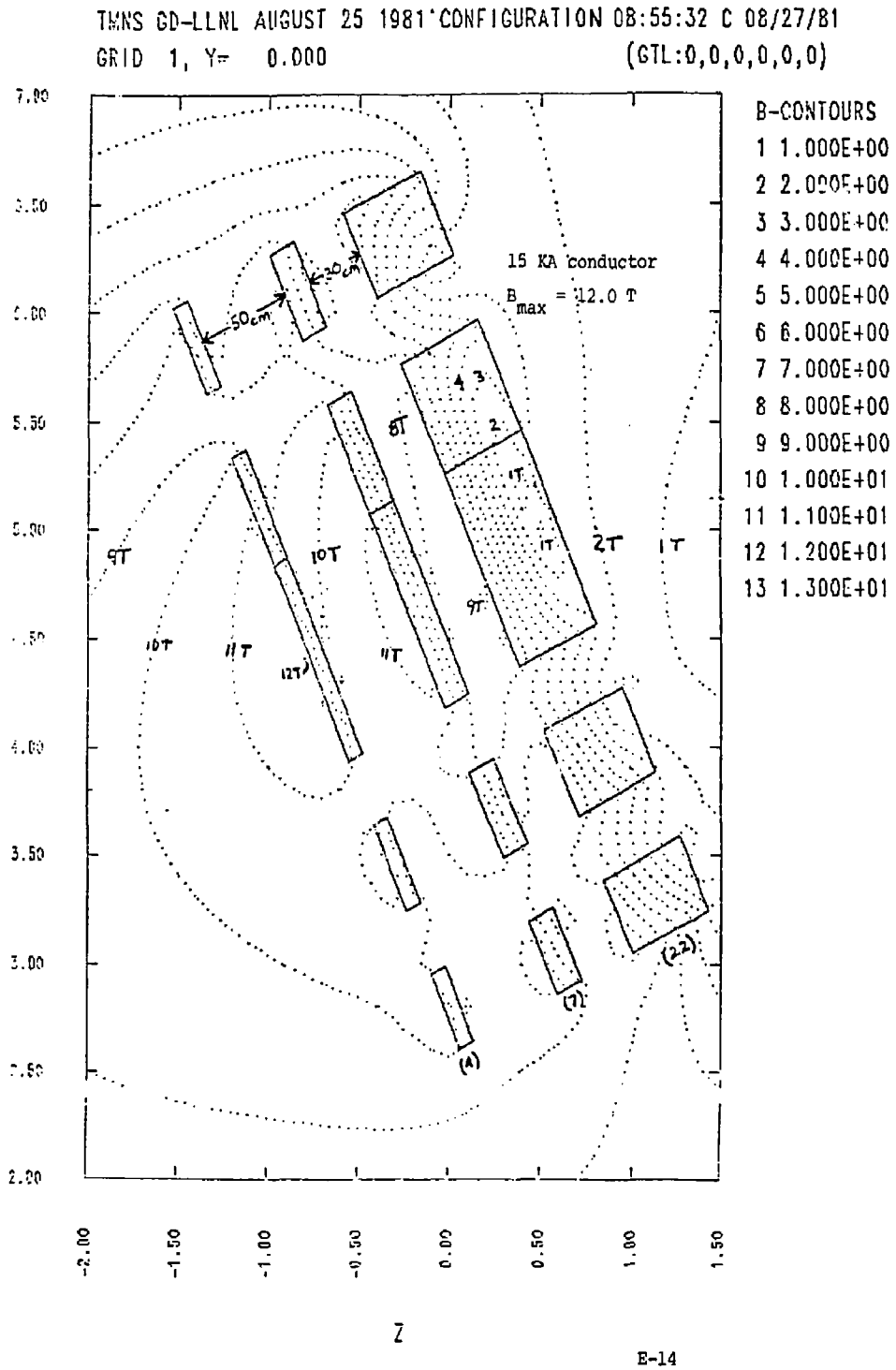
TMNS GD-LLNL AUGUST 25 1981 CONFIGURATION 08:55:32 C 08/27/81
GRID 1, Y= 0.000
(GTL:0,0,0,0,0,0)
B-CONTOURS
1 1.000E+00
2 2.000E+00
3 3.000E+00
4 4.000E+00
5 5.000E+00
6 6.000E+00
7 7.000E+00
8 8.000E+00
9 9.000E+00
10 1.000E+01
11 1.100E+01
12 1.200E+01
13 1.300E+01
15 KA conductor
B max = 12.0 T
50cm
20cm
9T
10T
11T
12T
8T
4 3
2
1T
2T
7.00
6.50
6.00
5.50
5.00
4.50
4.00
3.50
3.00
2.50
2.00
-2.00
-1.50
-1.00
-0.50
0.00
0.50
1.00
1.50
X
Z

FIGURE E-10

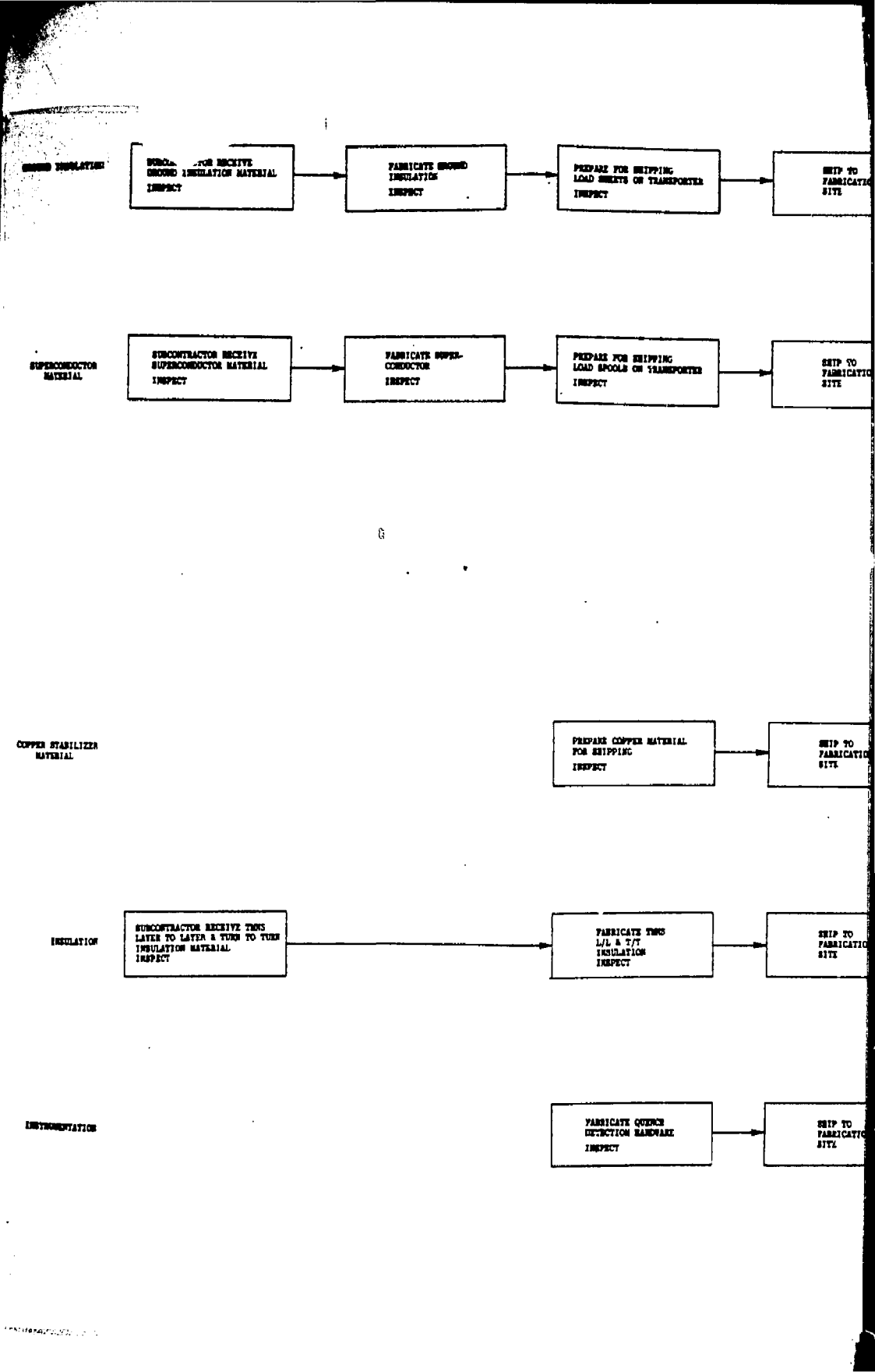
GROUND INSULATION
SUBCONTRACTOR RECEIVE GROUND INSULATION MATERIAL INSPECT
FABRICATE GROUND INSULATION INSPECT
PREPARE FOR SHIPPING LOAD SHEETS ON TRANSPORTER INSPECT
SHIP TO FABRICATION SITE
SUPERCONDUCTOR MATERIAL
SUBCONTRACTOR RECEIVE SUPERCONDUCTOR MATERIAL INSPECT
FABRICATE SUPER-CONDUCTOR INSPECT
PREPARE FOR SHIPPING LOAD SPOOLS ON TRANSPORTER INSPECT
SHIP TO FABRICATION SITE
COPPER STABILIZER MATERIAL
PREPARE COPPER MATERIAL FOR SHIPPING INSPECT
SHIP TO FABRICATION SITE
INSULATION
SUBCONTRACTOR RECEIVE THIN LAYER TO LAYER & TURN TO TURN INSULATION MATERIAL INSPECT
FABRICATE THIN L/L & T/T INSULATION INSPECT
SHIP TO FABRICATION SITE
INSTRUMENTATION
FABRICATE QUENCH DETECTION HARDWARE INSPECT
SHIP TO FABRICATION SITE

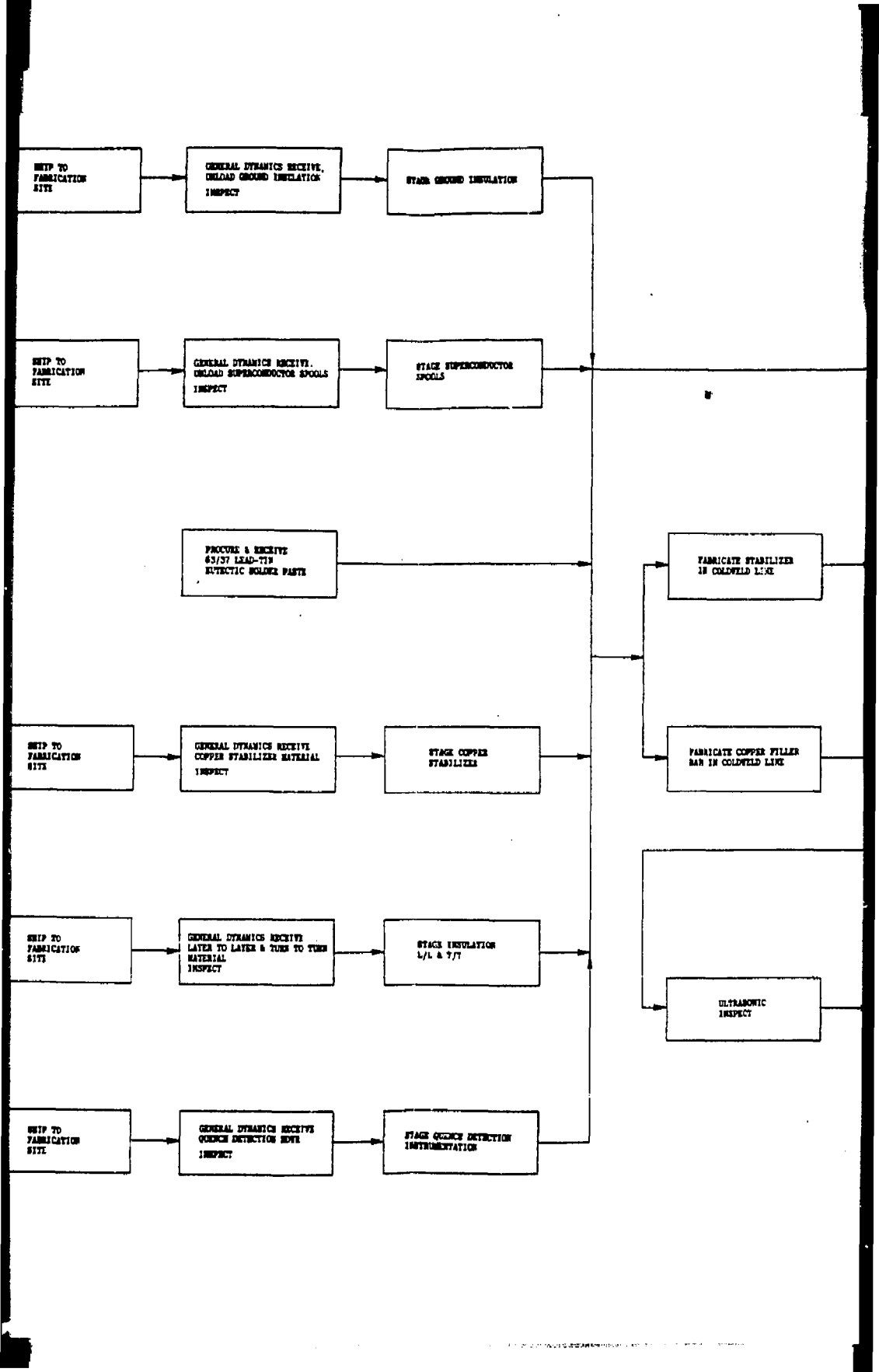
SHIP TO FABRICATION SITE
GENERAL DYNAMICS RECEIVE, UNLOAD GROUND INSULATION INSPECT
STAGE GROUND INSULATION
SHIP TO FABRICATION SITE
GENERAL DYNAMICS RECEIVE, UNLOAD SUPERCONDUCTOR SPOOLS INSPECT
STAGE SUPERCONDUCTOR SPOOLS
PROCURE & RECEIVE 63/37 LEAD-TIN EUTECTIC SOLDER PASTE
FABRICATE STABILIZER IN COILFELD LINE
SHIP TO FABRICATION SITE
GENERAL DYNAMICS RECEIVE COPPER STABILIZER MATERIAL INSPECT
STAGE COPPER STABILIZER
FABRICATE COPPER FILLER BAR IN COILFELD LINE
SHIP TO FABRICATION SITE
GENERAL DYNAMICS RECEIVE LAYER TO LAYER & TURN TO TURN MATERIAL INSPECT
STAGE INSULATION L/L & T/T
ULTRASONIC INSPECT
SHIP TO FABRICATION SITE
GENERAL DYNAMICS RECEIVE QUENCH DETECTION HEVE INSPECT
STAGE QUENCH DETECTION INSTRUMENTATION

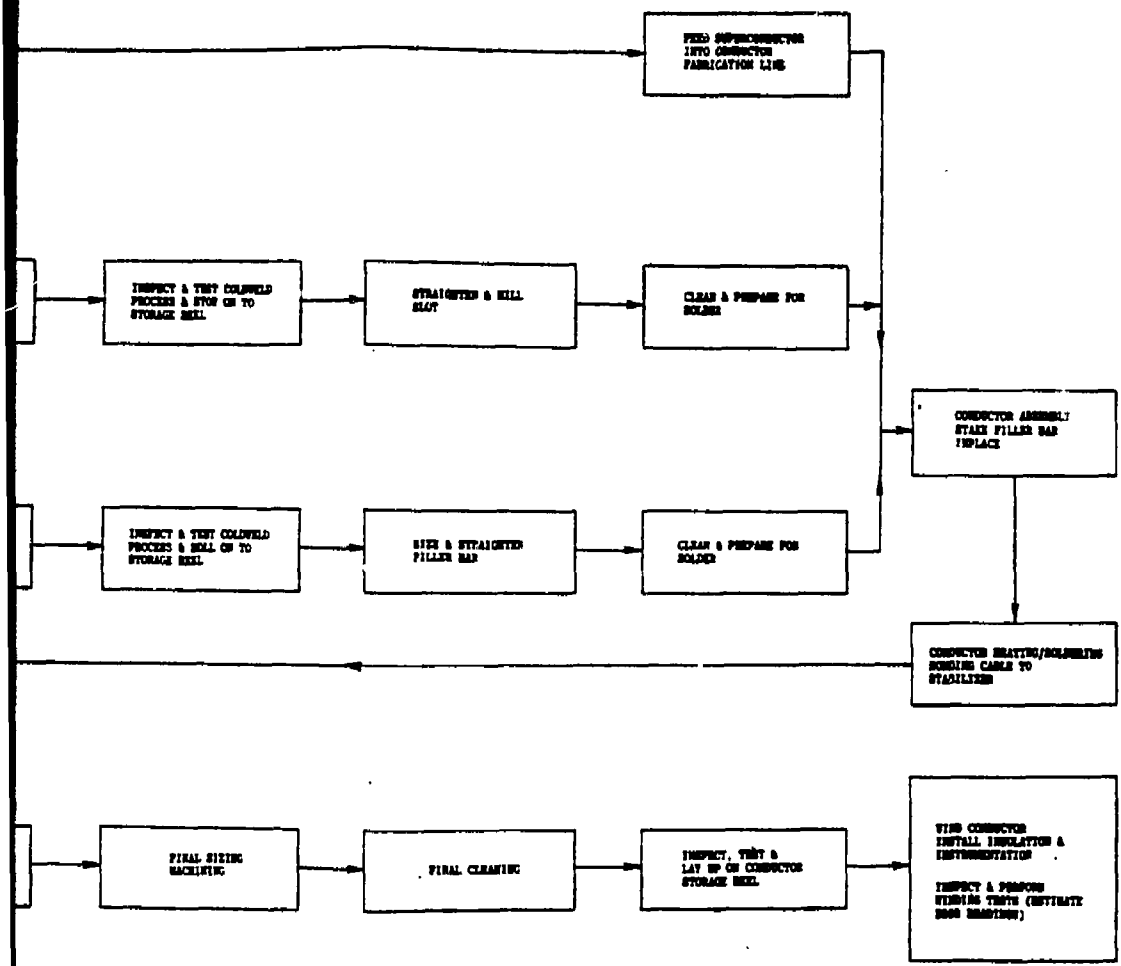

MANUFACTURING ENGINEERING	
TWIS CONDUCTOR FABRICATION & WINDING SEQUENCE & FLOW DIAGRAM	
PREPARED BY Greg Rowe	APPROVED BY [illegible] DATE 7/27/81